STRINGQFT

String-Theoretic Construction
of Quantum Field Theory

VOLUME X

Brane Webs and Magnetic Quivers

Xingyang Yu

StringQFT v1.0

Drafted with AI assistance under the supervision of the author.
Manuscript free to read. All rights reserved.

Contents

X.1 Five-brane webs and five-dimensional gauge theories 1

X.1.1 A finite five-brane face poses a five-dimensional question 1
X.1.2 Charge conservation fixes a supersymmetric junction 2
X.1.3 The pure SU(2) web has one local Coulomb deformation 5
X.1.4 A wrapped D3 measures the metric and magnetic-string tension 8
X.1.5 One-loop roots and weights resolve a mass chamber 10
X.1.6 Pure SU(3) tests the rank-two Coulomb metric 13
X.1.7 The perpendicular grid counts possible finite faces 15
X.1.8 What the shrinking web does and does not establish 18
X.1.9 Exercises 19
X.1.10 Take-home message 20
Status and sources 20

X.2 Seven-branes, junctions and charge monodromy 22

X.2.1 A flavor brane at the end of an E_1 web 22
X.2.2 Charge transport around one seven-brane 25
X.2.3 Moving a cut changes the brane word 27
X.2.4 From drawn strings to invariant prongs 29
X.2.5 Junction intersections make simple roots 31
X.2.6 The $BCBC$ loop and finite flavor 33
X.2.7 The W-boson and instanton junctions 36
X.2.8 Finite exceptional labels and five-dimensional phases 40
X.2.9 Exercises 42
X.2.10 Take-home message 43
Status and sources 43

X.3 Five-dimensional fixed points and exceptional symmetry 45

X.3.1 What shrinks when a five-dimensional face collapses? 45
X.3.2 The cubic prepotential and the flavor boundary 47
X.3.3 A flavor threshold in two Coulomb chambers 49
X.3.4 Exceptional flavor symmetry needs a construction 52
X.3.5 The two pure endpoints and the E0 transition 56
X.3.6 The E3 Higgs branch has two cones 59
X.3.7 What remains beyond the fixed-point examples 63
X.3.8 Exercises 64

X.3.9 Take-home message . . . 65
Status and sources . . . 65

X.4 Six-dimensional theories from NS5-D6-D8 systems 67
X.4.1 Dynamical endpoints in six dimensions . . . 67
X.4.2 D6 intervals, tensor scalars and instanton strings . . . 68
X.4.3 D8 charge fixes the rank profile . . . 70
X.4.4 Gauge anomalies from the brane inventory . . . 73
X.4.5 Tensor strings cancel the gauge anomaly . . . 77
X.4.6 Decoupling gravity and the conformal point . . . 80
X.4.7 What a magnetic quiver must still supply . . . 83
X.4.8 Exercises . . . 84
X.4.9 Take-home message . . . 85
Status and sources . . . 85

X.5 Magnetic quivers and Coulomb-branch geometry 87
X.5.1 A Higgs branch seen through a different theory . . . 87
X.5.2 Compact gauge data and the monopole sum . . . 88
X.5.3 The charge-one SQED ring . . . 90
X.5.4 An affine A_2 quiver and its centre . . . 93
X.5.5 Two cones from a five-brane web . . . 95
X.5.6 Two M5 branes and the affine D_4 quiver . . . 99
X.5.7 What the dictionary can and cannot identify . . . 103
X.5.8 Exercises . . . 105
X.5.9 Take-home message . . . 105
Status and sources . . . 106

X.6 Higgs branches at strong coupling 108
X.6.1 Why a Higgs branch changes at a singular limit . . . 108
X.6.2 Shared seven-branes turn five subwebs into a cycle . . . 109
X.6.3 Two maximal decompositions make a reducible branch . . . 113
X.6.4 Separated M5 branes and the affine D_4 magnetic quiver . . . 115
X.6.5 A small E_8 instanton transition changes the slice . . . 117
X.6.6 When quiver subtraction describes a transverse slice . . . 121
X.6.7 What the examples establish . . . 123
X.6.8 Exercises . . . 124
X.6.9 Take-home message . . . 125
Status and sources . . . 125

X.7 Hilbert series and the stratification of moduli spaces 127
X.7.1 One five-dimensional Higgs branch, two cones . . . 127
X.7.2 Magnetic flux and the monopole Hilbert sum . . . 129
X.7.3 The A-series ring and Molien counting . . . 131
X.7.4 A nonabelian sum and the D-series surface . . . 134
X.7.5 The affine A2 quiver and its missing center . . . 136
X.7.6 Symplectic leaves and the Hasse diagram . . . 138

X.7.7 What quiver subtraction can and cannot decide 142
X.7.8 Exercises 146
X.7.9 Take-home message 147
Status and sources 147

X.8 An atlas of webs and magnetic quivers 150
X.8.1 A source object becomes an atlas row 150
X.8.2 The pure SU(2) face, scalar map and theta fork 151
X.8.3 Charge and tensor data that do not become a magnetic ring . . 153
X.8.4 The E3 origin is a union of unequal cones 154
X.8.5 Separated M5s, electric four flavors and the D4 star 156
X.8.6 Cycles and aligned subtraction 158
X.8.7 Exercises 159
X.8.8 Take-home message 160
Status and sources 160

Chapter X.1

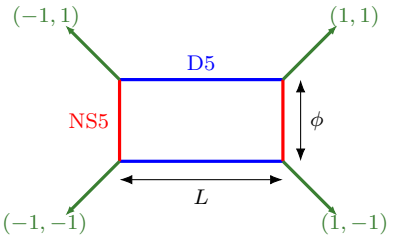
Five-brane webs and five-dimensional gauge theories

X.1.1 A finite five-brane face poses a five-dimensional question

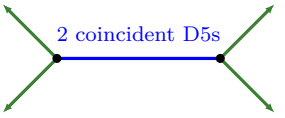
Two horizontal D5 segments can join two vertical NS5 segments to enclose a rectangle. Four diagonal five-branes carry the charge away to infinity. If the rectangle changes size while the distant legs stay on the same lines, the motion is confined to a finite part of the configuration. That simple distinction is the entry point to a five-dimensional gauge theory. A finite motion can become a dynamical Coulomb scalar; changing a distant leg instead changes a parameter of the theory.

The example in this chapter is the pure $SU(2)$ gauge phase. It has one independent compact face, hence one candidate local Coulomb coordinate. A fundamental string stretched vertically between the horizontal D5s gives a massive W particle. A D-string stretched horizontally between the NS5s gives an instanton particle. A D3 occupying the face and one spacetime direction gives a magnetic string. Their masses and tension turn the web from a drawing into a calculation.

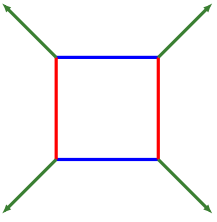
The five-branes share $x^{0,1,2,3,4}$. We draw x^6 to the right and x^5 upward. A horizontal D5 spans 012346, a vertical NS5 spans 012345, and 789 are transverse. A suitable junction preserves eight real supercharges, the amount denoted $\mathcal{N} = 1$ in five dimensions. We use the normalized drawing with Type IIB axiodilaton $\tau = i$ until the physical meaning of the drawing is discussed. Charges on every ray point outward.



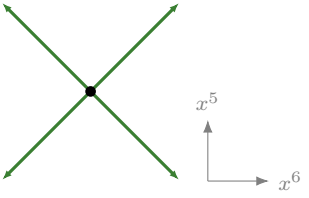
(a) $m_A > 0,\ \phi > 0$: rectangle



(b) $m_A > 0,\ \phi = 0$: segment



(c) $m_A = 0,\ \phi > 0$: square



(d) $m_A = \phi = 0$: point

Figure X.1.1: One charged web in four parameter limits. Blue and red finite edges are D5 and NS5 segments, respectively; green rays carry the same four diagonal charges in every panel. The face closes to a segment at $\phi = 0, m_A > 0$, stays a square at $m_A = 0, \phi > 0$, and becomes a point only when both parameters vanish. The collapsed segment in panel (b) retains two coincident D5s. The drawings show the local geometry, not a derivation of the ultraviolet theory.

The same face will support three complementary calculations. Charge and supersymmetry fix its edges. A wrapped D3 and a moving-edge calculation give its string tension and scalar metric. The one-loop prepotential then supplies a field-theory comparison with an explicitly different Cartan coordinate. We finally use the integer grid dual to the web to count possible faces. Each step answers a narrower question than the existence of a decoupled ultraviolet fixed point.

X.1.2 Charge conservation fixes a supersymmetric junction

A D5 ending on an unbent NS5 would leave a charge mismatch at the endpoint. The NS5 must bend into a bound-state five-brane. To see both the required charge and the angle, orient each half-edge away from the vertex and write its integer charge as (p, q), with p counting D5 charge and q counting NS5 charge. Reversing an edge reverses both

integers. For a trivalent junction, conservation is the pair of equations

$$\sum_{i=1}^{3} p_i = 0, \qquad \sum_{i=1}^{3} q_i = 0. \tag{X.1.1}$$

An elementary example uses a D5 extending left, an NS5 extending down, and a diagonal ray extending northeast. In our outward convention its charges are

$$(-1,0) + (0,-1) + (1,1) = (0,0). \tag{X.1.2}$$

The opposite simultaneous orientation gives the equally valid triple $(1,0), (0,1), (-1,-1)$. It is the arrows, not unsigned labels printed next to a source drawing, that decide which triple is being used.

The original endpoint construction offers a complementary local derivation of the bend. In the old physical axes, the D5 endpoint is a source for the NS5 transverse profile. After the coordinate relabelling to our x^6 horizontal and x^5 vertical axes, its one-dimensional profile equation in normalized units is

$$\frac{d^2x^6}{d(x^5)^2} = \delta(x^5). \tag{X.1.3}$$

Choose the asymptotic NS5 below the endpoint to remain on $x^6 = 0$. Integrating across the source gives a unit jump in slope and fixes the piecewise linear solution

$$x^6(x^5) = \frac{|x^5| + x^5}{2} = \begin{cases} 0, & x^5 < 0, \\ x^5, & x^5 > 0. \end{cases} \tag{X.1.4}$$

The upper part is the northeast diagonal in Figure X.1.2. The profile calculation explains physically why the NS5 cannot remain a straight vertical line. The charge calculation identifies the new leg as a $(1,1)$ bound state; the BPS slope then agrees with the unit jump for $\tau = i$. At general τ, the source-normalized drawing must be transformed with A_τ rather than keeping the same Euclidean angle.

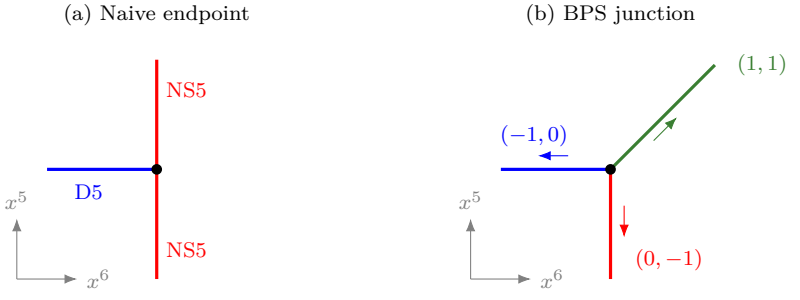


Figure X.1.2: The same D5 and NS5 legs at an endpoint. A vertical NS5 through the naive endpoint would not conserve the two charges there. The corrected configuration has a northeast $(1,1)$ outgoing leg. All charge arrows in panel (b) point away from the junction in the physical x^6 right, x^5 up plane.

The angle is fixed by the BPS condition. For a constant axiodilaton $\tau = u + iv$, $v > 0$, a (p, q) five-brane has tension, in the source's relative units,

$$T_{(p,q)} = T_{\mathrm{D5}}|p + \tau q|. \tag{X.1.5}$$

Its directed tangent in the physical plane is parallel to the complex number $p + \tau q$. Thus the physical force vector of an outward leg is proportional to

$$\boldsymbol{f}_{(p,q)} = T_{\mathrm{D5}}(p + uq,\, vq). \tag{X.1.6}$$

Applying the same linear map to the charge equation gives

$$\sum_i \boldsymbol{f}_i = T_{\mathrm{D5}} \left(\sum_i p_i + u \sum_i q_i,\, v \sum_i q_i \right) = \mathbf{0}. \tag{X.1.7}$$

At $\tau = i$, the legs in Figure X.1.2 are horizontal, vertical and at 45°, exactly as their charge vectors require. Charge conservation and BPS slope together imply planar equilibrium. Neither condition alone supplies a five-dimensional field theory.

It is useful to separate physical distance from the integer drawing. If $(\tilde{x}, \tilde{y})$ are normalized coordinates in the basis $(1, \tau)$, then

$$\begin{pmatrix} x^6 \\ x^5 \end{pmatrix} = A_\tau \begin{pmatrix} \tilde{x} \\ \tilde{y} \end{pmatrix}, \qquad A_\tau = \begin{pmatrix} 1 & u \\ 0 & v \end{pmatrix}. \tag{X.1.8}$$

The physical squared-length form on a normalized vector is therefore

$$G_\tau = A_\tau^{\mathsf{T}} A_\tau = \begin{pmatrix} 1 & u \\ u & u^2 + v^2 \end{pmatrix}. \tag{X.1.9}$$

For example, at $\tau = 1 + 2i$, a normalized NS5 unit vector has physical length $\sqrt{5}$, while physical areas acquire the factor $\det A_\tau = 2$. An edge perpendicular in the normalized integer grid is generally not Euclidean perpendicular in the physical plane. The source proposes that compensating a change of τ by this plane transformation leaves the low-energy theory unchanged within an appropriate energy window. We use that proposal only to compare normalized drawings; force balance itself does not establish it.

The older physical drawing labels a horizontal D5 by $(0, 1)$ because it orders the components as (NS5,D5). Swapping those components and then assigning outward signs yields the charges used here. This translation is especially useful in the next chapter, where seven-brane branch cuts make the ordered charge and its orientation indispensable.

One can test the force rule away from the square drawing without relying on a visual angle. At $\tau = 1 + 2i$, the same outward triple has directed force vectors, divided by T_{D5},

$$\boldsymbol{f}_{(-1,0)} = (-1, 0), \qquad \boldsymbol{f}_{(0,-1)} = (-1, -2), \qquad \boldsymbol{f}_{(1,1)} = (2, 2). \tag{X.1.10}$$

They still add to zero, but the NS5 and diagonal directions have changed from the $\tau = i$ picture. In particular, retaining a Euclidean 45° diagonal while changing τ would

keep the charges but violate the BPS slope condition. This example separates two inputs that are often collapsed into a single sketch: the integer conservation law and the axiodilaton-dependent physical embedding.

The five-dimensional particle interpretation also needs the common worldvolume directions. Both basic five-branes extend over 01234, so a finite web drawn in the 56 plane leaves a common five-dimensional spacetime. A D5 edge extends along 6 beyond that common spacetime, and an NS5 edge along 5; a diagonal bound state extends along the corresponding line in the 56 plane. The three unused spatial directions 789 supply the transverse rotation group. This geometrical count explains why the construction can preserve the eight supercharges of a five-dimensional $\mathcal{N} = 1$ theory, while an arbitrary redrawing of the slopes need not preserve the same supersymmetry. It still leaves the separation of brane modes from bulk string and gravity modes as a further physical premise.

X.1.3 The pure SU(2) web has one local Coulomb deformation

Which motion of the rectangle is a field, and which merely changes the theory? Set $\phi \geq 0$, $m_A \geq 0$, and follow the source's pure $SU(2)$ finite-face configuration. In its normalized mass coordinates,

$$L = m_A + \phi. \tag{X.1.11}$$

The corners, read from northeast through northwest and southwest to southeast, are

$$\begin{aligned} V_{\mathrm{NE}} &= (L/2, \phi/2), & V_{\mathrm{NW}} &= (-L/2, \phi/2), \\ V_{\mathrm{SW}} &= (-L/2, -\phi/2), & V_{\mathrm{SE}} &= (L/2, -\phi/2). \end{aligned} \tag{X.1.12}$$

The top and bottom segments are D5s; the left and right segments are NS5s. At the corresponding corners the outward diagonal rays carry

$$(p,q)_{\mathrm{NE}} = (1,1), \quad (p,q)_{\mathrm{NW}} = (-1,1), \quad (p,q)_{\mathrm{SW}} = (-1,-1), \quad (p,q)_{\mathrm{SE}} = (1,-1). \tag{X.1.13}$$

For example, the two finite directions away from the northeast vertex have charges $(-1,0)$ and $(0,-1)$. The ray $(1,1)$ makes their sum zero. Rotating this check through the other three corners verifies all four junctions. It also shows why the exterior legs cannot be assigned charges without declaring arrows.

The apparent motion of every corner when ϕ varies does not mean the external theory changes. A ray of charge (p,q) lies on a line of fixed support $p\tilde{y} - q\tilde{x} = c$. At the northeast corner, for instance,

$$c_{\mathrm{NE}} = \frac{\phi - L}{2} = -\frac{m_A}{2}. \tag{X.1.14}$$

The other three rays obey, in the same cyclic order,

$$(c_{\mathrm{NE}}, c_{\mathrm{NW}}, c_{\mathrm{SW}}, c_{\mathrm{SE}}) = \frac{m_A}{2}(-1,1,-1,1). \tag{X.1.15}$$

All four supporting lines are independent of ϕ at fixed m_A. Changing ϕ therefore moves only finite edges. In the web description that local zero mode is assigned to a vector-multiplet scalar. Changing m_A moves the asymptotic lines and changes a coupling parameter. The distinction is an asymptotic boundary condition, not a visual judgment that one displacement looks smaller than another.

There is a useful independent way to count the local motion before identifying it with ϕ. The compact part of this graph has four finite edges and four trivalent vertices. For a connected planar web with a fixed asymptotic configuration, the edge displacements obey one linear meeting constraint per vertex, with one relation among those constraints. The count for this rectangle is

$$n_{\text{local}} = E_{\text{finite}} - V + 1 = 4 - 4 + 1 = 1. \tag{X.1.16}$$

The same count is the number of compact faces by Euler's relation. It does not say that each of the four edges supplies a separate vector. The source's geometric dictionary associates the single motion with one low-energy abelian multiplet; the physical decoupling and normalizability of that motion remain part of the construction.

There is one compact face and one independent local motion. The two finite horizontal D5s do not provide two independent interacting Coulomb coordinates. Their relative separation is the scalar in the $SU(2)$ gauge frame; a putative center-of-mass motion either shifts external data or is a decoupled translation. At the generic point the low-energy gauge field is abelian. The nonabelian W state becomes light when the horizontal D5s meet.

In the source-native normalization a fundamental string stretched between the D5s and a D-string stretched between the NS5s have masses

$$m_W = \phi, \qquad m_{\text{inst}} = L = m_A + \phi. \tag{X.1.17}$$

The first equality fixes the scalar coordinate rather than following from an unlabeled geometric length. The second is the instanton-particle interpretation in this gauge chamber. Their string species and endpoints are shown on the same face in Figure X.1.3.

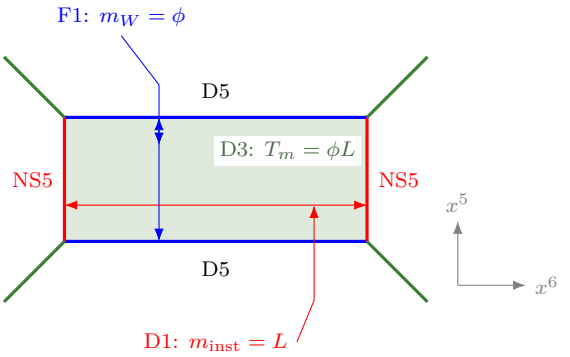


Figure X.1.3: Three probes of the same pure $SU(2)$ face. The vertical F1 path measures the W mass, the horizontal D1 path measures the instanton mass, and a D3 covering the shaded face and extending along x^1 makes a magnetic string. Paths indicate the source-native relative normalization; absolute brane-action factors have not been inferred from the drawing.

The limits are geometrically distinct. At $\phi = 0$ with $m_A > 0$, the two horizontal D5 edges coincide and the face becomes a segment of length m_A. At $m_A = 0$ with $\phi > 0$, $L = \phi$ and the face is a square of positive area. Only $m_A = \phi = 0$ shrinks the face to a point. This distinction will matter when a geometric degeneration is interpreted as a strong-coupling limit. A face drawn as a point at $m_A = 0$ would discard the remaining Coulomb coordinate.

For a numerical picture in the normalized units, choose $m_A = 2$ and $\phi = 1$. The horizontal D5 edges then have length three, while the vertical NS5 edges have length one. The W particle has mass one and the instanton particle mass three. Decreasing ϕ at fixed $m_A = 2$ shortens both the vertical separation and the horizontal length, yet the four diagonal supporting lines remain fixed. Increasing m_A at fixed $\phi = 1$ lengthens the horizontals and shifts those supporting lines. These two operations can look similar in a cropped drawing of the compact face; their different effect at infinity is why one is a Coulomb expectation value and the other a coupling change.

The same example can be checked directly at the northeast vertex. At $(m_A, \phi) = (2, 1)$ it is $(x, y) = (3/2, 1/2)$, and its $(1, 1)$ ray lies on $y - x = -1$. At $(m_A, \phi) = (2, 2)$ the vertex has moved to $(2, 1)$, but the ray still lies on that very line:

$$(y - x)\big|_{(3/2,1/2)} = (y - x)\big|_{(2,1)} = -1. \tag{X.1.18}$$

At the original $\phi = 1$ with $m_A = 3$, by contrast, the vertex is $(2, 1/2)$ and the support value is $-3/2$. This small calculation shows how an apparently moving external ray can keep its asymptotic line while the face changes, and how a coupling deformation really moves that line. Chapter 3 will use this separation when it compares distinct strong-coupling limits of pure and flavored webs.

X.1.4 A wrapped D3 measures the metric and magnetic-string tension

The compact face has a direct field-theory observable. A D3 wrapping its interior and extending along x^1 is a string in the common five-dimensional spacetime. Its tension in the normalized units is the face area. The three probes in Figure X.1.3 use the same rectangle, so their mass and tension comparisons share a geometry. For the ordered corners in (X.1.12), the shoelace sum gives

$$A_{\text{face}} = \frac{1}{2}\left|\sum_{j=1}^{4}(x_j y_{j+1} - y_j x_{j+1})\right| = L\phi. \tag{X.1.19}$$

The string tension is consequently

$$T_m^A(\phi) = \phi(m_A + \phi) = m_A\phi + \phi^2. \tag{X.1.20}$$

The superscript A reminds us that ϕ is the Aharony–Hanany–Kol coordinate. The area comparison fixes relative terms in that convention; it does not by itself restore every factor of 2π, α' or the Type IIB string tension.

There is a second geometric calculation of the scalar metric. A change $d\phi$ moves each of the four finite edges normally by $d\phi/2$. The two horizontal edges each have length L and the two vertical ones each have length ϕ. With the weighted moving-edge rule, their contributions add to

$$g_{\text{eff}}^{-2} = 2\sum_e \ell_e \left(\frac{\delta_e}{d\phi}\right)^2 = 2\left(\frac{1}{2}\right)^2 (2L + 2\phi) = m_A + 2\phi. \tag{X.1.21}$$

This explicitly uses all four edges. Using only the horizontal D5 lengths would miss the same low-energy field's participation in the NS5 edges. The source kinetic convention is

$$\mathcal{L}_{\text{kin}}^A = \frac{1}{4} g_{\text{eff}}^{-2}(\phi)(\partial_\mu\phi)(\partial^\mu\phi). \tag{X.1.22}$$

Thus the positive length $m_A + 2\phi$ is also the local Coulomb metric in this source-native comparison.

The magnetic string and scalar metric constrain a single cubic prepotential. Taking $T_m^A = \partial_\phi \mathcal{F}_A$ and choosing $\mathcal{F}_A(0) = \mathcal{F}_A'(0) = 0$ gives

$$\mathcal{F}_A(\phi) = \int_0^\phi (m_A t + t^2)\, dt = \frac{1}{2} m_A \phi^2 + \frac{1}{3}\phi^3. \tag{X.1.23}$$

Differentiating twice reproduces the edge calculation,

$$\mathcal{F}_A''(\phi) = m_A + 2\phi = g_{\text{eff}}^{-2}(\phi). \tag{X.1.24}$$

The agreement is informative because the first route measures a D3 area and the second follows the motion of five-brane edges. They share the same physical web premise, however, so agreement is a consistency check within that construction.

The two measurements also have different derivatives. The first derivative of the area with respect to the Coulomb separation is the weighted perimeter relevant to the kinetic motion,

$$\frac{dA_{\text{face}}}{d\phi} = \frac{d}{d\phi}\big[\phi(m_A+\phi)\big] = m_A + 2\phi. \tag{X.1.25}$$

The dependence of L on ϕ is essential here. Differentiating $A = L\phi$ as if L were fixed would give only L and miss the motion of the vertical NS5 edges. At $m_A = 2$, $\phi = 1$, the face area and string tension are three, while the effective inverse coupling is four. Area and metric therefore carry related but distinct physical units and need not be numerically equal.

Before comparing this result with the standard compact-Cartan prepotential, we must translate its electric and magnetic units. Let

$$H = \operatorname{diag}(1,-1), \qquad \Phi = aH, \qquad a \geq 0, \qquad \operatorname{Tr} H^2 = 2. \tag{X.1.26}$$

The compact $SU(2)$ roots evaluate to $\pm 2a$ and a full fundamental has weights $\pm a$. The physical W mass in this Cartan coordinate is $2a$. Comparing it with $m_W = \phi$ determines

$$\phi = 2a. \tag{X.1.27}$$

The massive fundamental provides a separate check. Its two masses are $|m \pm a|$ in the Cartan description and $|m \pm \phi/2|$ in the web description. The agreement uses the full pair of weights, not a single scalar replacement in a polynomial.

The electric and magnetic lattices clarify the factor of two. In the $H/2$ electric basis the W has charge one and the fundamental has charge one-half. The primitive magnetic coroot pairs integrally with the fundamental only when its component is two. In the smallest pair,

$$q^A_{\text{fund}} = \frac{1}{2}, \qquad n_m(H) = 2, \qquad q^A_{\text{fund}} n_m(H) = 1. \tag{X.1.28}$$

Had we assigned the coroot component one merely because the web has one face, this electric-magnetic pairing would be half-integral. The face count and the normalization of magnetic charge answer different questions. The former counts local deformations; the latter uses the chosen compact group and its weight lattice.

In the electric basis where a W has charge one, a fundamental has charge $\pm\frac{1}{2}$. The primitive compact $SU(2)$ magnetic coroot H has component two in that rescaled basis. Consequently the canonical prepotential for differentiation with respect to ϕ is $\mathcal{F}_A/2$, and a magnetic object of component n_m has relative tension

$$T(n_m) = \frac{n_m}{2}\mathcal{F}'_A(\phi), \qquad n_m(H) = 2. \tag{X.1.29}$$

For the primitive string this is $\mathcal{F}'_A$. In the compact Cartan coordinate the corresponding derivative is $\mathcal{F}'_I(a)$. Matching the same string fixes $m_A = m_I$ in the compared source-native magnetic unit. We may call this common parameter m_0 only after that comparison; m_I is a bare IMS parameter, whereas $m_{\text{inst}} = m_A + \phi$ is a particle mass.

The resulting relative map is more than a substitution of variables,

$$\mathcal{F}_A(2a) = 2\mathcal{F}_I(a), \qquad \mathcal{F}'_A(2a) = \mathcal{F}'_I(a), \qquad \mathcal{F}''_I(a) = 2\mathcal{F}''_A(2a). \tag{X.1.30}$$

In particular the two kinetic conventions agree after pullback,

$$\frac{1}{4}\mathcal{F}_A''(2a)(d\phi)^2 = \frac{1}{2}\mathcal{F}_I''(a)(da)^2, \qquad d\phi = 2\,da. \tag{X.1.31}$$

These equalities compare relative low-energy normalizations. Absolute BPS action constants, line-operator spectra and a discrete theta choice require additional physical input. In the stated chamber $m_A, \phi \geq 0$, the metric is nonnegative and the string tension vanishes as the face closes. That local result is necessary for this gauge phase; it is not a general theorem that every such web has a decoupled ultraviolet completion.

For completeness, the pure compact-Cartan polynomial can be placed beside its web version with the compared bare parameter explicit,

$$\mathcal{F}_I(a) = m_I a^2 + \frac{4}{3}a^3, \qquad \mathcal{F}_A(2a) = 2m_A a^2 + \frac{8}{3}a^3. \tag{X.1.32}$$

The cubic coefficients already obey the factor-two relation. Equality of the quadratic terms in that relation requires $m_A = m_I$, which came from matching the same primitive magnetic string. This is why a bare symbol m_0 appearing in two papers should not be identified before the charged objects and their kinetic conventions are compared.

X.1.5 One-loop roots and weights resolve a mass chamber

The field-theory prepotential gives a way to test the web's cubic without assuming the two scalar coordinates coincide. In the compact Cartan basis used above, the exact perturbative five-dimensional prepotential is piecewise cubic. For a simple group with Cartan scalar Φ, real masses m_f, roots R and full representation weight sets W_f, its form is

$$\mathcal{F}_I = \frac{m_I}{2}\operatorname{Tr}\Phi^2 + \frac{c_{\mathrm{cl}}}{6}d(\Phi,\Phi,\Phi) + \frac{1}{12}\left(\sum_R |R(\Phi)|^3 - \sum_f \sum_{w\in W_f} |w(\Phi)+m_f|^3\right). \tag{X.1.33}$$

Here m_I is the bare quadratic coefficient and c_{cl} is a classical cubic level when that invariant exists. The absolute values record which massive modes have been integrated out in a given Coulomb chamber. The cubic form follows from the five-dimensional gauge invariance restriction on the low-energy prepotential. It does not fix which global gauge group or discrete theta theory the local Lie-algebra calculation describes.

The two sums in (X.1.33) play different roles as one moves through a Weyl chamber. The signs of root evaluations are fixed inside that chamber; a root can vanish only on a nonabelian boundary. A shifted matter weight $w(\Phi) + m_f$ can vanish on an interior wall. Its absolute-value cube is twice differentiable there, but its third derivative changes. This is why a five-dimensional massive hypermultiplet can change the local cubic coefficient without making the scalar metric discontinuous. The calculation below keeps both weights of a full fundamental and the same bare quadratic coefficient on both sides of the wall.

For pure $SU(2)$, $\mathrm{Tr}\,\Phi^2 = 2a^2$ and the two roots have values $2a$ and $-2a$. With $a \geq 0$ and no classical cubic term,

$$\sum_R |R(\Phi)|^3 = 2(2a)^3 = 16a^3. \tag{X.1.34}$$

The pure prepotential and metric are therefore

$$\mathcal{F}_I^{(0)}(a) = m_I a^2 + \frac{4}{3}a^3, \qquad (\mathcal{F}_I^{(0)})'' = 2m_I + 8a. \tag{X.1.35}$$

Substitution into (X.1.30) gives exactly the web-derived $\mathcal{F}_A$ and its metric at $\phi = 2a$. This checks the root coefficient, the scalar scale and the magnetic comparison together.

A massless full fundamental contributes both weights $+a$ and $-a$. Its weight sum and the resulting prepotential are

$$\sum_{w=\pm 1} |wa|^3 = 2a^3, \qquad \mathcal{F}_I^{(1,0)} = m_I a^2 + \frac{7}{6}a^3. \tag{X.1.36}$$

Thus one full flavor changes the Hessian from $2m_I + 8a$ to

$$(\mathcal{F}_I^{(1,0)})'' = 2m_I + 7a. \tag{X.1.37}$$

This is a field-theory calculation of a protected gauge-phase function. It does not draw a flavor web or identify an enhanced symmetry.

Now give that fundamental a positive mass m. The two absolute values $|a+m|^3$ and $|m-a|^3$ change algebraic form at $a = m$. Outside the wall, $a \geq m \geq 0$, their sum is

$$(a+m)^3 + (a-m)^3 = 2a^3 + 6am^2. \tag{X.1.38}$$

Inside, $m \geq a \geq 0$, it is

$$(m+a)^3 + (m-a)^3 = 2m^3 + 6ma^2. \tag{X.1.39}$$

Keeping the same bare m_I in the two expressions gives

$$\mathcal{F}_{\text{out}} = m_I a^2 + \frac{7}{6}a^3 - \frac{1}{2}am^2, \qquad \mathcal{F}_{\text{in}} = \left(m_I - \frac{m}{2}\right)a^2 + \frac{4}{3}a^3 - \frac{1}{6}m^3. \tag{X.1.40}$$

The cubic changes at the wall, while the metric remains continuous. Indeed, direct differentiation yields

$$\mathcal{F}''_{\text{out}} = 2m_I + 7a, \qquad \mathcal{F}''_{\text{in}} = 2m_I - m + 8a. \tag{X.1.41}$$

At $a = m$ the two values are both $2m_I + 7m$. The functions and first derivatives also meet there, whereas

$$\mathcal{F}'''_{\text{out}} - \mathcal{F}'''_{\text{in}} = 7 - 8 = -1. \tag{X.1.42}$$

This is the characteristic change of a five-dimensional cubic when a charged state crosses zero mass. Figure X.1.4 isolates the continuous metric and its kink.

The continuity can be checked without relying only on the smoothness of $|z|^3$. Substituting $a = m$ into both chamber polynomials and their first derivatives gives

$$\mathcal{F}_{\text{out}}(m) = \mathcal{F}_{\text{in}}(m) = m_I m^2 + \frac{2}{3}m^3, \tag{X.1.43}$$

$$\mathcal{F}'_{\text{out}}(m) = \mathcal{F}'_{\text{in}}(m) = 2m_I m + 3m^2. \tag{X.1.44}$$

The second derivatives agree as shown above. These three checks tell the reader exactly what is smooth across the threshold. They also expose a common shortcut that gives the wrong coefficient: subtracting only one fundamental weight would halve the matter contribution, change the outer cubic and spoil the comparison with the source's massive web normalization.

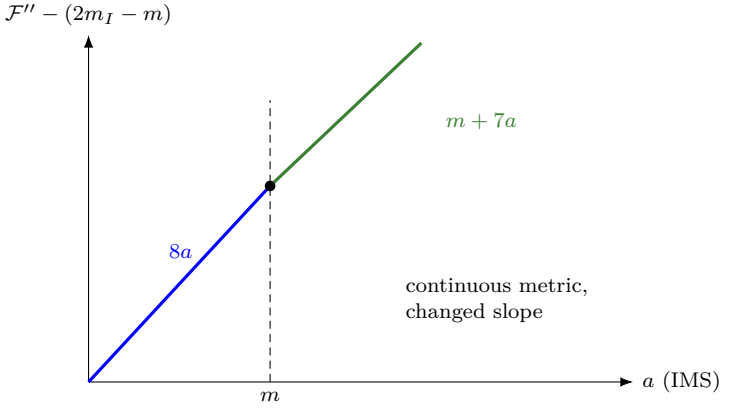


Figure X.1.4: One massive full fundamental in the IMS coordinate. The plotted quantity subtracts the common inner-chamber intercept $2m_I - m$; its piecewise slopes are 8 and 7. The point $a = m$ is a mass wall, not a singularity in the scalar metric. Physical metric nonnegativity must be imposed in addition to the indicated chamber inequalities.

In the inner chamber the smallest value of the metric on $0 \le a \le m$ is $2m_I - m$ at $a = 0$. Thus the whole inner interval is a physical positive-metric gauge region only if

$$2m_I \ge m. \tag{X.1.45}$$

The branch condition $m \ge a$ alone does not ensure this. For example, $m = 3$ and $m_I = 1$ satisfy the algebraic inner-chamber condition at $a = 0$, but the calculated metric there is -1. The polynomial can still be evaluated; that does not make the entire interval a positive kinetic-energy gauge phase. At $a = m$ the metric has risen to $2m_I + 7m = 23$, so the same formula can describe a positive region nearer the wall. The physical domain must be stated with the chamber formula. A heavy hypermultiplet also reveals why the bare parameter must be specified. Holding m_I fixed while $m \to \infty$ leaves an unbounded quadratic shift. Defining and holding fixed

$$m_{\text{eff}} = m_I - \frac{m}{2} \tag{X.1.46}$$

instead leaves $m_{\rm eff}a^2 + 4a^3/3$, plus the a-independent constant $-m^3/6$. The dynamical pure prepotential is recovered in that renormalized limit.

The same normalization map can be checked against a massive rather than a pure observable. In the AHK coordinate, the full-fundamental term contains the two masses $|m \pm \phi/2|$ and carries coefficient $-1/6$; in the IMS coordinate the term has coefficient $-1/12$. Consequently, after $\phi = 2a$, the matter terms obey

$$-\frac{1}{6}\left(\left|m+\frac{\phi}{2}\right|^3+\left|m-\frac{\phi}{2}\right|^3\right)_{\phi=2a} = 2\left[-\frac{1}{12}(|m+a|^3+|m-a|^3)\right]. \tag{X.1.47}$$

This check is sensitive to the full weight multiplicity. It supports the relative source-native prepotential factor used in Section X.1.4; it does not supply the topology of the one-flavor web from a polynomial alone.

The actual one-flavor web has distinct configurations on the two sides of its mass wall. The algebra above explains its low-energy cubic change, but does not replace the charge and seven-brane analysis required to construct those configurations. The exceptional-symmetry interpretation of their strong-coupling limits belongs to Chapter 3.

X.1.6 Pure SU(3) tests the rank-two Coulomb metric

A single Coulomb coordinate can conceal the matrix structure of a higher rank theory. Pure $SU(3)$ gives a small example with two independent Cartan coordinates. Choose the ordered Weyl chamber and zero bare quadratic and classical cubic terms,

$$\Phi = \mathrm{diag}(x, y, -x-y), \qquad x \geq y \geq -x-y. \tag{X.1.48}$$

The six roots occur in positive and negative pairs. Their three positive values in this chamber are

$$\alpha_{12}(\Phi) = x-y, \quad \alpha_{13}(\Phi) = 2x+y, \quad \alpha_{23}(\Phi) = x+2y. \tag{X.1.49}$$

Each pair contributes twice the cube of its positive value to the root sum in (X.1.33). The resulting polynomial is

$$\mathcal{F}_{SU(3)}(x,y) = \frac{1}{6}\left[(x-y)^3+(2x+y)^3+(x+2y)^3\right]. \tag{X.1.50}$$

The condition that the three differences remain nonnegative is essential for this polynomial form. Outside the ordered chamber, the absolute values must be restored or the eigenvalues permuted.

The chamber itself can be described by two independent nonnegative separations. Put $s_1 = x-y$ and $s_2 = x+2y$. The remaining positive-root mass is their sum, so

$$s_1 \geq 0, \qquad s_2 \geq 0, \qquad 2x+y = s_1+s_2. \tag{X.1.51}$$

At $s_1 = 0$ the first two eigenvalues meet, while at $s_2 = 0$ the last two meet. These are different walls of the rank-two Weyl chamber. A calculation along one ray through the

chamber could miss a problem on the other wall, which is why the full Hessian is the appropriate object for a rank-two metric test. The source's pure $SU(3)$ web likewise has two independent compact-face motions; a single rectangle width cannot parameterize both.

To see the metric rather than just its value along one path, write the three linear forms as $\ell_j = \boldsymbol{v}_j \cdot (x, y)$ with

$$\boldsymbol{v}_{12} = (1, -1), \qquad \boldsymbol{v}_{13} = (2, 1), \qquad \boldsymbol{v}_{23} = (1, 2). \tag{X.1.52}$$

Twice differentiating a term $\ell^3/6$ gives

$$\partial_i \partial_j \frac{\ell^3}{6} = \ell \, v_i v_j. \tag{X.1.53}$$

Summing the three rank-one matrices yields the full two-coordinate Hessian,

$$\mathcal{H}(x, y) = \begin{pmatrix} 10x + 5y & 5x + 7y \\ 5x + 7y & 7x + 8y \end{pmatrix}. \tag{X.1.54}$$

The off-diagonal entry is a physical part of the kinetic form in these coordinates. Two separate second derivatives along the coordinate axes would not determine whether an arbitrary Coulomb motion has positive kinetic energy.

The matrix construction makes that issue explicit. For a small displacement $\delta\boldsymbol{a} = (\delta x, \delta y)$, its quadratic kinetic form is a sum over root directions,

$$\delta\boldsymbol{a}^{\mathsf{T}} \mathcal{H} \delta\boldsymbol{a} = \sum_{\alpha > 0} \alpha(\Phi) \big(\boldsymbol{v}_\alpha \cdot \delta\boldsymbol{a}\big)^2. \tag{X.1.55}$$

This expression explains the Hessian entries rather than merely displaying them. A root contributes according to how strongly the chosen Coulomb motion changes its associated charged-particle mass. The mixed term appears because a single root mass depends on both x and y. In a web picture, the two local face motions similarly share edges, so their kinetic terms need not diagonalize in the coordinates suggested by a first drawing.

For a concrete interior point take eigenvalues $(2, 0, -2)$, so $(x, y) = (2, 0)$. The three positive differences are $(2, 4, 2)$ and

$$\mathcal{F}_{SU(3)}(2, 0) = \frac{2^3 + 4^3 + 2^3}{6} = \frac{40}{3}. \tag{X.1.56}$$

At that point the metric matrix, its leading minor and determinant are

$$\mathcal{H}(2, 0) = \begin{pmatrix} 20 & 10 \\ 10 & 14 \end{pmatrix}, \qquad \mathcal{H}_{11} = 20, \qquad \det \mathcal{H} = 180. \tag{X.1.57}$$

Both principal tests are positive. Equivalently, the eigenvalues are

$$\lambda_\pm = 17 \pm \sqrt{109} > 0. \tag{X.1.58}$$

This fully works the rank-two example rather than checking only a diagonal entry. A positive matrix at one point is still a local result. To see exactly where the entries at this point came from, keep the three root terms separate before adding them:

$$\mathcal{H}(2,0) = 2\begin{pmatrix} 1 & -1 \\ -1 & 1 \end{pmatrix} + 4\begin{pmatrix} 4 & 2 \\ 2 & 1 \end{pmatrix} + 2\begin{pmatrix} 1 & 2 \\ 2 & 4 \end{pmatrix}. \tag{X.1.59}$$

The coefficients $2, 4, 2$ are the three charged-vector masses in this Cartan slice. The first contribution alone would have a null direction; the other two roots supply kinetic cost along it. This is a concrete reason to retain the entire root system rather than read a rank-two metric from one charged state or one visible web edge. It is instructive to test two different motions at the same point. Moving with $(\delta x, \delta y) = (1, 1)$ gives quadratic value 54, whereas $(1, -1)$ gives 14:

$$(1,1)\mathcal{H}(2,0)\begin{pmatrix} 1 \\ 1 \end{pmatrix} = 54, \qquad (1,-1)\mathcal{H}(2,0)\begin{pmatrix} 1 \\ -1 \end{pmatrix} = 14. \tag{X.1.60}$$

The different costs are not captured by a single effective-coupling number. The full matrix is the rank-two counterpart of the one-dimensional $m_A + 2\phi$ metric. A different Cartan coordinate basis would change the entries by a basis transformation while preserving positivity of the quadratic form at this physical point. To make a statement about an entire gauge chamber one must examine the full physical cone, its walls and the chosen matter and classical-level data. A pure $SU(3)$ web has two face motions in the source construction; its picture supports the rank-two interpretation but does not itself select the zero classical level used in this algebraic slice.

The example prepares the atlas later in this volume. A web face count can suggest a rank, while the field-theory Hessian decides whether a specified motion has positive local kinetic energy. The two questions must be kept distinct when the web topology changes or flavors are added.

X.1.7 The perpendicular grid counts possible finite faces

The web tells us how finite edges meet; an integer grid dual to it makes the number of possible compact faces easier to read. In the normalized charge plane, assign to an oriented web edge $\boldsymbol{c} = (p, q)$ a perpendicular grid displacement

$$J\boldsymbol{c} = (-q, p), \qquad J = \begin{pmatrix} 0 & -1 \\ 1 & 0 \end{pmatrix}. \tag{X.1.61}$$

The sign of a particular grid edge depends on which neighboring web region is crossed first. Its length is the primitive multiplicity of the charged web edge. The simple rotation is Euclidean in the normalized integer plane; at general τ the physical metric is (X.1.9), so the drawn grid need not be physically perpendicular to the transformed five-brane.

At a balanced trivalent web vertex, the three charges close. Linearity of the rotation then gives a closed dual polygon,

$$\sum_{i=1}^{3} J\boldsymbol{c}_i = J\left(\sum_{i=1}^{3} \boldsymbol{c}_i\right) = 0. \tag{X.1.62}$$

Each web vertex becomes a grid polygon, each web edge a grid edge, and a compact web face a grid point. This exchange is the useful part of the dictionary. It is a statement about the sourced five-brane construction, not a theorem that every integer polygon by itself gives a normalizable five-dimensional vector multiplet.

For the four external rays of the pure $SU(2)$ web, an equivalent normalized grid has successive vertices

$$P_E = (1,0), \quad P_N = (0,1), \quad P_W = (-1,0), \quad P_S = (0,-1). \tag{X.1.63}$$

Its boundary steps, starting at P_E, are

$$(-1,1), \quad (-1,-1), \quad (1,-1), \quad (1,1). \tag{X.1.64}$$

Their outward normals are, in order,

$$(1,1), \quad (-1,1), \quad (-1,-1), \quad (1,-1), \tag{X.1.65}$$

which recover exactly the northeast, northwest, southwest and southeast web rays. Figure X.1.5 keeps the web and the triangulated diamond side by side to make this rotation visible.

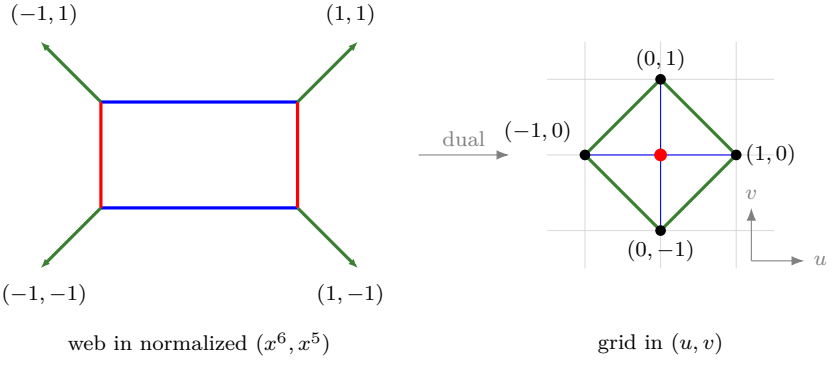


Figure X.1.5: The charged pure-$SU(2)$ web and its normalized integer grid. Each boundary step of the diamond is perpendicular to the corresponding outward web ray in the normalized plane. Four spokes from the red interior point produce four triangles of lattice area $1/2$. The point records a possible local face under the web dictionary; it is not by itself a normalizability or fixed-point test.

The diamond has area two. One way to see it is to partition it into four right triangles of legs one. Every boundary edge is primitive, so its only lattice points are its

four corners. Hence

$$A_{\text{grid}} = 4\left(\frac{1}{2}\right) = 2, \qquad B_{\text{grid}} = 4. \tag{X.1.66}$$

Pick's formula then yields

$$I_{\text{grid}} = A_{\text{grid}} - \frac{B_{\text{grid}}}{2} + 1 = 2 - 2 + 1 = 1. \tag{X.1.67}$$

The unique interior point is $(0,0)$. Joining it to the four corners produces four unimodular triangles, since every adjacent pair of corner vectors has determinant one. The count matches the one finite face and one local Coulomb motion found directly in the rectangular web.

The determinant statement can be checked on an actual triangle. For the triangle with vertices $(0,0)$, $P_E = (1,0)$ and $P_N = (0,1)$,

$$|\det(P_E, P_N)| = 1, \qquad A_{\triangle} = \frac{1}{2}. \tag{X.1.68}$$

Quarter-turning this calculation gives the other three triangles. The four exterior normals retain the charge information, while the single interior point retains the possible compact-face count. This separation is useful because the polygon remains the same as m_A and ϕ vary, whereas the effective metric $m_A + 2\phi$ changes continuously. The grid records a combinatorial possibility, not its kinetic coefficient.

The grid has discarded the lengths L and ϕ. It therefore cannot distinguish the positive-area square from the segment or point limits in Figure X.1.1. It also omits the compact electric and magnetic line lattices, the Type IIB decoupling limit and possible nonlocal modes. Later geometric-engineering chapters use the same perpendicular orientation convention, but they must supply their own physical map from lattice geometry to field-theory observables.

There are two different uses of the word "perpendicular" here. In the normalized plane, the dot product of a charge direction and its grid edge vanishes exactly,

$$(p,q)\cdot(-q,p) = -pq + qp = 0. \tag{X.1.69}$$

In the physical plane at general τ, the relevant squared-length form is G_τ, so the ordinary Euclidean dot product of the transformed directions need not vanish. Keeping the lattice drawing in its own normalized coordinates prevents an accidental inference about angles or tensions in a different physical axiodilaton background. For the normalized D5 direction $(1,0)$ and its grid direction $(0,1)$, the physical dot product at $\tau = 1+2i$ is

$$(1,0)G_{1+2i}\begin{pmatrix}0\\1\end{pmatrix} = 1, \tag{X.1.70}$$

even though their normalized dot product is zero. The grid's integer perpendicularity is therefore a rule for constructing the dual polygon, not a statement about the physical angle between two branes at this axiodilaton.

X.1.8 What the shrinking web does and does not establish

At fixed positive m_A, the face closes to a segment as $\phi \to 0$. The W mass then vanishes, while the instanton mass approaches m_A. This is the ordinary gauge-theory origin at finite bare coupling in the chosen chamber. Sending $m_A \to 0$ at fixed $\phi > 0$ instead leaves a square, a massive W, and a positive string tension ϕ^2. The simultaneous limit $m_A = \phi = 0$ is the point where those face scales vanish together. The source associates that particular web fixture with the E_1 fixed point.

The calculations in this chapter constrain the interpretation. The local metric $m_A + 2\phi$ and tension $\phi(m_A + \phi)$ are nonnegative in the declared quadrant. The compact-Cartan prepotential reproduces them after the explicit electric and magnetic normalization map. The diamond has one interior point. These facts make the proposed rank-one gauge phase coherent. To call the simultaneous degeneration a decoupled five-dimensional fixed point also requires a limit in which gravity and unwanted nonlocal string modes separate, plus a consistent physical Coulomb region. Neither force balance nor Pick's formula supplies that dynamical step.

The three geometric limits can be read directly against the same observables. The table uses the source-native relative units of the finite-web calculation and keeps the limiting operation explicit.

Limit of the face	Geometry	Particle and magnetic-string data
$\phi = 0$, $m_A > 0$	finite segment	$m_W = 0$, $m_{\text{inst}} = m_A$, $T_m = 0$, $g_{\text{eff}}^{-2} = m_A$
$m_A = 0$, $\phi > 0$	square of area ϕ^2	$m_W = m_{\text{inst}} = \phi$, $T_m = \phi^2$, $g_{\text{eff}}^{-2} = 2\phi$
$m_A = \phi = 0$	point	both particle masses, T_m and g_{eff}^{-2} vanish in these relative units

Table X.1.1: Three distinct limits of the same pure $SU(2)$ web. The final row is the selected strong-coupling candidate; the table lists calculated local data rather than establishing the existence of a decoupled theory.

The first row shows why a vanishing face area alone cannot identify the strong-coupling point: the magnetic string also has zero tension at the finite-coupling gauge origin, where the instanton particle remains massive. The second row shows the opposite error. Setting the bare inverse coupling to zero does not set the Coulomb expectation value to zero; the finite square still supports massive particles and a tense magnetic string. The last row takes both operations, so the local mass scales displayed here vanish together. Whether their limit defines a complete interacting ultraviolet theory is a further physical question.

The local cubic also leaves discrete information unresolved. Different pure $SU(2)$ ultraviolet theories can share the same perturbative rank-one prepotential. The source's E_1 name applies to the selected web, while a different strong-coupling configuration may

select a different theta theory. Compact line spectra and the theta choice cannot be reconstructed by differentiating the cubic. Chapter 3 takes up those questions together with flavor and exceptional symmetry.

The scope of a construction also differs from a field-theory existence criterion. The early simple webs explicitly cover fewer flavors than the seven-flavor $SU(2)$ field-theory analysis permits. A failure to find a state in this restricted web family is not a general exclusion theorem. The next chapter adds seven-brane endpoints and their ordered charge monodromy, which enlarge the available descriptions. Later magnetic quivers examine Higgs-branch geometry at strong coupling; a match of that geometry is a narrower statement than equality of full five-dimensional quantum field theories.

X.1.9 Exercises

1. At $\tau = i$, two outward legs of a trivalent junction have charges $(1, 0)$ and $(0, 1)$. Find the third outward charge. Explain why the BPS slope rule turns charge balance into force balance, and say which part of the argument fails if the legs are drawn at arbitrary angles.

2. In the AHK coordinate $m_W = \phi$, suppose a rank-one face has $T_m = m_A\phi + \phi^2$ and $\mathcal{F}(0) = \mathcal{F}'(0) = 0$. Determine the coefficients c_2, c_3 in $\mathcal{F} = c_2 m_A \phi^2 + c_3\phi^3$. Derive the effective metric and compare it with the four-edge displacement calculation.

3. Use $H = \operatorname{diag}(1, -1)$, $\operatorname{Tr} H^2 = 2$, $\Phi = aH$ and $a \geq 0$. Starting from the full root-minus-weight expression, calculate the coefficients c_2, c_3 in $\mathcal{F} = c_2 m_I a^2 + c_3 a^3$ for one massless full fundamental of $SU(2)$. Show the vector and hypermultiplet terms separately.

4. For pure $SU(3)$ with vanishing bare quadratic and classical cubic terms, evaluate $\mathcal{F}$ at eigenvalues $(2, 0, -2)$. List the three positive roots used in the calculation, then compute the full Hessian in the (x, y) coordinates to decide whether the metric is positive at that point.

5. Draw the grid polygon for outward web charges $(1, 1)$, $(-1, 1)$, $(-1, -1)$ and $(1, -1)$ in cyclic order. Mark every interior lattice point and relate it to a possible finite face. State the extra physical assumptions needed to interpret a shrinking web as a five-dimensional ultraviolet fixed point, and explain why the polygon calculation alone cannot supply them.

X.1.10 Take-home message

Take-home message

A BPS five-brane junction combines outward $(D5, NS5)$ charge conservation with a slope fixed by $p + \tau q$. In the pure $SU(2)$ finite web, one compact face gives one local Coulomb motion. Its F1, D1 and D3 probes measure $m_W = \phi$, $m_{\text{inst}} = m_A + \phi$ and $T_m = \phi(m_A + \phi)$. The moving edges and the cubic prepotential both give $g_{\text{eff}}^{-2} = m_A + 2\phi$. The compact-Cartan comparison uses $\phi = 2a$ and a magnetic-charge map; equal symbol names alone do not establish equal normalization. The dual diamond counts one possible face. Identifying a decoupled ultraviolet theory requires physical input beyond these local and combinatorial calculations.

Status and sources

The charge, tension and BPS-slope construction in Section X.1.2 follows Aharony, Hanany, and Kol (1998, PDF pp. 8–9, eqs. (8)–(11)). The physical D5 endpoint and its bent NS5 are in Aharony and Hanany (1997, PDF pp. 21–23, Fig. 4 and eqs. (3.1)–(3.3)); that paper orders the two charges as (NS5,D5), opposite to the house $(p, q) = (D5, NS5)$ order. The relative general-τ plane map is Aharony, Hanany, and Kol (1998, PDF p. 12, eq. (18)). Its compensated low-energy τ invariance is conjectural and energy-window qualified. The associated five-dimensional QFT identification uses a decoupling premise [DEC]; the local charge and linear-algebra checks are exact within the stated BPS setup. The web uses the stated axes and the charge order $(D5, NS5)$.

Sections X.1.3 and X.1.4 use the pure-web figures and probe assignments of Aharony, Hanany, and Kol (1998, PDF pp. 9, 11, 13–17, Figs. 1(b)–3 and eqs. (14)–(25)) and the finite-web deformation of Aharony and Hanany (1997, PDF pp. 23–25, Fig. 5). The D3 area and moving-edge metric are source-native protected effective quantities; the equality of their polynomials is algebraic under the stated normalization. The AHK/IMS electric, magnetic and kinetic map uses the stated relative normalization. Absolute action factors use the brane-action convention. The E_1 identity of this particular source fixture is physical source input [DEC], not an inference from the cubic. The two sources share the web premise and are not independent validation of a general geometric dictionary [GEO-E].

The field-theory root-minus-weight formula in Sections X.1.5 and X.1.6 is Intriligator et al. (1997, PDF p. 10, eq. (2.22), and pp. 11–12). The $SU(2)$ and $SU(3)$ specializations, wall continuity, third-derivative jump and displayed Hessian are algebraic consequences [MATH] in the specified Weyl chambers and classical-level choices. The actual one-flavor web chambers occur in Aharony, Hanany, and Kol (1998, PDF pp. 42–43, Fig. 16 and eqs. (59)–(61)). The pure $SU(3)$ two-face web context is Aharony and Hanany (1997, PDF p. 29, Fig. 7); its image alone does not fix our zero-level field-theory choice. These statements concern five-dimensional gauge-phase functions, not a three-dimensional Coulomb ring.

The grid construction and pure-web diamond in Section X.1.7 follow Aharony, Hanany, and Kol (1998, PDF pp. 17–19, Figs. 5–6 and eqs. (26)–(27)). The count of

one interior point is exact lattice arithmetic; the step from that point to a dynamical five-dimensional field uses the sourced web dictionary [GEO-E] and a normalizability/decoupling premise [DEC]. Section X.1.8 uses the selected E_1 assignment in Aharony, Hanany, and Kol (1998, PDF p. 16), the alternative pure-web limits in Aharony and Hanany (1997, PDF p. 26), and the physical-chamber and flavor discussion in Intriligator et al. (1997, PDF pp. 11–14). The local convexity criterion is necessary within the declared gauge phase, not a universal ultraviolet-existence theorem. No full-QFT equivalence, compact line spectrum or discrete-theta classification is established here.

References

Aharony, O. and A. Hanany (1997). "Branes, superpotentials and superconformal fixed points". In: *Nucl. Phys. B* 504, pp. 239–271. DOI: 10.1016/S0550-3213(97)00472-0. arXiv: hep-th/9704170.

Aharony, O., A. Hanany, and B. Kol (1998). "Webs of (p,q) five-branes, five-dimensional field theories and grid diagrams". In: *JHEP* 01, p. 002. DOI: 10.1088/1126-6708/1998/01/002. arXiv: hep-th/9710116.

Intriligator, K. A., D. R. Morrison, and N. Seiberg (1997). "Five-dimensional supersymmetric gauge theories and degenerations of Calabi-Yau spaces". In: *Nucl. Phys. B* 497, pp. 56–100. DOI: 10.1016/S0550-3213(97)00279-4. arXiv: hep-th/9702198.

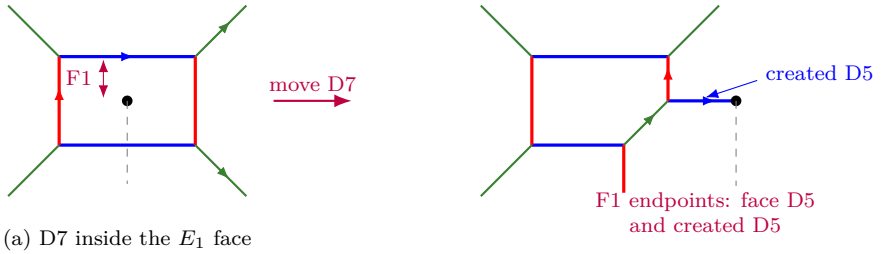
Chapter X.2

Seven-branes, junctions and charge monodromy

X.2.1 A flavor brane at the end of an E_1 web

The finite face of Chapter 1 supports massive strings as well as a Coulomb motion. We now add a D7 to that same pure $SU(2)$ web. A fundamental string can run from a horizontal D5 to the D7, so the new object supplies a fundamental quark. What happens when the D7 moves across the vertical NS5? The answer is visible before any monodromy calculation: a D5 prong is created, and the string can end on it. A five-dimensional particle keeps its quantum numbers although the drawing of its endpoint has changed.

The common five-brane directions are $x^{0,1,2,3,4}$. D5 and NS5 also span x^6 and x^5, respectively. The D7 of this construction spans $x^{0,1,2,3,4,7,8,9}$. The web is drawn with x^6 rightward and x^5 upward. Its five-brane charge column counts $(D5, NS5)$ charges. A string ending on a seven-brane instead carries the distinct $(F1, D1)$ column. An $X_{[p,q]}$ seven-brane allows a string with that latter charge to end; its label and $[-p, -q]$ differ by orientation. In the local frame used below, $A = X_{[1,0]}$ is a D7, $B = X_{[1,-1]}$ and $C = X_{[1,1]}$. Equal pairs of integers in the two doublets do not specify equal planar slopes. At $\tau = i$, matching string and five-brane segments are perpendicular in this source frame.



(a) D7 inside the E_1 face

(b) D7 past the NS5

Outward house-frame labels: blue D5 $(1,0)$; red NS5 $(0,1)$;
upper diagonals $(-1,1),(1,1)$; lower diagonals $(-1,-1),(1,-1)$.
After crossing, the lower-right external leg is NS5: outward $(0,-1)$ in the new chart.

Figure X.2.1: The source's one-D7 flavor construction in the fixed x^6 horizontal, x^5 vertical frame. Both panels use the same physical web before and after the allowed move. The lower-right external leg changes its charge label in the new cut chart. A black dot marks the D7 and a dashed line its downward cut. Crossing the right NS5 creates the D5 prong. The after-crossing F1 is specified by its allowed endpoints rather than a straight geodesic. The strokes are normalized schematics.

In the first panel of Figure X.2.1, fix the Coulomb face and let m_{q} denote the mass of the selected quark string between its D5 and D7 endpoints. In relative units this string mass is its tension times the shortest allowed length,

$$|m_{\mathrm{q}}| = T_{\mathrm{F1}}\ell_{\mathrm{F1}}. \tag{X.2.1}$$

A motion of the D7 along the appropriate prong changes where the string ends but does not change this shortest length. Moving it in the transverse direction changes this string mass at a fixed face. The D7 height relative to a fixed external reference specifies the bare flavor mass parameter; the chosen D5 height also enters the displayed string length and varies with the Coulomb face. D7 height is external; the face modulus is dynamical. This physical identification assumes brane creation, an allowed continuous motion, and a decoupling limit that leaves the five-dimensional low-energy theory unchanged.

The two carriers in this operation have matching entries in this particular frame but different charge meanings:

$$z_A^{\mathrm{string}} = (F1, D1) = (1,0), \qquad z_{\mathrm{prong}}^{\mathrm{fivebrane}} = (D5, NS5) = (1,0). \tag{X.2.2}$$

The first pair specifies the string allowed to end on the D7. The second labels the created horizontal five-brane segment. Equal entries do not turn a string monodromy into a five-brane slope rule.

The source figure makes the mass statement more precise than the phrase "moving a seven-brane does not matter." In the normalized constant-τ drawing, put the horizontal D5 supporting the quark at height y_D and the D7 at (x_7, y_7) in the face. The source's quark string is vertical before the crossing, so its relative length is

$$\ell_{\mathrm{F1}} = |y_7 - y_D|. \tag{X.2.3}$$

After the crossing, a horizontal displacement may lengthen the created D5 prong while leaving the quark mass fixed:

$$L_{\mathrm{D5}} = |x_7 - x_{\mathrm{NS5}}|, \qquad \Delta L_{\mathrm{D5}} = \Delta x \quad (x_7 > x_{\mathrm{NS5}},\ \Delta x > 0). \tag{X.2.4}$$

The growing segment belongs to the external brane presentation. It is not the F1 whose length measures this selected quark-string mass. An allowed horizontal displacement holds y_7 and the finite face fixed. Consequently this particular length is independent of x_7, whereas a vertical displacement changes it:

$$\left.\frac{\partial |m_{\mathrm{q}}|}{\partial x_7}\right|_{y_7, y_D} = 0. \tag{X.2.5}$$

The transverse displacement has a different effect:

$$|m_{\mathrm{q}}(y_7')| - |m_{\mathrm{q}}(y_7)| = T_{\mathrm{F1}}\big(|y_7' - y_D| - |y_7 - y_D|\big). \tag{X.2.6}$$

The source's before-and-after mass identification can therefore be written in the stated horizontal-motion regime as

$$|m_{\mathrm{q}}^{\mathrm{before}}| = T_{\mathrm{F1}}|y_7 - y_D| = |m_{\mathrm{q}}^{\mathrm{after}}|. \tag{X.2.7}$$

The absolute-value cusp only records that the shortest vertical segment switches orientation as the D7 passes the D5 height. It is not a claim that the full BPS mass at arbitrary axiodilaton equals a Euclidean distance. Once the D7 crosses the NS5, the source replaces the direct D5-to-D7 string by one reaching the newly created D5 prong. The endpoint displacement along that prong remains the same mass-preserving operation in the source's continuous construction.

There is a charge reason that a D7 can support precisely this prong. Its allowed string endpoint is the A charge $(F1, D1) = (1, 0)$, while the five-brane ending on it after the crossing is a D5 with $(D5, NS5) = (1, 0)$. The equality of these two integer pairs reflects the selected Type-IIB frame and endpoint compatibility, not identity of a string with a five-brane. If the five-brane pair is reversed in a different source convention, the physical D5 endpoint must still be identified from the brane directions and figure. In the source's discussion one sentence prints $(0, 1)$ for both D5 and NS5 endpoints; its own definitions and drawings give the D5 value used here.

Before the D7 crosses the NS5, a reader can detect the quark by a finite F1 path from the D7 to a D5 in the face. After the crossing, the same reader should follow the path through the created prong, not erase the prong and compare only the locations of black dots. This is the first example of a recurring principle: a brane move changes the presentation of a charged object while conserving its physical charge. The algebraic version will replace the drawn endpoint path by invariant prong integers.

The five-dimensional gauge group acts on the quark, while the D7 has an eight-dimensional worldvolume gauge theory before the decoupling limit. Calling its entire eight-dimensional gauge group the global symmetry of the five-dimensional fixed point would skip the endpoint and normalizability questions. The one-D7 construction is the source's E_2 flavor example. The pure E_1 web will remain our calculable charge example, and Chapter 3 will return to the fixed-point interpretation. We next need a rule that explains why a string can acquire a new charge label as it crosses the D7 cut.

X.2.2 Charge transport around one seven-brane

A branch cut is a choice of charge chart. Put every cut downward, order the seven-branes left to right, and take a string crossing a cut from left to right *below* its brane. This is the counterclockwise crossing path in the seven-brane plane. For a string column $v = (r, s)^{\mathsf{T}}$ and a brane column $z = (p, q)^{\mathsf{T}}$, define the integral antisymmetric form and its determinant convention by

$$S = \begin{pmatrix} 0 & -1 \\ 1 & 0 \end{pmatrix}, \qquad \det(v, z) = rq - sp = z^{\mathsf{T}} S v. \tag{X.2.8}$$

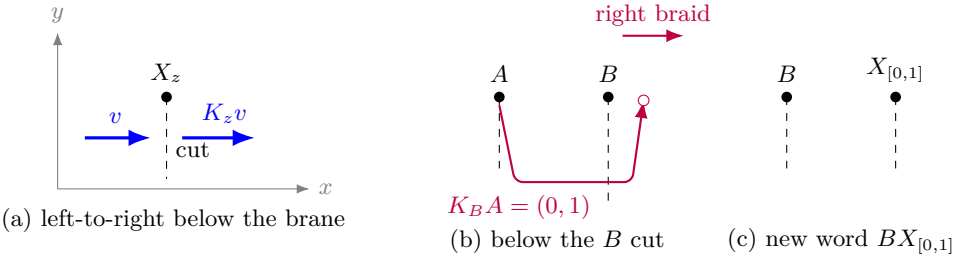
The counterclockwise crossing acts by

$$K_z = I + z z^{\mathsf{T}} S = \begin{pmatrix} 1 + pq & -p^2 \\ q^2 & 1 - pq \end{pmatrix}. \tag{X.2.9}$$

Multiplying this matrix by v gives the prong-creation rule directly,

$$K_z v = v + \det(v, z) z. \tag{X.2.10}$$

The added multiple of z can end on X_z. Crossing the same cut in the reverse direction uses $K_z^{-1} = I - z z^{\mathsf{T}} S$, because $(z z^{\mathsf{T}} S)^2 = 0$. The sign is determined by the path, not by requiring determinant one.



(a) left-to-right below the brane

(b) below the B cut

(c) new word $BX_{[0,1]}$

Figure X.2.2: Panel (a) fixes the oriented cut crossing used throughout. The horizontal coordinate is an auxiliary position in the seven-brane plane; the drawn arrow represents charge transport rather than a five-brane slope. Panels (b) and (c) show the right braid of the ordered word AB: A follows the marked contour below B and crosses its downward cut from left to right before taking the new right position. Both final cuts point downward. The later junction calculation transports prong coordinates as well as the brane labels.

Two elementary checks make the physical content of K_z clearer. The brane's own endpoint charge is unchanged, and a global Type-IIB duality rotation changes the matrix by conjugation:

$$K_z z = z, \qquad \det K_z = 1, \tag{X.2.11}$$

$$K_{gz} = g K_z g^{-1}, \qquad g \in SL(2, \mathbb{Z}). \tag{X.2.12}$$

The second identity follows from $g^{\mathsf{T}} S g = S$. Neither identity chooses which side of a downward cut is the starting chart. That choice was fixed by the crossing path before the matrix was written.

It is useful to derive these properties without relying on the three special branes. Set $N_z = z z^{\mathsf{T}} S$. Antisymmetry gives $z^{\mathsf{T}} S z = 0$, so the rank-one part is nilpotent:

$$N_z^2 = z(z^{\mathsf{T}} S z) z^{\mathsf{T}} S = 0. \tag{X.2.13}$$

Thus $K_z^{-1} = I - N_z$. The matrix determinant lemma also gives $\det(I + N_z) = 1 + z^{\mathsf{T}} S z = 1$. If we cross right to left, the created-prong contribution changes sign:

$$K_z^{-1} v = v - \det(v, z) z. \tag{X.2.14}$$

These calculations show why the same brane can support both a forward and a reversed description of a junction. They do not tell us which motion is counterclockwise; the orientation of the path in Figure X.2.2 supplies that information.

For the three branes used here in the source's ordered charge frame, the matrices are concrete:

$$K_A = \begin{pmatrix} 1 & -1 \\ 0 & 1 \end{pmatrix}, \quad K_B = \begin{pmatrix} 0 & -1 \\ 1 & 2 \end{pmatrix}, \quad K_C = \begin{pmatrix} 2 & -1 \\ 1 & 0 \end{pmatrix}. \tag{X.2.15}$$

The D7 cut itself gives a quick orientation check. A pure F1 string is fixed by K_A, since it can end on A. A D1 crossing below the same D7 picks up a negative F1 prong in the stated direction:

$$K_A \begin{pmatrix} 1 \\ 0 \end{pmatrix} = \begin{pmatrix} 1 \\ 0 \end{pmatrix}, \qquad K_A \begin{pmatrix} 0 \\ 1 \end{pmatrix} = \begin{pmatrix} -1 \\ 1 \end{pmatrix}, \qquad K_A^{-1} \begin{pmatrix} 0 \\ 1 \end{pmatrix} = \begin{pmatrix} 1 \\ 1 \end{pmatrix}. \tag{X.2.16}$$

The last two columns differ because they describe opposite crossing paths. Neither is a new seven-brane type. This small example also returns the transport rule to the D7 that supplied the quark at the start of the chapter. For example, a $(1, 0)$ string below B picks up a B prong and emerges with charge $(0, 1)$. Crossing C next gives $(-1, 0)$:

$$\begin{pmatrix} 1 \\ 0 \end{pmatrix} \xrightarrow{B} K_B \begin{pmatrix} 1 \\ 0 \end{pmatrix} = \begin{pmatrix} 0 \\ 1 \end{pmatrix} \xrightarrow{C} K_C K_B \begin{pmatrix} 1 \\ 0 \end{pmatrix} = \begin{pmatrix} -1 \\ 0 \end{pmatrix}. \tag{X.2.17}$$

The individual determinants expose the two creation steps. For $v_0 = (1, 0)$, $\det(v_0, B) = -1$, so the first crossing adds $-B$. For $v_1 = (0, 1)$, $\det(v_1, C) = -1$, so the second adds $-C$:

$$v_1 = v_0 - B = (0, 1), \qquad v_2 = v_1 - C = (-1, 0). \tag{X.2.18}$$

Each equality has a direct endpoint interpretation. The string segment changes its chart charge as a compensating prong reaches the brane whose cut it crossed. If the route is retraced, the inverse matrices remove these contributions in reverse order:

$$K_B^{-1} K_C^{-1} v_2 = v_0. \tag{X.2.19}$$

That path check is stronger than noting that every K has unit determinant. It also anticipates why the order of a four-brane word must be recorded explicitly. This

example is the first half of the four-cut loop in Section X.2.6. It also displays the central pitfall: a transported string charge is a column in a chosen cut chart. It need not retain its initial numerical pair across a cut. Moreover, the normalized straight strokes in our figures are not exact geodesics when the axiodilaton varies near the seven-branes. The charge rule survives as an integral transport statement; the dynamical BPS path requires the local metric and string tension.

X.2.3 Moving a cut changes the brane word

The D7 motion suggests a sharper question. In Figure X.2.2, can we pass one brane below another brane's downward cut and still describe the same transported charge? An ordered seven-brane word records the cuts encountered from left to right. For two adjacent columns z_1, z_2, let

$$d = \det(z_1, z_2). \tag{X.2.20}$$

The right braid changes the ordered pair to

$$X_{z_1} X_{z_2} = X_{z_2} X_{z_1 + dz_2}. \tag{X.2.21}$$

This is an equality of cut presentations under the specified move, with the source's physical brane-motion premise understood. It is not an instruction to keep both old brane labels fixed while swapping their positions.

The charge action itself explains the new label. As the first brane passes the second cut, its column is transported by K_{z_2}:

$$z_1' = K_{z_2} z_1 = z_1 + \det(z_1, z_2) z_2 = z_1 + dz_2. \tag{X.2.22}$$

Using the conjugation identity (X.2.12) with $g = K_{z_2}$ then gives an identity of total ordered actions,

$$K_{z_1'} K_{z_2} = (K_{z_2} K_{z_1} K_{z_2}^{-1}) K_{z_2} = K_{z_2} K_{z_1}. \tag{X.2.23}$$

The product identity is an algebraic consequence of the transported brane label. It does not know whether the motion preserves the decoupled theory, and it does not yet tell us how a junction ending on the moving brane should be represented. That second question requires T below.

The simplest example uses $A = (1, 0)$ and $B = (1, -1)$. Their determinant is -1, so the new right brane has charge $A - B = (0, 1)$:

$$d_{AB} = -1, \qquad AB = B X_{[0,1]}. \tag{X.2.24}$$

The ordered total matrix multiplies from the rightmost encountered factor acting last. Direct multiplication gives

$$K_B K_A = K_{[0,1]} K_B = \begin{pmatrix} 0 & -1 \\ 1 & 1 \end{pmatrix}. \tag{X.2.25}$$

This matrix test catches many orientation mistakes. It does not yet track a junction ending on the two branes. For that, introduce canonical integer prongs $Q = (Q_1, Q_2)^{\mathsf{T}}$

and assemble the brane columns into $Z_{\rm old} = (z_1\ z_2)$. The asymptotic string charge is $Z_{\rm old}Q$ in this presentation. With $Z_{\rm new} = (z_2\ z_1 + dz_2)$, solve for a prong-coordinate map:

$$Q_{\rm new} = TQ_{\rm old}, \qquad T = \begin{pmatrix} -d & 1 \\ 1 & 0 \end{pmatrix}. \tag{X.2.26}$$

The first new prong subtracts d times the old first one; the second new prong is the old first. Their total charge is unchanged because

$$Z_{\rm new}T = \begin{pmatrix} z_2 & z_1 + dz_2 \end{pmatrix} \begin{pmatrix} -d & 1 \\ 1 & 0 \end{pmatrix} = \begin{pmatrix} z_1 & z_2 \end{pmatrix} = Z_{\rm old}. \tag{X.2.27}$$

For AB, $T = \left(\begin{smallmatrix} 1 & 1 \\ 1 & 0 \end{smallmatrix}\right)$. The test charge $Q = (2, -3)$ therefore becomes $(-1, 2)$; both presentations have asymptotic charge $2A - 3B = (-1, 3)$.

The same braid must preserve junction intersection, including any spectator brane. The canonical prong e_i has one oriented endpoint on brane i and none on the others. Write $J = \sum_i Q_i e_i$. For ordered columns z_i, the symmetric source intersection pairing defines the full Gram matrix by

$$\begin{aligned} &G_{ii} = (e_i, e_i) = -1, \\ &G_{ij} = (e_i, e_j) = \tfrac{1}{2}\det(z_i, z_j) \quad (i < j), \qquad G_{ji} = G_{ij}, \qquad (J, J) = Q^{\mathsf{T}}GQ. \end{aligned} \tag{X.2.28}$$

The half-integral mixed entries combine to give integral squares for integral Q. Section X.2.5 will use this same pairing to extract roots. Extend T by the identity on all spectators. The source pairing obeys the stronger identity

$$T^{\mathsf{T}}G_{\rm new}T = G_{\rm old}. \tag{X.2.29}$$

For an AB pair followed by C, the old ordered Gram and the new one are

$$G_{ABC} = \begin{pmatrix} -1 & -\frac{1}{2} & \frac{1}{2} \\ -\frac{1}{2} & -1 & 1 \\ \frac{1}{2} & 1 & -1 \end{pmatrix}, \qquad G_{B,[0,1],C} = \begin{pmatrix} -1 & \frac{1}{2} & 1 \\ \frac{1}{2} & -1 & -\frac{1}{2} \\ 1 & -\frac{1}{2} & -1 \end{pmatrix}. \tag{X.2.30}$$

Here T acts on the first two entries and leaves the C entry unchanged. Both the asymptotic map and the entire Gram form agree under that same transformation. Reversing a brane label $z \mapsto -z$ also reverses its oriented prong $Q_i \mapsto -Q_i$; only their simultaneous change preserves ZQ. This is why equal total monodromy alone would be too weak to identify a charged state. The next section builds the pairing and makes its root content explicit.

The spectator provides a useful numerical test that cannot be reduced to the two-by-two monodromy equality. Extend $Q = (2, -3)$ to the ABC junction $Q_{\rm old} = (2, -3, 5)$. With the charge columns and Gram form just displayed, the two invariant quantities are

$$Z_{ABC}Q_{\rm old} = \begin{pmatrix} 4 \\ 8 \end{pmatrix}, \qquad Q_{\rm old}^{\mathsf{T}}G_{ABC}Q_{\rm old} = -52. \tag{X.2.31}$$

The right braid acts on the first two prongs, leaving the third unchanged. In the new word $BX_{[0,1]}C$ this gives

$$Q_{\rm new} = (-1, 2, 5), \qquad Z_{B,[0,1],C}Q_{\rm new} = \begin{pmatrix} 4 \\ 8 \end{pmatrix}, \quad Q_{\rm new}^{\mathsf{T}}G_{B,[0,1],C}Q_{\rm new} = -52. \tag{X.2.32}$$

The last equality probes the off-diagonal intersections with C. Had we transported only the pair's internal form, a mistaken sign in the pair-to-spectator intersections could have escaped. This explicit state shows what (X.2.29) means for a junction that actually reaches beyond the braided pair.

For completeness, a sign reversal of a single brane is a different coordinate operation. If D is diagonal with one entry -1 and all others $+1$, then the same physical endpoint data are represented by

$$Z' = ZD, \qquad Q' = DQ, \qquad G' = DGD, \qquad Z'Q' = ZQ. \tag{X.2.33}$$

It is easy to overlook the Q transformation because X_z and X_{-z} name the same brane. Yet the oriented canonical prong has changed. In a later root calculation, such an omission would change the apparent signs of cross-pairings even though the physical junction is the same.

X.2.4 From drawn strings to invariant prongs

The braid carried a vector Q of canonical prongs, but why does that vector retain physical information when a cut moves? A string network may cross a branch cut without ending on the brane. Dragging that network across the brane removes the crossing and creates an endpoint prong. Counting visible endpoints alone would therefore assign two different charges to the same continuous junction. The source's invariant charge adds a crossing contribution to the endpoint count. The oriented crossing in Figure X.2.2 fixes the sign.

For the ith brane $z_i = (p_i, q_i)$, let $n_{i,+}$ count outgoing canonical prongs and $n_{i,-}$ incoming ones. If oriented string segments of charge $v_k = (r_k, s_k)$ cross its cut in the positive direction, the invariant integer is

$$Q_i(J) = n_{i,+} - n_{i,-} + \sum_{k \in \text{cut crossings}} \det(v_k, z_i). \tag{X.2.34}$$

The orientation of a reverse crossing changes the sign of its term. This definition is local to the chosen downward-cut presentation; it is the step between a drawn string and a canonical lattice coordinate. A junction with no visible prong can still have nonzero Q_i if it crosses a cut.

Apply the rule to the B crossing already calculated. The incoming string has $v_0 = (1, 0)$ and its determinant with $B = (1, -1)$ is -1. Before the crossing is traded for an endpoint, the invariant B charge comes entirely from the cut:

$$Q_B^{\text{before}} = 0 + \det(v_0, B) = -1. \tag{X.2.35}$$

After the continuous deformation, the string no longer crosses that cut, but an oriented prong with coefficient -1 ends on B:

$$Q_B^{\text{after}} = -1 + 0 = -1. \tag{X.2.36}$$

The same junction has acquired a new visible branch, while its invariant charge has stayed fixed. Its outgoing string column changes from v_0 to $v_1 = v_0 - B = (0, 1)$,

precisely as the monodromy rule required. The negative sign records orientation of the canonical prong; it does not mean a negative number of physical strings.

There is also a useful conservation equation when a distinguished incoming tail is present. If that tail carries v_{in} and the crossings are converted into canonical prongs Q_i, the outgoing tail carries

$$v_{\mathrm{out}} = v_{\mathrm{in}} + \sum_i Q_i z_i. \tag{X.2.37}$$

For a B crossing followed by a C crossing, both coefficients are -1. Because $B + C = (2, 0)$, the outgoing charge is

$$v_{\mathrm{out}} = (1, 0) - B - C = (-1, 0). \tag{X.2.38}$$

This repeats the matrix calculation in a different language. The matrix transports the charge on the tail; the invariant integers record what has been deposited at branes along the way. Keeping these two descriptions together prevents a misleading statement that the charge of a fixed physical junction changed merely because its tail passed a cut.

For a junction described wholly by canonical prongs, without the separate incoming tail, the asymptotic charge is ZQ. A braid changes the canonical basis itself. The matrix T from (X.2.26) is exactly the coordinate transformation that keeps ZQ and the intersection form fixed in the new basis. If a single brane label is negated, the corresponding oriented basis element is negated as well. A visible drawing can therefore change in three ways: a crossing becomes a prong, adjacent cuts braid, or a brane orientation is reversed. Each has an explicit charge rule; none authorizes a free relabeling of only one side of an equation.

Two short kernel calculations distinguish prong conservation from zero asymptotic charge. With only one B and one C brane, the charge map is invertible over the rationals:

$$Z_{BC} = \begin{pmatrix} 1 & 1 \\ -1 & 1 \end{pmatrix}, \qquad \det Z_{BC} = 2, \qquad \ker_{\mathbb{Z}} Z_{BC} = 0. \tag{X.2.39}$$

Its image inside the integer charge plane has index two. Solving $Z_{BC}(u, v) = (p, q)$ gives

$$u = \frac{p - q}{2}, \qquad v = \frac{p + q}{2}, \qquad (p, q) \in Z_{BC}\mathbb{Z}^2 \iff p \equiv q \pmod 2. \tag{X.2.40}$$

This parity describes only the asymptotic charges generated by these two canonical brane columns. It is not a statement about the global line-operator lattice of a five-dimensional gauge theory. In particular, an open string with a separate incoming tail may have an outgoing charge outside this image even though the deposited prongs lie inside it. Our B-then-C crossing nevertheless had nonzero invariant prongs. It was an *open* network with an incoming and an outgoing tail, so $v_{\mathrm{out}} - v_{\mathrm{in}} = ZQ$ need not vanish. No root can be inferred from the crossing picture alone.

For three identical A branes, by contrast, zero asymptotic charge is possible. Since all columns are $(1, 0)$, the kernel equation is

$$Z_{AAA}Q = 0 \quad \iff \quad Q_1 + Q_2 + Q_3 = 0. \tag{X.2.41}$$

Every integer solution can be written using two adjacent differences,

$$Q = u(1,-1,0) + v(0,1,-1) = (u, -u+v, -v), \qquad u, v \in \mathbb{Z}. \tag{X.2.42}$$

This identifies the *candidate* zero-charge lattice before any intersection is computed. The next section supplies the pairing that decides which primitive vectors act as simple roots. It also shows why the three mutually local branes give finite A_2, whereas the four-brane $BCBC$ presentation has an affine null combination.

The point is physical as well as algebraic. The source's five-seven deformation of a particle can move its endpoint across several cuts. Invariant prongs let us carry the particle's junction information through the deformation before asking whether a BPS representative exists at the final positions. The next section supplies the intersection form on these prongs. That form will identify simple roots, while the source's brane motion and decoupling assumptions remain separate from the lattice arithmetic.

X.2.5 Junction intersections make simple roots

A network of strings may have several representatives because cut moves create or absorb prongs. Its *invariant prong charge* at brane i counts signed endpoints together with the signed contributions from crossings of that brane's cut. This is the source's conserved integer under the local Hanany–Witten move. Once an ordered cut chart is fixed, we collect these integers into $Q \in \mathbb{Z}^n$. The asymptotic string charge, if the network extends away from the branes, is

$$ZQ = \sum_{i=1}^{n} Q_i z_i = \begin{pmatrix} p \\ q \end{pmatrix}, \qquad Z = (z_1 \ \cdots \ z_n). \tag{X.2.43}$$

Changing the chart changes Q and Z together as in (X.2.27). Thus a displayed integer vector is meaningful only with its ordered brane word.

The source's canonical prong pairing is symmetric and bilinear. Its diagonal remembers the boundary of a single prong, while its ordered off-diagonal part remembers oriented crossings:

$$(e_i, e_i) = -1, \qquad (e_i, e_j) = \frac{1}{2}\det(z_i, z_j) \quad (i < j). \tag{X.2.44}$$

The symmetric entry for $i > j$ equals that for $j < i$. If G is this Gram matrix, the self-intersection of $J = \sum_i Q_i e_i$ is

$$(J, J) = Q^{\mathsf{T}} G Q = -\sum_i Q_i^2 + \sum_{i<j} Q_i Q_j \det(z_i, z_j). \tag{X.2.45}$$

The minus sign on the diagonal is essential. A shorthand sign printed in the source after the canonical-pairing equations conflicts with its explicit negative diagonal; we retain the explicit form (X.2.44). A root Cartan matrix is *minus* the intersection of its chosen simple roots.



(a) ordered AAA (b) ordered $BCBC$

Figure X.2.3: Symbolic canonical-basis connectors in two fixed ordered presentations. The arrows encode the full Q vectors printed in each panel; they are not literal string paths across cuts. In (a), the two AAA vectors give finite A_2 roots. In (b), like-brane differences give affine A_1 roots whose sum is null only inside the zero-asymptotic root span. Downward cuts sit below all connectors.

For three mutually local A branes all pairwise determinants vanish, so $G_{AAA} = -I_3$. Two open-string simple roots have no asymptotic charge:

$$\alpha_1 = (1, -1, 0), \qquad \alpha_2 = (0, 1, -1), \qquad Z\alpha_1 = Z\alpha_2 = 0. \tag{X.2.46}$$

They have self-intersection -2 and mutual intersection $+1$:

$$\big((\alpha_i, \alpha_j)\big) = \begin{pmatrix} -2 & 1 \\ 1 & -2 \end{pmatrix}. \tag{X.2.47}$$

Hence the Cartan matrix is

$$C_{A_2} = -\big((\alpha_i, \alpha_j)\big) = \begin{pmatrix} 2 & -1 \\ -1 & 2 \end{pmatrix}. \tag{X.2.48}$$

There is a useful distinction already in this elementary example. The root intersection identifies a Lie *algebra* associated with the coincident seven-brane stack. To call it a five-dimensional flavor algebra requires an attached web and a physical account of which junctions survive the decoupling limit. The root lattice also does not determine the global compact group or its line-operator lattice. Chapter 3 will use actual five-dimensional states to address flavor enhancement; the present section supplies the integral geometry those states can carry.

The three-A example is also the first member of a controlled source family. For n mutually local A branes, $G_{A^n} = -I_n$ and the adjacent roots $e_{A_i} - e_{A_{i+1}}$ have pairings -2 on the diagonal, $+1$ for neighbors, and zero otherwise. Hence

$$C_{ij} = 2\delta_{ij} - \delta_{i,j+1} - \delta_{i+1,j}, \qquad 1 \le i, j \le n-1. \tag{X.2.49}$$

This generalization is still a statement about the root system of a specified mutually local stack. It does not turn every A stack into five-dimensional flavor. Indeed, the three-A calculation tells us how to read a Cartan link only after the physical branes and their order have been named.

A nontrivial finite comparison in the same source is the ordered A^5BCC stack. Denote its five A prongs by a_i, its B prong by b, and its two C prongs by c_1, c_2. The

source gives four families of square--2, zero-asymptotic roots. One may count them without asserting a classification of arbitrary brane words:

$$\begin{aligned} &\pm(c_1 - c_2), \qquad \pm(a_i - a_j) \quad (i < j), \\ &\pm(a_i + a_j - b - c_k) \quad (i < j,\ k = 1, 2), \\ &\pm\left(\sum_{j \neq i} a_j - 2b - c_1 - c_2\right) \quad (i = 1, \ldots, 5). \end{aligned} \tag{X.2.50}$$

The family sizes are 2, $2\binom{5}{2} = 20$, $4\binom{5}{2} = 40$, and $2 \cdot 5 = 10$, totaling 72 roots. For a representative that uses all three brane types, the charge cancels because $2A - B - C = 0$:

$$Z(a_1 + a_2 - b - c_1) = 2A - B - C = (0, 0), \qquad (a_1 + a_2 - b - c_1)^2 = -2. \tag{X.2.51}$$

The second equality uses the ordered form (X.2.44); the A to B and A to C cross-pairings enter with opposite signs. Checking only the zero charge would miss that intersection condition.

The source's six simple junctions in its exact Cartan order are

$$\begin{aligned} &\alpha_1 = a_1 - a_2, && \alpha_2 = a_2 - a_3, && \alpha_3 = a_3 - a_4, \\ &\alpha_4 = a_4 + a_5 - b - c_1, && \alpha_5 = c_1 - c_2, && \alpha_6 = a_4 - a_5. \end{aligned} \tag{X.2.52}$$

In the A^5BCC order each has $Z\alpha_i = 0$. For the mixed root, the diagonal terms contribute -4, and the ordered cross terms contribute $+2$, so $(\alpha_4, \alpha_4) = -2$. The A–B and A–C cross terms cancel here, while the B–C pairing supplies the remaining $+2$. For the adjacent roots the mixed terms cancel and $(\alpha_3, \alpha_4) = (-a_4, a_4) = 1$. Let R have these six prong columns. The finite matrix is explicitly $-R^{\mathsf{T}}GR$:

$$C_{E_6} = -R^{\mathsf{T}}GR = \begin{pmatrix} 2 & -1 & 0 & 0 & 0 & 0 \\ -1 & 2 & -1 & 0 & 0 & 0 \\ 0 & -1 & 2 & -1 & 0 & -1 \\ 0 & 0 & -1 & 2 & -1 & 0 \\ 0 & 0 & 0 & -1 & 2 & 0 \\ 0 & 0 & -1 & 0 & 0 & 2 \end{pmatrix}, \qquad \det C_{E_6} = 3. \tag{X.2.53}$$

This fixture demonstrates how a less trivial exceptional root system can arise from canonical prongs. Its 72 roots and six simple vectors belong to the explicit A^5BCC source family; they are neither a rule for arbitrary seven-brane words nor evidence that every root appears as a stable five-dimensional particle. The next $BCBC$ example uses the same pairing for a different purpose. There the Cartan form becomes affine, and the physical five-brane loop selects a finite flavor reading.

X.2.6 The $BCBC$ loop and finite flavor

The pure E_1 web has a useful ordered seven-brane presentation $BCBC$. The same canonical-prong rule that produced finite A_2 now produces an affine Cartan matrix.

Why does this not give an infinite-dimensional five-dimensional flavor symmetry? The answer requires two steps. First we calculate exactly which direction is null and which string charge goes around the cuts. Then we apply the source's physical condition on a junction ending on the finite five-brane loop.

With branes ordered B_1, C_1, B_2, C_2, their charge map is

$$Z = \begin{pmatrix} 1 & 1 & 1 & 1 \\ -1 & 1 & -1 & 1 \end{pmatrix}. \tag{X.2.54}$$

The ordered determinants include $\det(B, C) = 2$ and $\det(C, B) = -2$. Substituting them into (X.2.44) gives the full form

$$G = \begin{pmatrix} -1 & 1 & 0 & 1 \\ 1 & -1 & -1 & 0 \\ 0 & -1 & -1 & 1 \\ 1 & 0 & 1 & -1 \end{pmatrix}, \qquad \det G = 1. \tag{X.2.55}$$

The determinant matters because it immediately forbids treating a null root as a radical vector of the entire canonical-prong lattice.

The simple roots joining like branes are

$$\alpha_0 = e_{B_1} - e_{B_2} = (1, 0, -1, 0), \qquad \alpha_1 = e_{C_1} - e_{C_2} = (0, 1, 0, -1). \tag{X.2.56}$$

Both have vanishing asymptotic charge. Their self-intersections are -2 and their mutual pairing is $+2$, so

$$-\big((\alpha_i, \alpha_j)\big) = \begin{pmatrix} 2 & -2 \\ -2 & 2 \end{pmatrix}. \tag{X.2.57}$$

This is the affine A_1 Cartan form. Its primitive null combination is

$$\delta = \alpha_0 + \alpha_1 = (1, 1, -1, -1), \qquad Z\delta = 0, \quad (\delta, \delta) = 0. \tag{X.2.58}$$

The word *null* here has a precise domain. Although δ is orthogonal to both roots in their zero-asymptotic span, it pairs with general prongs:

$$G\delta = (-1, 1, -1, 1)^{\mathsf{T}} \neq 0. \tag{X.2.59}$$

If J has asymptotic charge $(p, q) = ZQ$, then

$$(\delta, J) = (-1, 1, -1, 1)Q = q, \qquad k := -(\delta, J) = -q. \tag{X.2.60}$$

The source calls k the affine level. For strings terminating on the finite five-brane loop in its E_1 picture, the endpoint restricts to level zero. The affine grade may change when a junction is slid around that loop; it is not a separate conserved five-dimensional flavor charge. The finite A_1 algebra remains the flavor algebra of this source phase.

This restriction has an algebraic consequence that explains why a formal affine tower need not produce distinct local flavor charges. Adding an integral multiple of the null root leaves asymptotic charge unchanged, since $Z\delta = 0$. Its effect on self-intersection is

$$(J + n\delta, J + n\delta) = (J, J) + 2n(\delta, J) + n^2(\delta, \delta) = (J, J) + 2nq. \tag{X.2.61}$$

On the level-zero subspace $q = 0$, all members of this algebraic orbit have the same charge and square. In the source's loop picture, sliding a junction around the five-brane loop changes the affine grade. This is the physical step that relates those presentations; the quadratic identity alone cannot identify their states. Away from level zero, the $2nq$ term explicitly prevents the same conclusion. The full-lattice covector $G\delta$ in (X.2.59) was needed to see this difference.

One can see the geometric origin of the null direction in charge transport. Starting with $(1, 0)$ and crossing the ordered cuts B, C, B, C gives

$$\begin{pmatrix}1\\0\end{pmatrix} \xrightarrow{B} \begin{pmatrix}0\\1\end{pmatrix} \xrightarrow{C} \begin{pmatrix}-1\\0\end{pmatrix} \xrightarrow{B} \begin{pmatrix}0\\-1\end{pmatrix} \xrightarrow{C} \begin{pmatrix}1\\0\end{pmatrix}. \tag{X.2.62}$$

With the outgoing-prong rule, the four crossings contribute $(-1, -1, 1, 1) = -\delta$: this directed orbit realizes the negative of the chosen positive null root. Reversing its orientation reverses all four prong signs and gives δ. The four segments can close after transport. But the full word monodromy is not the identity:

$$K_C K_B K_C K_B = \begin{pmatrix}1 & 8\\0 & 1\end{pmatrix}, \qquad (K_C K_B K_C K_B)\begin{pmatrix}1\\0\end{pmatrix} = \begin{pmatrix}1\\0\end{pmatrix}. \tag{X.2.63}$$

It fixes the particular charge $(1, 0)$ while shearing other charges. For a general incoming string this statement reads

$$\begin{pmatrix}r\\s\end{pmatrix} \longmapsto \begin{pmatrix}r + 8s\\s\end{pmatrix}. \tag{X.2.64}$$

Thus the fixed primitive charge lies along the $(1, 0)$ direction. The $q = 0$ endpoint condition found from the intersection pairing selects that same direction. The agreement connects the monodromy calculation with the null-root calculation, yet the two calculations are not identical: one transports an external string, while the other pairs an integral junction with δ. Figure X.2.4 separates this algebraic orbit from the five-brane loop that the source associates with it. A cut orbit and a source's web identification have different logical jobs; even a perfectly closed charge polygon is not, by itself, a geodesic or a proof of a BPS state.

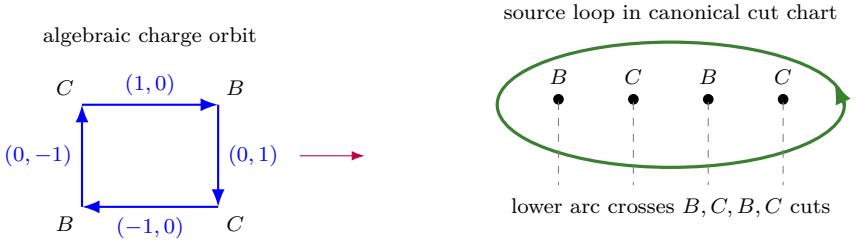


Figure X.2.4: Left, the $BCBC$ sequence of transported $(F1, D1)$ charges. Right, a canonical downward-cut deformation of the enclosed loop used in this section: the five-brane loop encloses all four seven-branes, and its lower arc crosses their cuts in $BCBC$ order. The source's physical loop requires brane creation and the allowed geodesic regime; the charge orbit alone does not establish a five-dimensional spectrum.

The finite-versus-affine distinction also prevents a common leap in the exceptional series. A larger ordered word can exhibit affine junction data without admitting an infinite-dimensional global symmetry in a decoupled five-dimensional QFT. The relevant flavor charges are selected by the attached web, endpoint conditions, and physical limit. Our calculation identifies the precise lattice direction that needs that selection.

X.2.7 The W-boson and instanton junctions

The loop calculation has so far produced root and asymptotic string charges. Can it distinguish particles in the five-dimensional gauge theory? In the source's pure E_1 phase, the W-boson and the instanton particle have the same positive electric charge but opposite weights under the finite $E_1 \simeq SU(2)$ flavor algebra. The source deforms their five-five strings into five-seven junctions. This is a specific physical identification, not a consequence of the Cartan matrix alone.

Start with the W in the actual web. In the source's three-panel drawing the initial fundamental string runs between the upper and lower D5 portions of the finite face. After the four external legs have ended on seven-branes and those branes have moved inside the face, the five-brane is a single loop. Hold the upper string endpoint on its D5 portion and slide the lower endpoint counterclockwise along the right side of that loop. Passing the lower-right B cut replaces the crossing by a B prong; the remaining string segment continues towards the upper-right C. Sliding that endpoint to the top creates the C prong. Both external legs of the resulting junction end on seven-branes, while its two outgoing $(1,0)$ tails end on the top D5 portion of the loop. Figure X.2.5 follows the three source panels rather than drawing a new geodesic.

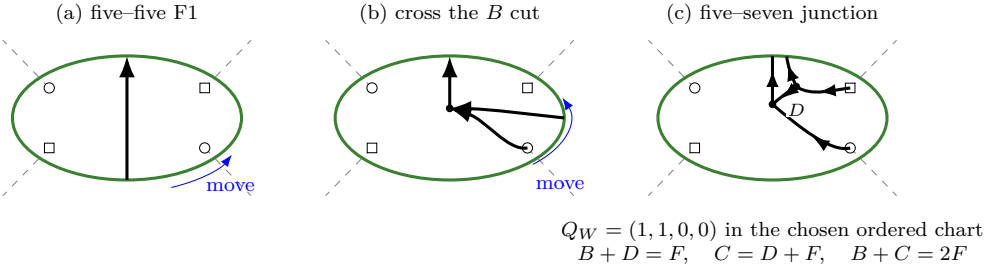


Figure X.2.5: The W endpoint deformation redrawn from the source's three-panel W sequence, after its seven-brane loop construction. Circles mark B and squares C seven-branes. Dashed rays are their cuts. Blue arrows indicate endpoint motion; black arrows show the oriented string-charge flow. The middle panel has its moving endpoint on the loop. The final panel is a connected two-vertex tree with B and C prongs, two top D5 tails and an internal $D = (0,1)$ segment. The diagram is topological: the physical metric does not justify straight geodesics in this drawing.

The final drawing tests charge conservation locally, before any ordered-chart assignment. Put $F = (1,0)$ and $D = (0,1)$; orient both seven-brane prongs out of their

branes and both F tails toward the top D5 loop. At the lower vertex the incoming $B = (1, -1)$ and internal D balance the outgoing F, since $B + D = F$. At the upper vertex the incoming $C = (1, 1)$ balances the internal D and the second outgoing F, since $C = D + F$. Adding these equations removes the internal edge and gives $B + C = 2F$. The global equation alone would also hold for two disconnected paths, although each such path would have a residual charge $B - F = -D$ or $C - F = D$. The internal edge resolves these opposite local mismatches. The blue motion arrow describes endpoint deformation and carries no string charge.

The charge chart needs one further step. The symbols in the source figure identify the two seven-brane types, but do not label the canonical left-to-right cut order or the orientation of every prong. The visible endpoint record is

source panel	visible seven-brane prongs	top-loop tail chart
(a)	0	not yet applicable
(b)	B	incomplete: one endpoint still moving
(c)	$B + C$	two $(1, 0)$ tails

(X.2.65)

The first two rows are physical intermediate drawings; they are not separate $BCBC$ vectors for a junction whose tails already all lie on the top loop. Only the final row is translated into that chart. Transport the final junction into the ordered $BCBC$ presentation used above and choose the oriented representative with one B_1 and one C_1 prong. The original drawing does not specify the braid and grade needed to identify its spatial right-hand pair with those ordered labels. That identification remains a source-specific choice fixed by its W charge assignment, rather than a deduction from unlabeled symbol positions. The resulting charge balance is

$$Q_W = (1, 1, 0, 0), \qquad ZQ_W = B + C = (1, -1) + (1, 1) = (2, 0). \tag{X.2.66}$$

Thus the $p = 2$ tail count follows from the two created canonical prongs. Adding the null loop to Q_W changes the grade while leaving the five-dimensional charges fixed; the displayed vector chooses one grade. The source's string deformation and particle-charge calculation, rather than the unlabeled geometry alone, identify this as the W and assign its finite-flavor label $a = 1$. Its lower row similarly starts from a D1 string between the two NS5 portions and moves its endpoints to the top loop. The source assigns that particle $p = 2, a = -1$; below we use the corresponding integral $BCBC$ representative. An endpoint slide preserves the particle identification as a physical premise; the cut and intersection calculation checks the resulting charge coordinates, not the existence of a geodesic BPS representative.

Restrict to its $q = 0$, $p \geq 0$ charge chart. Write the four invariant prongs as $Q = (b, c, h, j)$ in $BCBC$ order. The source's particle-charge formula groups the same labels as $(Q_{B_1}, Q_{B_2}, Q_{C_1}, Q_{C_2})$; our ordered word uses $(b, c, h, j) = (Q_{B_1}, Q_{C_1}, Q_{B_2}, Q_{C_2})$. This is a coordinate reorder of the *labeled* prongs, distinct from the unmarked spatial-to-canonical identification in the figure. The lower component of $ZQ = (p, 0)^{\mathsf{T}}$ sets the last prong in terms of the others:

$$-b + c - h + j = 0, \qquad j = b + h - c. \tag{X.2.67}$$

The upper component then gives $p = 2(b+h)$. The finite E_1 root is the C-to-C junction $\alpha_C = (0, 1, 0, -1)$ from Section X.2.6. Its action measures the Dynkin label by minus intersection. Equivalently, the source's grouped-label formula is $a = Q_{C_1} - Q_{C_2} + 2Q_{B_2} = c - j + 2h$; after the $q = 0$ condition both give $a = -b + 2c + h$. This is a flavor weight because the source identifies the root action on the attached web as the five-dimensional finite E_1 symmetry. Its instanton number is a different input: the source's pure-gauge particle assignment identifies $I = (p/2 - a)/2$. Thus

$$p = 2(b + h), \qquad a = -b + 2c + h, \qquad I = b - c. \tag{X.2.68}$$

The electric relation $n_e = p/2$ comes from the source's top D5 endpoint counting, once every tail has reached that segment; it is not determined by the root pairing. It is useful to keep both the source electric unit and the fundamental-weight unit visible:

$$n_e = \frac{p}{2} = b + h, \qquad q_{\mathrm{wt}} = 2n_e = p. \tag{X.2.69}$$

Thus the W has $n_e = 1$, whereas a compact $SU(2)$ fundamental has $n_e = 1/2$; the latter has unit charge only in the explicitly rescaled q_{wt} unit. The two numbers should not be interchanged in a state table.

Eliminating b, c, h from a makes the flavor-instanton relation transparent. Since $N = b + h = p/2$ and $I = b - c$,

$$a = N - 2I = \frac{p}{2} - 2I, \qquad I = \frac{p/2 - a}{2}. \tag{X.2.70}$$

At fixed electric charge $p = 2$, changing the finite $SU(2)$ Dynkin label from $+1$ to -1 changes I from zero to one. That is why the source's W and instanton can form a flavor doublet while retaining distinct five-dimensional particle interpretations. A single seven-brane root matrix would not identify which of them is the Yang–Mills instanton; the identification uses the web and its gauge phase.

Integral prongs impose a parity condition on the allowed (p, a). Let $N = p/2 = b + h$. From $a = N + 2(c - b)$ we obtain

$$p \in 2\mathbb{Z}, \qquad a \equiv \frac{p}{2} \pmod 2. \tag{X.2.71}$$

Conversely, if $p = 2N$ and $a \equiv N \pmod 2$, choosing

$$(b, c, h, j) = \left(0, \frac{a - N}{2}, N, N - \frac{a - N}{2}\right) \tag{X.2.72}$$

gives an integral $q = 0$ junction with those charges. The congruence is therefore an exact characterization of the integral chart, not merely a necessary test obtained by reducing one example modulo two.

Substitute $j = b + h - c$ into the full Gram form (X.2.55). After collecting terms one obtains a compact identity for the self-intersection:

$$(J, J) = Q^{\mathsf{T}} G Q = -\frac{a^2}{2} + \frac{p^2}{8}. \tag{X.2.73}$$

The identity depends on the stated $BCBC$ chart and $q = 0$ restriction. It is a polynomial reduction of the string junction intersection, not an independent mass formula. In particular, the value can be nonzero even when each constituent junction has zero square.

For the first two integral prongs the direct full-Gram calculation is short enough to display. Their separate self-intersections vanish, but their mutual intersection is one:

$$Q_W = (1,1,0,0), \quad Q_I = (1,0,0,1), \qquad Q_W^{\mathsf{T}} G Q_W = Q_I^{\mathsf{T}} G Q_I = 0, \quad Q_W^{\mathsf{T}} G Q_I = 1. \tag{X.2.74}$$

Consequently the sum has square two rather than zero,

$$(Q_W + Q_I)^{\mathsf{T}} G (Q_W + Q_I) = 2. \tag{X.2.75}$$

This is a useful warning against adding self-intersections as if they were linear charges. The cross term records how the two junctions intersect in the ordered $BCBC$ presentation.

Here are four charge assignments that make the distinction concrete. The source's W and instanton states admit the first two prong vectors. The other two rows test the intersection rule rather than asserting new single-particle states.

junction	$Q = (b, c, h, j)$	(p, a)	n_e	I	(J, J)	bound	result
W	$(1,1,0,0)$	$(2,1)$	1	0	0	0	source state
instanton	$(1,0,0,1)$	$(2,-1)$	1	1	0	0	source state
$W + I$	$(2,1,0,1)$	$(4,0)$	2	1	2	2	passes
$2W$	$(2,2,0,0)$	$(4,2)$	2	0	0	2	excluded

Table X.2.1: All entries use the source's pure E_1, $q = 0$ chart. The bound is the right side of the necessary intersection inequality for the displayed p. Passing that inequality does not assert BPS existence. The first two rows are identified particles in the source; the last two are junction arithmetic tests.

The necessary condition used in the final column is

$$(J, J) \geq -2 + \gcd(p, q). \tag{X.2.76}$$

For $p = 2, q = 0$, the lower bound is zero and both source particles saturate it. Their sum has $(J, J) = 2$ at $p = 4$, again saturating its bound. Twice the W has $(J, J) = 0$ at the same $p = 4$, below the bound two, so this candidate cannot be a single BPS junction of the stated type. The converse would be wrong: satisfying an intersection inequality cannot establish that a stable BPS representative exists in the varying seven-brane metric. This difference between an exact lattice filter and a physical spectrum will matter again for the fixed-point states in Chapter 3.

Figure X.2.5 supplies the physical route behind the first charge row. The corresponding lower-row D1 deformation supplies the distinct D1 starting object for the instanton row. The deformations preserve the particle charges in the stated construction, while the detailed geodesic representative can change. Electric charge n_e, instanton number

I, finite-flavor weight a, and the original eight-dimensional seven-brane gauge charge are different roles for charge. None is the three-dimensional GNO flux introduced for magnetic quivers in Chapter 5.

X.2.8 Finite exceptional labels and five-dimensional phases

The $BCBC$ computation is an affine presentation of a particular pure-$SU(2)$ source phase. To understand the familiar E_n labels, one must separate that presentation from the finite seven-brane configuration and from the five-dimensional ultraviolet limit. The source records three distinct finite words near the small-rank end:

$$E_1 = BCC, \qquad \widetilde{E}_1 = AX_{[2,-1]}C, \qquad E_0 = X_{[2,-1]}C. \tag{X.2.77}$$

Their surrounding-loop presentations are different larger words, respectively

$$BCBC, \qquad AX_{[2,-1]}X_{[-1,2]}C, \qquad X_{[2,-1]}X_{[-1,2]}C. \tag{X.2.78}$$

The extra brane in a loop presentation cannot be erased when comparing monodromies, and it must not be silently included when computing a finite root system. In the source's finite zero-asymptotic sectors, the primitive root forms are $[-2]$ for E_1, $[-8]$ for $\widetilde{E}_1$, and rank zero for E_0. A one-dimensional kernel therefore need not contain a vector of square -2.

The finite-word distinction can be checked without any claim about theta angle. For $E_1 = BCC$, the zero-asymptotic condition on (u, v, w) reads $u + v + w = 0$ and $-u + v + w = 0$, hence $u = 0$ and $w = -v$. The primitive finite root is $c_1 - c_2$ and its square is

$$\ker Z_{BCC} = \mathbb{Z}(0, 1, -1), \qquad (0, 1, -1)^{\mathsf{T}} G_{BCC} (0, 1, -1) = -2. \tag{X.2.79}$$

The two coincident C branes therefore provide a finite A_1 root. This is the finite root left after the extra loop brane in $BCBC$ has been separated conceptually from the finite word. A physical statement that the C pair collapses in a limit must still specify the web motion; it does not mean all branes in the finite word become one stack.

For $\widetilde{E}_1 = AX_{[2,-1]}C$, the charge matrix has one primitive integer kernel vector, but its intersection differs:

$$Z_{AX_{[2,-1]}C} = \begin{pmatrix} 1 & 2 & 1 \\ 0 & -1 & 1 \end{pmatrix}, \qquad \ker_{\mathbb{Z}} Z = \mathbb{Z}(-3, 1, 1), \quad (-3, 1, 1)^{\mathsf{T}} G (-3, 1, 1) = -8. \tag{X.2.80}$$

Every nonzero vector in this rank-one kernel has square $-8m^2$ for an integer m; there is no square--2 root in that finite sector. Finally, the two columns of the E_0 word are linearly independent:

$$Z_{X_{[2,-1]}C} = \begin{pmatrix} 2 & 1 \\ -1 & 1 \end{pmatrix}, \qquad \det Z = 3, \quad \ker_{\mathbb{Z}} Z = 0. \tag{X.2.81}$$

These three calculations explain the finite algebraic contrast. They do not infer which pure-$SU(2)$ theta sector a web realizes. That choice is a physical input tied to the source's phase analysis, and E_0 is not simply the same gauge phase with one fewer visible root.

The comparison can be organized by asking which object each word describes. The finite word controls a zero-asymptotic root calculation for the cluster associated with the source's collapsed configuration. The larger word includes a surrounding-loop brane needed for the charge orbit of the web. The phase label is a statement about the five-dimensional theory reached in a particular limit. These are three connected but separate inputs. The following table keeps the correspondence explicit.

phase	finite word	surrounding-loop word	finite root square
E_1	BCC	$BCBC$	-2
$\widetilde{E}_1$	$AX_{[2,-1]}C$	$AX_{[2,-1]}X_{[-1,2]}C$	-8
E_0	$X_{[2,-1]}C$	$X_{[2,-1]}X_{[-1,2]}C$	no root

Table X.2.2: Source-native finite and surrounding-loop words. The last column is the primitive zero-asymptotic junction square in the finite word, not a list of five-dimensional particles or a theta calculation.

For E_1, the finite C-pair root of (X.2.79) and the affine null direction of (X.2.58) are compatible precisely because they live in different presentations. Adding the extra B needed to surround the web creates the $BCBC$ affine calculation. It does not enlarge the local flavor algebra to affine A_1. Conversely, deleting that extra brane from an affine word while keeping its monodromy would invalidate the very ordered product that produced the loop orbit. The distinction is a useful test whenever an exceptional-looking seven-brane word is used to name a five-dimensional phase.

The associated five-dimensional readings are also distinct. The E_1 configuration is the theta-zero pure $SU(2)$ phase with finite $su(2)$ flavor algebra. The $\widetilde{E}_1$ configuration is the theta-pi pure $SU(2)$ phase, read in the source as having an abelian flavor algebra. E_0 is an endpoint without a weakly coupled $SU(2)$ gauge phase. These phase and theta assignments come from the source's physical analysis. Neither the cubic prepotential nor the matrix product in this chapter derives the discrete theta angle. Likewise, the finite root form identifies algebraic information but does not settle the global form of the flavor group. For example, the $[-2]$ root in the finite E_1 word determines the $su(2)$ root length and its Weyl reflection. It does not say which weight representations occur as genuine local operators, nor which line charges are permitted in the decoupled theory. Those questions require the spectrum and boundary conditions of the attached web. The separate particle example above supplies two source states in a chosen gauge phase, but even that pair is not a determination of the full global-form data.

For the broader rank-one family, Seiberg's strong-coupling argument uses $SU(2)$ with $N_f \leq 7$ fundamental flavors and the label

$$E_{N_f+1}, \qquad 0 \leq N_f \leq 7. \tag{X.2.82}$$

The notation is tied to that family and its decoupling path. It does not license $N_f = 8$ by formal continuation, nor does an affine seven-brane word construct an E_9 five-dimensional fixed point. The global form, line spectrum, and parameter-space identifications need separate input. Chapter 3 will investigate the five-dimensional fixed points and their finite enhancement. Here the charge and junction calculations have made precise which parts of that story can be read directly from an ordered seven-brane presentation.

X.2.9 Exercises

The following four calculations use the downward-cut and ordered-prong conventions of this chapter. Show the matrix or lattice steps, even when the final charge is short. The last task asks for a physical explanation of the one-D7 construction.

1. For $A = (1, 0)$, $B = (1, -1)$ and $C = (1, 1)$, calculate K_A, K_B and K_C, then give the charge of the right brane after the AB braid. Explain why determinant one alone cannot select the sign of the cut action.

2. Starting with a $(1, 0)$ string, cross the cuts of $BCBC$ from left to right below their branes. Give all five successive charge columns, including the initial one. Multiply the four monodromy matrices in their acting order. Explain which charge closes and why the product matrix need not equal the identity.

3. For AAA, calculate the minus-intersection (Cartan) matrix of $(1, -1, 0)$ and $(0, 1, -1)$. For $BCBC$, do the same for $(1, 0, -1, 0)$ and $(0, 1, 0, -1)$, then give a primitive null vector in their span. Explain why this calculation alone cannot identify a five-dimensional flavor group.

4. In the E_1 chart $q = 0, p \geq 0$, calculate n_e, I and (J, J) for the source W state $(p, a) = (2, 1)$ and instanton state $(2, -1)$. Do the same intersection calculation for $(p, a) = (4, 2)$ and decide whether this double-W candidate passes the necessary BPS inequality. Explain the logical status of a passing result.

5. Describe the one-D7 version of the E_1 web and the D5 prong created when the D7 crosses the NS5. Identify the five-dimensional quark object, the direction that changes its bare mass, and the physical premise needed to read the continued drawing as the same decoupled theory. Distinguish five-dimensional gauge charge, finite flavor charge and the D7 worldvolume gauge charge.

X.2.10 Take-home message

Take-home message

An ordered seven-brane cut chart turns a physical prong-creation move into an exact charge-transport rule, $K_z v = v + \det(v, z)z$. A right braid changes the brane word and the canonical prongs together, preserving asymptotic charge and intersection. Three A branes give finite A_2 roots. In the pure-E_1 $BCBC$ presentation, two roots give affine A_1, but its null vector is null only in the zero-asymptotic root span. The attached five-brane loop and level-zero condition select the finite five-dimensional flavor reading. In the source's $q = 0$ chart, integral junctions obey p even and $a \equiv p/2 \pmod 2$; the W and instanton have equal electric charge and different instanton number. Their intersection arithmetic supplies a necessary BPS filter, while the spectrum and theta phase require physical input.

Status and sources

The one-D7 E_2 flavor construction and created D5 prong in Section X.2.1 follow DeWolfe, Hanany, et al. (1999, PDF pp. 5–7, Figs. 1–3). Its physical identification of continued webs uses brane motion and five-dimensional decoupling premises [DEC]. The comparison pure web and five-brane charge orientation follow Aharony et al. (1998, PDF pp. 8–13, Figs. 1–3). The source's printed D5 endpoint charge on PDF p. 6 conflicts with its definitions and figures; the D5 has five-brane charge $(1, 0)$ in the present $(D5, NS5)$ convention. Seven-brane labels instead refer to the $(F1, D1)$ string doublet. The ordered web and junction calculations use the physical axes and charge doublets defined above.

Sections X.2.2 and X.2.3 use the downward-cut, left-to-right counterclockwise path of DeWolfe and Zwiebach (1999, PDF pp. 8–9, eqs. (2.1)–(2.3) and Fig. 1) and the ordered product and right braid of DeWolfe, Hanany, et al. (1999, PDF pp. 24–25, eqs. (7.40)–(7.46)). The latter source prints an ill-typed outer product in (7.43); its explicit matrices (7.40) and (7.44) fix the column expression $zz^{\mathsf{T}}S$. The matrix, charge and full-prong-pairing identities displayed here are exact for the declared ordered chart [MATH]. Their physical use in brane motion remains [DEC]; equal monodromy is not a general full-QFT equivalence test.

The invariant-prong definition, canonical pairing, three-A roots and their finite Cartan form in Section X.2.5 follow DeWolfe and Zwiebach (1999, PDF pp. 8, 15, 19, eqs. (2.1), (3.5)–(3.6), (3.23) and Fig. 5). Its equation (3.8) has a sign inconsistent with the explicit negative diagonal in (3.9)–(3.10); the latter and the canonical pairings fix G, while the Cartan form is minus the root intersection. The bounded A^5BCC family, its 72 roots and six finite E_6 simple junctions are from DeWolfe and Zwiebach (1999, PDF pp. 22–23, eqs. (3.37)–(3.40) and Fig. 7); the displayed count and determinant are checks of that source family [MATH], not a classification of arbitrary seven-brane words. The $BCBC$ roots, null loop, level, charge orbit and source's finite-loop interpretation in Section X.2.6 use DeWolfe, Hanany, et al. (1999, PDF pp. 7, 11–13 and 25, Fig. 3(b) and eqs. (4.11)–(4.14), (7.47)). The loop drawing is recast in the canonical downward-cut chart. The matrices, determinant, null-span statement and level reduction are exact junction-lattice arithmetic [MATH]; the five-brane-loop and finite-flavor selection include

physical endpoint premises [DEC]. No infinite-dimensional five-dimensional flavor group is inferred.

Section X.2.7 uses the source's W and instanton junctions and E_1 charge chart in DeWolfe, Hanany, et al. (1999, PDF pp. 8, 13–14, Fig. 4 and eqs. (4.14), (5.15)–(5.18)). Its Fig. 4 upper row supplies the W endpoint sequence; its lower row supplies the separate D1 instanton sequence. The printed inverse electric relation on PDF p. 19 is inconsistent with those equations; here $n_e = p/2$, and a fundamental has $n_e = 1/2$ in these units. The integer lift, parity, J^2 values and necessary-bound comparison are exact [MATH] within the stated chart. The physical W and instanton assignments are source-specific [DEC]; a passing intersection inequality is not a BPS existence theorem.

The finite E_1, $\widetilde{E}_1$ and E_0 words, distinct loop words and phase scope in Section X.2.8 follow DeWolfe, Hanany, et al. (1999, PDF pp. 19–20, 24–26, appendix table). The E_{N_f+1} strong-coupling family with $N_f \leq 7$ follows Seiberg (1996, PDF pp. 10–11, Section 4). The phase and discrete-theta readings are sourced physical claims [DEC], not derived from the monodromy or a cubic prepotential. The ordered junction lattice does not select a compact global form, a five-dimensional line spectrum, or the three-dimensional GNO lattice of Chapter 5. The calculation concerns the junction lattice, with full-QFT equivalence outside its scope.

References

Aharony, O., A. Hanany, and B. Kol (1998). "Webs of (p,q) five-branes, five-dimensional field theories and grid diagrams". In: *JHEP* 01, p. 002. DOI: 10.1088/1126-6708/1998/01/002. arXiv: hep-th/9710116.

DeWolfe, O., A. Hanany, et al. (1999). "Five-branes, seven-branes and five-dimensional E(n) field theories". In: *JHEP* 03, p. 006. DOI: 10.1088/1126-6708/1999/03/006. arXiv: hep-th/9902179.

DeWolfe, O. and B. Zwiebach (1999). "String junctions for arbitrary Lie algebra representations". In: *Nucl. Phys. B* 541, pp. 509–565. DOI: 10.1016/S0550-3213(98)00743-3. arXiv: hep-th/9804210.

Seiberg, N. (1996). "Five-dimensional SUSY field theories, nontrivial fixed points and string dynamics". In: *Phys. Lett. B* 388, pp. 753–760. DOI: 10.1016/S0370-2693(96)01215-4. arXiv: hep-th/9608111.

Chapter X.3

Five-dimensional fixed points and exceptional symmetry

X.3.1 What shrinks when a five-dimensional face collapses?

A finite face in a five-brane web has a size that can vary without moving the distant legs. In the pure $SU(2)$ example of Chapter 1 this motion gives a real Coulomb coordinate, while the separation of the external supporting lines fixes a coupling. The physical question is what remains when both scales approach zero. The local answer is concrete: a W particle, an instanton particle and a magnetic string become light. Calling their common endpoint an interacting five-dimensional theory additionally uses the brane decoupling and BPS-state construction.

We retain the charge convention $(p, q) = (D5, NS5)$, with rays directed away from junctions. For the finite rectangular face, let ϕ be the mass of the fundamental-string W particle and let m_A denote the source-normalized bare web parameter. Its horizontal and vertical dimensions and its D3 string tension are

$$L = m_A + \phi, \qquad h = \phi, \qquad T_m^A = Lh = \phi(m_A + \phi). \tag{X.3.1}$$

These are the same objects as in Chapter 1. At fixed $m_A > 0$, taking $\phi \to 0$ leaves a segment of length m_A. At $m_A = 0$ and $\phi > 0$, it leaves a finite square. The point contraction needs both coordinates to vanish.

The distinction between a modulus and a coupling can be checked without using the area. In the normalized x^6-x^5 drawing, the northeast corner is $(L/2, \phi/2)$ and the outgoing $(1, 1)$ ray lies on $x^5 - x^6 = c_{\mathrm{NE}}$. Its supporting-line constant is

$$c_{\mathrm{NE}} = \frac{\phi - L}{2} = -\frac{m_A}{2}. \tag{X.3.2}$$

Varying ϕ at fixed m_A slides that corner along the same asymptotic line. Varying m_A moves the line itself. This is why one can let a finite face shrink dynamically while

treating the external separation as a deformation of the theory. The same reasoning applies at the other three corners with corresponding signs. It also explains why a picture of a small face is ambiguous unless the distant legs are shown or their support constants stated.

The area formula can be integrated in the web's source coordinate. With $\mathcal{F}_A(0) = \mathcal{F}'_A(0) = 0$, the primitive magnetic-string convention of that comparison gives

$$\mathcal{F}'_A = T^A_m, \qquad \mathcal{F}_A(\phi) = \frac{1}{2} m_A \phi^2 + \frac{1}{3}\phi^3. \tag{X.3.3}$$

The moving-edge metric agrees with the second derivative,

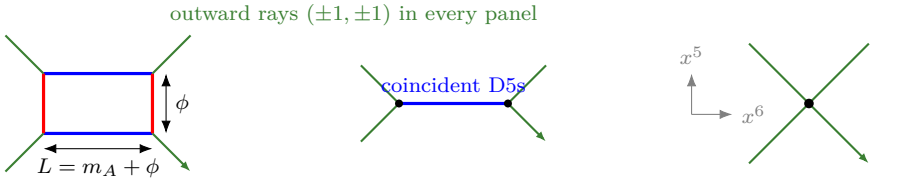
$$g_A^{-2}(\phi) = \mathcal{F}''_A(\phi) = m_A + 2\phi. \tag{X.3.4}$$

For example, at $(m_A, \phi) = (2, 1)$ the face has width 3, height 1, string tension 3 and metric 4. A zero string tension at $\phi = 0$ with $m_A = 2$ does not mean that the whole face has collapsed.

The two particle probes make the distinction even more direct. In the same normalized web the vertical F1 sees $m_W = \phi$, while the horizontal D1 sees $m_{\text{inst}} = m_A + \phi$. Their difference is the external separation,

$$m_{\text{inst}} - m_W = m_A. \tag{X.3.5}$$

At fixed positive m_A, only the W particle can become massless as the Coulomb height reaches zero. At $m_A = 0$ and positive ϕ, neither particle is massless and the face has nonzero area. This probe calculation gives the reader a way to distinguish the two limits without trusting the visual size of a drawing. It also shows why a bare inverse coupling acts as a deformation rather than another Coulomb coordinate in this rank-one example.



(a) finite face (b) $\phi = 0$, $m_A > 0$ (c) $\phi = m_A = 0$

Figure X.3.1: The same four outward diagonal charges surround the pure $SU(2)$ face. The blue horizontal edges are D5s and the red vertical edges are NS5s in the x^6-x^5 plane. The first limit contracts only the Coulomb height; the second also removes the external separation. The local area and the source assignment of the E_1 endpoint have different logical roles.

For comparison with the compact gauge calculation, write $\Phi = \operatorname{diag}(a, -a)$, $a \geq 0$. The same W mass sets $\phi = 2a$. In the separately normalized primitive-coroot comparison for the pure web, $m_A = m_0^{\text{IMS}}$ and

$$\mathcal{F}_A(2a) = 2\mathcal{F}^{(0)}_{\text{IMS}}(a), \qquad \mathcal{F}''_A(2a) = \tfrac{1}{2}(\mathcal{F}^{(0)}_{\text{IMS}})''(a). \tag{X.3.6}$$

The factor two depends on the electric coordinate and magnetic-charge comparison. It is a relative statement in the chosen pure gauge phase; it does not determine an absolute five-brane action or a line-operator spectrum. The next section computes the gauge-side cubic directly. This distinction matters when flavor masses later split the Weyl ray into chambers.

In particular, the face's two visually simple limits are not interchangeable. At $m_A = 0$ and $\phi > 0$, the instanton and W masses are both ϕ, but the magnetic string still has tension ϕ^2. At $m_A > 0$ and $\phi = 0$, the string tension vanishes while the instanton particle retains mass m_A. Only the simultaneous point limit drives all three source-normalized quantities to zero. The endpoint interpretation requires the modes associated with the external legs and the ambient string theory to decouple in the intended energy limit. Geometry fixes the local configuration but does not perform that decoupling argument by itself.

X.3.2 The cubic prepotential and the flavor boundary

What can the compact gauge phase itself calculate? Five-dimensional $\mathcal{N} = 1$ supersymmetry makes its effective Abelian prepotential piecewise cubic. The root-minus-weight expression contains the particle thresholds; differentiating twice gives the metric on the real Coulomb ray. Choose the primitive cocharacter $H = \mathrm{diag}(1, -1)$, $\Phi = aH$, $\mathrm{Tr}\, H^2 = 2$, and N_f full fundamental hypermultiplets of masses m_f. In the IMS convention the source formula specializes to

$$\mathcal{F}(a) = \frac{1}{2} m_0 \,\mathrm{Tr}\,\Phi^2 + \frac{1}{12}\left[\sum_{\alpha\in\Delta} |\alpha(\Phi)|^3 - \sum_{f=1}^{N_f}\sum_{w\in\mathbf{2}} |w(\Phi) + m_f|^3\right]. \tag{X.3.7}$$

Here $m_0 = m_0^{\mathrm{IMS}}$ is the bare inverse-coupling coordinate in this formula. A classical cubic invariant is absent for $SU(2)$. Roots are $\alpha = \pm 2a$, while each full fundamental has the two weights $w = \pm a$. Explicitly counting both signs gives

$$\sum_{\alpha\in\Delta} |\alpha(\Phi)|^3 = |2a|^3 + |-2a|^3 = 16a^3, \tag{X.3.8}$$

$$\sum_{f=1}^{N_f}\sum_{w\in\mathbf{2}} |w(\Phi)|^3 = N_f\big(|a|^3 + |-a|^3\big) = 2N_f a^3. \tag{X.3.9}$$

The full weight pair is essential. Counting only one weight would shift the cubic coefficient and move the apparent flavor boundary.

The coefficient is also insensitive to how one names the two weights. The Weyl reflection $a \mapsto -a$ exchanges them and exchanges the two roots. Restricting to $a \geq 0$ avoids double counting the physical Coulomb ray, but it does not authorize dropping one member of either root or weight sum. A full five-dimensional hypermultiplet in the doublet supplies both signed electric masses in this effective formula. This is precisely why the root contribution is $16a^3$, not $8a^3$, and each flavor subtracts $2a^3$, not a^3.

At zero masses the resulting polynomial and its first two derivatives are

$$\mathcal{F}_{N_f}(a) = m_0 a^2 + \frac{8 - N_f}{6} a^3, \tag{X.3.10}$$

$$\mathcal{F}'_{N_f}(a) = 2m_0 a + \frac{8 - N_f}{2} a^2, \tag{X.3.11}$$

$$g_{aa}^{-2} = \mathcal{F}''_{N_f}(a) = 2m_0 + (8 - N_f)a. \tag{X.3.12}$$

In this compact coordinate the first derivative is the magnetic-string central-charge expression under the declared primitive charge normalization. The second derivative is the local kinetic coefficient; the two derivatives should not be confused with a full theory's global data.

The quick test is to set $m_0 = 0$. Seven flavors give a positive metric at every $a > 0$, whereas eight give zero everywhere on the ray,

$$g_{aa}^{-2}\big|_{N_f=7, m_0=0} = a, \qquad g_{aa}^{-2}\big|_{N_f=8, m_0=0} = 0. \tag{X.3.13}$$

The $N_f = 8$ limit has lost its rank-one kinetic scale throughout the putative strong-coupling phase. It does not supply another isolated five-dimensional E fixed point by simply continuing the list. At positive m_0, its metric is the constant $2m_0$ for all a; when m_0 is set to zero, that coefficient collapses everywhere. The limiting problem is therefore more severe than an isolated charged threshold at one point of the ray.

The two neighboring endpoint calculations display the difference at every derivative order. With $N_f = 7$ and $m_0 = 0$, the cubic, primitive-coroot string expression and metric are respectively

$$\mathcal{F}_7 = \frac{a^3}{6}, \qquad \mathcal{F}'_7 = \frac{a^2}{2}, \qquad \mathcal{F}''_7 = a. \tag{X.3.14}$$

They vanish at the origin at different rates but are nonzero on the open ray. With $N_f = 8$ in the same formal limit, all three expressions vanish identically. A vanishing value of $\mathcal{F}'$ only at $a = 0$ can signal a tensionless string localized at the endpoint; an identically vanishing $\mathcal{F}''$ deprives the entire ray of the gauge kinetic coefficient in this description. The difference is why the eight-flavor observation is not merely one more tensionless-string example.

For a positive bare m_0, both examples regain a quadratic term, but that term is a deformation. Setting it to zero is the step that tests whether the candidate fixed-point description has a scale-free gauge phase. The field-theory formula tests that necessary local condition without constructing the would-be endpoint states. In the seven-flavor case the string construction supplies the separate E_8 identification; in the eight-flavor case the zero metric blocks the same rank-one five-dimensional inference. This is a comparison of controlled limits of one gauge formula, not a classification of all possible ultraviolet completions.

The actual condition within the massless gauge chamber is

$$a \geq 0, \qquad 2m_0 + (8 - N_f)a \geq 0. \tag{X.3.15}$$

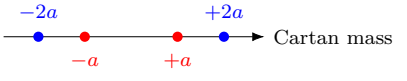
This is necessary for a sensible local gauge-phase metric. It is not a sufficient existence criterion for a decoupled ultraviolet theory. The distinction is already visible in the $N_f = 7$ example: $g^{-2} = a$ is an algebraic result, while identifying its endpoint with the E_8 theory uses a string construction and BPS flavor currents.

The necessary character of this test can be phrased directly in terms of small displacements. If a slowly varying Coulomb scalar has a local kinetic term proportional to $g_{aa}^{-2}(a)(\partial a)^2$, negative g_{aa}^{-2} is incompatible with the chosen weak gauge-phase description. A positive coefficient permits that local fluctuation but says nothing about additional states at $a = 0$. When $N_f = 8$ and $m_0 = 0$, the coefficient vanishes not just at the endpoint but for every positive a. The failure is therefore stronger than a single massless charged particle at a threshold. It signals that this rank-one five-dimensional gauge-phase metric no longer provides a nondegenerate direction in the putative limit.

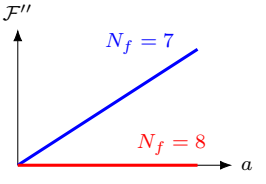
The prepotential also makes the scale of the deformation explicit. Since a and each real mass carry mass dimension one, m_0 must also have dimension one and $\mathcal{F}$ has dimension three. At $m_0 = 0$, the surviving polynomial is homogeneous of degree three,

$$\mathcal{F}_{N_f}(\lambda a; 0) = \lambda^3 \mathcal{F}_{N_f}(a; 0), \qquad \lambda \geq 0. \tag{X.3.16}$$

That scale behavior is necessary for an endpoint with no bare inverse-coupling scale. It cannot identify its conserved currents. In particular, a homogeneous zero function for $N_f = 8$ is not evidence of a new interacting fixed point.



(a) roots (blue), full-fundamental weights (red)



(b) $m_0 = 0$

Figure X.3.2: The compact $SU(2)$ Cartan ray. Each full fundamental contributes both weights $\pm a$ against the roots $\pm 2a$. At $m_0 = 0$ the $N_f = 7$ Hessian rises linearly, while the $N_f = 8$ Hessian vanishes on the whole ray. These slopes test the gauge phase and do not supply the endpoint symmetry.

As another arithmetic check, with $N_f = 3$ the vector term contributes $4a^3/3$ and the three hypers subtract $a^3/2$. Thus $\mathcal{F} = m_0 a^2 + 5a^3/6$ and $\mathcal{F}'' = 2m_0 + 5a$. Exercise 1 asks the reader to reproduce both coefficients, retaining a full hypermultiplet rather than one signed weight. Real masses now turn the single cubic into separate chamber polynomials.

X.3.3 A flavor threshold in two Coulomb chambers

One massive fundamental provides the smallest example in which the absolute values do work. Let $m > 0$ and $a \geq 0$. The two charge-one masses are $|a + m|$ and $|m - a|$.

The point $a = m$ is a charged threshold inside the Weyl ray, so the relevant polynomial must be expanded on each side. Define

$$W(a, m) = |a + m|^3 + |m - a|^3. \tag{X.3.17}$$

For $a \geq m$, the pair is $2a^3 + 6am^2$; for $0 \leq a \leq m$, it is $2m^3 + 6ma^2$,

$$W(a, m) = \begin{cases} 2m^3 + 6ma^2, & 0 \leq a \leq m, \\ 2a^3 + 6am^2, & a \geq m. \end{cases} \tag{X.3.18}$$

The $2m^3$ term is independent of the Coulomb coordinate. Keeping it makes the continuity of the prepotential transparent, while dropping it would leave the same derivatives.

Substitution into the same root sum gives two actual cubic functions,

$$\mathcal{F}_{\text{in}}(a) = \left(m_0 - \frac{m}{2}\right) a^2 + \frac{4}{3}a^3 - \frac{1}{6}m^3, \qquad 0 \leq a \leq m, \tag{X.3.19}$$

$$\mathcal{F}_{\text{out}}(a) = m_0 a^2 + \frac{7}{6}a^3 - \frac{1}{2}am^2, \qquad a \geq m. \tag{X.3.20}$$

They have different cubic coefficients because one weight changes sign across the threshold. Their gradients and Hessians are

$$\mathcal{F}'_{\text{in}} = 2\left(m_0 - \frac{m}{2}\right) a + 4a^2, \qquad \mathcal{F}''_{\text{in}} = 2m_0 - m + 8a, \tag{X.3.21}$$

$$\mathcal{F}'_{\text{out}} = 2m_0 a + \frac{7}{2}a^2 - \frac{1}{2}m^2, \qquad \mathcal{F}''_{\text{out}} = 2m_0 + 7a. \tag{X.3.22}$$

At $a = m$, both polynomials give the same value and first derivative,

$$\mathcal{F}(m) = m_0 m^2 + \frac{2}{3}m^3, \qquad \mathcal{F}'(m) = 2m_0 m + 3m^2, \tag{X.3.23}$$

while their Hessians meet at

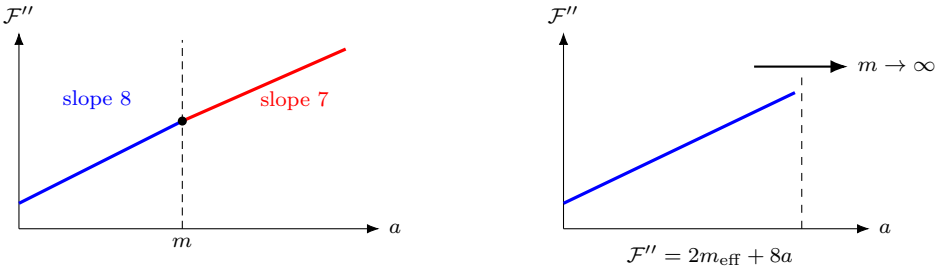
$$\mathcal{F}''_{\text{in}}(m) = \mathcal{F}''_{\text{out}}(m) = 2m_0 + 7m. \tag{X.3.24}$$

The third derivative changes from 8 inside to 7 outside. That one-unit jump is the signature of the changing charged hypermultiplet contribution, not a discontinuity in the metric.

One can see the regularity directly from the absolute-value term. The function $|a - m|^3$ and its first two derivatives vanish at $a = m$, while its third derivative is -6 on one side and $+6$ on the other. After the factor $-1/12$ in the prepotential, this produces the one-unit change in the cubic derivative. The other weight $|a + m|^3$ stays smooth throughout the nonnegative ray. Thus the threshold leaves $\mathcal{F}$ of class C^2 but changes its cubic coefficient,

$$\mathcal{F}'''_{\text{in}} = 8, \qquad \mathcal{F}'''_{\text{out}} = 7. \tag{X.3.25}$$

The magnetic-string central-charge expression $\mathcal{F}'$ is continuous as well. A drawing that jumps the metric at $a = m$ would contradict the source's exact cubic threshold form, even if its two asymptotic slopes were correct.



(a) fixed m, m_0; $|a - m| = 0$ at the wall (b) finite a stays inside

Figure X.3.3: The same $m > 0$ flavor in two Coulomb chambers. The mass $|a - m|$ closes at $a = m$; the piecewise Hessian is continuous and changes slope from 8 to 7. The right panel sends m outward while holding $m_{\text{eff}} = m_0 - m/2$ fixed.

For $m = 2$ and $m_0 = 3$, $a = 1$ lies inside, $a = 3$ outside, and $a = 2$ is the wall. Equation (X.3.21) gives 12, the outer formula gives 27, and either formula at the wall gives 20. The numbers test both the chamber assignment and the continuity condition.

The same numerical choice can test more than the Hessian. At the wall, the full prepotential and its first derivative have the common values

$$\mathcal{F}(2) = \frac{52}{3}, \qquad \mathcal{F}'(2) = 24, \qquad \mathcal{F}''(2) = 20. \tag{X.3.26}$$

Substituting $a = 2$ into the inner polynomial gives $2(2)^2 + 4(2)^3/3 - 8/6 = 52/3$; the outer polynomial gives $3(2)^2 + 7(2)^3/6 - 2(2)^2/2 = 52/3$. Their first derivatives likewise agree. This checks that the additive mass-dependent constant in the inner prepotential has been retained correctly. Omitting that constant would leave the metric exercise unchanged, but it would spoil continuity of the displayed prepotential as written.

A formula is physically used only where its chamber and metric conditions hold. The inner interval has $0 \le a \le m$ and $2m_0 - m + 8a \ge 0$; the outer has $a \ge m$ and $2m_0 + 7a \ge 0$,

$$\begin{aligned} \mathcal{C}_{\text{in}} &= \{0 \le a \le m : \ 2m_0 - m + 8a \ge 0\}, \\ \mathcal{C}_{\text{out}} &= \{a \ge m : \ 2m_0 + 7a \ge 0\}. \end{aligned} \tag{X.3.27}$$

If the entire inner interval is required to have nonnegative metric, its minimum at $a = 0$ imposes $2m_0 \ge m$. A positive metric only near the wall does not rescue a negative-metric interval near the origin.

The numerical example gives a useful view of the wall as a physical location rather than a notation switch. At $m = 2$, the inner polynomial applies from the origin through $a = 2$ and the outer one from $a = 2$ onward. Its intercept is $2m_0 - m = 4$, so every point in the inner interval has positive metric. The outer metric starts at 20 on the wall and rises with slope 7. Both chambers are admitted locally for this choice. If instead $m_0 = 1$ and $m = 3$, the inner intercept is -1, even though the wall value $2m_0 + 7m = 23$ is positive. The near-origin part of that formal chamber cannot be used as a healthy gauge phase. This is why the chamber inequalities must accompany the polynomial.

When the flavor is sent far away, a fixed low-energy pure theory requires the shifted coefficient

$$m_{\text{eff}} = m_0 - \frac{m}{2}, \qquad m \to \infty \quad \text{with } m_{\text{eff}} \text{ fixed.} \tag{X.3.28}$$

For any finite a, one eventually remains in the inner chamber, and the a-dependent part tends to $m_{\text{eff}}a^2 + 4a^3/3$. Holding m_0 fixed instead changes the pure theory's metric intercept without bound. This simple threshold prepares the signed mass flow, where the two pure endpoints have different physical theta data despite the same local cubic.

The opposite limit returns the massless one-flavor polynomial. For fixed $a > 0$, making m small enough puts that point in the outer chamber, and

$$\lim_{m\to 0^+} \mathcal{F}_{\text{out}}(a) = m_0 a^2 + \frac{7}{6}a^3, \qquad \lim_{m\to 0^+} \mathcal{F}''_{\text{out}}(a) = 2m_0 + 7a. \tag{X.3.29}$$

The wall itself moves to the origin. At $a = 0$, the inner expression differs by the mass-only constant $-m^3/6$, which also vanishes in this limit. These checks show that the two chamber formulas rejoin the massless full-weight result without changing the source convention. They do not identify the strong-coupling symmetry after the flavor is removed; that question requires the signed physical flow of Section X.3.5.

X.3.4 Exceptional flavor symmetry needs a construction

At the massless origin the perturbative gauge phase makes $SO(2N_f)$ flavor transformations of the hypers and an instanton-number current visible. The proposed E_{N_f+1} symmetry is larger. Where do its extra currents come from? The Hessian tests the gauge phase but does not count the states that become light at the string-theory endpoint. Seiberg's D4 probe construction supplies that missing physical step.

The conserved topological current has the schematic form

$$j_I \propto * \operatorname{Tr}(F \wedge F), \qquad d{*}j_I = 0. \tag{X.3.30}$$

Its charge is the instanton number. At finite coupling an instanton on the D4 is a massive particle. In Seiberg's local source variables, a BPS particle with electric charge I_3 and instanton charge I has the central-charge expression

$$Z\big|_{\text{S96}} = (I_3 + cI)\phi + Im_0, \qquad c = 2(8 - N_f). \tag{X.3.31}$$

Here m_0 is the source's inverse-coupling parameter; the cI term shows that an instanton can also carry gauge electric charge. The formula identifies a charge direction and its deformation, but does not count endpoint particles. Why should its current be related to the exceptional symmetry? Seiberg starts one frame earlier: in type I, the probe is a five-brane wrapped on a circle. The source relates its five-dimensional inverse coupling to the circle radius R, string scale M_s and the two dual-frame couplings by

$$g^{-2} \sim \frac{RM_s^2}{\lambda_I} \sim \frac{M_s}{\lambda_{I'}}. \tag{X.3.32}$$

The proportionality is source-native; it is not an absolute normalization of the IMS prepotential. An instanton on the type-I five-brane is a string wrapped on that circle, identified there with a heterotic string. Thus the five-dimensional instanton number is tied to the winding $U(1)$ of the dual heterotic description. This identifies a charge carried by the probe particle; it does not compute its complete strong-coupling spectrum.

The bulk enhancement has a separate starting point. Compactify the $SO(32)$ heterotic string on a circle and choose Wilson lines and radius so that an $SO(14) \times U(1)$ subgroup and the circle's left-moving $U(1)$ enhance to $E_8 \times U(1)$. The new massless *bulk gauge bosons* are heterotic winding modes. The extra $U(1)$ is retained in this statement; the source does not give a state-by-state winding spectrum here. Heterotic/type-I duality, followed by circle T-duality to type I$'$, places the corresponding bulk enhancement at an orientifold endpoint where the type-I$'$ coupling diverges. This is the source's nonperturbative duality step, rather than an implication of the D4 one-loop Hessian.

In the type-I$'$ interval there are two orientifold endpoints and sixteen background D8-branes. The T-dual of the wrapped probe is a D4 localized along the interval. Its position is its real Coulomb coordinate: in the interior its gauge group is broken to $U(1)$, while at an endpoint it is $SU(2)$. To keep the source's two ends distinct, let n_L D8-branes sit at the left, p in the interior and n_R at the right; its right-end coordinate and flavor count obey

$$n_L + p + n_R = 16, \qquad N_f = n_R < 8, \qquad \phi_R = R^{-1} - \phi \geq 0. \tag{X.3.33}$$

These are Seiberg's local interval coordinates, not the IMS scalar a. Strings stretching to D8-branes supply the probe quark hypermultiplets; the N_f coincident right-end D8-branes give massless quarks there. Their positions away from it set real quark masses. By contrast, the circle size and endpoint dilaton control the inverse coupling deformation of the probe. The position-dependent probe coupling is related to that dilaton, and near the right endpoint the source obtains

$$g_{\text{eff}}^{-2}(\phi_R) = g_0^{-2} + 2(8 - N_f)\phi_R. \tag{X.3.34}$$

The slope reads the net orientifold/D8 charge in this gauge phase. The vanishing endpoint intercept g_0^{-2} is the local limit used in the strong-coupling argument; this equation does not identify its normalization with the IMS m_0 used above.

At an endpoint with seven coincident D8-branes, the type-I$'$ bulk has the sourced E_8 enhancement. On an isolated D4 probe, transformations of that background gauge symmetry act as *global flavor* transformations of the five-dimensional theory; the D4's $SU(2)$ remains its dynamical gauge group. Seiberg argues that the long-distance probe theory reaches an interacting fixed point as the endpoint coupling diverges. This physical endpoint and decoupling argument transfers the bulk enhancement to global E_8 flavor on the probe. Moving D8-branes away breaks it and gives quark masses, leading to the stated E_{N_f+1} pattern for $N_f \leq 7$. Neither the bulk-to-probe step nor the existence of the isolated fixed point is proved by the cubic metric.

frame	charged object or local process	parameter and probe meaning
heterotic S^1	winding modes become bulk gauge bosons at the special $E_8 \times U(1)$ locus	circle radius and Wilson lines select the enhancement locus
type I S^1	instanton string on the wrapped five-brane winds the circle	its wrapped particle carries the D4 instanton charge $U(1)_I$
type I′ interval	one orientifold endpoint has divergent coupling; D8-branes can sit on it or move into the interval	endpoint coupling controls the probe inverse coupling; D8 displacements give quark masses
D4 probe	D4–D8 strings give quarks; D4 instantons are particles	endpoint bulk gauge symmetry acts as probe flavor, distinct from the probe's dynamical $SU(2)$

Table X.3.1: The states and parameters in the circle-to-endpoint argument. The rows are dual descriptions and a probe, not a computed one-to-one spectrum of winding states and endpoint particles.

The parameter count provides a useful check on what the enhanced symmetry must organize. The weak gauge frame has N_f independent real flavor masses and one inverse-coupling deformation. At the proposed endpoint these are interpreted as Cartan deformations of the enhanced flavor algebra. In the two cases used below, the counts are

$$\operatorname{rank}(E_2) = 2 = 1 + 1, \qquad \operatorname{rank}(E_3) = 3 = 2 + 1. \tag{X.3.35}$$

The equalities test the number of deformation parameters, not the non-Abelian commutators of the missing currents. In particular, $SU(2) \times U(1)$ and two unrelated $U(1)$ factors have the same rank. The D4 endpoint construction supplies the enhancement claim; the rank check only locates its Cartan deformations.

The one-flavor E_2 endpoint makes the missing generators explicit without requiring a winding-state formula. At finite coupling, its visible flavor algebra is $\mathfrak{u}(1)_{\text{quark}} \oplus \mathfrak{u}(1)_I$. Morrison and Seiberg identify the source-native deformation m with the $U(1)$ factor of E_2, while their $m_0^{\text{MS}} = t_0^{\text{MS}} - 2m$ breaks its $SU(2)$ factor. At $m = m_0^{\text{MS}} = 0$ the proposed flavor algebra is therefore

$$\begin{aligned} \mathfrak{e}_2 &= \mathfrak{su}(2)_{\text{enh}} \oplus \mathfrak{u}(1)_{\text{sp}}, \quad & \mathfrak{su}(2)_{\text{enh}} &= \langle J_3, J_+, J_- \rangle, \\ [J_3, J_\pm] &= \pm J_\pm, & [J_+, J_-] &= 2J_3. \end{aligned} \tag{X.3.36}$$

Here J_3 is the Cartan direction selected by m_0^{MS}, and $J_\pm$ are the two additional root currents with opposite charges under it. In the positive-m flow, where $m_0^{\text{MS}} = 0$ leaves the E_1 $SU(2)$, Seiberg identifies its Cartan $U(1)_I$ with instanton number. The spectator label $\mathfrak{u}(1)_{\text{sp}}$ refers to varying m at fixed m_0^{MS}; it does not identify that current with the weak quark current. Holding $m_0^{\text{MS}} = t_0^{\text{MS}} - 2m$ fixed also changes t_0^{MS} as m varies, so the dual current basis must change with the parameters. The displayed commutators fix only a Lie basis, not the primitive charge of a five-dimensional particle. Thus the enhancement adds two current generators, not just a second deformation parameter. Their physical existence is the source's strong-coupling claim; the cubic and the algebraic decomposition do not construct their BPS states.

At weak coupling, the manifest mass rotations for the hypermultiplets give $SO(2N_f)$, while the instanton-number charge supplies an additional $U(1)_I$. The proposed endpoint

enhancement can be represented schematically as

$$SO(2N_f) \times U(1)_I \;\longrightarrow\; E_{N_f+1}, \qquad N_f \le 7, \tag{X.3.37}$$

where the arrow records that string construction. For $N_f = 2$ the left side has the Lie algebra of $SU(2) \times SU(2) \times U(1)$, while the endpoint algebra is $SU(3) \times SU(2)$. The extra generators depend on light states at the endpoint. A web with seven-brane endpoints gives a complementary geometric presentation of their charges, developed in Chapter 2.

For orientation, the small-E names used here mean

$$E_1 = SU(2), \quad \widetilde{E}_1 \text{ has } U(1) \text{ flavor}, \quad E_2 = SU(2) \times U(1), \quad E_3 = SU(3) \times SU(2). \tag{X.3.38}$$

These are local source names for flavor symmetries. E_2 and E_3 are products, not simple exceptional Lie groups. The source also uses E_0 for a theory with no continuous flavor algebra. It would therefore be wrong to insert all these labels into one simple-group dual-Coxeter formula.

A concrete one-flavor operation makes the distinction visible. DeWolfe, Hanany, Iqbal and Katz place a D7 inside the E_1 face, with its cut away from the web. Fundamental strings from that D7 to the two D5 edges give the quark. Sliding the D7 horizontally across the right NS5 creates a D5 prong ending on it; the string can then end on that prong. Its vertical displacement changes the quark length and hence the bare mass, while horizontal motion does not change that length. Figure X.3.4 follows this move on the same initial face. Tuning the flavor mass to zero and contracting the face yields the sourced E_2 endpoint. The field-theory calculation records the new weights $\pm a$,

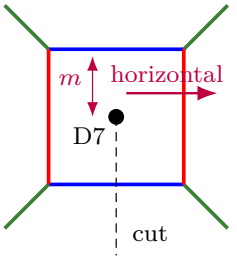
$$M_{q,+} = |a + m|, \qquad M_{q,-} = |m - a|. \tag{X.3.39}$$

At $m = 0$ the pair becomes degenerate on the Weyl ray; at $a = m > 0$ only one of these charge-one masses closes. The vertical D7 displacement is a deformation rather than a Coulomb modulus. The same weights shift the metric slope by one,

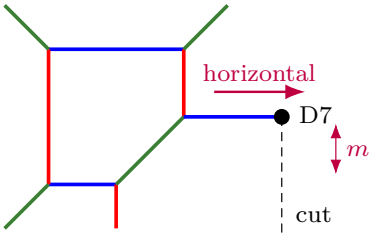
$$\mathcal{F}''_{N_f=0} = 2m_0 + 8a, \qquad \mathcal{F}''_{N_f=1} = 2m_0 + 7a. \tag{X.3.40}$$

The slope change checks the charged flavor threshold. The D7 move shows which physical object supplies the flavor; the endpoint enhancement still uses the string construction.

The seven-flavor case is the D4 probe of the E_8 string endpoint just described. At $m_0 = 0$ its metric is a for $a > 0$; that positive slope is compatible with, but does not generate, the exceptional currents. Eight flavors instead give an identically zero metric in this rank-one strong-coupling gauge limit, so the same five-dimensional inference stops there.



(a) D7 inside the E_1 face



(b) D5 prong after NS5 crossing

Figure X.3.4: Adding a D7 in the x^6-x^5 plane: blue horizontal edges are D5s, red vertical edges are NS5s and the diagonal legs are (p, q) five-branes. The filled dot is the same D7, and its dashed cut points away from the web. Moving it horizontally past the right NS5 creates a D5 prong; changing its vertical position changes the quark mass. The drawing explains the flavor operation, while the E_2 current enhancement uses the source's endpoint construction.

N_f	source name	input beyond the cubic
0	E_1 or $\widetilde{E}_1$	pure theta and asymptotic web choice
1	$E_2 = SU(2) \times U(1)$	D7 flavor and endpoint current identification
2	$E_3 = SU(3) \times SU(2)$	strong-coupling branch construction
7	E_8	string construction and BPS currents
8	no isolated rank-one E_9 here	zero strong-coupling gauge metric

Table X.3.2: What the local cubic does and what the endpoint construction must supply. The $N_f = 0$ row has two pure endpoints with the same cubic. The $N_f = 8$ row records a limitation of this five-dimensional gauge phase, not a new flavor group.

The mass deformations are relevant at the candidate fixed point and carry flavor Cartan data. At weak coupling they simply move charged thresholds. At strong coupling they can select different endpoint phases. That selection is the next question, and the pure theory is the cleanest demonstration because its cubic cannot distinguish its two choices.

X.3.5 The two pure endpoints and the E0 transition

Pure compact $SU(2) \simeq Sp(1)$ has a $\mathbb{Z}_2$ theta choice associated with $\pi_4(SU(2)) = \mathbb{Z}_2$. Both choices have the same local root contribution and therefore the same pure prepotential,

$$\mathcal{F}^{(\theta=0)}_{\text{pure}}(a) = \mathcal{F}^{(\theta=\pi)}_{\text{pure}}(a) = m_0 a^2 + \frac{4}{3} a^3. \tag{X.3.41}$$

This equality is a statement about the perturbative Coulomb function, not an equality of the resulting complete theories. With a massless fundamental, the theta parameter can be rotated away as an independent choice; after the fundamental acquires a mass,

the determinant-mass sign can carry the distinction. The sourced theta-zero pure web is called E_1 and has $SU(2)$ flavor. The other pure endpoint is $\widetilde{E}_1$ with $U(1)$ flavor. This assignment uses physical source information, not a calculation of $\mathcal{F}''$.

To track the signed flow, one must keep the Morrison–Seiberg coordinates separate from the IMS bare parameter. In the one-flavor source convention define t_0^{MS} and

$$m_0^{\mathrm{MS}} = t_0^{\mathrm{MS}} - 2m, \tag{X.3.42}$$

so that the old gauge-phase formula reads

$$t_{\mathrm{MS}}(\phi) = m_0^{\mathrm{MS}} + 2m + 16\phi - |\phi - m| - |\phi + m|. \tag{X.3.43}$$

Here ϕ is the source's charge-one matter-mass coordinate. Equation (X.3.43) has the source domain

$$s := m_0^{\mathrm{MS}} + 4m > 0, \qquad m_0^{\mathrm{MS}} \geq 0. \tag{X.3.44}$$

The equality $s = 0$ is its limiting wall. Continuing the old gauge expression to $s < 0$ would assign a negative origin metric and would miss the proposed E_0 region.

A relative map to our compact IMS gauge coordinate follows by comparing the actual Hessians. In common matter-mass units and one declared finite mass counterterm scheme, set $\phi_{\mathrm{MS}} = a$ and $m_{\mathrm{MS}} = m_{\mathrm{IMS}} = m$. The two formulas then obey

$$t_{\mathrm{MS}}(a) = 2\mathcal{F}''_{\mathrm{IMS}}(a), \qquad t_0^{\mathrm{MS}} = 4m_0^{\mathrm{IMS}}, \tag{X.3.45}$$

$$m_0^{\mathrm{MS}} = 4m_0^{\mathrm{IMS}} - 2m, \qquad s = 4m_0^{\mathrm{IMS}} + 2m. \tag{X.3.46}$$

For $m > 0$ and $a < m$, the IMS metric is $2m_0^{\mathrm{IMS}} - m + 8a$. Twice this is $4m_0^{\mathrm{IMS}} - 2m + 16a$, exactly the old MS expression there. For $a > m$, twice $2m_0^{\mathrm{IMS}} + 7a$ gives $4m_0^{\mathrm{IMS}} + 14a$, also the old expression after its absolute values are expanded. This is a kinetic or metric dictionary. The factors do not fix an absolute action, nor do they assign a primitive MS magnetic string to the IMS cocharacter.

The coordinate map can be checked in the massless subcase before following a sign. Setting $m = 0$ gives $t_{\mathrm{MS}} = t_0^{\mathrm{MS}} + 14a$ for one flavor, while IMS gives $\mathcal{F}'' = 2m_0^{\mathrm{IMS}} + 7a$. Their slopes and intercepts both obey the factor of two. For the pure theory the same comparison yields $t_{\mathrm{MS}} = t_0^{\mathrm{MS}} + 16a$ and $\mathcal{F}'' = 2m_0^{\mathrm{IMS}} + 8a$. The factor remains two even though the number of flavors changes,

$$t_{\mathrm{MS}}^{(N_f)}(a) = 4m_0^{\mathrm{IMS}} + 2(8 - N_f)a = 2\mathcal{F}''_{\mathrm{IMS}}(a), \qquad m_f = 0. \tag{X.3.47}$$

This comparison guards against identifying t_0^{MS} with m_0^{IMS}. It also isolates the finite mass-linear shift in the one-flavor problem: the source's m_0^{MS} already contains $-2m$, whereas IMS m_0 is the coefficient of a^2 before the hypermultiplet term is expanded.

The signed origin exposes the two paths. Write $m = \mu > 0$ or $m = -\mu < 0$. Evaluating the old formula at $\phi = 0$ gives

$$t_{\mathrm{MS}}(0) = \begin{cases} m_0^{\mathrm{MS}}, & m = +\mu, \\ m_0^{\mathrm{MS}} - 4\mu, & m = -\mu. \end{cases} \tag{X.3.48}$$

Thus the positive-mass path reaches its E_1 wall at $m_0^{\rm MS} = 0$, while the negative-mass path reaches the $\widetilde{E}_1$ wall at $m_0^{\rm MS} = 4\mu$, or $s = 0$. These wall locations are algebraic inside the flow picture. Their endpoint names and distinct flavor symmetries come from the source's physical construction.

The signed origin formula is instructive because the two paths use the same absolute-value expression. For positive mass, both $|\phi - m|$ and $|\phi + m|$ equal m at the origin, canceling the explicit $2m$ in $t_0^{\rm MS}$. For negative mass they contribute 2μ while the explicit term is -2μ, leaving a difference of 4μ. The asymmetric source coordinate and the physical mass flow together expose the two endpoints. Replacing every occurrence of m by $|m|$ would erase the distinction.

At $m = -\mu$ the old domain condition reads $m_0^{\rm MS} > 4\mu$. Within that open region the gauge expression has a nonnegative origin value. As the boundary is approached from above, that value tends to zero. Beyond it, the old expression would produce a negative origin metric, so a different phase description is needed. The wall equation itself is exact within the old expression; the E_0 interpretation beyond it is sourced separately.

The complete old piecewise metrics make the sign dependence visible away from the origin as well. With $M = m_0^{\rm MS}$ and $\mu > 0$, expansion of the two absolute values gives

$$t_{\rm old}(\phi; m = +\mu) = \begin{cases} M + 16\phi, & 0 \le \phi \le \mu, \\ M + 2\mu + 14\phi, & \phi \ge \mu, \end{cases} \tag{X.3.49}$$

$$t_{\rm old}(\phi; m = -\mu) = \begin{cases} M - 4\mu + 16\phi, & 0 \le \phi \le \mu, \\ M - 2\mu + 14\phi, & \phi \ge \mu. \end{cases} \tag{X.3.50}$$

Each pair agrees at $\phi = \mu$, so the wall in the Coulomb ray remains continuous. The two origin intercepts differ by 4μ. It is this intercept, together with the source's endpoint construction, that separates the positive- and negative-mass paths. The displayed negative-mass pair remains an old gauge-phase expression only for $M > 4\mu$.

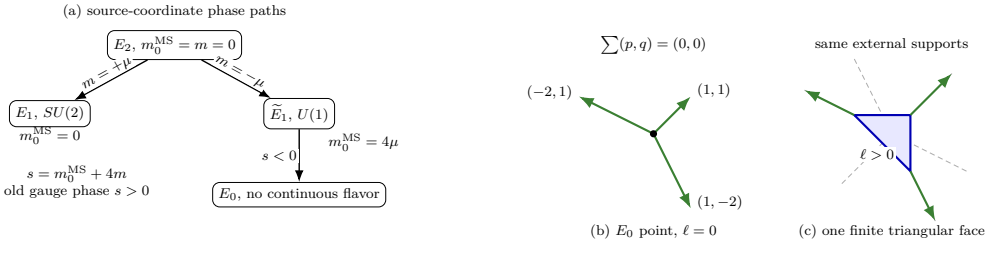


Figure X.3.5: The one-flavor E_2 deformation has two signed-mass paths in source-native $(m_0^{\rm MS}, m)$ coordinates. The old gauge expression ends at $s = 0$; its $s < 0$ continuation toward E_0 is separately sourced. Panels (b) and (c) show the local web deformation: the same three external charge supports surround a point at $\ell = 0$ or a triangular face at $\ell > 0$. The physical Coulomb branch is the source's web statement, beyond the charge sum.

For $s < 0$, the source proposes a different expression, with the origin of ϕ held fixed

and $m_0^{\mathrm{MS}} \geq 0$,

$$t_{E_0}(\phi) = \frac{m_0^{\mathrm{MS}}}{2} + 3\left|m + \frac{m_0^{\mathrm{MS}}}{4}\right| + 17\phi \\ - |\phi + m| - |\phi - m| - \left|\phi + m + \frac{m_0^{\mathrm{MS}}}{4}\right|. \tag{X.3.51}$$

Its source argument follows the movement of an additional Abelian singularity away from the origin. As a concrete comparison, take $m_0^{\mathrm{MS}} = 2$ and $m = -1$, so $s = -2$. The forbidden continuation of the old expression gives $t_{\mathrm{old}}(0) = -2$ and $t_{\mathrm{old}}(1) = 14$. The separately proposed expression instead gives

$$t_{E_0}(0) = 0, \qquad t_{E_0}(1) = 17. \tag{X.3.52}$$

The example shows exactly where using the old chamber formula would change the physics. It does not independently establish that the proposed new phase exists.

The new expression also illustrates why a continued effective metric need not have the same list of charged singularities as the old one. Besides $|\phi + m|$ and $|\phi - m|$, it contains $|\phi + m + m_0^{\mathrm{MS}}/4|$. For $m = -1$ and $m_0^{\mathrm{MS}} = 2$, that last argument closes at $\phi = 1/2$, while the old two-weight formula had only the $\phi = 1$ positive threshold. A piecewise linear slope change at the additional location encodes the source's proposed Abelian particle leaving the origin. The value $t_{E_0}(0) = 0$ is consistent with the proposed new endpoint, but the web or geometric argument is needed for its physical existence.

The web realization supplies a second physical view. In the house outward-charge order, one sourced E_0 three-leg junction has

$$(1, 1) + (-2, 1) + (1, -2) = (0, 0). \tag{X.3.53}$$

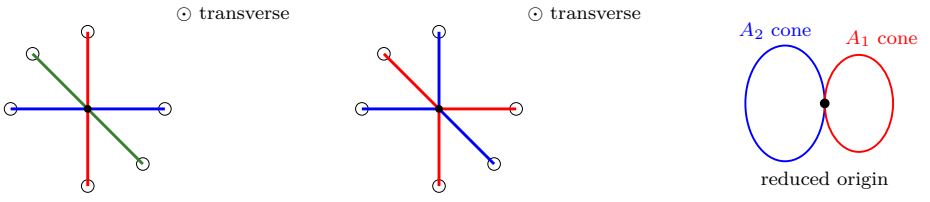
Each component of the sum vanishes. The web deformation also opens this point into one finite triangular face. Let $\ell \geq 0$ be its local size parameter. In Figure X.3.5(c), its vertices lie at $\ell(1, 1)$, $\ell(-2, 1)$ and $\ell(1, -2)$ in the local x^6-x^5 plane: increasing ℓ opens the face while each external ray stays on its original supporting line. This is one real size modulus, and the source identifies its motion as the E_0 Coulomb branch. There is no ordinary weakly coupled $SU(2)$ gauge region assigned to it. Charge balance alone would hold for many junctions with no such branch. Nor does the absence of a Higgs branch at $\widetilde{E}_1$ make that endpoint a trivial theory. The three endpoints require physical construction data beyond their local cubic.

X.3.6 The E3 Higgs branch has two cones

The two-flavor endpoint gives a different question. A five-dimensional real Coulomb metric describes a vector-multiplet scalar, while the Higgs branch consists of hypermultiplet vacua. In the finite configuration used for comparison the coupling is finite and both flavor masses and the Coulomb vev are nonzero. Its web moves as one object along the matching seven-branes; removing that common translation leaves no relative Higgs motion in this selected configuration. The sourced limit sends the inverse coupling,

both masses and the Coulomb vev to zero together. At that origin, two inequivalent balanced partitions acquire independent motions transverse to the x^6-x^5 page. The physical result proposed for the five-dimensional Higgs space is

$$\mathcal{H}_{\infty}^{E_3} = \overline{\mathcal{O}}_{\min}(\mathfrak{sl}_3) \cup \overline{\mathcal{O}}_{\min}(\mathfrak{sl}_2), \qquad \overline{\mathcal{O}}_{\min}(\mathfrak{sl}_3) \cap \overline{\mathcal{O}}_{\min}(\mathfrak{sl}_2) = \{0\}. \tag{X.3.54}$$



(a) three moving subweb classes A_2, $\dim_{\mathbb{H}} = 2$

(b) two moving subweb classes A_1, $\dim_{\mathbb{H}} = 1$

(c) $R_{A_2} \times_{\mathbb{C}} R_{A_1}$

Figure X.3.6: Two partitions of the same massless infinite-coupling $N_f = 2$ web in the x^6-x^5 plane. Hollow circles are matching seven-branes; horizontal D5s carry $(\pm 1, 0)$, vertical NS5s $(0, \pm 1)$, and green or assigned diagonal legs $(-1, 1)$ or $(1, -1)$ outward. Orientation fixes the charge; color identifies a balanced movable subweb in each panel; $\odot$ denotes motion transverse to the page. Removing common translation gives $3-1=2$ in (a) and $2-1=1$ in (b). Panel (c) shows the two reduced cones meeting only at their common origin.

These are reduced one-instanton cones, with the free center-of-mass $\mathbb{H}$ removed. In Figure X.3.6, hollow circles mark matching seven-branes: each horizontal D5 carries $(\pm 1, 0)$, each vertical NS5 carries $(0, \pm 1)$, and the diagonal endpoints carry $(-1, 1)$ or $(1, -1)$ according to their outward direction. In panel (a), each opposite pair is separately balanced and all three classes can move transversely. In panel (b), each colored trivalent set is balanced, and the two sets move independently. One motion in either partition translates all pieces together and is removed, leaving $3-1=2$ or $2-1=1$ relative quaternionic motions. Identifying those motions with five-dimensional Higgs branches is a physical source premise. The coordinate-ring calculation below starts from that premise.

For $n = 2, 3$, represent the minimal A_{n-1} cone by a traceless rank-one matrix $M = uv^{\mathsf{T}}$ with $u \in \mathbb{C}^n$, $v \in (\mathbb{C}^n)^*$ and $v \cdot u = 0$. The rescaling $(u, v) \sim (\lambda u, \lambda^{-1} v)$ leaves M unchanged. Thus its coordinate algebra can be written

$$R_{A_{n-1}} = \left(\mathbb{C}[u_1, \ldots, u_n, v_1, \ldots, v_n]/(v \cdot u)\right)^{\mathbb{C}^*} . \tag{X.3.55}$$

The moment-map entries $M_i{}^j = u_i v^j$ have local degree one. This ring realizes the rank-one and trace-zero equations without imposing a separate arbitrary relation at each degree.

Its dimension can be found before any series is summed. The pair (u, v) has $2n$ complex coordinates. The nonzero trace condition $v \cdot u = 0$ removes one dimension on the nonzero rank-one locus, and quotienting by the rescaling removes another. Closure

adds the zero matrix but no new top-dimensional component, so

$$\dim_{\mathbb{C}} \overline{\mathcal{O}}_{\min}(\mathfrak{sl}_n) = 2n-2, \qquad n=2,3. \tag{X.3.56}$$

For $n=2$, M is a traceless 2×2 rank-one matrix; its determinant vanishes. This is the familiar A_1 surface cone. For $n=3$, the rank-one equations describe a four-complex-dimensional cone. They are different irreducible varieties, so writing their union does not turn them into one cone of an intermediate dimension.

Before the trace equation, an invariant polynomial of degree k in M has bidegree (k,k) in (u,v). Its vector-space dimension is

$$b_n(k) = \dim \mathrm{Sym}^k \mathbb{C}^n \, \dim \mathrm{Sym}^k (\mathbb{C}^n)^* = \binom{k+n-1}{n-1}^2. \tag{X.3.57}$$

Multiplication by the nonzero invariant $v\cdot u$ injects the degree-$(k-1,k-1)$ space into degree (k,k) of the polynomial domain. Quotienting by its ideal therefore subtracts exactly the previous degree,

$$\dim R_{A_{n-1},k} = b_n(k) - b_n(k-1), \qquad b_n(-1)=0. \tag{X.3.58}$$

This is an all-degree derivation, not a fit to the first few coefficients.

For the two cases, the subtraction can be made completely explicit. At $n=2$, $b_2(k)=(k+1)^2$, so every degree has $2k+1$ independent functions. At $n=3$, $b_3(k)=\binom{k+2}{2}^2$ and subtraction gives

$$\dim R_{A_2,k} = \binom{k+2}{2}^2 - \binom{k+1}{2}^2 = (k+1)^3. \tag{X.3.59}$$

The last equality follows by factoring the difference of squares. It offers a direct check of the rational expression below at every nonnegative degree. In degree one it gives the eight independent traceless 3×3 moment-map entries. In degree two it gives 27 functions after the trace-generated relations are removed.

Let x count one moment-map degree. Summing the last equation gives

$$H_{A_{n-1}}(x) = (1-x)\sum_{k\ge 0} \binom{k+n-1}{n-1}^2 x^k. \tag{X.3.60}$$

For $n=2$, the summand is $(k+1)^2$. Its geometric-series derivatives yield

$$\sum_{k\ge 0}(k+1)^2 x^k = \frac{1+x}{(1-x)^3}, \qquad H_{A_1}(x) = \frac{1+x}{(1-x)^2}. \tag{X.3.61}$$

There is a familiar presentation of the A_1 result. Write the traceless matrix as

$$M = \begin{pmatrix} Z & X \\ Y & -Z \end{pmatrix}, \qquad \det M = 0 \quad\Longleftrightarrow\quad XY + Z^2 = 0. \tag{X.3.62}$$

The three degree-one generators have one degree-two relation, so their complete-intersection series is $(1-x^2)/(1-x)^3 = (1+x)/(1-x)^2$. A change of sign of Y

gives the conventional $XY = Z^2$ equation. This small example turns the abstract invariant construction into a concrete surface and independently checks the A_1 generating function. Its complex dimension is $3 - 1 = 2$, as found from the general rank-one quotient. For $n = 3$, the summand is $[(k+1)(k+2)/2]^2$. The same differentiation gives

$$\sum_{k\geq 0} \binom{k+2}{2}^2 x^k = \frac{1+4x+x^2}{(1-x)^5}, \qquad H_{A_2}(x) = \frac{1+4x+x^2}{(1-x)^4}. \tag{X.3.63}$$

The denominator orders imply complex dimensions 2 and 4, hence quaternionic dimensions 1 and 2 for these hyperkähler cones,

$$\dim_{\mathbb{H}} \overline{\mathcal{O}}_{\min}(\mathfrak{sl}_2) = 1, \qquad \dim_{\mathbb{H}} \overline{\mathcal{O}}_{\min}(\mathfrak{sl}_3) = 2. \tag{X.3.64}$$

The subtraction of the center-of-mass $\mathbb{H}$ is essential. Adding it back would increase both dimensions by one and change the Hilbert series by a free-factor contribution.

The two factors $SU(3)$ and $SU(2)$ have distinct minimal nilpotent cones, and a generic point on one component cannot move into the other without returning to their common origin. In the specified finite-coupling comparison, the masses and Coulomb vev are also nonzero. The selected connected web therefore has only the removable common motion; the two relative partitions appear at the simultaneous massless, zero-Coulomb, infinite-coupling origin. Finite coupling alone is not a general criterion for absence of Higgs branches. The physical premise of the union is this specified source limit.

To turn a set-theoretic union into a ring formula, specify the scheme at the intersection. If both cones are reduced and meet in one reduced origin, their coordinate ring is the fiber product

$$R_{E_3} = R_{A_2} \times_{\mathbb{C}} R_{A_1} = \{(f, g) : f(0) = g(0)\}. \tag{X.3.65}$$

The difference of the two constant evaluations yields the exact sequence

$$0 \longrightarrow R_{E_3} \longrightarrow R_{A_2} \oplus R_{A_1} \xrightarrow{(f,g)\mapsto f(0)-g(0)} \mathbb{C} \longrightarrow 0. \tag{X.3.66}$$

Therefore the constant function is counted once,

$$H_{E_3}(x) = H_{A_2}(x) + H_{A_1}(x) - 1. \tag{X.3.67}$$

Expansion through degree four supplies a check of the ring statement,

$$H_{E_3}(x) = 1 + 11x + 32x^2 + 71x^3 + 134x^4 + O(x^5). \tag{X.3.68}$$

For example, degree one consists of eight A_2 moment-map entries and three A_1 entries, giving 11. Degree zero is 1, rather than 2, because the two branches share their origin.

There is a second coefficient check that keeps the two branches visibly separate. Through local degree four, the component dimensions are

k	0	1	2	3	4
$\dim R_{A_2,k}$	1	8	27	64	125
$\dim R_{A_1,k}$	1	3	5	7	9

. (X.3.69)

For $k > 0$ the union ring adds the component dimensions. For $k = 0$ the exact sequence removes one of the two constants. This reproduces $11, 32, 71, 134$ without manipulating a rational function. It also shows what a wrong direct sum would do: it would have constant coefficient two and would describe two disconnected origins rather than a union meeting at one point.

The component dimensions yield an all-degree version of the same check. For every $k \geq 1$, the degree-k piece of the fiber product is the direct sum of the positive-degree pieces of the two factors. Consequently

$$\dim R_{E_3,k} = (k+1)^3 + (2k+1), \qquad k \geq 1, \quad \dim R_{E_3,0} = 1. \tag{X.3.70}$$

The cubic growth at large k comes from the four-complex-dimensional A_2 component. The linear growth from A_1 is subleading but never absent. Thus a calculation that extracts only the dimension of the union would report the larger component and overlook the second cone. The full graded ring retains both. This is why the two-component source premise carries more information than one quoted quaternionic dimension.

The book's Coulomb-ring fugacity is $t^{2\Delta}$. For these degree-one moment maps define the local polynomial variable $x = t^2$, so the same series begins

$$H_{E_3}(t) = 1 + 11t^2 + 32t^4 + 71t^6 + 134t^8 + O(t^{10}). \tag{X.3.71}$$

There are no odd powers of the book t in this ring. The source associates each component separately with a three-dimensional $\mathcal{N} = 4$ magnetic-quiver Coulomb ring. That protected-ring dictionary is a physical construction premise. It does not identify the entire five-dimensional QFT with either three-dimensional quiver, nor does a Hilbert series establish equality of metrics or an unexamined nonreduced scheme structure. Chapters 5–7 will calculate such three-dimensional Coulomb rings and study how their components intersect.

X.3.7 What remains beyond the fixed-point examples

The computations answer different questions. The compact real Coulomb coordinate a gives a piecewise cubic $\mathcal{F}$ and a local metric. A choice of global theta data and a source construction distinguish pure endpoints that share that cubic. The massless two-flavor five-dimensional Higgs space is a proposed union; once the reduced-point premise is specified, its coordinate-ring series follows exactly. The three-dimensional magnetic-quiver Coulomb rings enter only as component-wise descriptions of that Higgs space.

Object	Direct result here	Further physical input
5d real Coulomb ray	$\mathcal{F}'' = 2m_0 + (8 - N_f)a$ and massive chambers	endpoint existence, global theta, current enhancement
Pure endpoints	same perturbative cubic and different signed-flow walls	E_1, $\widetilde{E}_1$ and E_0 identification
5d E_3 Higgs space	conditional fiber-product Hilbert series	reduced union and web branch identification
3d quiver Coulomb rings	candidate component rings	component-wise five-dimensional Higgs dictionary

Table X.3.3: Each calculation has a different target. The E_0 source web shows why balanced external legs alone are insufficient; the E_3 union shows why one dimension or one polynomial cannot represent every component.

These examples also set the transition to the next construction. Chapter 4 uses a six-dimensional IIA brane system with tensor and anomaly conditions, where a finite tensor vev and an SCFT limit again have distinct meanings. Chapters 5–7 take up the component-wise magnetic-quiver proposal and its graded rings. The useful common habit is to name the physical space first, then ask which calculation sees it and which premise connects the two.

X.3.8 Exercises

1. Take compact $SU(2)$ with $\Phi = \mathrm{diag}(a, -a)$, $a \geq 0$, three massless full fundamentals and the IMS quadratic term $m_0 a^2$. Sum every root and weight in the one-loop formula. Find the coefficient of a^3 in $\mathcal{F}$ and the coefficient of a in $\mathcal{F}''$. Explain why counting one weight per fundamental changes both answers.

2. For one fundamental of positive mass $m = 2$ and $m_0 = 3$ in the same convention, compute $\mathcal{F}''$ at $a = 1$ in the inner chamber, at $a = 3$ in the outer chamber and at $a = 2$ on the wall. State the three values in that order and check the wall using both formulas.

3. Suppose the infinite-coupling E_3 Higgs space is the union of reduced minimal A_2 and A_1 cones meeting only at a reduced origin. With moment maps of local degree one in x, derive the Hilbert-series coefficients through x^4. Translate those degrees into the book variable $x = t^2$, and explain why only one constant survives.

4. Tabulate or draw the outward external five-brane charges $(1, 1)$, $(-2, 1)$ and $(1, -2)$ of the sourced E_0 junction. Check balance component by component. Using the physical endpoint construction, compare the E_1 and $\widetilde{E}_1$ theta choices and explain why neither charge balance nor the shared pure cubic certifies the hidden Coulomb direction or an isolated fixed point.

X.3.9 Take-home message

Take-home message

The compact $SU(2)$ root and full-weight sums give $\mathcal{F} = m_0 a^2 + (8 - N_f)a^3/6$ in the massless gauge phase. One mass produces two cubic chambers with a continuous metric at $a = m$. The $N_f = 8$ zero metric is a boundary of this five-dimensional diagnostic. Source constructions supply the exceptional currents, pure theta endpoints and the E_0 continuation. At the sourced infinite-coupling E_3 origin, the two reduced Higgs components have quaternionic dimensions two and one. Under a reduced-point intersection, their exact coordinate ring has $H_{E_3} = H_{A_2} + H_{A_1} - 1$. These are five-dimensional physical spaces and their associated protected rings, with three-dimensional magnetic-quiver Coulomb rings entering component by component.

Status and sources

The pure finite-face quantities and the relative AHK/IMS charge-normalized comparison in Section X.3.1 use Aharony, Hanany, and Kol (1998, PDF pp. 16–17, eqs. (24)–(25)) and the relative electric, magnetic and kinetic normalization of Chapter 1. The E_1 theta-zero source web is DeWolfe et al. (1999, PDF pp. 4–5, Fig. 1a). The web-to-five-dimensional endpoint and decoupling step is a construction premise [DEC], not an algebraic consequence of the face area.

The compact root-minus-weight calculation, mass chambers, Hessian continuity and metric criterion in Sections X.3.2 and X.3.3 use Intriligator et al. (1997, PDF pp. 10–11, eq. (2.22)). Their displayed specializations and limits are [MATH] within the specified Weyl chambers. The $N_f = 8$ zero-metric discussion also follows Morrison and Seiberg (1997, PDF pp. 5–6, eqs. (2.6)–(2.7)) and Seiberg (1996, PDF p. 5 and p. 10). Metric positivity is necessary, not a UV theorem. The source-native MS/IMS comparison in Section X.3.5 uses the stated relative metric and finite-counterterm scheme. It does not fix an absolute action or primitive string normalization.

The E_{N_f+1} endpoint construction and small-E names in Section X.3.4 follow Seiberg (1996, PDF pp. 7–10, eqs. (3.8) and (4.1)–(4.5)); the source-native BPS charge expression is on PDF p. 7, the wrapped-instanton/winding identification is on PDF pp. 7–9, and the heterotic E_8 enhancement and probe flavor inference are on PDF p. 10. The E_2 deformation assignment and source-native m_0^{MS} are Morrison and Seiberg (1997, PDF pp. 6–7, eqs. (2.7)–(2.9)); the D7 flavor operation is DeWolfe et al. (1999, PDF pp. 5–6, Figs. 1–2). The string/BPS flavor-current argument is [GEO-E] with decoupling input [DEC]; the cubic only checks a local gauge-phase condition. The pure $\mathbb{Z}_2$ theta observation follows Intriligator et al. (1997, PDF p. 5). The signed source coordinates, $s > 0$ domain, wall and separately proposed E_0 continuation are Morrison and Seiberg (1997, PDF pp. 6–8, eqs. (2.8)–(2.10) and Fig. 1). The alternative web and hidden real Coulomb branch are Aharony and Hanany (1997, PDF pp. 33–34, Figs. 11–12). The charge sum is [MATH]; the endpoint identifications and Coulomb branch are sourced physical claims [GEO-E].

The two-component five-dimensional E_3 Higgs premise in Section X.3.6 is Morrison

and Seiberg (1997, PDF p. 6, eq. (2.7)) and Cabrera et al. (2019, PDF pp. 7–9, eqs. (2.1)–(2.3), Figs. 2–3). The rank-one matrix count and fiber-product series are [MATH] conditional on a reduced-point intersection. Each component's identification with a three-dimensional magnetic-quiver Coulomb ring is the source's protected-space proposal [GEO-E]; no full-QFT duality or metric identification follows.

References

Aharony, O. and A. Hanany (1997). "Branes, superpotentials and superconformal fixed points". In: *Nucl. Phys. B* 504, pp. 239–271. DOI: 10.1016/S0550-3213(97)00472-0. arXiv: hep-th/9704170.

Aharony, O., A. Hanany, and B. Kol (1998). "Webs of (p,q) five-branes, five-dimensional field theories and grid diagrams". In: *JHEP* 01, p. 002. DOI: 10.1088/1126-6708/1998/01/002. arXiv: hep-th/9710116.

Cabrera, S., A. Hanany, and F. Yagi (2019). "Tropical Geometry and Five Dimensional Higgs Branches at Infinite Coupling". In: *JHEP* 01, p. 068. DOI: 10.1007/JHEP01(2019)068. arXiv: 1810.01379 [hep-th].

DeWolfe, O. et al. (1999). "Five-branes, seven-branes and five-dimensional E(n) field theories". In: *JHEP* 03, p. 006. DOI: 10.1088/1126-6708/1999/03/006. arXiv: hep-th/9902179.

Intriligator, K. A., D. R. Morrison, and N. Seiberg (1997). "Five-dimensional supersymmetric gauge theories and degenerations of Calabi-Yau spaces". In: *Nucl. Phys. B* 497, pp. 56–100. DOI: 10.1016/S0550-3213(97)00279-4. arXiv: hep-th/9702198.

Morrison, D. R. and N. Seiberg (1997). "Extremal transitions and five-dimensional supersymmetric field theories". In: *Nucl. Phys. B* 483, pp. 229–247. DOI: 10.1016/S0550-3213(96)00592-5. arXiv: hep-th/9609070.

Seiberg, N. (1996). "Five-dimensional SUSY field theories, nontrivial fixed points and string dynamics". In: *Phys. Lett. B* 388, pp. 753–760. DOI: 10.1016/S0370-2693(96)01215-4. arXiv: hep-th/9608111.

Chapter X.4

Six-dimensional theories from NS5-D6-D8 systems

X.4.1 Dynamical endpoints in six dimensions

Imagine several parallel D6 stacks suspended between successive NS5-branes. The six directions common to every stack are ordinary spacetime directions. Moving one NS5 relative to another changes the length of a D6 interval, and therefore changes the gauge coupling measured by a six-dimensional observer. In five dimensions it is tempting to regard such a separation as an externally chosen coupling. Here the NS5 worldvolume carries a tensor multiplet. Its relative position is a dynamical scalar, and a D2 stretched across the interval is a string whose tension changes with that scalar.

This one configuration poses three linked questions. Which D6 ranks can end on the NS5-branes when D8-branes are present? Why does the resulting chiral gauge theory have no irreducible gauge anomaly? What cancels the reducible anomaly that survives the rank constraint? The answer to the last question uses the very interval strings that measure the tensor scalars. The brane inventory, the rank equation, and the tensor pairing will therefore be developed for the same ordered chain.

Our principal small example has three NS5-branes, two rank-four D6 intervals, and four semi-infinite flavor D6s at each end. Its gauge sector is $SU(4) \times SU(4)$ on a specified semisimple cover. A second example has four NS5-branes and interval ranks $(6, 5, 4)$; it exposes the D8 jumps that the constant-rank example hides. Both examples are local noncompact constructions. A local charge and anomaly calculation is valuable even though a complete massive-IIA vacuum, when D8s are present, needs further global information.

We use six-dimensional $\mathcal{N} = (1, 0)$ names for eight real supercharges. Some of the original IIA literature calls the same eight-supercharge arrangement $(0, 1)$. Its "Coulomb branch" in this setting is the tensor branch. A $(1, 0)$ vector multiplet has no scalar whose expectation value could supply a six-dimensional vector Coulomb branch. This distinction will matter again when Chapter 5 introduces a separate three-dimensional magnetic-quiver Coulomb branch.

X.4.2 D6 intervals, tensor scalars and instanton strings

The first task is to read the configuration without hiding a direction. Let x^0 be time, let the NS5-branes be ordered along x^6, and use the directions in Table X.4.1. The common 012345 worldvolume is six-dimensional. A D6 continues along the suspended direction 6; a D8 replaces that direction by 789. A D6–D8 string has four relative Neumann–Dirichlet directions, namely $6, 7, 8, 9$, and supplies the familiar hypermultiplet matter in this local brane description. Rotations of 789 have spin cover $SU(2)_R$.

object	shared 012345	suspension 6	transverse 789	role
NS5	$\times$	position	position	tensor endpoint
D6	$\times$	$\times$	position	gauge interval
D8	$\times$	position	$\times$	fundamental matter
D2	01	$\times$	position	string on 01

Table X.4.1: Coordinates of the local IIA construction. The D2 row specifies the representative string stretched between adjacent NS5-branes, not a new spacetime-filling D2 stack.

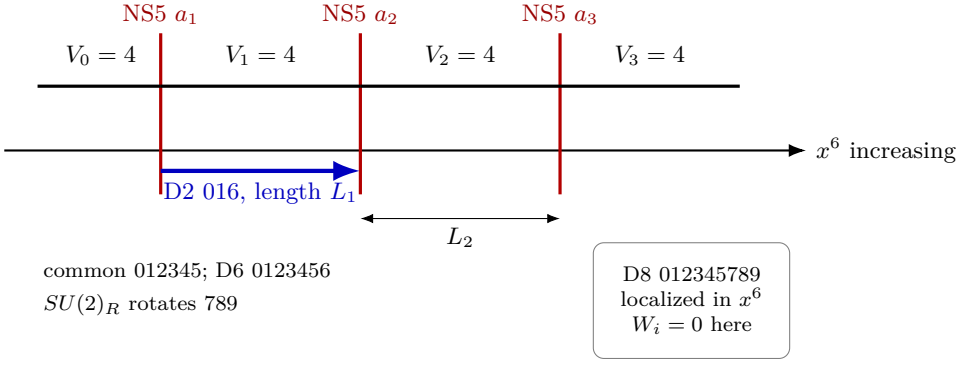


Figure X.4.1: The same three NS5-branes at $a_1 < a_2 < a_3$ support two rank-four D6 intervals. The blue D2 occupies 01 and spans the first interval in x^6; the other string spans $[a_2, a_3]$. The exterior rank-four D6 stacks define flavor groups, while the inset records the D8 orientation. There are no D8-branes in this equal-rank example.

The two positive separations are $L_i = a_{i+1} - a_i$, $i = 1, 2$. More generally, N NS5-branes have $n = N - 1$ independent relative positions. The simultaneous translation of all a_i is a free center-of-mass mode, whereas each difference couples to a suspended D6 interval. This is a geometric reason to expect $N - 1$ interacting tensor directions. It is not the reason the D6 trace $U(1)$ factors become massive; that involves a different field and a different mechanism.

At a single interval, the Chan–Paton group first appears as $U(V_i)$. The source's dynamical axion or FI hypermultiplets make each gauge trace $U(1)$ massive in its local low-energy description. The resulting semisimple gauge-anomaly calculation will use the simply connected compact cover $SU(V_i)$ for every node. We have not silently divided by its center. Indeed

$$U(V_i) = \frac{SU(V_i) \times U(1)}{\mathbb{Z}_{V_i}} \tag{X.4.1}$$

already shows why the original $U(V_i)$ flux sectors cannot be reconstructed by taking two unrelated flux lattices. The remaining discrete Stückelberg sector and faithful flavor quotient need more information than the local anomaly polynomial supplies.

The physical size of L_i becomes a coupling after reducing the leading D6 Yang–Mills term. In the house normalization $\mathrm{Tr_f}(T^a T^b) = \delta^{ab}/2$, write

$$S_7 = -\frac{1}{2g_7^2} \int_{M_6 \times [a_i, a_{i+1}]} \mathrm{Tr_f}\, F_{MN} F^{MN}, \qquad g_7^2 = 2(2\pi)^4 g_s (\alpha')^{3/2}. \tag{X.4.2}$$

For a zero mode constant along the interval, integrating x^6 gives

$$S_{6,i} = -\frac{1}{2g_{6,i}^2} \int_{M_6} \mathrm{Tr_f}\, F_{\mu\nu} F^{\mu\nu}, \qquad \frac{1}{g_{6,i}^2} = \frac{L_i}{g_7^2}. \tag{X.4.3}$$

Thus $\phi_i := g_{6,i}^{-2}$ is a useful tensor-branch coordinate with mass dimension two. We do not thereby assert that the independent ϕ_i have diagonal, unit-normalized scalar kinetic terms. The leading flat-patch reduction fixes the local coefficient; in a warped massive-IIA region it is not an exact reduction formula without further input.

The D2 provides a second measurement of precisely this coefficient. Its tension per unit length along x^1 is its brane tension times the stretched length,

$$\tau_2 = \frac{1}{(2\pi)^2 g_s (\alpha')^{3/2}}, \qquad T_i = \tau_2 L_i = \frac{L_i}{(2\pi)^2 g_s (\alpha')^{3/2}}. \tag{X.4.4}$$

Using the normalized g_7 in (X.4.2), rather than a schematic proportionality, produces the exact local leading-order match

$$T_i = \frac{8\pi^2}{g_{6,i}^2} = 8\pi^2 \phi_i. \tag{X.4.5}$$

The factor $8\pi^2$ can also be recovered from a unit instanton in the four spatial directions transverse to the string. With the same fundamental trace,

$$q_{\mathrm{phys}} = \frac{1}{8\pi^2} \int_{M_4} \mathrm{Tr_f}(F_{\mathrm{phys}} \wedge F_{\mathrm{phys}}), \qquad |q_{\mathrm{phys}}| = 1. \tag{X.4.6}$$

For a self-dual representative, the four-dimensional kinetic integral is $16\pi^2$ in this convention. Substitution in (X.4.3) therefore gives

$$E_{\mathrm{inst}}/\text{string length} = \frac{16\pi^2}{2g_{6,i}^2} = \frac{8\pi^2}{g_{6,i}^2}. \tag{X.4.7}$$

An anti-self-dual representative reverses the oriented charge but keeps the positive tension. The string can be read both as a stretched D2 and as an instanton of the D6 gauge field. It is also electrically and magnetically charged under the six-dimensional tensor sector in the source's description. We will turn that tensor charge into an integral pairing in Section X.4.5.

For the two-node rank-four example, $g_{6,1}^{-2}$ and $g_{6,2}^{-2}$ are independent because L_1 and L_2 are. Their string tensions vanish separately if one interval closes. A simultaneous relative collapse is needed to reach the origin of this two-dimensional tensor cone. The dimension count also explains a common mistake. Since $[g_6^2] = \text{mass}^{-2}$, g_6^2 is dimensionful; the condition for a weak gauge-theory expansion at energy E is $g_6^2 E^2 \ll 1$, not a dimensionless small-coupling statement.

The field assignments can be reconstructed from the intersections. Strings with both ends on one finite D6 interval supply a vector zero mode along 012345. The endpoint boundary conditions remove an independent D6 displacement along the suspended direction; its length is instead the separation of the NS5s. Strings across the D6 stacks on opposite sides of an NS5 supply a full bifundamental hypermultiplet. A D8 crossing interval i supplies a fundamental hypermultiplet. A semi-infinite D6 at either exterior end gives a flavor representation but no finite-interval six-dimensional gauge kinetic term. The equal-rank example therefore has

$$[SU(4)] - SU(4)_1 - SU(4)_2 - [SU(4)], \qquad n_{\text{tensor}} = 2. \tag{X.4.8}$$

The square brackets denote external flavor factors. They do not add a tensor or gauge node to either semi-infinite stack. There are three full hypers in the drawing: one interior bifundamental of dimension 16 and two end hypers of dimension 16 each. This explains why the later weighted hyper count is 48 rather than three or eight.

The action trace defines an oriented instanton number q_{phys}, while the source anomaly trace below will use $q_O = -q_{\text{phys}}$. Both conventions describe a unit-tension BPS object when their absolute charges are one. The sign conversion belongs to the curvature convention, not to a reversal of the D2's geometric length $L_i > 0$. Two local checks are therefore

$$\frac{T_i}{\phi_i} = 8\pi^2, \qquad \frac{\phi_1}{\phi_2} = \frac{L_1}{L_2} \quad \text{in the common flat D6 patch.} \tag{X.4.9}$$

The first fixes an absolute brane/action normalization; the second is a relative interval statement. A formula preserving only the ratio could still miss a common factor of two in the D6 coupling and D2 tension. This matters when comparing schematic source formulas with the explicit local reduction.

X.4.3 D8 charge fixes the rank profile

What changes if a D8 sits inside an interval? The source charge equation relates the D6s ending on each NS5 to an integer Romans quantity. We need only its dimensionless charge units. Label the ordered NS5-branes by $i = 1, \ldots, N$, the D6 ranks in the intervals by V_i for $i = 1, \ldots, N-1$, and the exterior ranks by $V_0 = W_L$ and $V_N = W_R$.

The exterior stacks extend away from the finite system and are flavor data. The charge mechanism was also formulated in a source with a rotated brane coordinate frame. To use that argument while retaining our x^6 suspension direction, Table X.4.2 shows the same objects on both sides of the relabeling.

frame	NS5	D6	D8	ordered suspension
source	012389	0123789	012345689	x^7
book	012345	0123456	012345789	x^6

Table X.4.2: The coordinate translation used for the endpoint-charge argument. The signed relabeling preserves ten-dimensional orientation and maps increasing source x^7 to increasing book x^6; the endpoint sign is fixed in the book-axis source.

Explicitly, the six noncommon coordinates map as

$$(x^4, x^5, x^6, x^7, x^8, x^9)_{\text{source}} \longmapsto (x^7, x^8, -x^9, x^6, x^4, x^5)_{\text{book}}. \tag{X.4.10}$$

The permutation has odd parity and the extra reflection restores orientation. It does not assign a sign to an RR component; the endpoint convention below is pinned separately in the frame of Table X.4.1. No four-dimensional D4 sector of the rotated source is imported into this six-dimensional chapter.

The massive-IIA charge equation has the schematic local form

$$dF_2 = J_{\text{D6}} - mH. \tag{X.4.11}$$

Around an NS5 endpoint, H detects its charge and J_{D6} detects the oriented D6 ends. Integrating over a small linking region relates the left-minus-right D6 number to the local integer m. Across a positive D8 wall this integer increases by one. These are the physical source inputs for the discrete equations that follow. The integer argument does not supply a dimensionful RR/Wess–Zumino normalization.

Write $W_i \geq 0$ for the number of positive D8 walls in interval i. The oriented endpoint rule is

$$m_i = V_{i-1} - V_i, \qquad i = 1, \ldots, N. \tag{X.4.12}$$

The second source rule says a positive D8 raises the Romans integer as x^6 increases,

$$m_{i+1} - m_i = W_i. \tag{X.4.13}$$

It follows immediately, by substituting two adjacent endpoint equations, that the ranks obey a discrete second-difference condition,

$$W_i = 2V_i - V_{i-1} - V_{i+1}. \tag{X.4.14}$$

This is a charge-balance result in the specified local source family. It does not assign a dimensionful normalization to F_0 and does not by itself construct a globally complete massive-IIA background.

The sign is worth following on an actual chain. Choose four NS5-branes, three interval ranks $(V_1, V_2, V_3) = (6, 5, 4)$, and exterior ranks $(V_0, V_4) = (6, 2)$. Then the four endpoint differences give

$$(m_1, m_2, m_3, m_4) = (6-6, 6-5, 5-4, 4-2) = (0, 1, 1, 2). \tag{X.4.15}$$

Taking the successive differences gives

$$(W_1, W_2, W_3) = (1, 0, 1). \tag{X.4.16}$$

The zero middle entry means no D8 jump between the second and third NS5-branes, even though the D6 rank changes there. This distinguishes a rank slope from its discrete change of slope.

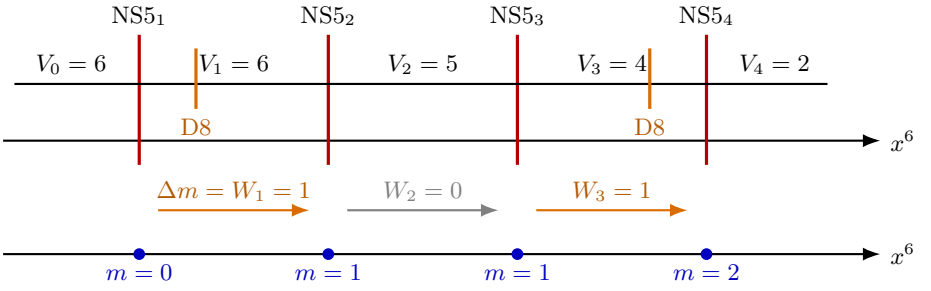


Figure X.4.2: One fixed four-NS5 inventory in two views. The upper panel keeps exterior D6 ranks $6, 2$ and interval ranks $6, 5, 4$ at the same four positions $a_1 < \cdots < a_4$; D8 walls lie only in the first and third intervals. The lower panel plots $m_i = V_{i-1} - V_i$ at those very NS5s. The arrows label positive jumps toward increasing x^6.

Each gauge node also sees fundamentals from the D8s and from its two neighbors. A bifundamental of $SU(V_i) \times SU(V_{i+1})$ has V_{i+1} copies of the fundamental when inspected at node i. Thus the effective fundamental multiplicity of node i is

$$N_{f,i}^{\text{eff}} = V_{i-1} + W_i + V_{i+1}. \tag{X.4.17}$$

For the displayed chain, including the exterior flavors, this yields

$$(N_{f,1}^{\text{eff}}, N_{f,2}^{\text{eff}}, N_{f,3}^{\text{eff}}) = (6+1+5,\ 6+0+4,\ 5+1+2) = (12, 10, 8). \tag{X.4.18}$$

Every entry equals twice the corresponding gauge rank. The equality is not a generic six-dimensional flavor slogan; it is precisely (X.4.14) rewritten for this matter inventory.

With nonnegative W_i, the ranks are discretely concave. Indeed (X.4.14) says that the slope $V_i - V_{i-1}$ cannot increase as one moves right. This gives a quick diagnostic for a proposed positive-D8 chain. For example, changing only the last D8 count from one to two while holding all four NS5 positions and all D6 ranks fixed would demand $m_4 - m_3 = 2$, whereas the endpoint differences still give $m_4 - m_3 = 1$. One cannot repair that contradiction by moving the D8 wall inside the interval; its net charge jump is fixed.

The equal-rank chain has a useful complementary property. If $(V_0, V_1, V_2, V_3) = (4, 4, 4, 4)$, then

$$(m_1, m_2, m_3) = (0, 0, 0), \qquad (W_1, W_2) = (0, 0). \tag{X.4.19}$$

It isolates the tensor and anomaly calculation from D8 walls. The unequal chain is a numerical specialization of the source's NS5–D6–D8 family, not a separately exhibited complete vacuum. Its rank condition will reappear, coefficient for coefficient, in the irreducible anomaly.

The second-difference equation can construct a chain as well as check one afterward. Given V_0, an initial m_1, and ordered D8 counts, the first gauge rank is $V_1 = V_0 - m_1$. Every later rank follows from the running Romans integer:

$$m_{i+1} = m_1 + \sum_{j=1}^{i} W_j, \qquad V_i = V_0 - \sum_{a=1}^{i} m_a. \tag{X.4.20}$$

The D8 walls change a slope, not a rank directly. For the $(6, 5, 4)$ chain with $m_1 = 0$ and $W = (1, 0, 1)$, the partial sums give $m = (0, 1, 1, 2)$ and then $V = (6, 6, 5, 4, 2)$, including both exterior ranks. The right end is consequently fixed if the left end and D8 charges are fixed. Conversely, fixing both exterior ranks imposes the integrated constraint

$$V_N = V_0 - Nm_1 - \sum_{j=1}^{N-1} (N - j) W_j. \tag{X.4.21}$$

For $N = 4$, $V_0 = 6$, $m_1 = 0$ and $W = (1, 0, 1)$, the right side is $6 - (3 + 1) = 2$. Omitting the first D8 changes it by three units, because that jump affects three subsequent endpoint slopes. This weighted sum checks a diagram whose D8 walls are visually far from the right boundary.

Let $\Delta_i = V_i - V_{i-1} = -m_i$. Equation (X.4.14) then gives

$$\Delta_{i+1} - \Delta_i = -W_i \leq 0. \tag{X.4.22}$$

The profile bends downward at each positive D8 wall. An upward bend would require a negative jump in this orientation or a different source ingredient. This local restriction does not decide whether the finite positive ranks embed in a compact setup satisfying global RR charges.

X.4.4 Gauge anomalies from the brane inventory

A six-dimensional chiral gauge theory can fail before any question about its strong-coupling limit is asked. The obstruction has a piece proportional to an independent $\operatorname{tr} F_i^4$. A Green–Schwarz square is built from four-forms, and therefore cannot remove that independent quartic invariant. We will calculate the coefficient from the actual matter at a node, keeping the sign convention fixed throughout. The calculation also leaves a reducible quadratic-trace piece for the next section.

The Yang–Mills action above used a Hermitian physical curvature. For the anomaly polynomial we switch explicitly to the source's anti-Hermitian, 2π-normalized curvature

$$F_{O,i} = -\frac{iF_{\mathrm{phys},i}}{2\pi}, \qquad s_i = \mathrm{tr_f}\, F_{O,i}^2, \qquad u_i = \mathrm{tr_f}\, F_{O,i}^4. \tag{X.4.23}$$

The fundamental trace $\mathrm{tr_f}$ acts in the same representation as $\mathrm{Tr_f}$ in the action, but its argument is now F_O. Quadratic traces acquire a minus sign under this conversion, whereas quartic traces do not. We retain the source characteristic classes $c = c_2(R)$, $p_1 = p_1(T)$ and $p_2 = p_2(T)$ without assigning their signs from the Hermitian action.

There is a useful charge check on the conversion. The normalized adjoint trace of the anomaly source is $\mathrm{Tr}_O = \mathrm{tr_{adj}}\,/k$ for $SU(k)$, so $\mathrm{Tr}_O\, F_O^2 = 2s_i$. On one fixed oriented four-cycle,

$$q_O = \frac{1}{4}\int \mathrm{Tr}_O\, F_O^2 = -\frac{1}{8\pi^2}\int \mathrm{Tr_f}\, F_{\mathrm{phys}} \wedge F_{\mathrm{phys}} = -q_{\mathrm{phys}}. \tag{X.4.24}$$

The positive D2 tension uses $|q_O| = |q_{\mathrm{phys}}|$. It does not identify the two sources' opposite oriented-instanton labels. In particular, Tr_O is not the fundamental trace of the kinetic action.

The one-loop sign will be the normalized anomaly convention in which a hypermultiplet contributes $+\mathrm{tr}_R\, F_O^4/24$ and a vector contributes $-\mathrm{tr_{adj}}\, F_O^4/24$. To see what these terms contain, restrict a traceless $SU(k)$ curvature to Cartan eigenvalues x_a with $\sum_a x_a = 0$. The adjoint nonzero weights are $x_a - x_b$. The quadratic sum is

$$\sum_{a,b}(x_a - x_b)^2 = 2k\sum_a x_a^2. \tag{X.4.25}$$

Expanding the fourth power, the terms cubic in one eigenvalue vanish by tracelessness. The remaining terms give

$$\sum_{a,b}(x_a - x_b)^4 = 2k\sum_a x_a^4 + 6\left(\sum_a x_a^2\right)^2, \tag{X.4.26}$$

or, in the defined traces,

$$\mathrm{tr_{adj}}\, F_O^4 = 2ku_i + 6s_i^2, \qquad \mathrm{tr_{adj}}\, F_O^2 = 2ks_i. \tag{X.4.27}$$

The zero Cartan weights do not change these positive-degree traces. For $k = 5$, for example, the adjoint fourth trace is $10u + 6s^2$. The coefficient ten comes from the pair of root sums, not from counting the 24 vector components as 24 fundamentals.

A full bifundamental hyper between $SU(k)$ and $SU(\ell)$ has weights $x_a - y_b$. Its quartic expansion gives a different, equally useful identity,

$$\mathrm{tr}_{(k,\bar{\ell})}\, F_O^4 = \ell u_k + k u_\ell + 6 s_k s_\ell. \tag{X.4.28}$$

In particular, a $(4, \bar{5})$ hyper contributes $5u_4 + 4u_5 + 6s_4 s_5$. The mixed term is essential. It is the only source of the adjacent-node quadratic-trace term in this chain. The analogous quadratic sum is

$$\mathrm{tr}_{(k,\bar{\ell})}\, F_O^2 = \ell s_k + k s_\ell. \tag{X.4.29}$$

At a flavor end, the flavor curvature is set to zero in the restricted polynomial below, but the hyper still contributes k copies of the gauged fundamental. Setting a flavor background to zero does not delete its matter field.

The local contributions can now be read in Table X.4.3. The coefficient of u_i from the vector is $-2V_i/24$; the two neighboring full hypers provide $(V_{i-1}+V_{i+1})/24$, and W_i D8 fundamentals add $W_i/24$. Thus

$$[I_{8,1\text{loop}}]_{u_i} = \frac{W_i + V_{i-1} + V_{i+1} - 2V_i}{24}. \tag{X.4.30}$$

For $V_i \geq 4$ this multiplies an independent quartic invariant. The rank condition (X.4.14) sets it to zero at each node, as the brane charge argument promised.

field seen by node i	coefficient of u_i	coefficient of s_i^2	adjacent $s_i s_j$
adjoint vector	$-2V_i/24$	$-6/24$	0
left full hyper	$V_{i-1}/24$	0	$6/24$ if gauged
right full hyper	$V_{i+1}/24$	0	$6/24$ if gauged
W_i D8 hypers	$W_i/24$	0	0

Table X.4.3: Pure-gauge fourth-trace contributions at one node in the normalized one-loop polynomial. An adjacent gauged link is one full bifundamental and its cross term is counted once for the pair; an exterior link has zero flavor curvature. The table represents (X.4.27) and (X.4.28), not a count of independent fields per node.

For the $(6,5,4)$ chain the three quartic numerators are

$$1+6+5-12=0, \qquad 0+6+4-10=0, \qquad 1+5+2-8=0. \tag{X.4.31}$$

Each zero uses a different part of the inventory. In particular, omitting the right exterior rank would change the last numerator to -2. This is the promised anomaly fingerprint of the D8/rank equation. It checks an irreducible local gauge obstruction; it is not an ultraviolet existence proof or a full background anomaly calculation for this flavored chain.

After the independent u_i pieces vanish, the vector's $-6s_i^2/24$ and the adjacent hyper's $+6s_is_{i+1}/24$ survive. They form the negative Cartan quadratic form

$$[I_{8,1\text{loop}}]_{\text{pure gauge}} = -\frac{1}{4}\sum_{i=1}^{n} s_i^2 + \frac{1}{4}\sum_{i=1}^{n-1} s_i s_{i+1} = -\frac{1}{8} s^{\mathsf{T}} A_n s. \tag{X.4.32}$$

For the unequal-rank chain, this is the pure-gauge reducible statement we need. We have not included its full flavored or gravitational background polynomial. For the equal-rank, flavor-curvature-zero chain, the vector's $-12ks_ic/24$ adds a mixed gauge–R term. The complete gauge-dependent one-loop piece in that restricted frame is

$$I_{8,1\text{loop}}^{\text{gauge}} = -\frac{1}{8} s^{\mathsf{T}} A_n s - \frac{k}{2} c\, \mathbf{1}^{\mathsf{T}} s. \tag{X.4.33}$$

The $s_i p_1$ coefficients cancel separately between the vector and its effective $2k$ fundamentals. This cancellation must be checked in the same source frame. A formula in an early brane discussion writes the reducible obstruction with the opposite overall sign and without this full normalized I_8 convention; it is a diagnostic of factorization, not an alternative sign for (X.4.33).

The p_1 cancellation can be seen explicitly at an interior equal-rank node. The vector contributes $-2ks_ip_1/48$. The left and right bifundamentals each contribute $+ks_ip_1/48$, so

$$[I_{8,1\text{loop}}]_{s_ip_1} = \frac{-2k+k+k}{48} = 0. \tag{X.4.34}$$

At the end node one of these hypers is an exterior flavor link. Its flavor curvature has been set to zero, but its gauge trace still contributes the same $+ks_ip_1/48$. This is why simply deleting end matter from a flavor-zero polynomial gives a false gravitational-mixed gauge anomaly as well as a false quartic coefficient.

For the unequal-rank $SU(6)\times SU(5)\times SU(4)$ chain, the pure-gauge part of (X.4.32) is concretely

$$I_{8,1\text{loop}}^{\text{pure gauge}} = -\frac{1}{4}(s_1^2+s_2^2+s_3^2)+\frac{1}{4}(s_1s_2+s_2s_3). \tag{X.4.35}$$

It is independent of the rank values once the quartics have cancelled, because the s_i^2 coefficient comes from the universal adjoint identity and each adjacent full hyper carries one universal cross term. This observation motivates the same A_3 quadratic form used for relative interval strings. It does not provide the full GS four-forms for the unequal-rank flavored theory, so we refrain from promoting (X.4.35) to a complete anomaly result.

There is a genuine low-rank qualification. For a traceless two- or three-eigenvalue matrix the characteristic equation implies

$$\operatorname{tr}_{\mathrm{f}} F_O^4 = \frac{1}{2}\big(\operatorname{tr}_{\mathrm{f}} F_O^2\big)^2, \qquad SU(2), SU(3). \tag{X.4.36}$$

For $SU(2)$, use eigenvalues $(x,-x)$; for $SU(3)$, use $(x,y,-x-y)$ and expand both sides. Hence u_i is not an independent obstruction there. One must first reduce the fourth trace to s_i^2 and then analyze the resulting reducible anomaly. The rank-four-and-above argument cannot simply be read as a universal $N_f = 2N_c$ condition at small rank, nor can a GS square cancel a genuinely independent quartic.

For clarity, the $SU(3)$ identity can be derived without a general trace theorem. Tracelessness gives $z=-x-y$, and expansion shows

$$x^4+y^4+z^4 = 2(x^2+y^2+xy)^2 = \frac{1}{2}(x^2+y^2+z^2)^2. \tag{X.4.37}$$

At $SU(4)$, choose $(x,-x,y,-y)$. The square of the quadratic trace contains $8x^2y^2$, whereas the fourth trace has no mixed x^2y^2 term. Thus the identity fails for a generic $SU(4)$ curvature and the coefficient of u_i must vanish independently. This Cartan comparison explains why our rank-four and larger examples can use (X.4.30) as an independent obstruction. It does not address global anomalies, which are separate from the local eight-form calculation.

X.4.5 Tensor strings cancel the gauge anomaly

The leftover expression (X.4.33) has exactly the shape that tensor fields can address. The appropriate pairing is not chosen merely to complete a square. Each elementary D2 interval string joins neighboring NS5-branes. Introduce N unit endpoint directions e_a and take the relative charges to be $d_i = e_i - e_{i+1}$ for $i = 1, \ldots, N-1$. Their integer Gram matrix is

$$A_{ij} = d_i \cdot d_j = 2\delta_{ij} - \delta_{i,j+1} - \delta_{i+1,j}. \tag{X.4.38}$$

Writing the rows d_i as a matrix D makes the origin of the pairing visible, $A = DD^{\mathsf{T}}$. For any nonzero relative vector v,

$$v^{\mathsf{T}} A v = \|D^{\mathsf{T}} v\|^2 > 0. \tag{X.4.39}$$

The common translation $(1, \ldots, 1)$ is in the kernel of D, not in the relative lattice paired by A. It is the free NS5 center tensor and is excluded from the interacting anomaly count.

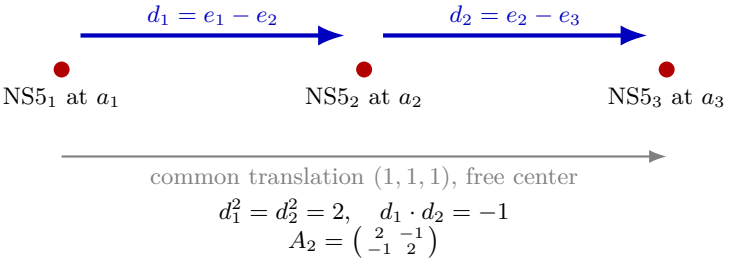


Figure X.4.3: Three ordered NS5 positions yield two oriented relative strings $d_1 = e_1 - e_2$ and $d_2 = e_2 - e_3$. These vectors have squared length two and $d_1 \cdot d_2 = -1$, giving the A_2 Gram matrix. Each arrow has $+e_i$ at its tail and $-e_{i+1}$ at its head. The separate gray translation direction is free; the diagram depicts tensor charge, not three-dimensional monopole flux.

Care is needed in translating the tensor indices of the anomaly source. It writes Bianchi four-forms with lower labels I_i and the numerical pairing with upper labels Ω^{ij}. We define our displayed arrays entry by entry as

$$X^i := I_i \text{ (source)}, \qquad A_{ij} := \Omega^{ij} \text{ (source)}, \qquad I_{8,\mathrm{GS}} = \frac{1}{2} X^{\mathsf{T}} A X. \tag{X.4.40}$$

This is a relabeling of two arrays, not the result of raising an I_i index with a metric. If we instead define the genuinely dual array $Y = AX$, then and only then may we write

$$I_{8,\mathrm{GS}} = \frac{1}{2} Y^{\mathsf{T}} A^{-1} Y. \tag{X.4.41}$$

Using A^{-1} directly with X would change the polynomial. The distinction will also separate this tensor-string lattice from the gauge cocharacters discussed at the end of the chapter.

For equal ranks k and zero flavor curvature, the source Bianchi forms translated to this basis have a direct solution. Let $\mathbf{1} = (1, \ldots, 1)^{\mathsf{T}}$ and set

$$X = \frac{s}{2} + kA^{-1}\mathbf{1}\, c. \tag{X.4.42}$$

Expanding the quadratic form independently of the loop expression gives

$$I_{8,\mathrm{GS}} = \frac{1}{8} s^{\mathsf{T}} A s + \frac{k}{2} c\, \mathbf{1}^{\mathsf{T}} s + \frac{k^2}{2} (\mathbf{1}^{\mathsf{T}} A^{-1} \mathbf{1}) c^2. \tag{X.4.43}$$

The first two terms cancel (X.4.33) term by term. The surviving c^2 term is a background $SU(2)_R$ anomaly. A consistent decoupled QFT can have an anomaly for a global symmetry. It cannot have the uncancelled dynamical gauge terms that have just disappeared.

The rank-four, two-node example permits every matrix entry to be seen. The relative-charge pairing and its inverse are

$$A_2 = \begin{pmatrix} 2 & -1 \\ -1 & 2 \end{pmatrix}, \qquad A_2^{-1} = \frac{1}{3} \begin{pmatrix} 2 & 1 \\ 1 & 2 \end{pmatrix}, \qquad A_2^{-1}\mathbf{1} = \begin{pmatrix} 1 \\ 1 \end{pmatrix}. \tag{X.4.44}$$

Consequently the two four-forms and the one-loop gauge terms are

$$X = \begin{pmatrix} s_1/2 + 4c \\ s_2/2 + 4c \end{pmatrix}, \qquad I_{8,1\mathrm{loop}}^{\mathrm{gauge}} = -\frac{s_1^2 - s_1 s_2 + s_2^2}{4} - 2c(s_1 + s_2). \tag{X.4.45}$$

Multiplication by the actual integral A_2 gives, without an inverse matrix substitution,

$$I_{8,\mathrm{GS}} = \frac{s_1^2 - s_1 s_2 + s_2^2}{4} + 2c(s_1 + s_2) + 16c^2. \tag{X.4.46}$$

Thus one-loop plus GS is independent of s_1, s_2. The two tensor four-forms are not arbitrary tunable counterterms; their pairing follows from the oriented interval strings and their source coupling.

The inverse matrix also gives an efficient general calculation. Write $z = A^{-1}\mathbf{1}$ and impose $z_0 = z_N = 0$. The equations are

$$2z_i - z_{i-1} - z_{i+1} = 1, \qquad i = 1, \ldots, N-1. \tag{X.4.47}$$

The quadratic sequence $z_i = i(N-i)/2$ satisfies both the difference equation and the endpoints. Therefore

$$\mathbf{1}^{\mathsf{T}} A^{-1} \mathbf{1} = \sum_{i=1}^{N-1} \frac{i(N-i)}{2} = \frac{N^3 - N}{12}. \tag{X.4.48}$$

For completeness, the Green function of the same Dirichlet difference operator has entries

$$(A^{-1})_{ij} = \frac{\min(i,j)\,[N - \max(i,j)]}{N}. \tag{X.4.49}$$

The cubic $N^3 - N$ growth is therefore a consequence of summing a quadratic solution along the chain, not a fit to a few low-rank examples.

A nonuniform background shift first appears with three relative tensors. For $N = 4$, $k = 4$, the construction has

$$A_3 = \begin{pmatrix} 2 & -1 & 0 \\ -1 & 2 & -1 \\ 0 & -1 & 2 \end{pmatrix}, \qquad A_3^{-1}\mathbf{1} = \begin{pmatrix} 3/2 \\ 2 \\ 3/2 \end{pmatrix}. \tag{X.4.50}$$

Its Bianchi four-forms are

$$X = \begin{pmatrix} s_1/2 + 6c \\ s_2/2 + 8c \\ s_3/2 + 6c \end{pmatrix}. \tag{X.4.51}$$

The larger middle entry follows from the full Dirichlet solution $z_i = i(N - i)/2$, rather than from the local number of neighbors alone. Inserting this X into the integral pairing gives

$$I_{8,\mathrm{GS}} = \frac{1}{4}\left(\sum_{i=1}^{3} s_i^2 - s_1 s_2 - s_2 s_3\right) + 2c\sum_{i=1}^{3} s_i + 40c^2. \tag{X.4.52}$$

The first two pieces cancel the three-node version of (X.4.33); the last follows independently from $16(3/2 + 2 + 3/2)/2 = 40$. This example shows that $A^{-1}\mathbf{1}$ is sensitive to position along the chain. Assigning every tensor the same shift merely because all gauge ranks are equal would fail already for four NS5-branes.

To retain all gravitational and R backgrounds, count multiplets with their representation dimensions. There are N full bifundamentals, including the two flavor ends, $N - 1$ adjoint vectors, and $N - 1$ interacting tensors. Their weighted counts are

$$H = Nk^2, \qquad V = (N - 1)(k^2 - 1), \qquad T = N - 1. \tag{X.4.53}$$

Here H is a weighted quaternionic count. It is not the number N of links in the drawing. For $N = 3, k = 4$ this gives

$$(H, V, T) = (48, 30, 2). \tag{X.4.54}$$

The source's multiplet polynomials, with flavor curvature zero, contribute the following background pieces before GS:

$$\begin{aligned} I_{8,H}^{\mathrm{back}} &= H\,\frac{7p_1^2 - 4p_2}{5760}, \\ I_{8,V}^{\mathrm{back}} &= -V\left(\frac{c^2}{24} + \frac{cp_1}{48} + \frac{7p_1^2 - 4p_2}{5760}\right), \\ I_{8,T}^{\mathrm{back}} &= T\left(\frac{c^2}{24} + \frac{cp_1}{48} + \frac{23p_1^2 - 116p_2}{5760}\right). \end{aligned} \tag{X.4.55}$$

These terms already include the interacting tensor contribution and do not include a free center tensor. The one-loop gauge terms used above are the other pieces of the same vector and hyper polynomials.

For the concrete A_2 chain, the c^2 coefficient is visibly assembled from the three sources,

$$[I_8]_{c^2} = -\frac{30}{24} + \frac{2}{24} + 16 = \frac{89}{6}. \tag{X.4.56}$$

The remaining three coefficients follow without an unexplained quoted answer:

$$\begin{aligned} [I_8]_{cp_1} &= \frac{-30+2}{48} = -\frac{7}{12}, \\ [I_8]_{p_1^2} &= \frac{(48-30)7 + 2\cdot 23}{5760} = \frac{43}{1440}, \\ [I_8]_{p_2} &= \frac{(48-30)(-4) + 2(-116)}{5760} = -\frac{19}{360}. \end{aligned} \tag{X.4.57}$$

The complete restricted background result for this example is hence

$$I_8\big|_{F_{\text{flavor}}=0} = \frac{89}{6}c^2 - \frac{7}{12}cp_1 + \frac{43}{1440}p_1^2 - \frac{19}{360}p_2. \tag{X.4.58}$$

This is a four-coefficient polynomial after dynamical gauge cancellation, not the full polynomial with nonzero flavor backgrounds.

The same steps give the equal-rank family as a further check. Combining (X.4.48), (X.4.53) and (X.4.55) yields

$$\begin{aligned} I_8\big|_{F_{\text{flavor}}=0} = &\frac{(N^3-N)k^2 - (N-1)(k^2-2)}{24}c^2 \\ &- \frac{(N-1)(k^2-2)}{48}cp_1 \\ &+ \frac{7k^2 + 30(N-1)}{5760}p_1^2 - \frac{4k^2 + 120(N-1)}{5760}p_2. \end{aligned} \tag{X.4.59}$$

At $N = 2$, $A = (2)$ and $A^{-1} = (1/2)$, while one $SU(k)$ node sees $2k$ effective fundamentals. This one-node limit checks both the inverse pairing and the matter count. We require $k \geq 4$ for the independent quartic argument and do not treat the formal $N = 1$ substitution as an empty physical theory.

One last count prevents a misleading interpretation. In the $N = 3, k = 4$ example, $H - V + 29T = 48 - 30 + 58 = 76$. The familiar number 273 is a gravitational-anomaly constraint for a six-dimensional supergravity system, not a requirement that this decoupled QFT's background anomaly vanish. Adding the free NS5 center tensor to T would change all four background coefficients, but it would mix a decoupled multiplet with the relative sector we are calculating. The tensor center is also distinct from every trace $U(1)$ removed by the local Stückelberg mechanism.

X.4.6 Decoupling gravity and the conformal point

The anomaly calculation concerns a candidate low-energy QFT on a positive tensor vacuum. It does not say that every limit of the brane picture is the same theory. Three operations should be kept apart: making the string length small while retaining a

positive tensor coordinate, moving those coordinates to zero in a decoupled theory, and compactifying a worldvolume direction. Their light states and dimensional couplings differ.

First consider the finite interval at an energy well below its geometric and string scales. A useful perturbative regime requires

$$E \ll \min_i L_i^{-1}, \qquad E \ll (\alpha')^{-1/2}, \qquad g_{6,i}^2 E^2 \ll 1. \tag{X.4.60}$$

The first inequality excludes interval excitations, the second excludes fundamental oscillator states, and the third makes the dimensionful gauge interaction weak at the chosen energy. The D2 strings remain present at tension $8\pi^2\phi_i$ even when the point-particle gauge theory is an adequate low-energy approximation. The gauge theory cannot describe all string excitations when their tension is sent to zero.

The zero-D8 rank-four example permits a transparent formal scaling. Put $\alpha' = \epsilon^2\alpha'_0$, hold a small g_s and each ϕ_i fixed, and choose $L_i = \epsilon^3 L_{i,0}$. The D6 coupling indeed stays fixed, because

$$g_7^2 \propto g_s\epsilon^3, \qquad \phi_i = \frac{L_i}{g_7^2} \propto \epsilon^0. \tag{X.4.61}$$

The two high-energy thresholds move away at different rates,

$$M_{\mathrm{KK,i}} \sim L_i^{-1} \propto \epsilon^{-3}, \qquad M_{\mathrm{osc}} \sim (\alpha')^{-1/2} \propto \epsilon^{-1}. \tag{X.4.62}$$

At the same time, the string tension stays finite and the bulk gravitational coupling decreases,

$$T_i = 8\pi^2\phi_i \propto \epsilon^0, \qquad \kappa_{10}^2 \propto g_s^2(\alpha')^4 \propto \epsilon^8. \tag{X.4.63}$$

These are scale statements in the leading local, massless-IIA patch. They are conditional on the existence of the decoupled brane theory; the powers of ϵ alone do not construct the interacting six-dimensional completion. The D8 example has a varying Romans background and is not assigned the same universal scaling argument here.

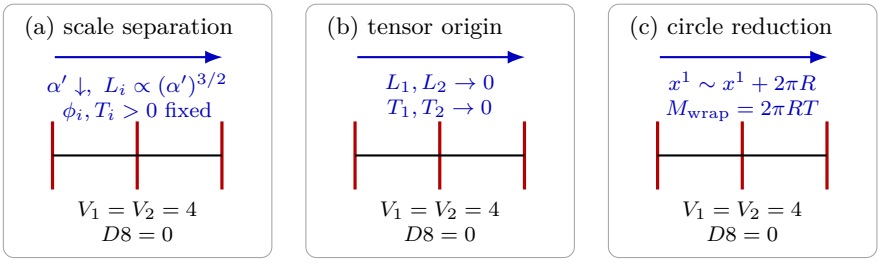


Figure X.4.4: Three distinct operations applied to the same three-NS5, two-interval rank-four chain. Panel (a) shrinks α' and both L_i at fixed positive ϕ_i, raising KK and oscillator scales. Panel (b) moves the same relative NS5 positions together after decoupling, making both D2 strings tensionless. Panel (c) compactifies x^1, the spatial direction of the D2=016 string already specified, on a circle of radius R. That string winding the circle becomes a five-dimensional particle. The arrows represent parameter operations, not a brane motion that changes the ranks.

At the tensor origin we instead take $\phi_i \to 0$ in the decoupled system. Equation (X.4.5) then forces the corresponding D2-string tension to vanish. In the rank-four, two-node example, moving only a_2 toward a_1 closes the first interval but leaves the second positive; the simultaneous relative origin requires $L_1, L_2 \to 0$. A BPS string becoming tensionless is new light physics, not a better perturbative gauge expansion. The source identifies a six-dimensional fixed-point interpretation for the appropriate configuration. Its dynamics does not follow merely by inserting $L = 0$ into the leading D6 action. Perturbative Yang–Mills control is lost because $g_{6,i}^2 E^2 = E^2/\phi_i$ diverges at fixed positive energy, while the D2 strings become tensionless. The formal interval KK scale $1/L_i$ increases as the interval shrinks.

Nor is taking $g_s \to 0$ at fixed α' automatically the same as removing all extended string degrees of freedom. The fundamental string scale remains finite in that operation. In specified compact and dual frames, the source discusses a gravity-decoupled little-string regime at fixed string length. That argument is not a blanket construction of a massive-IIA completion for every local D8 distribution. The lesson is physical: gravity can become weak while finite-tension string excitations remain in the decoupled sector. The parameter that removes gravity and the parameter that sends an interval D2 tension to zero answer different questions.

Now compactify a worldvolume direction on a circle of circumference $2\pi R$, staying in a zero-mode regime. Integrating the same kinetic term as before gives

$$\frac{1}{g_{5,i}^2} = \frac{2\pi R}{g_{6,i}^2} = 2\pi R \phi_i. \tag{X.4.64}$$

The dimensions are consistent: $[g_5^2] = \text{mass}^{-1}$, while $[g_6^2] = \text{mass}^{-2}$ and $[R] = \text{mass}^{-1}$. A D2 string wrapped on that circle becomes a particle with mass

$$M_{i,\text{wrapped}} = 2\pi R T_i = \frac{16\pi^3 R}{g_{6,i}^2}. \tag{X.4.65}$$

This is a direct kinematic consequence of its six-dimensional tension. It does not say that the six-dimensional vector multiplet had a Coulomb scalar. The scalar of a reduced five-dimensional vector can arise from a component along the circle, but that is a statement about a different effective theory and its compactification regime.

There is also a useful order-of-limits check. At fixed positive ϕ_i, $R \to 0$ makes the wrapped particle light according to (X.4.65), while the six-dimensional string remains tense. At fixed R, $\phi_i \to 0$ makes both the six-dimensional string and its wrapped particle light. The same vanishing five-dimensional mass can therefore arise from two physically different operations. A proposed five-dimensional or three-dimensional dictionary must specify which operation it uses before matching spectra or moduli spaces.

The dimensionless ratios expose the distinction more directly. At positive fixed ϕ_i, the tension defines a dimensional scale $\sqrt{T_i}$; this does not determine an excitation spectrum or gap. Under the ϵ scaling above, the oscillator and interval thresholds move far above this tension scale:

$$\frac{M_{\text{osc}}}{\sqrt{T_i}} \propto \epsilon^{-1}, \qquad \frac{M_{\text{KK,i}}}{\sqrt{T_i}} \propto \epsilon^{-3}. \tag{X.4.66}$$

The D2 string is retained while those two kinds of microscopic excitation are removed. At a later tensor-origin limit with the microscopic scales already removed, $\sqrt{T_i} \to 0$ relative to any fixed positive energy. Perturbative Yang–Mills is then precisely the wrong description for the new string degrees of freedom, even though one may still write $g_{6,i}^2 = 1/\phi_i$ formally.

Circle reduction gives another pair of scales: the worldvolume-circle KK energy $1/R$ and the mass of an interval string wrapped on it. Their ratio is

$$\frac{M_{i,\mathrm{wrapped}}}{M_{\mathrm{KK,circle}}} = 2\pi R^2 T_i = 16\pi^3 R^2 \phi_i. \tag{X.4.67}$$

If $16\pi^3 R^2 \phi_i \ll 1$, the wrapped string can be light even when circle KK modes are heavy. This is a particle in the reduced description, not a new fundamental interval gauge boson. In the opposite regime it is heavier than the first circle KK excitation. A comparison between a five-dimensional particle spectrum and six-dimensional strings must therefore state $R^2\phi_i$, not just a relation between g_5 and g_6.

Each limit has a different object held fixed. The local $\alpha' \to 0$ scaling fixes the positive tensor coordinates and compares them with diverging microscopic masses. At the conformal point the tensor coordinates themselves change and the interacting string sector survives. Circle reduction fixes a radius and changes which states are particles after wrapping. A protected anomaly computed on the tensor branch can constrain the fixed point without making perturbative Yang–Mills a complete description of it.

X.4.7 What a magnetic quiver must still supply

The construction so far supplies six-dimensional tensor-branch data: gauge ranks, flavor links, relative-string charges, and a restricted anomaly. It does not produce a three-dimensional magnetic quiver. That later object has its own compact gauge group, monopole flux lattice and Coulomb-branch coordinate ring. A claim that this Coulomb branch equals a Higgs branch of the six-dimensional system must specify the tensor-vacuum regime, any decoupled factors, and the precise global group on both sides.

The lattice distinction is particularly sharp. For our chosen simply connected semisimple gauge cover, a cocharacter at node i is represented by integer diagonal entries with zero sum,

$$\lambda_i = \mathrm{diag}(m_{i,1}, \dots, m_{i,V_i}), \qquad m_{i,a} \in \mathbb{Z}, \qquad \sum_a m_{i,a} = 0, \tag{X.4.68}$$

modulo the node Weyl group. This is neither an arbitrary $PSU(V_i)$ coweight nor the full cocharacter set of the initial $U(V_i)$ Chan–Paton factor. Endpoint fundamentals and bifundamentals must also descend to any proposed center quotient. For instance, a fundamental weight detects a fractional $PSU(4)$ cocharacter that would not be allowed on an isolated $SU(4)$ cover with the stated matter.

The interval-string lattice instead has generators d_i and pairing A_n, as in (X.4.38). Its dual has pairing A_n^{-1}; the finite discriminant group records the difference between

that dual and the integral root lattice. Neither this discriminant group nor the matrix inverse by itself determines a quotient of the gauge group. A three-dimensional monopole lattice belongs to the magnetic quiver's own compact gauge group and will be defined afresh in Chapter 5. Matching a protected ring or a branch of moduli space is a specific claim about those objects. It is not, by itself, an equality of complete QFTs or a general IIA/M-theory lift. Here the sourced six-dimensional field content and anomaly can be compared; the precise massless lift is treated later.

X.4.8 Exercises

The first four questions admit a bounded algebraic check, but a complete solution must show the indicated reasoning. The fifth question is written work. All use the conventions of this chapter.

1. Four ordered NS5-branes bound D6 intervals of ranks $(6, 5, 4)$, with exterior ranks 6 and 2. Use $m_i = V_{i-1} - V_i$ and a positive D8 jump toward increasing x^6. Find all four m_i, all three W_i, and the effective fundamental multiplicity at each SU node, including the neighboring bifundamentals. Explain why the exterior ranks label flavors rather than additional six-dimensional gauge nodes.

2. For traceless $SU(5)$ curvature, derive constants a, b in $\operatorname{tr}_{\mathrm{adj}} F^4 = a \operatorname{tr}_{\mathrm{f}} F^4 + b(\operatorname{tr}_{\mathrm{f}} F^2)^2$. For a full $(4, \bar{5})$ hyper, derive the three coefficients of $\operatorname{tr}_4 F_4^4$, $\operatorname{tr}_5 F_5^4$ and $\operatorname{tr}_4 F_4^2 \operatorname{tr}_5 F_5^2$. Use Cartan weights, and explain why the independent-quartic step changes for $SU(2)$ and $SU(3)$.

3. In the $[SU(4)] - SU(4) - SU(4) - [SU(4)]$ example, take $s_i = \operatorname{tr}_{\mathrm{f}} F_{O,i}^2$, $c = c_2(R)$ and $A = \left(\begin{smallmatrix} 2 & -1 \\ -1 & 2 \end{smallmatrix}\right)$. The gauge-dependent one-loop term is $-(s_1^2 - s_1 s_2 + s_2^2)/4 - 2c(s_1 + s_2)$. Find the two coefficients v_i in $X^i = s_i/2 + v_i c$ and expand the entire $I_{8,\mathrm{GS}} = X^{\mathsf{T}} A X/2$, including the background term. Explain why that remaining background term is compatible with gauge consistency. Use the entrywise source-to-book array translation given in (X.4.40).

4. For the same $N = 3, k = 4$ chain, compute A^{-1} and the weighted counts (H, V, T) with the free NS5 center excluded. A hyper of dimension d contributes $d(7p_1^2 - 4p_2)/5760$ to the gravitational terms; a vector contributes $-d[c^2/24 + cp_1/48 + (7p_1^2 - 4p_2)/5760]$; a tensor contributes $c^2/24 + cp_1/48 + (23p_1^2 - 116p_2)/5760$. Add the GS term from the previous question and determine, in order, the four coefficients of c^2, cp_1, p_1^2, p_2. Explain why the resulting decoupled theory is not required to obey $H - V + 29T = 273$.

5. Compare shrinking α' at fixed positive ϕ_i, sending all relative ϕ_i to zero after decoupling, and compactifying a worldvolume circle. State the behavior of $g_{6,i}$, interval KK scales, D2 tensions, and wrapped-string masses in each operation. Explain why $g_s \to 0$ at fixed string length can leave little-string excitations. Finally distinguish the original $U(V_i)$ Chan–Paton cocharacters, our chosen $SU(V_i)$ cover cocharacters, the A_n tensor-string lattice and a future three-dimensional monopole

lattice. What further physical data would be needed for a complete global-form or magnetic-quiver claim?

X.4.9 Take-home message

Take-home message

An ordered NS5–D6–D8 chain gives six-dimensional gauge intervals whose relative NS5 separations are tensor scalars. The leading normalized D6 action and the stretched D2 agree on $T_i = 8\pi^2/g_{6,i}^2$. Positive D8 charge imposes $W_i = 2V_i - V_{i-1} - V_{i+1}$, exactly the condition that removes the independent $\operatorname{tr} F_i^4$ obstruction at rank at least four. The remaining gauge-dependent anomaly is cancelled by the integral pairing of interval strings. For two rank-four nodes, the surviving flavor-zero background polynomial is $89c^2/6 - 7cp_1/12 + 43p_1^2/1440 - 19p_2/360$. The finite tensor vacuum, tensionless-string origin, compactified theory and future magnetic-quiver Coulomb branch answer different physical questions.

Status and sources

The coordinate inventory, six-dimensional fields, local trace-$U(1)$ mechanism, D2 string and tensor-branch interpretation in Sections X.4.1–X.4.2 follow Hanany and Zaffaroni (1998a, printed pp. 3–6, Fig. 1 and eqs. (2.1)–(2.6)) and Brunner and Karch (1997, printed pp. 9–11, Fig. 4). The numerical g_7 and T_{D2} factors follow the stated brane-action normalization and the displayed leading DBI reduction [MATH]; the original source's coupling and tension wording is schematic. The normalized equality is local and does not assert an exact warped D8 reduction. The $(0,1)$ to $(1,0)$ name translation converts the source's (NS,D) order to the book's (D,NS) order.

Section X.4.3 uses Hanany and Zaffaroni (1998a, printed pp. 10–11, eq. (2.13)) and the underlying IIA endpoint charge argument in Hanany and Zaffaroni (1998b, printed pp. 13, 15–17, Figs. 2–3 and eqs. (2.10), (3.1)–(3.2)). The latter source uses NS′=012389, D6=0123789, D8=012345689 and suspension x^7. Its signed coordinate relabeling to our axes is $(x^4,x^5,x^6,x^7,x^8,x^9)_{\text{source}} \mapsto (x^7,x^8,-x^9,x^6,x^4,x^5)_{\text{book}}$, with orientation preserved; the endpoint sign is independently fixed by the first citation. The $(6,5,4)$ ranks are a local specialization of the sourced family [MATH] subject to its physical brane premise [DEC]. No full massive-IIA completion or dimensionful F_0 normalization follows.

Sections X.4.4–X.4.5 use the normalized multiplet polynomials, trace identities, tensor pairing and relative spectrum in Ohmori et al. (2014, printed pp. 5–8, 25–26, eqs. (1.12)–(1.21), (2.3)–(2.8) and (A.1)–(A.8)). The convention is $F_O = -iF_{\text{phys}}/(2\pi)$ and $X^i := I_i$, $A_{ij} := \Omega^{ij}$ entry by entry. The local quartic factorization discussion in Brunner and Karch (1997, printed pp. 9–10) writes an oppositely signed unnormalized obstruction, not the full source-frame I_8 used here. The independent quartic calculation assumes $V_i \geq 4$; the $SU(2)$ and $SU(3)$ identity is treated separately. Pure-gauge unequal-rank cancellation is [ANOM]; its full flavored anomaly has not been calculated

here. For equal rank $k \geq 4$, zero flavor curvatures and no free center tensor, the four displayed background coefficients are [ANOM]. The anomaly calculation compares sourced field content and does not transfer a full-QFT identity from a massless M-theory description.

The finite-tensor and fixed-point interpretation in Section X.4.6 uses Hanany and Zaffaroni (1998a, printed p. 12 and pp. 30–31) and Brunner and Karch (1997, printed pp. 10–11). The formal ϵ scaling and circle zero-mode equations are conditional calculations [MATH]/ [DEC]; they do not construct a general massive-IIA decoupling limit. The known source's fixed-point premise is separate from the vanishing of a leading DBI length. The six-dimensional tensor-charge lattice and the simply connected gauge cover used here are distinct from the three-dimensional magnetic quiver's still-to-be-specified compact group. Residual discrete Stückelberg and correlated flavor quotients are outside the present global-form calculation. No complete IIA/M-theory lift, full QFT duality or magnetic-quiver ring is asserted in this chapter.

References

Brunner, I. and A. Karch (1997). "Branes and six-dimensional fixed points". In: *Phys. Lett. B* 409, pp. 109–116. DOI: 10.1016/S0370-2693(97)00935-0. arXiv: hep-th/9705022.

Hanany, A. and A. Zaffaroni (1998a). "Branes and six-dimensional supersymmetric theories". In: *Nucl. Phys. B* 529, pp. 180–206. DOI: 10.1016/S0550-3213(98)00355-1. arXiv: hep-th/9712145.

Hanany, A. and A. Zaffaroni (1998b). "Chiral symmetry from type IIA branes". In: *Nucl. Phys. B* 509, pp. 145–168. DOI: 10.1016/S0550-3213(97)00595-6. arXiv: hep-th/9706047.

Ohmori, K. et al. (2014). "Anomaly polynomial of general 6d SCFTs". In: *PTEP* 2014.10, 103B07. DOI: 10.1093/ptep/ptu140. arXiv: 1408.5572 [hep-th].

Chapter X.5

Magnetic quivers and Coulomb-branch geometry

X.5.1 A Higgs branch seen through a different theory

At the origin of a five-dimensional brane web, two pieces of the web can move independently even though a weak-coupling gauge description sees only one configuration. The new flat directions belong to its Higgs branch. A direct description by five-dimensional hypermultiplet expectation values can miss them when instanton particles become massless. A magnetic quiver gives a different route to the same geometric question. It assigns a three-dimensional $\mathcal{N} = 4$ gauge theory to the chosen brane phase, then studies the *Coulomb branch of that three-dimensional theory.*

We will keep the two sides of this assignment distinct. Write $\mathcal{H}_{5d}(P)$ or $\mathcal{H}_{6d}(P)$ for the Higgs branch in a specified higher-dimensional phase P, and $\mathcal{C}_{3d}(Q_P)$ for the Coulomb branch of the proposed magnetic quiver Q_P. The physical proposal has the form $\mathcal{H}_{5d/6d}(P) \simeq \mathcal{C}_{3d}(Q_P)$. It concerns a moduli space in a stated phase. The spacetime dimensions, microscopic theories and their metrics are not identified by this equation. The calculation in this chapter starts on the right, after the compact three-dimensional gauge group and matter charges have been specified.

There are three progressively stronger statements in play. One can calculate a Hilbert series for a declared quiver. One can identify its coordinate ring, including multiplication and relations. One can then propose that this ring describes the Higgs geometry of a particular higher-dimensional theory. The first statement does not imply the second, because a graded vector-space count need not fix products. The second does not imply the third, because the brane construction must select both the graph and the correct phase. The examples below make each implication, and its extra input, explicit.

The first physical object is the massless, infinite-coupling origin of five-dimensional $SU(2)$ theory with two fundamental hypermultiplets. Its source web has two maximal decompositions. One leads to a triangular quiver and a quaternionic two-dimensional cone; the other leads to a double edge and a quaternionic one-dimensional cone. The

proposed Higgs space is their union at a common origin. The second object has two separated M5 branes on an A_1 singularity, at a finite relative tensor expectation value. Its electric description is six-dimensional $SU(2)$ with four full flavors. The proposed magnetic quiver has a central $U(2)$ node and four separate $U(1)$ leaves. Its Coulomb dimension is five, matching a regular Higgs dimension calculation on the electric side.

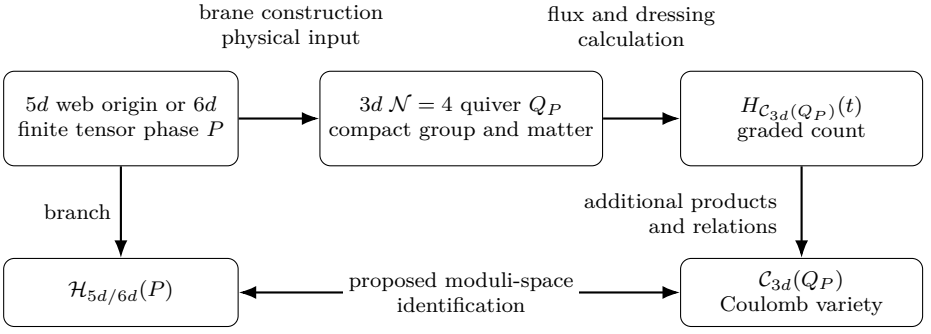


Figure X.5.1: The arrows used in this chapter. A specified five-dimensional web limit or six-dimensional tensor phase supplies a magnetic quiver by a physical construction. The monopole sum computes a protected graded count of the resulting three-dimensional Coulomb branch. Identifying that branch with the higher-dimensional Higgs space is an additional physical step.

Why use the word *magnetic*? In the quiver, coordinates on $\mathcal{C}_{3d}$ include monopole operators labelled by magnetic flux. Their dressing by residual vector-multiplet scalars gives a tractable graded ring. This is not the real-scalar Coulomb branch of the original five-dimensional gauge theory. In particular, the word does not turn the five-dimensional Coulomb expectation value into a three-dimensional monopole charge. We first build the compact flux dictionary, then calculate an abelian surface and an affine cycle. Only after those examples do we return to the five- and six-dimensional brane systems.

X.5.2 Compact gauge data and the monopole sum

Which magnetic charges enter a Coulomb-branch count? A quiver drawing gives node ranks and edges, but a flux sum also needs the *compact gauge group*. For compact G, magnetic charges are cocharacters of G modulo its Weyl group. A quotient by a central circle can change both this lattice and the scalar dressings. We use circular nodes for gauge factors and square nodes for flavor factors. An edge of multiplicity e means e full bifundamental hypermultiplets. For each full hypermultiplet in $R \oplus \overline{R}$, the weight sum below runs over R once: its pair of $\mathcal{N} = 2$ chirals is already accounted for. Thus n charge-one full hypers contribute $n|m|$ to 2Δ, not $2n|m|$.

For a good or ugly three-dimensional $\mathcal{N} = 4$ theory without a Chern–Simons coupling, let m denote a GNO cocharacter. With the book's grading $t^{2\Delta}$, the bare

monopole has degree

$$2\Delta(m) = \sum_{\text{full hypers } R} \sum_{\rho \in R} |\rho(m)| - 2 \sum_{\alpha > 0} |\alpha(m)|. \tag{X.5.1}$$

The first term counts hypermultiplet weights. The second subtracts the positive roots of the vector multiplet. At a fixed flux, the unbroken centralizer $H_m \subseteq G$ supplies invariant scalar polynomials. If its Casimir degrees are d_j, their dressing factor is

$$P_G(t; m) = \prod_j (1 - t^{2d_j})^{-1}. \tag{X.5.2}$$

The protected Hilbert series is the sum of these dressed sectors,

$$H_G(t) = \sum_{m \in \mathrm{cochar}(G)/W_G} t^{2\Delta(m)} P_G(t; m). \tag{X.5.3}$$

An optional topological fugacity can retain a flux charge instead of setting it to one. The formula is useful here because every selected example has a nonnegative, locally finite grading. In a bad theory the ultraviolet monopole dimension need not be the exact infrared grading, so the same manipulation would need new input.

The dressing factor deserves a direct explanation. A monopole flux breaks some gauge generators and leaves a group H_m unbroken. The complex scalar in its vector multiplet can multiply the bare monopole without changing the flux. Gauge-invariant polynomials in that scalar produce one geometric series for every independent homogeneous generator. If $H_m = U(1)^r$, all r generators have degree one as Casimirs, hence physical grading degree two and factor

$$P_{U(1)^r}(t; m) = (1 - t^2)^{-r}. \tag{X.5.4}$$

If the residual group is $U(2)$, symmetric polynomials in its two eigenvalues are generated by a trace and determinant of Casimir degrees one and two. That produces the first factor in (X.5.6). Thus the dressing change across $a = b$ is a change in the stabilizer of the flux, rather than a numerical exception inserted into the series.

The same weights also explain the matter term. For a full bifundamental between $U(2)$ with flux (a, b) and a rank-one node with flux l, the two central weights contribute

$$2\Delta_{\text{edge}} = |a - l| + |b - l|. \tag{X.5.5}$$

Four distinct leaves give four copies with independently chosen l_i. The central $U(2)$ positive root contributes $-2|a - b|$. This small calculation previews the affine D_4 sum and shows why node ranks alone cannot supply its coefficient. By comparison, an edge between two rank-one circles has the single contribution $|m_i - m_j|$, the ingredient of the affine triangle.

A $U(2)$ node already shows why a flux sum cannot be replaced by a count of node ranks. Diagonalize its cocharacter and order the integers $a \leq b$. At $a = b$, the full $U(2)$ remains, with Casimir degrees one and two. At $a < b$, only $U(1)^2$ remains, with two degree-one Casimirs. Before any central quotient, the two dressings are therefore

$$P_{U(2)}(t; a, a) = \frac{1}{(1 - t^2)(1 - t^4)}, \qquad P_{U(2)}(t; a, b) = \frac{1}{(1 - t^2)^2} \quad (a < b). \tag{X.5.6}$$

For example, $(a,b)=(0,1)$ breaks $U(2)$ to two circles, while $(0,0)$ does not. Equal and unequal central fluxes will consequently contribute different coefficients to the affine D_4 example.

$U(2)$ flux	residual central group	Casimir degrees	scalar factor
(a,a)	$U(2)$	$1,2$	$(1-t^2)^{-1}(1-t^4)^{-1}$
(a,b), $a<b$	$U(1)^2$	$1,1$	$(1-t^2)^{-2}$

Table X.5.1: One node with two different residual groups. The remaining factors of a larger quiver must be included before taking a common central quotient.

The gauge group also determines whether a common circle is physical. On a connected unitary graph with only bifundamental matter, simultaneous central phases can act trivially on every hypermultiplet. In the examples below we specify the *primitive* quotient by this circle. It removes one scalar Casimir and one entire common-flux direction. These are two parts of one compact-group decision, not two optional corrections to a series. A physical central factor with Chern–Simons or BF couplings would require its own analysis before any such quotient.

The quotient can be understood directly from charges. On an edge from node i to node j, a simultaneous central phase $e^{i\theta}$ acts as $e^{i\theta}e^{-i\theta}=1$. A common flux similarly changes both endpoint cocharacters by the same integer, leaving their difference fixed. For three rank-one nodes this action is generated by $(1,1,1)$, whose integer components have greatest common divisor one. The quotient lattice therefore has no torsion:

$$[m_0,m_1,m_2]\longmapsto(0,m_1-m_0,m_2-m_0)\quad\text{is an integral bijection.}\tag{X.5.7}$$

Deleting the common flux while retaining its scalar would be a different, inconsistent operation. Conversely, retaining the flux can leave infinitely many zero-degree sectors. The flux and scalar tests must be applied together before any series expansion.

The series records dimensions of graded spaces of chiral operators. A coefficient can suggest a symmetry representation, but a few matching coefficients do not construct an isomorphism of branches. The calculation below keeps that distinction visible. Chapter 7 develops broader Hilbert-series and stratification methods; the present chapter needs only the precise flux and dressing data of four small objects.

X.5.3 The charge-one SQED ring

The smallest complete calculation begins with compact $U(1)$ and $n\geq 2$ full charge-one hypermultiplets. Its integral magnetic lattice is $m\in\mathbb{Z}$. There are no positive roots, and the unbroken vector scalar remains at every flux. Calling that scalar ϕ, its degree is two. Equation (X.5.1) becomes

$$2\Delta(m)=\sum_{i=1}^{n}|m|=n|m|.\tag{X.5.8}$$

The primitive monopoles V_+ and V_- carry flux $+1$ and -1, respectively, so each has degree n. A fugacity z for topological charge retains the distinction between them.

The sum over nonzero fluxes consists of two geometric tails. Writing $q = t^n$ makes their resummation transparent,

$$H_n(t,z) = \frac{1}{1-t^2}\sum_{m\in\mathbb{Z}} z^m t^{n|m|} = \frac{1}{1-t^2}\left(1 + \frac{zq}{1-zq} + \frac{z^{-1}q}{1-z^{-1}q}\right). \tag{X.5.9}$$

Combining the two tails gives the exact rational function

$$H_n(t,z) = \frac{1-t^{2n}}{(1-t^2)(1-zt^n)(1-z^{-1}t^n)}. \tag{X.5.10}$$

The denominator has the degrees and charges of ϕ, V_+, V_-, and the numerator has the degree of one relation. This observation counts a candidate presentation. The actual physical operator product is a separate input from the Coulomb-ring construction,

$$V_+V_- = \phi^n. \tag{X.5.11}$$

It would be an error to deduce this operator product solely from the numerator. Distinct multiplication laws can share a Hilbert series.

There is, however, a direct algebraic proof of the abstract hypersurface presentation once the physical generators and product are known. Let $\omega^n = 1$ act on $\mathbb{C}[u,v]$ by

$$(u,v) \longmapsto (\omega u, \omega^{-1}v). \tag{X.5.12}$$

A monomial $u^r v^s$ is invariant exactly when $r - s \equiv 0 \pmod n$. If $r \geq s$, write it as $(uv)^s(u^n)^{(r-s)/n}$; if $s \geq r$, write it as $(uv)^r(v^n)^{(s-r)/n}$. Thus every invariant has a normal form built from three elements,

$$X = u^n, \qquad Y = v^n, \qquad P = uv, \qquad XY = P^n. \tag{X.5.13}$$

The two normal-form families meet only on powers of P, so this relation accounts for their overlap. Consequently

$$\mathbb{C}[u,v]^{\mathbb{Z}_n} \simeq \frac{\mathbb{C}[X,Y,P]}{(XY - P^n)}. \tag{X.5.14}$$

To see that there is no hidden second relation, reduce any polynomial in X, Y, P by replacing each occurrence of XY with P^n. The surviving monomials have one of the forms X^jP^k or Y^jP^k, with $j > 0$, together with the pure P^k. Their images in $\mathbb{C}[u,v]$ have distinct exponent pairs. Linear independence of monomials in u, v then makes the map injective. The preceding factorization of invariant monomials makes it surjective. This two-sided argument proves the ring presentation rather than merely matching its Hilbert function.

The grading and topological charge are also compatible with that normal form. Give u and v degree one and opposite cyclic weights. The invariant $P = uv$ has degree two, while $X = u^n$ and $Y = v^n$ have degree n. Assign topological charges $+1$ to X, -1 to Y and zero to P. Then the relation is homogeneous in both gradings,

$$(\deg, q_{\mathrm{top}})(X) = (n,1), \quad (\deg, q_{\mathrm{top}})(Y) = (n,-1), \quad (\deg, q_{\mathrm{top}})(P) = (2,0). \tag{X.5.15}$$

Counting the normal forms gives the same refined numerator and denominator as (X.5.10). That equality is a nontrivial consistency test of the physical generator assignment, but the assignment itself came from the monopole operators and their OPE. The match $X \leftrightarrow V_+$, $Y \leftrightarrow V_-$ and $P \leftrightarrow \phi$ identifies the Coulomb chiral ring with the A_{n-1} surface ring. It does not determine an exact hyperkähler metric.

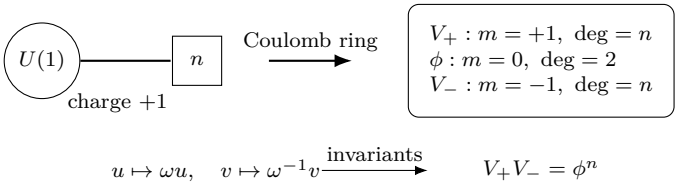


Figure X.5.2: The invariant-coordinate description of the charge-one SQED Coulomb ring. The primitive opposite fluxes give X and Y, while the degree-two scalar gives P. The cyclic action fixes precisely the monomials whose exponent difference is divisible by n. The relation connects the two flux directions at degree $2n$.

For $n = 2$, all three generators have degree two. Setting $z = 1$ in the rational series and expanding gives

$$H_2(t, 1) = \frac{1 - t^4}{(1 - t^2)^3} = 1 + 3t^2 + 5t^4 + 7t^6 + \cdots . \tag{X.5.16}$$

The three degree-two elements obey the quadratic A_1 relation. For $n = 3$, the scalar still has degree two but the primitive monopoles have degree three. The full low-degree series is

$$H_3(t, 1) = 1 + t^2 + 2t^3 + t^4 + 2t^5 + 3t^6 + O(t^7). \tag{X.5.17}$$

In particular, reporting only even coefficients would erase the first two monopole contributions. This distinction matters when the same A_1 ring appears as the double-edge component of the five-dimensional example. There the physical web identifies which three-dimensional quiver to use; the abelian ring calculation supplies its protected coordinate algebra.

The low-degree terms can be read directly without expanding a rational function. At degree two in the $n = 3$ model, only ϕ contributes. At degree three, V_+ and V_- contribute separately. At degree four, the only monomial is ϕ^2. At degree five, the two dressings ϕV_+ and ϕV_- appear. At degree six one has ϕ^3, V_+^2 and V_-^2; the apparent fourth monomial V_+V_- equals ϕ^3. In symbols,

$$R_6\big|_{n=3} = \operatorname{span}_{\mathbb{C}}\{\phi^3, V_+^2, V_-^2\}, \qquad \dim R_6 = 3. \tag{X.5.18}$$

This explicit degree-six check ties the physical OPE to a missing monomial in the Hilbert count. It also makes clear why the relation has degree $2n$, not degree n.

The hypersurface equation also reveals the geometry of this elementary model. Let $F = XY - P^n$. Its gradient is

$$\nabla F = (Y, X, -nP^{n-1}). \tag{X.5.19}$$

For $n \geq 2$, all three derivatives vanish together only at $X = Y = P = 0$. Thus the ring describes a surface smooth away from its cone point. The $n = 2$ case has a quadratic cone at the origin; the $n = 3$ case has a higher-order P term but the same two-complex-dimensional generic size. This local calculation explains why the component used in the E_3 web has one quaternionic dimension. It does not turn the surface equation into a statement about its exact metric.

There is a practical distinction between an unrefined and a refined test. Setting $z = 1$ adds operators of opposite topological charge into one coefficient. Keeping z makes the first monopole terms visible as

$$H_n(t, z) = \frac{1}{1 - t^2}\big[1 + (z + z^{-1})t^n + (z^2 + z^{-2})t^{2n} + \cdots\big]. \tag{X.5.20}$$

At degree $2n$, the relation identifies the neutral product of the opposite primitive monopoles with ϕ^n; the two charged squares remain distinct. A coefficient alone hides this charge separation.

X.5.4 An affine A_2 quiver and its centre

An affine cycle tests the compact-group part of the dictionary. Put one $U(1)$ at each vertex of a triangle and one full bifundamental hyper on each edge. Every edge has charge difference, so the common diagonal $U(1)$ acts trivially. We take the effective compact group to be

$$G_{A_2} = U(1)^3/U(1)_{\mathrm{diag}}, \qquad \mathrm{cochar}(G_{A_2}) = \mathbb{Z}^3/\mathbb{Z}(1, 1, 1). \tag{X.5.21}$$

The diagonal vector is primitive. Subtracting the zeroth component from each flux gives a unique integral representative $(0, m_1, m_2)$ of every class. No half-integral or fractional sector is introduced.

The three edge weights are $m_1, m_2, m_1 - m_2$ up to signs. There are no nonabelian roots. Hence

$$2\Delta(m_1, m_2) = |m_1| + |m_2| + |m_1 - m_2| = 2\big[\max(0, m_1, m_2) - \min(0, m_1, m_2)\big]. \tag{X.5.22}$$

The quotient leaves two degree-two scalars. If r denotes the range in the last expression, the fluxes of range one are

$$(1, 0),\ (0, 1),\ (1, 1),\ (-1, 0),\ (0, -1),\ (-1, -1). \tag{X.5.23}$$

They are the six primitive nonzero degree-two sectors. Along with two scalar dressings of the zero flux, they produce eight degree-two operators. The coefficient is a useful test of whether the diagonal was removed consistently.

The entire bare-shell count is equally elementary. For $r > 0$, the integer points with range r lie on the boundary of a hexagon in the (m_1, m_2) lattice; each of its six sides contributes r new points. Thus the shell population is $6r$. With $x = t^2$, the bare sum and the fully dressed Hilbert series are

$$\sum_{m_1, m_2 \in \mathbb{Z}} x^{r(m_1, m_2)} = 1 + \sum_{r \geq 1} 6r x^r = 1 + \frac{6x}{(1 - x)^2}, \tag{X.5.24}$$

For completeness, one can count the same shell without relying on the picture. If $0 \le m_1, m_2 \le r$, range r requires that at least one coordinate equal r, giving $2r+1$ points. The opposite quadrant gives another $2r+1$; for positive r these two sets do not overlap. The mixed sign quadrants have $m_1 - m_2 = r$ or its negative; each gives $r-1$ strictly mixed points. Together these contributions give

$$(2r+1) + (2r+1) + (r-1) + (r-1) = 6r. \tag{X.5.25}$$

The six degree-two fluxes in (X.5.23) are precisely the $r = 1$ instance. This direct count also shows how the hexagon grows: moving from range $r-1$ to r adds six longer boundary segments while leaving the scalar dressing unchanged.

$$H_{A_2}(t) = \frac{1}{(1-x)^2}\left(1 + \frac{6x}{(1-x)^2}\right) = \frac{1+4x+x^2}{(1-x)^4}. \tag{X.5.26}$$

Expanding gives

$$H_{A_2}(t) = 1 + 8t^2 + 27t^4 + 64t^6 + O(t^8). \tag{X.5.27}$$

One can check the first two nonconstant coefficients sector by sector. At t^2, the six range-one bare monopoles and two zero-flux scalars give $6+2$. At t^4, range-two fluxes contribute twelve, the six range-one sectors each have two scalar dressings, and the zero sector has three quadratic scalar monomials. Therefore

$$[t^2]H_{A_2} = 6 + 2 = 8, \qquad [t^4]H_{A_2} = 12 + 6 \cdot 2 + 3 = 27. \tag{X.5.28}$$

This decomposition identifies exactly which terms would change if an edge, a flux class or a scalar were mistakenly retained or deleted. At any cutoff L, the condition $2\Delta \le L$ implies $|m_1|, |m_2| \le \lfloor L/2 \rfloor$. The shell calculation therefore also gives a finite bound for direct enumeration; no unexamined fluxes can contribute below that degree.

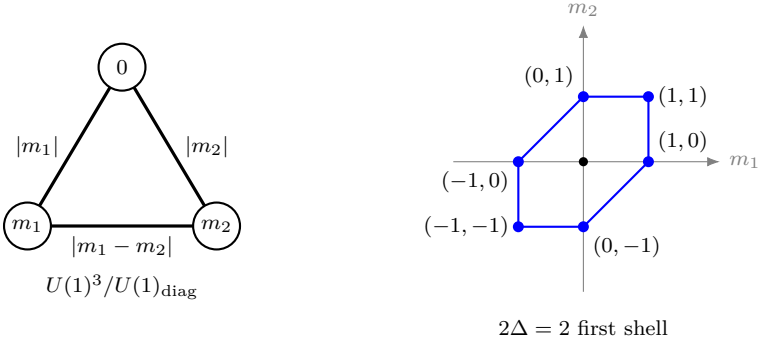


Figure X.5.3: The affine A_2 triangle and its primitive flux slice. The three unit edges measure the differences m_1, m_2 and $m_1 - m_2$ after $m_0 = 0$. The six points on the first hexagonal shell have bare degree two. The common diagonal flux has already been removed from both panels.

Two tempting operations give different wrong answers. If one fixes the common flux but keeps its scalar Casimir, one has only partially removed the circle. This

multiplies (X.5.26) by $(1-t^2)^{-1}$, so the coefficient of t^2 becomes nine. If one keeps the full $U(1)^3$ instead, every simultaneous flux (c,c,c) has zero bare degree. There are infinitely many such sectors already at degree zero, and the ultraviolet sum is not locally finite in this grading. Neither operation describes the effective group in (X.5.21).

The degree-two coefficient eight is compatible with the adjoint of $SU(3)$. The source identifies this Coulomb branch with the reduced one-instanton space associated with A_2; that symmetry and instanton interpretation uses the three-dimensional physical dictionary. The triangle's own Higgs branch is a different variety. In the next section the triangle will model one, but only one, component of the selected five-dimensional Higgs branch.

There is a useful exact character consistency check behind the first four numbers. The elementary generating identity

$$\sum_{p\geq 0}(p+1)^3 x^p = \frac{1+4x+x^2}{(1-x)^4} \tag{X.5.29}$$

matches the dimensions of the $SU(3)$ representations with highest weights (p,p). The equality of these two power series follows from the rational function. Calling those graded pieces actual symmetry representations requires the sourced symmetry action, since an unrefined integer coefficient cannot by itself specify how a group acts. This distinction will matter again when 28 and 300 appear in the affine D_4 example.

The rational expression also makes the complex dimension visible. Near $x=1$ its numerator tends to six while the denominator has a fourth-order pole. The associated affine cone therefore has complex dimension four, or quaternionic dimension two in the hyperkähler interpretation. This agrees with the rank calculation $\operatorname{rank}(U(1)^3/U(1)_{\mathrm{diag}})=2$. The two tests use different features of the same three-dimensional object: the pole measures growth of graded functions, while the rank counts independent Coulomb coordinates. Agreement is expected here but neither number alone specifies the affine A_2 ring.

One can see why the quotient matters even before evaluating a sum. The cycle charges span the rank-two sublattice generated by $(1,-1,0)$ and $(0,1,-1)$ in the dual charge lattice. Both annihilate $(1,1,1)$, and together they have no further continuous kernel. Removing exactly that primitive common circle therefore leaves two independent scalar directions. If an edge of the triangle is deleted, the charge graph changes; the six-point first shell and the rational series are no longer the ones calculated above. This charge-lattice view ties the visible edges to the integer flux slice, rather than treating the quotient as a cosmetic adjustment to a final coefficient.

X.5.5 Two cones from a five-brane web

At zero masses, zero five-dimensional Coulomb expectation value and vanishing inverse gauge coupling, the $SU(2)$ theory with two flavors has a web whose external charges can be partitioned in two inequivalent maximal ways. This is the E_3 example. The finite-coupling drawing used to approach the limit has generic nonzero masses and Coulomb expectation value. It does not establish a statement about every massless

finite-coupling Higgs branch. Here the three parameters are taken to zero together, and the external seven-brane endpoints remain part of the chosen web description.

In one decomposition, three distinct subwebs can move. Their charge directions are $(1,0)$, $(0,1)$ and $(1,-1)$ in the source's local orientation. The pairwise stable intersections in this fixture have magnitude one. The associated quiver has three rank-one nodes with one edge between each pair, namely the affine A_2 triangle. Its effective rank, after the primitive common circle is removed, is

$$\operatorname{rank} G_{\triangle} = 3 - 1 = 2. \tag{X.5.30}$$

The calculated Hilbert series is (X.5.26); the source identifies its Coulomb branch with the reduced minimal $\mathfrak{sl}_3$ nilpotent cone.

The unit edge count can be seen in the primitive charge vectors. For two transverse straight segments of charges (p_i, q_i) and (p_j, q_j), their local intersection multiplicity is the absolute determinant. In the chosen three-direction fixture,

$$|\det((1,0),(0,1))| = 1, \quad |\det((1,0),(1,-1))| = 1, \quad |\det((0,1),(1,-1))| = 1. \tag{X.5.31}$$

The three unit results account for the three edges of the triangle. They do not by themselves establish that these are the complete movable subwebs; that information comes from the physical decomposition of the limiting web. The same external seven-brane endpoints are kept through the comparison, so the two quivers represent alternatives for one origin rather than two unrelated five-dimensional theories.

In the other decomposition, two subwebs move. Their stable intersection is two, represented by two mixed-color unit squares in the source web. The quiver has two $U(1)$ nodes joined by two full hypermultiplet edges. Its primitive diagonal quotient leaves one relative circle. The two edge weights have charge one under that relative circle, so it is exactly the $n = 2$ SQED calculation of the preceding section. Its Coulomb rank is

$$\operatorname{rank} G_{\parallel} = 2 - 1 = 1, \qquad H_{\parallel}(t) = \frac{1 - t^4}{(1 - t^2)^3}. \tag{X.5.32}$$

The source identifies this component with the reduced minimal $\mathfrak{sl}_2$ cone. A single triangular quiver would lose the second component, while the double-edge quiver alone would lose the first.

For this second component, the two-node quotient can be made explicit. If its cocharacters are (r_1, r_2), their simultaneous shift is unphysical and the relative flux $m = r_1 - r_2$ is any integer. Each of the two edges contributes $|m|$. Thus

$$2\Delta_{\parallel}(m) = 2|m|, \qquad G_{\parallel} = (U(1)^2/U(1)_{\mathrm{diag}}) \simeq U(1). \tag{X.5.33}$$

The one remaining scalar dressing gives exactly the $n = 2$ SQED series, including its relation $V_+V_- = \phi^2$. This is a sharper test than merely observing that the proposed cone has quaternionic dimension one. If the double edge were mistaken for a single edge, the primitive monopoles would have degree one and the ring would change.

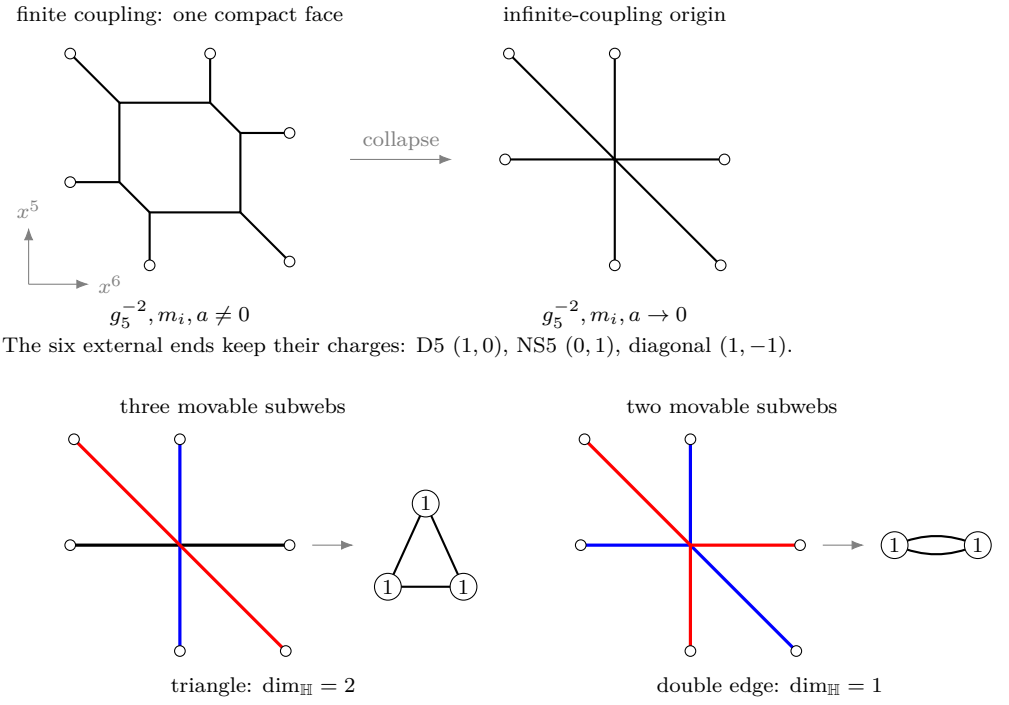


Figure X.5.4: The finite $SU(2)$, $N_f = 2$ web has one compact face; its six external legs collapse to the massless infinite-coupling web. The lower panels color that limiting web in two inequivalent ways and draw the corresponding rank-one magnetic graphs: a unit-edge triangle and a two-node double edge. Open circles are seven-brane endpoints of the indicated leg types. The web decomposition supplies the proposed branch dictionary, not an independent proof of the Higgs-branch assignment.

The two varieties meet at the origin according to the physical web analysis. To make a Hilbert-series statement about their union, we also take the intersection to be the *reduced* origin. Denote the two coordinate rings by R_{A_2} and R_{A_1}, with evaluation maps to $\mathbb{C}$ at their origins. The glued coordinate ring is their fiber product,

$$R_{\text{union}} = R_{A_2} \times_{\mathbb{C}} R_{A_1} = \{(f, g) : f(0) = g(0)\}. \tag{X.5.34}$$

The elementary exact sequence of graded vector spaces is

$$0 \longrightarrow R_{\text{union}} \longrightarrow R_{A_2} \oplus R_{A_1} \xrightarrow{(f,g)\mapsto f(0)-g(0)} \mathbb{C} \longrightarrow 0. \tag{X.5.35}$$

It subtracts precisely one duplicated constant, rather than a whole positive-degree series. The resulting series is

$$H_{\text{union}}(t) = H_{A_2}(t) + H_{A_1}(t) - 1 = 1 + 11t^2 + 32t^4 + O(t^6). \tag{X.5.36}$$

The coefficients follow from $8+3=11$ and $27+5=32$. They describe the union only under the reduced-origin gluing premise. A point-set intersection by itself would not determine its scheme structure.

The exact sequence also explains why the union is not obtained by multiplying two Hilbert series. Multiplication counts tensor products of independent coordinates, appropriate for a Cartesian product of varieties. Here a point lies on one cone or the other, and the two constant functions agree at their common origin. The vector space at every positive degree is a direct sum of the corresponding pieces on the two components. At degree zero there is only one copy of $\mathbb{C}$. This gives a transparent coefficient rule,

$$(R_{\text{union}})_0 \simeq \mathbb{C}, \qquad (R_{\text{union}})_d \simeq (R_{A_2})_d \oplus (R_{A_1})_d \quad (d>0). \tag{X.5.37}$$

For example, the two degree-two spaces have dimensions eight and three. Their direct sum has dimension eleven, with no second identity operator. The reduced-intersection assumption is essential to this simple positive-degree rule.

The union is reducible, so its dimension is the larger component dimension rather than the sum of both dimensions. In this example,

$$\dim_{\mathbb{H}}\left(\overline{\mathcal{O}}^{\mathfrak{sl}_3}_{\min} \cup \overline{\mathcal{O}}^{\mathfrak{sl}_2}_{\min}\right) = \max(2,1) = 2. \tag{X.5.38}$$

The degree-two coefficient eleven carries different information: it counts the first graded functions from both components, glued at the identity. Thus a dimension-two answer alone would miss the smaller branch. The web decomposition supplies precisely the extra discrete information that the dimension cannot detect.

There is also a limit to what the two separate Coulomb calculations say about the union. Each component's monopole sum determines its graded count under its own compact group. Their intersection and the rule for gluing functions are facts about the five-dimensional branch geometry supplied by the selected web analysis and the reduced origin premise. One cannot discover the second component by analytically continuing the triangle's series, nor can one extract the intersection scheme from the two component series alone. The exact sequence makes this missing physical input visible as the map to $\mathbb{C}$.

The edge rule also has a scope. For this local triple, the determinant of two primitive charge directions computes their unit stable intersection. With shared seven-brane endpoints, the sourced rule includes endpoint terms,

$$E = SI + \sum_i X_i - \sum_i Y_i. \tag{X.5.39}$$

Here SI is the stable intersection, and i labels a shared seven-brane. Each counted pair contains one five-brane from each subweb: X_i counts pairs ending on opposite sides of that seven-brane, and Y_i counts pairs ending on the same side. The correction cannot be discarded in a general web. Chapter 6 develops that construction. The result here is a protected geometry assigned to a particular five-dimensional origin; none of these steps equates the full five-dimensional and three-dimensional quantum theories.

X.5.6 Two M5 branes and the affine D_4 quiver

How does a separated pair of M5 branes produce the four leaves of an affine D_4 magnetic quiver? Put n M5 branes on a local A_{k-1} singularity and separate them along x^6 while keeping them on the singularity. In the massless equal-rank IIA description, each M5 becomes an NS5 along 012345 and the k D6 branes occupy 0123456 in the interior and exterior flavor regions. The M-theory circle is x^{10}, and the local transverse geometry lies in 78910. There are $n-1$ relative tensor separations. This local circle statement applies to the initial electric configuration, with no local D8, O8 or M9 object. It does not equate finite-radius ALF asymptotics with the limiting ALE singularity, and suspended D6 branes require the source's local treatment.

For $n = k = 2$, the finite relative-tensor phase has one electric $SU(2)$ gauge node with two full flavors at each end, giving four full fundamentals. At a regular, completely Higgsed point, the hyperkähler quotient dimension is

$$\dim_{\mathbb{H}} \mathcal{H}_{6d}^{\text{regular}} = 4 \dim_{\mathbb{C}} \mathbf{2} - \dim SU(2) = 8 - 3 = 5. \tag{X.5.40}$$

This electric arithmetic names the finite phase; it does not yet construct the magnetic quiver. The next operation changes the brane presentation. Bring two D8 branes from each end of the x^6 direction and rearrange the D6s so that they end on D8s. The resulting source configuration has four ordered D8s and D6 multiplicities $(1, 2, 1)$ in their three successive intervals. The two NS5 branes remain distinct in the central D8 interval, displaced from the D6s in the transverse 789 directions. These are the actual endpoint multiplicities of the D8 rearrangement in the source diagram. The source specifies bringing D8s from infinity and rearranging the D6s, but gives neither an order of individual NS5–D8 crossings nor a per-crossing count of created D6s for this example. The endpoint does not determine a unique crossing history. We therefore use its drawn stacks as the input to the D4 suspension prescription.

The two descriptions answer different questions. In the initial electric frame, an interval between adjacent NS5 branes supports the $SU(k)$ gauge factor, while the two exterior D6 regions supply flavor. For $n = 2$ there is one interval and therefore one relative tensor separation. Moving the NS5s together changes that phase; it does not merely tune a parameter inside a fixed Higgs quotient. In the magnetic prescription, D4s ending on m D6s within one D8 interval furnish the adjoint/vector of $U(m)$. Applied successively to the three stacks $(1, 2, 1)$, this gives the $U(1) - U(2) - U(1)$ tail. A D4 joining D6s in adjacent intervals gives one bifundamental for each of its two tail links. Each separated, dynamical NS5 supplies its own $U(1)$ vector; a D4 joining that NS5 to a D6 in the same central interval gives a $U(1) \times U(2)$ bifundamental. Thus the two NS5s add two distinct links to the central node. A D4 stretched between the two NS5s is massive at their nonzero x^6 separation and supplies no edge between the bouquet nodes. These D4s are the source's virtual magnetic probes, not additional electric color stacks. The two bouquet nodes cannot be merged without changing the physical phase and its monopole lattice.

The two tail ends and the two *separate* NS5 leaves make affine D_4, with one bifundamental on each of four edges. Its compact group and quaternionic Coulomb

rank are

$$G_{D_4} = \frac{U(2) \times U(1)^4}{U(1)_{\text{diag}}}, \qquad \operatorname{rank} G_{D_4} = 2 + 4 - 1 = 5. \tag{X.5.41}$$

The central quotient is primitive. Fixing the flux of one leaf to zero gives an integral slice isomorphic as a compact group to $U(2) \times U(1)^3$. It introduces no fractional sectors. The neutral adjoint hypermultiplet attached to each isolated source NS5 circle is omitted only in this Coulomb calculation. No additional factor is removed from the six-dimensional Higgs branch. Likewise, omitting the overall tensor center from the electric relative-tensor description is not the magnetic gauge-circle quotient.

The group isomorphism can be written without relying on a rank count. Represent a class of $(g; u_0, u_1, u_2, u_3)$ in the numerator of (X.5.41). Multiplying by the diagonal element u_0^{-1} sets the first leaf to the identity and sends the other factors to

$$[(g; u_0, u_1, u_2, u_3)] \longmapsto (u_0^{-1} g;\ u_0^{-1} u_1, u_0^{-1} u_2, u_0^{-1} u_3). \tag{X.5.42}$$

Because u_0 is an ordinary circle element, the map and its inverse are defined on the compact groups, not merely on their Lie algebras. On cocharacters it sends $(a, b; l_0, l_1, l_2, l_3)$ to $(a - l_0, b - l_0; l_1 - l_0, l_2 - l_0, l_3 - l_0)$. Every output remains integral. The Weyl exchange of a, b is the only remaining identification.

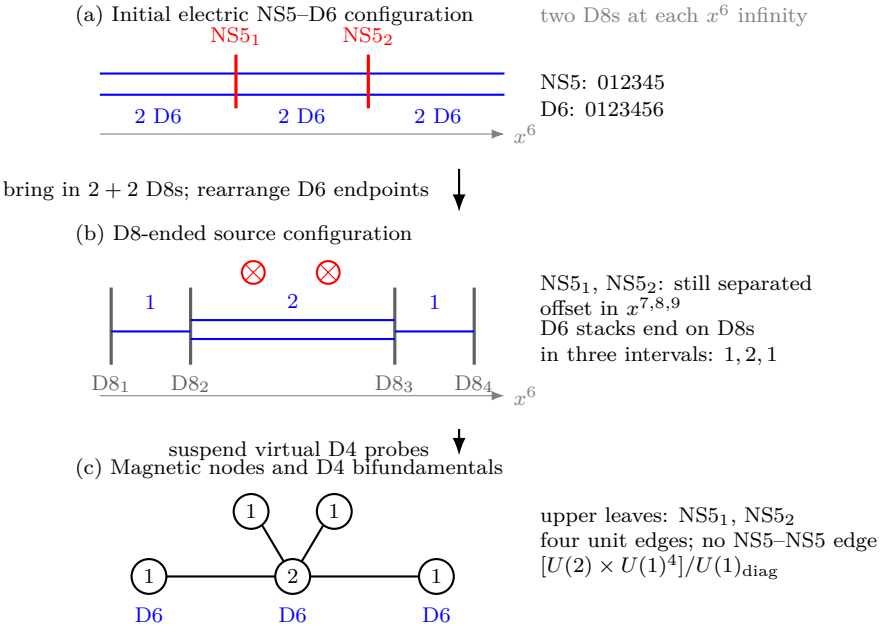


Figure X.5.5: The separated $n = k = 2$ construction. (a) Two NS5s divide the initial equal-rank electric D6 stack; the four D8s to be brought in are at infinity. (b) The source's rearranged endpoint has four ordered D8s, successive D6 stacks $1, 2, 1$, and the same two separated NS5s displaced in 789. The arrow specifies the sourced rearrangement, not a unique crossing movie. (c) D4 modes within each interval give the $1 - 2 - 1$ nodes; modes between adjacent D6 intervals and between each NS5 and the central D6 stack give the four unit edges. There is no massless NS5–NS5 edge at finite separation. The primitive common gauge circle is removed only after constructing the graph.

We can now calculate entirely on the three-dimensional side. Order the central cocharacter as $a \leq b$ and write the four leaf fluxes as l_0, l_1, l_2, l_3, with $l_0 = 0$ in the quotient slice. Every edge has central weights $a - l_i$ and $b - l_i$. The one positive root of $U(2)$ has value $b - a$. Thus

$$2\Delta(a, b; \mathbf{l}) = \sum_{i=0}^{3} \big(|a - l_i| + |b - l_i|\big) - 2|a - b|. \tag{X.5.43}$$

For the explicit flux $(a, b) = (0, 1)$ and all leaves zero, the four edges contribute four and the root subtracts two, so $2\Delta = 2$. The example tests both the edge multiplicity and the nonabelian root term. Replacing the four leaves by one rank-four leaf would define a different graph and a different lattice.

At equal central flux, the residual $U(2)$ supplies Casimir degrees one and two, while the three unfixed leaves supply three more degree-one Casimirs. At unequal central flux,

the centralizer is $U(1)^2$ and all five residual Casimirs have degree one. In the t grading,

$$P_{=}(t) = \frac{1}{(1-t^2)^4(1-t^4)}, \qquad P_{<}(t) = \frac{1}{(1-t^2)^5}. \tag{X.5.44}$$

The distinct dressing matters already at degree four. It cannot be recovered by treating each $U(2)$ eigenvalue as an unrelated abelian node.

There is a finite bound on the flux enumeration at any desired degree. Set $s = b - a \geq 0$ and let $\mathrm{dist}(l, [a, b])$ be the integer distance from l to the interval. For one leaf,

$$|a - l| + |b - l| = s + 2\,\mathrm{dist}(l, [a, b]). \tag{X.5.45}$$

Substituting all four leaves into (X.5.43) yields

$$2\Delta = 2\left[s + \sum_{i=0}^{3} \mathrm{dist}(l_i, [a, b])\right]. \tag{X.5.46}$$

If $2\Delta \leq L$, then $s + \sum_i \mathrm{dist} \leq L/2$. Because $l_0 = 0$, both endpoints obey $|a|, |b| \leq s + \mathrm{dist}(0, [a, b]) \leq \lfloor L/2 \rfloor$. Each other leaf obeys the same bound after adding its own distance. Consequently every independent flux coordinate lies in the finite box $[-\lfloor L/2 \rfloor, \lfloor L/2 \rfloor]$. This is why the following low-degree count is exhaustive rather than a cutoff guess.

The bare-shell populations at degrees zero, two and four are compact enough to display. Write $N_{d,=}$ for equal central flux and $N_{d,<}$ for unequal central flux. Directly evaluating the bounded integer solutions of (X.5.46) gives

$$(N_{0,=}, N_{2,=}, N_{2,<}, N_{4,=}, N_{4,<}) = (1, 8, 16, 32, 145). \tag{X.5.47}$$

The count can be reconstructed by the central interval length s. Writing $j = \Delta$, the nonzero populations through $j = 2$ are

	$s = 0$	$s = 1$	$s = 2$
$j = 0$	1	0	0
$j = 1$	8	16	0
$j = 2$	32	64	81

. (X.5.48)

For $s = 2$ and $j = 2$, every distance term must vanish. Since $l_0 = 0$, the interval $[a, b]$ can be $[-2, 0]$, $[-1, 1]$ or $[0, 2]$; each of the three movable leaves has three integer choices inside it. This gives $3 \cdot 3^3 = 81$. For $s = 1$ and $j = 1$, the intervals are $[-1, 0]$ and $[0, 1]$, and the three leaves each have two choices, giving $2 \cdot 2^3 = 16$. At $j = 2$, allowing one unit of distance gives 64 additional $s = 1$ sectors. For $s = 0$, the degree-one count is six ways to move one of three leaves from $a = 0$, plus the two common choices $a = \pm 1$ with all leaves equal to a; hence eight. The remaining $s = 0, j = 2$ count is 32. These decompositions expose the sources of the otherwise opaque number 145, namely $64 + 81$ unequal-central sectors. The equal-flux zero sector has four degree-two scalar dressings and eleven degree-four dressings. A degree-two equal-flux sector has four degree-two dressings; a degree-two unequal-flux sector has five. Hence

$$[t^2]H_{D_4} = 4 + 8 + 16 = 28, \tag{X.5.49}$$

$$[t^4]H_{D_4} = 11 + 8 \cdot 4 + 16 \cdot 5 + 32 + 145 = 300. \tag{X.5.50}$$

The number eleven in the first term can be read from the dressing factor itself. Four degree-two scalar generators give $\binom{4+2-1}{2} = 10$ quadratic monomials of total degree four. The degree-four $U(2)$ Casimir contributes one more, giving

$$[t^4]P_{=}(t) = \binom{5}{2} + 1 = 11. \tag{X.5.51}$$

For a nonzero bare sector of degree two, only one scalar insertion is allowed at degree four. There are four choices when $a = b$ and five when $a < b$. This explains each term in (X.5.50) without treating 300 as an unexplained output of a flux search. The Coulomb series begins

$$H_{D_4}(t) = 1 + 28t^2 + 300t^4 + O(t^6). \tag{X.5.52}$$

The degree-two coefficient equals the dimension of the $SO(8)$ adjoint, and the degree-four coefficient equals the dimension of its second Cartan power. The sourced finite Higgs branch is the closure of the minimal $SO(8)$ nilpotent orbit. These agreements give useful tests of the specified graph. The equality of the six-dimensional Higgs space and the three-dimensional Coulomb variety still rests on the physical brane and mirror arguments. If the M5 branes coincide, the source replaces the separated bouquet by a different nonabelian structure and obtains a different branch. In this low-rank example, the coincident $SO(7)$ branch is the $\mathbb{Z}_2$ quotient of the separated finite $SO(8)$ cone, where the exchange of the M5 branes is discretely gauged. That exchange quotient is a phase-changing physical operation; it is not the removal of the ineffective diagonal $U(1)$ in (X.5.41). The finite result here is not silently continued to that strong-coupling point.

The three operations sometimes compressed into a single phrase should be kept separate. Removing an overall tensor center concerns the electric six-dimensional description and leaves $n-1$ relative tensor multiplets. Omitting an isolated NS5 neutral adjoint concerns only the interacting Coulomb calculation of the magnetic theory. Quotienting by the primitive diagonal $U(1)$ fixes a compact magnetic gauge group and removes both a flux and a scalar. None is an instruction to divide the six-dimensional Higgs space by an additional factor. The dimension-five match would be easy to obtain for an incorrect graph, whereas the coefficient calculation tests all four separate leaves and their residual dressings.

This separated example supplies Chapter 6 with a concrete finite-tensor reference phase. When the branes coincide, the graph and Higgs space must be reconsidered there, rather than inferred by varying a parameter in the present flux series.

X.5.7 What the dictionary can and cannot identify

The four calculations give a compact way to remember the logical order. In SQED, the input is a compact three-dimensional theory and the output is an exact protected ring. In the affine triangle, the primitive common circle must be removed before the flux sum is meaningful. In the E_3 web and separated-M5 examples, a higher-dimensional

construction selects the magnetic graph. The subsequent monopole calculation tests its graded Coulomb geometry, while the Higgs/Coulomb identification remains a physical branch proposal in its specified phase.

Object	Phase and compact group	Computed statement and physical arrow
Charge-one SQED	$3d$ $U(1)$, $n = 2, 3$	$V_+V_- = \phi^n$ is the sourced operator product; the invariant normal forms give the abstract A_{n-1} ring.
Affine A_2	$3d$ $U(1)^3/U(1)_{\text{diag}}$	Flux shells give $1 + 8t^2 + 27t^4 + \cdots$; one-instanton meaning uses the physical dictionary.
E_3 origin	$5d$ $SU(2)$, $N_f = 2$, zero masses and vev, inverse coupling zero	Two proposed components give $1 + 11t^2 + 32t^4 + \cdots$ with reduced-origin gluing.
Separated M5/A_1	$6d$ finite relative-tensor phase; $3d$ $(U(2) \times U(1)^4)/U(1)_{\text{diag}}$	The protected count is $1 + 28t^2 + 300t^4 + \cdots$; its identification with the $6d$ Higgs space is sourced.

Table X.5.2: The object and phase attached to each calculation. A match of graded dimensions is narrower than an equality of moduli spaces, and an equality of moduli spaces is narrower than a full quantum-field-theory duality.

A further application is the subtraction of two magnetic quivers to model a transverse slice of a singular branch. In a selected $\mathfrak{sl}_5$ example, the ranks of two aligned graphs subtract as

$$(1, 2, 2, 1) - (1, 1, 1, 1) = (0, 1, 1, 0). \tag{X.5.53}$$

Both graphs are unitary chains. The first has one flavor at each of its two middle nodes, while the second has one flavor at each endpoint; these framings are part of the definition, not determined by the ranks. The chosen point lies in the orbit $(2, 1^3)$ inside the closure of $(2^2, 1)$. The subtraction retains the first graph's flavor framing, so the two surviving unit nodes each carry one flavor. The physical slice statement concerns an interior point of that specified orbit. The arithmetic alone does not make arbitrary graph subtraction valid at a singular boundary point. Chapter 6 studies the phase and slice constructions; Chapter 7 develops the ring and Hasse viewpoint, and Chapter 8 records examples with their limits. The useful lesson of this chapter is the order of operations. Specify a brane phase, construct the graph, declare its compact group, compute its protected Coulomb ring, and only then compare it with the proposed higher-dimensional Higgs space.

This order also tells a reader what a disagreement would mean. If the flux series changes when one retains a decoupled circle, the compact three-dimensional input was changed before any higher-dimensional comparison. If a sourced web has two maximal decompositions, a single-component series cannot represent the stated union even if its largest dimension agrees. If the six-dimensional tensor expectation value changes so that NS5 branes coincide, the magnetic graph itself must be reconstructed. Each failure occurs at a different arrow of Figure X.5.1.

The low-degree coefficients are best used as diagnostic consequences of specified objects. The A_2 shell identity and the D_4 finite bound make their enumerations exact through the reported orders. The SQED invariant normal forms establish an entire abstract ring once the physical OPE is supplied. The E_3 fiber product establishes an entire union ring only after the reduced-origin gluing input. These distinctions let a reader use the calculations without upgrading the brane proposals to complete dualities.

X.5.8 Exercises

1. For compact $U(1)$ with three full charge-one hypermultiplets, derive the relation among ϕ, V_+, V_- and give the coefficients of t^0 through t^6 in the unrefined Hilbert series, including zero coefficients. Explain why the primitive flux is integral.

2. For the affine A_2 triangle with one hypermultiplet on each edge, remove the common diagonal circle, fix one flux to zero and evaluate the monopole series through t^4. List all six primitive nonzero fluxes of degree two and explain the effect of retaining the deleted scalar.

3. At the massless infinite-coupling origin of five-dimensional $SU(2)$ with two flavors, use the two web decompositions to find the quaternionic dimensions of their components and the first three even coefficients of the reduced-origin union. Why does either component alone give the wrong branch?

4. For two separated M5 branes on A_1 in the finite relative-tensor phase, identify all five magnetic gauge-node ranks. Compute the Coulomb quaternionic dimension and the coefficients at t^0, t^2, t^4. Explain which part of the comparison with the six-dimensional Higgs space is a three-dimensional calculation.

5. Draw the physical and geometric arrows for one five-dimensional and one six-dimensional example in this chapter. Mark each coupling or tensor phase, the common-centre quotient, and the equality that concerns only moduli spaces. Give an example of how choosing the wrong compact global form changes a monopole lattice. This exercise calls for a written argument rather than a bounded numerical answer.

X.5.9 Take-home message

Take-home message

A magnetic quiver turns a proposed higher-dimensional Higgs-branch description into a three-dimensional Coulomb-ring calculation. The compact group fixes the integral flux lattice and residual dressings. Charge-one SQED gives $V_+V_- = \phi^n$; the effective affine A_2 triangle has $H = 1 + 8t^2 + 27t^4 + \cdots$. At the selected E_3 origin two quivers are needed, and reduced-origin gluing gives $1 + 11t^2 + 32t^4 + \cdots$. For separated M5 branes on A_1, the affine D_4 graph has Coulomb rank five and series $1 + 28t^2 + 300t^4 + \cdots$. The monopole calculations test the proposed branch dictionaries; the brane motions and cross-dimensional identifications remain physical premises of their stated phases.

Status and sources

The good/ugly monopole formula, GNO sum and residual Casimir dressing in Section X.5.2 follow Cremonesi et al. (2014, PDF pp. 7–8, eqs. (2.4)–(2.7)). The compact groups are specified in each example, and the grading is $t^{2\Delta}$ as in Volume IX. The finite calculations in Sections X.5.3 and X.5.4 are algebraic under those choices [MATH]. The physical SQED product is stated after eq. (3.2) of Cremonesi et al. (2014, PDF pp. 9–10); its invariant normal-form proof in this chapter establishes the abstract ring, not the operator product independently. The affine quotient and cycle come from that paper's eqs. (3.1), (3.5)–(3.6). The one-instanton interpretation is a sourced three-dimensional physical identification [GEO-E].

The two maximal web decompositions, triangle and double-edge quivers, and common-origin statement in Section X.5.5 follow Cabrera, Hanany, and Yagi (2019, PDF pp. 7–10, figs. 2–4 and eqs. (2.1)–(2.4)). The paper's shared-seven-brane correction is its eq. (3.1) on PDF p. 18. The cross-dimensional assumption and two-cone context are also stated by Ferlito et al. (2018, PDF p. 3). The reduced-origin fiber-product series is an algebraic consequence [MATH]; web motion, the physical Higgs/Coulomb arrow, and the reduced intersection remain sourced premises [GEO-E]. No full $5d/3d$ QFT or metric equality is asserted.

The massless local M/IIA interface and separate D8/D4 prescription in Section X.5.6 follow Cabrera, Hanany, and Sperling (2019, corrected complete article, PDF pp. 7, 9–11, table 1 and eqs. (2.4)–(2.10)). Its eq. (2.7) supplies the D8-ended endpoint, without an individual crossing sequence. The local-circle qualification, including suspended D6 branes, is explicit in Hanany and Zaffaroni (1998, PDF p. 25, sec. 5). The separated electric chain, finite $SU(2)$ four-flavor Higgs branch, and minimal $SO(8)$ orbit are in Hanany and Zafrir (2018, PDF pp. 5–6, 9–10, eqs. (2.1)–(2.2) and (2.17)–(2.25)). The rank, primitive quotient, flux bound and coefficients are conditional three-dimensional calculations [MATH] on the sourced graph. The six-dimensional Higgs/Coulomb identification and the D8/D4 and mirror steps are physical premises [GEO-E]; neither coefficient agreement nor the initial geometric lift proves them. The coincident-M5 phase is excluded from the finite branch result. The selected subtraction preview uses Cabrera and Hanany (2018, PDF pp. 4–7, eqs. (2.9)–(2.14)) and is not a general slice theorem.

References

Cabrera, S. and A. Hanany (2018). "Quiver Subtractions". In: *JHEP* 09, p. 008. DOI: 10.1007/JHEP09(2018)008. arXiv: 1803.11205 [hep-th].

Cabrera, S., A. Hanany, and M. Sperling (2019). "Magnetic quivers, Higgs branches, and 6d N=(1,0) theories". In: *JHEP* 06. [Erratum: JHEP 07, 137 (2019)], p. 071. DOI: 10.1007/JHEP06(2019)071. arXiv: 1904.12293 [hep-th].

Cabrera, S., A. Hanany, and F. Yagi (2019). "Tropical Geometry and Five Dimensional Higgs Branches at Infinite Coupling". In: *JHEP* 01, p. 068. DOI: 10.1007/JHEP01(2019)068. arXiv: 1810.01379 [hep-th].

Cremonesi, S., A. Hanany, and A. Zaffaroni (2014). "Monopole operators and Hilbert series of Coulomb branches of $3d$ $\mathcal{N} = 4$ gauge theories". In: *JHEP* 01, p. 005. DOI: 10.1007/JHEP01(2014)005. arXiv: 1309.2657 [hep-th].

Ferlito, G. et al. (2018). "3d Coulomb branch and 5d Higgs branch at infinite coupling". In: *JHEP* 07, p. 061. DOI: 10.1007/JHEP07(2018)061. arXiv: 1712.06604 [hep-th].

Hanany, A. and A. Zaffaroni (1998). "Branes and six-dimensional supersymmetric theories". In: *Nucl. Phys. B* 529, pp. 180–206. DOI: 10.1016/S0550-3213(98)00355-1. arXiv: hep-th/9712145.

Hanany, A. and G. Zafrir (2018). "Discrete Gauging in Six Dimensions". In: *JHEP* 07, p. 168. DOI: 10.1007/JHEP07(2018)168. arXiv: 1804.08857 [hep-th].

Chapter X.6

Higgs branches at strong coupling

X.6.1 Why a Higgs branch changes at a singular limit

A finite web can be pulled apart in ways that are invisible while its central face has positive size. At the massless infinite-coupling point of the five-dimensional $SU(2)$ theory with two flavors, the collapsed web admits two distinct maximal separations. Each separation proposes a different cone of Higgs vacua. The object at the singular point is their union, with a common origin. This is a sharper question than asking whether the number of massless fields has increased: what are the components, and how do they meet?

The corresponding six-dimensional question begins with separated M5-branes on an orbifold. Bringing branes together, or moving an M5 onto an M9 plane, changes that phase. A magnetic quiver offers a way to calculate a proposed Higgs space in each selected phase. Once a three-dimensional quiver and its compact gauge group have been fixed, its Coulomb operators can be counted independently.

We write $\mathcal{H}_{5d}(P)$ or $\mathcal{H}_{6d}(P)$ for the Higgs branch in a specified phase P, and $\mathcal{C}_{3d}(Q_P)$ for the Coulomb branch of a three-dimensional $\mathcal{N}=4$ quiver. The proposed dictionary in the examples of this chapter has the form

$$\mathcal{H}_{5d/6d}(P) \simeq \mathcal{C}_{3d}(Q_P). \tag{X.6.1}$$

It is an assertion about branches. It neither equates the complete quantum field theories nor identifies their metrics. The complex algebraic dimension of a hyperkähler cone is twice its quaternionic dimension,

$$\dim_{\mathbb{C}} \mathcal{H} = 2 \dim_{\mathbb{H}} \mathcal{H}. \tag{X.6.2}$$

Dimension is an early check of a proposed branch, but many distinct spaces have the same dimension.

In the two-flavor web, the contrast between finite and infinite coupling is concrete. At finite coupling with generic masses and a nonzero Coulomb vev, the source drawing

has one web whose allowed collective movement does not create the two new cones. At the simultaneous massless origin and vanishing inverse coupling, separate subwebs can move away from the collapsed configuration. The two ways of separating them are not successive stages of one smooth deformation. They are distinct components that return to the same unseparated web at their origins. Thus the limit changes the algebraic branch, not merely the size of a parameter in a fixed smooth quotient. The later fiber-product calculation will encode precisely the single shared point. With the reduced-origin premise, the chapter's first strong-coupling result can be previewed as

$$\mathcal{H}_{5d}(P_*) \simeq \mathcal{C}(Q_{A_2}) \cup_{\{0\}} \mathcal{C}(Q_{A_1}), \qquad P_* : \; g_5^{-2} = m_1 = m_2 = a = 0. \tag{X.6.3}$$

The two decompositions and their dimensions are drawn in Figure X.6.2; Section X.6.3 calculates the ring of their proposed union.

The three-dimensional calculation uses the compact form of the gauge group. For a connected unframed unitary quiver whose bifundamentals do not see the simultaneous central $U(1)$, that factor is removed before listing magnetic charges. If the remaining gauge group has rank r, then its Coulomb branch has quaternionic dimension r under the usual good-quiver assumptions. For the five-node example below this statement reads

$$\operatorname{rank}\big(U(1)^5/U(1)_{\mathrm{diag}}\big) = 5 - 1 = 4. \tag{X.6.4}$$

The count has content only after the physical subweb decomposition and the five matter links are specified. Chapter 5 supplied the compact-lattice and monopole conventions. Here we apply them to webs and six-dimensional brane phases; Chapter 7 will use the resulting rings to discuss strata.

X.6.2 Shared seven-branes turn five subwebs into a cycle

The massless $SU(2)$ web with three flavors at infinite coupling has five movable pieces. Calling them red, blue, green, orange and purple makes the endpoint incidence visible in Figure X.6.1. The central question is which pairs of pieces give bifundamental matter in the magnetic quiver. Their stable intersection alone gives the wrong graph: red–blue and red–green each intersect once in that sense, yet both proposed edges are cancelled by a same-side shared seven-brane endpoint.

For two selected subwebs W_i, W_j, let $SI(W_i, W_j)$ denote their stable intersection after a generic displacement. At each shared seven-brane, X_a counts cross-subweb pairs arriving on opposite sides, and Y_a counts pairs on the same side, with coincident multiplicities included. The source prescription assigns the weighted edge number

$$E_{ij} = SI(W_i, W_j) + \sum_a X_a(W_i, W_j) - \sum_a Y_a(W_i, W_j). \tag{X.6.5}$$

For the named web the three terms can be read on the same five colored objects. This is a sourced prescription for a maximal movable decomposition in its physical phase, not a theorem for arbitrary web drawings.

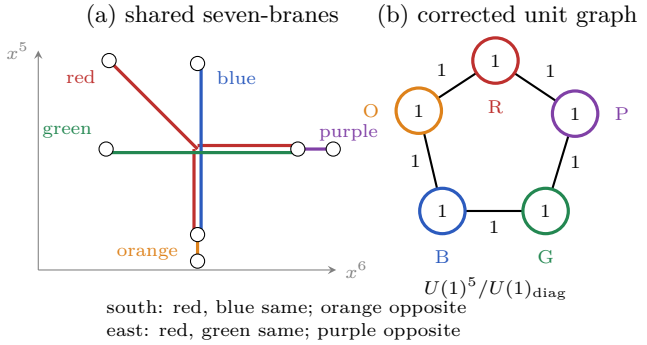


Figure X.6.1: The five source subweb colors, seven circular seven-brane endpoints, and their corrected magnetic graph. The south endpoint places red and blue on the same side of its seven-brane, with orange on the opposite side. At the east endpoint red and green are on the same side, with purple opposite. These two local incidences remove the red–blue and red–green links while creating the four orange and purple links. All five nodes are rank one; the graph is the unit cycle on the same named pieces.

Table X.6.1 records all ten unordered pairs. At the south endpoint, the red–blue same-side pair contributes $Y = 1$, while orange with red or blue contributes $X = 1$. The east endpoint similarly cancels red–green and joins purple to red and green. Blue–green has no shared endpoint correction, so its stable intersection survives. The last three pairs receive no edge from either mechanism. In particular, a positive stable intersection is not by itself a magnetic edge.

pair	SI	X	Y	E	pair	SI	X	Y	E
red, blue	1	0	1	0	red, green	1	0	1	0
blue, green	1	0	0	1	orange, red	0	1	0	1
orange, blue	0	1	0	1	purple, red	0	1	0	1
purple, green	0	1	0	1	blue, purple	0	0	0	0
green, orange	0	0	0	0	orange, purple	0	0	0	0

Table X.6.1: Every pair of the five movable subwebs in the massless $SU(2)$, $N_f = 3$ fixture. $E = SI + X - Y$ is a multiplicity, not merely a yes-or-no adjacency. The five positive entries form the cycle shown in Figure X.6.1.

Writing O, R, P, G, B for orange, red, purple, green and blue, respectively, the positive graph is

$$O - R - P - G - B - O, \qquad E_{OR} = E_{RP} = E_{PG} = E_{GB} = E_{BO} = 1. \tag{X.6.6}$$

This is affine A_4 as an unframed unitary quiver. Each subweb occurs once, so its gauge node has rank one. The simultaneous central gauge circle acts trivially on every edge,

giving the actual compact group

$$G_{E_4} = \frac{U(1)_O \times U(1)_R \times U(1)_P \times U(1)_G \times U(1)_B}{U(1)_{\mathrm{diag}}}, \qquad \dim_{\mathbb{H}} \mathcal{C}(Q_{E_4}) = 4. \quad \text{(X.6.7)}$$

The source calls the five-dimensional branch the minimal $\mathfrak{sl}_5$ nilpotent orbit closure. The affine-A_4 graph supplies a calculable three-dimensional candidate for that identification.

We can now turn the graph into a ring count. Magnetic charges are integer classes in $\mathbb{Z}^5/\mathbb{Z}(1,1,1,1,1)$. Fix the primitive integral representative $m_O = 0$. The source monopole formula commonly writes $t^{\Delta}_{\mathrm{src}}$. The convention used in this volume is the explicit change of variable

$$t_{\mathrm{src}} = t^2, \qquad t^{\Delta}_{\mathrm{src}} = t^{2\Delta}. \quad \text{(X.6.8)}$$

This regrades the same protected series before comparing coefficients with the equations of Chapter 5. With the book variable $t^{2\Delta}$, the monopole degree for this abelian graph is the total variation around its five links,

$$2\Delta(m) = |m_O - m_R| + |m_R - m_P| + |m_P - m_G| + |m_G - m_B| + |m_B - m_O|. \quad \text{(X.6.9)}$$

Each residual vector multiplet contributes a degree-two complex scalar. There are four such independent scalars, so the dressing factor and Hilbert sum are

$$P_{E_4}(t) = (1-t^2)^{-4}, \qquad H_{E_4}(t) = P_{E_4}(t) \sum_{\substack{m_O=0 \\ m_R,m_P,m_G,m_B \in \mathbb{Z}}} t^{2\Delta(m)}. \quad \text{(X.6.10)}$$

The shell at degree zero consists only of zero flux. Directly counting the integer solutions at degrees two and four gives

$$\sum_m t^{2\Delta(m)} = 1 + 20t^2 + 110t^4 + O(t^6). \quad \text{(X.6.11)}$$

Multiplication by $1 + 4t^2 + 10t^4 + \cdots$ yields

$$H_{E_4}(t) = 1+(20+4)t^2+(110+4\cdot 20+10)t^4+O(t^6) = 1+24t^2+200t^4+O(t^6). \quad \text{(X.6.12)}$$

The degree-two coefficient is the dimension of the adjoint of $SU(5)$. The degree-four coefficient agrees with the next $(2,0,0,2)$ character. These are protected statements about the specified three-dimensional quiver. The proposed five-dimensional identification still uses the web motion and the source's branch dictionary.

There is an independent representation-theoretic way to understand the first two coefficients. The minimal $\mathfrak{sl}_5$ orbit consists of nonzero rank-one nilpotent endomorphisms, and its closure adds the zero matrix. An element can be written $M = uv^{\mathsf{T}}$ with $v^{\mathsf{T}}u = 0$. Its coordinate ring, in the same degree-two normalization, decomposes into representations of highest weight $(k,0,0,k)$ at degree $2k$. The first nontrivial element is the traceless matrix M itself, with 24 components. At the next degree, relations remove all quadratic tensors except the $(2,0,0,2)$ piece. Explicitly,

$$\operatorname{tr} M = 0, \qquad \operatorname{rank} M \le 1, \qquad M^2 = u(v^{\mathsf{T}}u)v^{\mathsf{T}} = 0. \quad \text{(X.6.13)}$$

The Weyl dimension product for the partition $\lambda(k) = (2k, k, k, k, 0)$ is

$$\dim V_{(k,0,0,k)} = \prod_{1 \le i < j \le 5} \frac{\lambda_i(k) - \lambda_j(k) + j - i}{j - i}. \tag{X.6.14}$$

The first two positive evaluations give

$$\dim V_{(1,0,0,1)} = 24, \qquad \dim V_{(2,0,0,2)} = 200. \tag{X.6.15}$$

This comparison checks the graph count against a known cone at two degrees. It does not turn the web-derived branch proposal into a proof: the representation calculation begins with the orbit closure, whereas the monopole sum begins with the corrected five-cycle.

The finite shell count has a simple completeness argument. For any vertex i of the cycle, there are two edge-disjoint paths from O to i. Their total absolute variation obeys

$$2\Delta(m) \ge 2|m_i - m_O| = 2|m_i|. \tag{X.6.16}$$

Thus a flux of degree at most four has every $|m_i| \le 2$, and enumerating the radius-two box is exhaustive through t^4. The shell numbers can be checked without relying on a large formal power-series expansion. The degree-two configurations are those whose nonzero charges occupy a single interval avoiding O and equal $+1$ or -1 there. There are ten such intervals, hence twenty fluxes. At degree four, fluxes may have two disjoint unit intervals, nested height-two intervals, or configurations with both signs. Counting these disjoint types inside the radius-two box gives 110. The dressing then contributes four states above zero flux at degree two and ten at degree four, together with four dressings of each of the twenty degree-two bare monopoles. This is the decomposition behind (X.6.12); it also makes the grading convention observable rather than a silent rescaling of t.

If the orange–red link is doubled while the other edges stay fixed, its weight enters the exponent,

$$2\Delta'(m) = 2|m_O - m_R| + |m_R - m_P| + |m_P - m_G| + |m_G - m_B| + |m_B - m_O|, \tag{X.6.17}$$

and the resulting series begins

$$H'(t) = 1 + 16t^2 + 8t^3 + 100t^4 + O(t^5). \tag{X.6.18}$$

A binary adjacency table would miss this change. It would also miss the fact that the original degree-two coefficient encodes the cycle's balanced links. This prepares the more general Hilbert-series analysis of Chapter 7.

An especially sharp endpoint check appears in a different source web. Two displayed subwebs have stable intersection four. The three shared seven-branes contribute opposite-side counts $(0, 0, 2)$ and same-side counts $(1, 1, 4)$. The prescription gives

$$E = 4 + (0 + 0 + 2) - (1 + 1 + 4) = 0. \tag{X.6.19}$$

It is possible for endpoint effects to cancel every stable-intersection link. The resulting disconnected two-node fixture teaches the sign and coincident-multiplicity rule. It is not used here as an interacting good-quiver monopole example; a bare disconnected rank-one pair has free and bad-sector subtleties. The calculation answers the local edge question, not the full branch question.

X.6.3 Two maximal decompositions make a reducible branch

The massless infinite-coupling $SU(2)$ web with two flavors illustrates why a list of edges is sometimes still insufficient. At its singular origin, the source exhibits two inequivalent maximal decompositions of the same web. One moves three pieces whose directions can be represented by $(1,0)$, $(0,1)$ and $(1,-1)$. The other separates two composite pieces and has two unit stable-intersection squares. Figure X.6.2 shows both partitions of the same six endpoints. In the two-piece partition each trivalent junction balances charge: its outgoing vectors are $(-1,1)+(1,0)+(0,-1)=0$ for the red piece and $(0,1)+(-1,0)+(1,-1)=0$ for the blue piece.

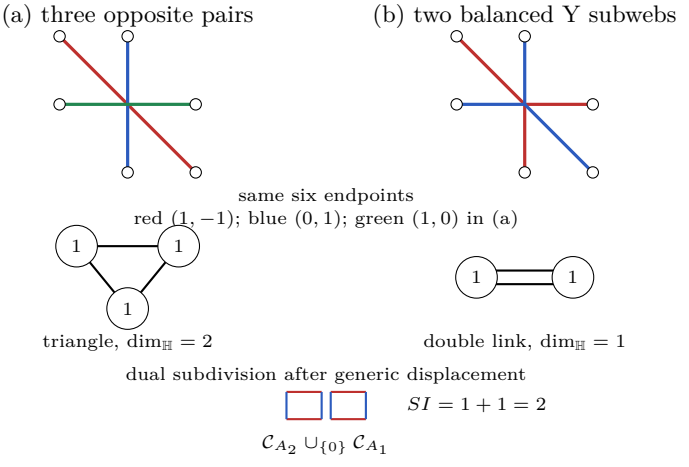


Figure X.6.2: The same six endpoint positions admit three straight colored pieces or two charge-balanced Y pieces. The first partition gives a triangle. For the second, a generic displacement resolves the stable intersection into two mixed unit cells and gives a double link. The reduced cones have quaternionic dimensions two and one and meet only at their common origin under the stated reduced-intersection premise.

For the three directions of the first separation, the three absolute determinants are all one,

$$|\det((1,0),(0,1))| = |\det((1,0),(1,-1))| = |\det((0,1),(1,-1))| = 1. \tag{X.6.20}$$

The resulting triangle is affine A_2. Removing its primitive common diagonal gives $U(1)^3/U(1)_{\mathrm{diag}}$ and rank two. In the other separation, the two mixed-color squares contribute stable intersection two between two rank-one nodes. The compact group is $U(1)^2/U(1)_{\mathrm{diag}}$, of rank one, with a double bifundamental link. The two candidate cones consequently have dimensions

$$\dim_{\mathbb{H}} \mathcal{C}(Q_{A_2}) = 3-1 = 2, \qquad \dim_{\mathbb{H}} \mathcal{C}(Q_{A_1}) = 2-1 = 1. \tag{X.6.21}$$

The distinction is visible in the monopole formula. For the triangle, fix $m_0 = 0$ and sum over two fluxes. For the double edge, fix one of the two fluxes to zero. Their bare degrees and scalar factors are

$$d_{A_2}(m,n) = |m| + |m-n| + |n|, \qquad d_{A_1}(q) = 2|q|, \tag{X.6.22}$$

$$H_{A_2}(t) = \frac{\sum_{m,n\in\mathbb{Z}} t^{d_{A_2}(m,n)}}{(1-t^2)^2}, \qquad H_{A_1}(t) = \frac{\sum_{q\in\mathbb{Z}} t^{2|q|}}{1-t^2}. \tag{X.6.23}$$

These two good-quiver series begin

$$H_{A_2}(t) = 1 + 8t^2 + 27t^4 + O(t^6), \qquad H_{A_1}(t) = 1 + 3t^2 + 5t^4 + O(t^6). \tag{X.6.24}$$

The eight and three degree-two operators distinguish the two components more directly than the label E_3 does.

The double-edge component can be summed without a cutoff. Its bare flux series is a geometric series in t^2,

$$\sum_{q\in\mathbb{Z}} t^{2|q|} = 1 + 2\sum_{q\geq 1} t^{2q} = \frac{1+t^2}{1-t^2}. \tag{X.6.25}$$

After scalar dressing it becomes

$$H_{A_1}(t) = \frac{1+t^2}{(1-t^2)^2} = \frac{1-t^4}{(1-t^2)^3}. \tag{X.6.26}$$

The last form is the Hilbert series of three degree-two generators with one degree-four relation. They may be called x, y, z with $xy = z^2$, an A_1 surface singularity. This is a useful reminder that the name of the two-node quiver refers to its Coulomb geometry and not to an extra three-dimensional gauge factor left unquotiented.

For the triangle, the degree $2k$ piece is the (k,k) representation of $SU(3)$. Its dimension is $(k+1)^3$. Summing the elementary cubic series gives

$$H_{A_2}(t) = \sum_{k\geq 0} (k+1)^3 t^{2k} = \frac{1 + 4t^2 + t^4}{(1-t^2)^4}. \tag{X.6.27}$$

This rational function has pole order four at $t = 1$, matching complex dimension four, whereas (X.6.26) has pole order two. The mismatch in pole orders is another reason a single uniform component cannot encode both separations. It also clarifies the notation: the first component is a minimal-A_2 orbit closure of quaternionic dimension two, not an A_2 surface singularity.

The source states that the physical components meet only at the origin. If the scheme is reduced and the intersection is the reduced point, the coordinate ring is a fiber product over their common constants,

$$R(\mathcal{C}_{A_2} \cup \mathcal{C}_{A_1}) = R(\mathcal{C}_{A_2}) \times_{\mathbb{C}} R(\mathcal{C}_{A_1}). \tag{X.6.28}$$

Therefore the Hilbert series adds the two components and subtracts the single over-counted degree-zero unit,

$$H_{E_3}(t) = H_{A_2}(t) + H_{A_1}(t) - 1 = 1 + 11t^2 + 32t^4 + O(t^6). \tag{X.6.29}$$

Without the subtraction, the constant term would be two, impossible for the connected reduced union described here. A single quiver also cannot replace the union: it would erase one maximal decomposition and its different component dimension. The fiber-product step is algebraic conditional on the intersection; the physical two-cone statement and the reduced-origin premise are separate inputs. In Chapter 7 these two components supply a first example of why a Hasse picture must retain branching rather than depict every degeneration as a single chain.

One can see the gluing directly on homogeneous functions. An element of the fiber product is a pair (f, g) with $f(0) = g(0)$. Positive-degree functions may live on either component independently; only their constants are identified. In degree zero there is one common unit, while in every positive degree the dimensions add. Thus the same coefficient rule follows without assuming a smooth intersection,

$$R_0 \cong \mathbb{C}, \qquad R_{d>0} \cong (R_{A_2})_d \oplus (R_{A_1})_d. \tag{X.6.30}$$

If the physical intersection carried an additional nonreduced structure, this formula would fail and the Hilbert series would need the corresponding intersection ring. The stated reduced-origin premise is therefore essential exactly at the step where the two component series are combined.

X.6.4 Separated M5 branes and the affine D_4 magnetic quiver

Chapter 5, Section 5.6 constructs the finite phase of two *separated* M5-branes on A_1. Its electric IIA picture has two NS5s at distinct x^6 positions and two D6s between them. The source then gives a rearranged four-D8 endpoint with D6 interval multiplicities $1, 2, 1$. It does not specify a unique sequence of crossings between these drawings. Suspended D4 modes at the endpoint give the affine-D_4 magnetic graph. Two chain leaves arise from the outer D6 intervals, while two separate bouquet leaves arise from the NS5s. The finite-D_4 figure there shows the construction and identifies its four edges.

What does this finite-branch example teach before a tensor transition? At a regular, fully Higgsed point, the electric $SU(2)$ with four fundamentals has quaternionic quotient dimension

$$\dim_{\mathbb{H}} \mathcal{H}_{\text{electric}} = 4 \cdot 2 - (2^2 - 1) = 5. \tag{X.6.31}$$

The specified magnetic graph has compact group and effective rank

$$G_{D_4} = \frac{U(2) \times U(1)^4}{U(1)_{\text{diag}}}, \qquad \operatorname{rank} G_{D_4} = 2 + 4 - 1 = 5. \tag{X.6.32}$$

The common circle is primitive and ineffective; it does not identify the four leaves. The source's general separated-phase dimension gives the same specialization,

$$(k^2 + n - 1)\big|_{k=n=2} = 5. \tag{X.6.33}$$

These three fives are consistency checks conditional on the selected physical phase. They do not reconstruct the D8 rearrangement.

The nodewise test says more than total rank. Every unit leaf sees the central rank two, and the center sees four unit leaves,

$$2r_{\text{leaf}} = 2 = r_{\text{center}}, \qquad 2r_{\text{center}} = 4 = \sum_{i=0}^{3} r_{\text{leaf},i}. \tag{X.6.34}$$

This is the balanced affine-D_4 incidence. The two bouquet leaves cannot be merged into one rank-two leaf. An NS5–NS5 suspended D4 is massive at their nonzero x^6 separation. At coincidence the source assigns a different magnetic object, so the finite count cannot be continued through that phase change by changing a coefficient.

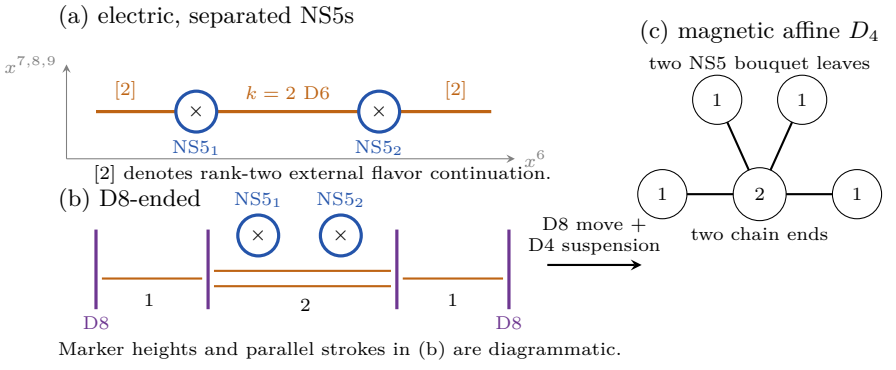


Figure X.6.3: Recall of the separated two-M5/A_1 phase constructed in Chapter 5, Section 5.6. The electric rank-two D6 interval and its four flavor continuations lead to the sourced four-D8 endpoint with $1, 2, 1$ D6 intervals. Two separate NS5s supply two of the four magnetic leaves; the outer D6 intervals supply the other two. The arrow denotes the sourced rearrangement and D4 dictionary, not a unique crossing history.

The nonabelian monopole formula supplies a sharper check. Fix one leaf flux $\ell_0 = 0$, order the central $U(2)$ fluxes as $a \le b$, and call the remaining leaf fluxes ℓ_1, ℓ_2, ℓ_3. The degree is

$$2\Delta(a, b; \ell) = \sum_{i=0}^{3} \big(|a - \ell_i| + |b - \ell_i|\big) - 2|a - b|. \tag{X.6.35}$$

The last term is the central positive root. Its residual dressings distinguish equal and unequal central flux,

$$P_{a=b}(t) = \frac{1}{(1 - t^2)^4 (1 - t^4)}, \tag{X.6.36}$$

$$P_{a<b}(t) = \frac{1}{(1 - t^2)^5}. \tag{X.6.37}$$

Chapter 5, Section 5.6 derives the finite flux bound and every shell population. For reference, putting $d = b - a$ gives the elementary identity

$$|a - \ell| + |b - \ell| = d + 2\,\mathrm{dist}(\ell, [a, b]), \tag{X.6.38}$$

and hence

$$2\Delta = 2d + 2\sum_{i=0}^{3} \mathrm{dist}(\ell_i, [a,b]). \tag{X.6.39}$$

Through degree four all independent fluxes lie in $[-2,2]$. Their bare shells and dressed coefficients are

$$B_{D_4}(t) = 1 + 24t^2 + 177t^4 + O(t^6), \tag{X.6.40}$$

$$[t^2]H_{D_4} = 4+8+16 = 28, \qquad [t^4]H_{D_4} = 11+8\cdot 4+16\cdot 5+32+145 = 300. \tag{X.6.41}$$

The 11 includes the degree-four Casimir of the unbroken $U(2)$; the unequal-flux sectors instead admit five degree-two scalar dressings. The resulting protected series is

$$H_{D_4}(t) = \sum_{\substack{a\le b \\ \ell_0=0,\ell_{1,2,3}\in\mathbb{Z}}} t^{2\Delta(a,b;\ell)} P_{a,b}(t) = 1 + 28t^2 + 300t^4 + O(t^6). \tag{X.6.42}$$

The coefficient 28 is the $SO(8)$ adjoint dimension expected at finite separation. Neutral adjoints of individual NS5 nodes were omitted only in this three-dimensional Coulomb count; no six-dimensional Higgs sector was removed. The next tensionless transition uses one M5 near an M9 on A_0, not a continuation of this two-M5/A_1 configuration.

X.6.5 A small E_8 instanton transition changes the slice

Place one M5 on A_0 outside an M9 plane and move it toward the wall. This is a different six-dimensional system from the separated pair on A_1. In the one-sided IIA drawing the M5 is a half NS5, the M9 is represented by O8$^-$ with eight local D8s, and one D6 reaches the D8/O8 region. The small-E_8 transition occurs when the half NS5 reaches the wall. How do its new Higgs directions acquire the magnetic fork that will carry the proposed 29-dimensional transverse slice?

The outside phase first brings one *additional* D8 from infinity to cap the original D6 on the left. The cap and the first of the eight local D8s bound one D6 segment; the half NS5 is off that D6 in the same interval. Their magnetic nodes are $U(1)_{\mathrm{D6}}$ and $U(1)_{\mathrm{NS5}}$ with one edge, as in Figure X.6.4(a),(b). The eight local D8s belong to the O8 system; their horizontal separation in the drawing resolves the count and does not impose eight distinct finite masses.

Now move the half NS5 past all eight *local* D8s, leaving it between the eighth and O8. The source's endpoint after this motion has one new D6 from each local D8 to the half NS5. The pre-existing external-cap segment remains. Counting intervals from left to right gives the brane multiplicities,

$$N_{\mathrm{created}} = \sum_{i=1}^{8} 1 = 8, \qquad N_{\mathrm{intervals}} = 1 \mid (1,2,3,4,5,6,7) \mid 8 \mid 0_{\mathrm{NS5-O8}}. \tag{X.6.43}$$

The eight increasing multiplicities in panel (c) count D6 ends on the NS5, not a rank-eight magnetic tail. The source shows the endpoint after all crossings; it does not specify eight separate intermediate trajectories.

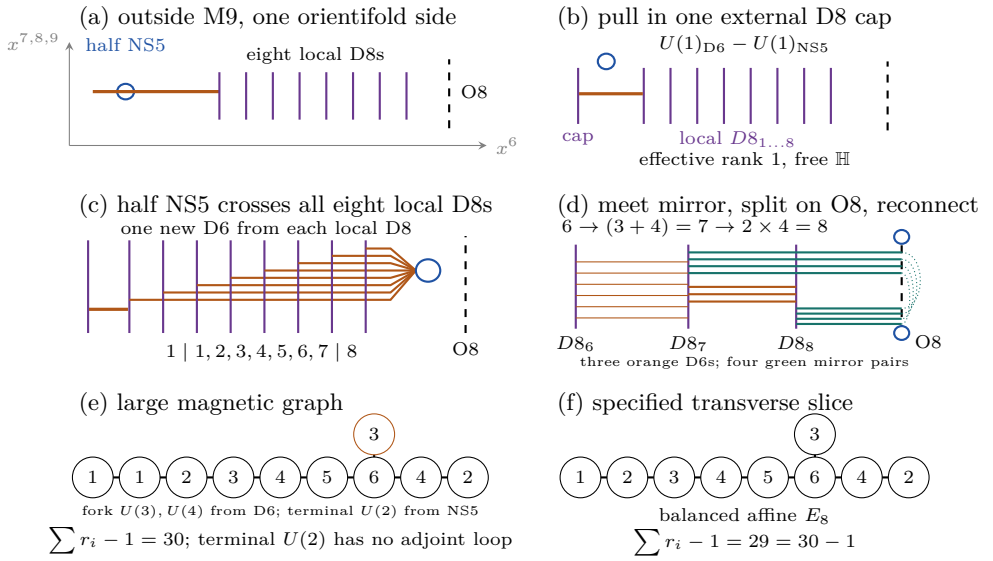


Figure X.6.4: The source's one-sided M5/M9 construction, with x^6 ordered to the right and $x^{7,8,9}$ transverse. (a) One half NS5 lies outside the O8 wall and its eight local D8s. (b) An extra D8 cap from infinity gives the outside 1–1 magnetic graph. (c) After the half NS5 crosses all eight local D8s, eight newly created D6s end on it; the interval multiplicities are $1 \mid 1, 2, 3, 4, 5, 6, 7 \mid 8$. (d) At O8, mirror reconnection splits the seven $D8_7$–$D8_8$ segments as $3 + 4$ and pairs eight near-wall half-segments as 2×4. Dotted links beyond the wall record mirror pairing, not physical turns; the two half NS5s remain distinct magnetic constituents. (e) The resulting large graph has a D6-derived rank-three/rank-four fork and an NS5-derived terminal rank two. (f) The source's specified transverse slice has balanced affine-E_8 topology. Panels (e) and (f) have effective ranks 30 and 29; panel (f) is a geometric comparison, not a further physical phase.

At O8 the half NS5 meets its mirror, and the two half NS5s split along the orientifold. The newly created D6s become free to move in the transverse directions. A D6 joining a D8 only to its own mirror does not give the desired massless BPS state, so the two intervals nearest the wall are rearranged as in panel (d). Of the seven D6 portions between local D8s 7 and 8, three end on those two D8s. The other four extend from $D8_7$ through O8 to the mirror of $D8_8$. Equivalently, each mirror representative runs from $D8_8$ to the mirror of $D8_7$: the two endpoint species are different, never a D8 and its own mirror. The eight near-wall half-segments pair into four mirror-connected objects,

$$7 = 3 + 4, \qquad 8 = 2 \times 4. \tag{X.6.44}$$

The $U(3)$ and $U(4)$ populations both meet the $U(6)$ interval between D8s 6 and 7; their bifundamentals produce the fork. The terminal $U(2)$ arises instead from the two half NS5s on O8 and joins $U(4)$ by the suspended-D4 dictionary. The orientifold freezes

their magnetic adjoint, so this $U(2)$ carries no adjoint loop. These are counts read from the source's reconnection, not an independently derived orientifold charge law. Extending the pre-wall ranks seven and eight as a linear tail would miss both the fork and the NS5 origin of its last node.

The source presents three actual graph objects. Before the transition, the outside-M9 phase has two rank-one nodes joined by one edge. After it, the large branch has horizontal ranks $(1,1,2,3,4,5,6,4,2)$ and a rank-three fork on the rank-six node. The specified slice graph has horizontal ranks $(1,2,3,4,5,6,4,2)$ with the same rank-three fork attached to rank six. Figure X.6.4(e),(f) displays the large graph and the specified slice after the counted brane panels. Panel (f) compares geometries; it is not another brane-motion stage.

For a connected unframed graph, sum the unitary ranks and remove one common diagonal. Thus the first and second graphs have effective ranks

$$r_{\text{outside}} = (1{+}1){-}1 = 1, \qquad r_{\text{large}} = (1{+}1{+}2{+}3{+}4{+}5{+}6{+}4{+}2{+}3){-}1 = 30. \tag{X.6.45}$$

The separately drawn slice has

$$r_{\text{slice}} = (1+2+3+4+5+6+4+2+3) - 1 = 29. \tag{X.6.46}$$

The rank jump is $30 - 1 = 29$, matching the slice rank. The outer graph is the Coulomb branch of a free hypermultiplet. The large branch retains a free factor, while its interacting transverse piece is associated with the minimal E_8 orbit closure. Saying that the singular origin has 29 free hypermultiplets would erase that interacting geometry.

The free small graph has a particularly transparent magnetic exponent. After fixing one of its two rank-one fluxes to zero, let the other be m. Its single bifundamental contributes $2\Delta(m) = |m|$. The residual scalar of the effective $U(1)$ gives

$$H_{\text{outside}}(t) = \frac{\sum_{m\in\mathbb{Z}} t^{|m|}}{1-t^2} = \frac{1}{(1-t)^2}. \tag{X.6.47}$$

The two degree-one generators are the coordinates of a free quaternionic line. This factor explains why the original small graph should not be presented as an interacting good cone. It also exposes the grading difference between the free factor and the balanced minimal-E_8 piece, whose first nonconstant generators occur at degree two.

The large graph also exposes its free factor without treating all its 30 effective directions as free. At the outermost horizontal rank-one node, the only neighbor has rank one. Its balance excess is

$$e_{\text{outer}} = \sum_{j\sim\text{outer}} r_j - 2r_{\text{outer}} = 1 - 2 = -1. \tag{X.6.48}$$

A primitive magnetic charge on that end node alone has one unit of matter variation and no central-root contribution, hence $2\Delta = 1$. It produces a degree-one free direction. The remaining balanced topology, after the source's specified slice operation, is the interacting affine-E_8 graph. This local flux check distinguishes the free factor from the rank-29 slice; it does not establish a global product decomposition beyond the one described by the source.

The slice's affine-E_8 balance can be checked node by node. For its horizontal rank vector $v = (1, 2, 3, 4, 5, 6, 4, 2)$, the neighbor-rank sum equals twice the rank at every node after including the fork rank three at the sixth node. At the fork and at rank six, for example,

$$2 \cdot 3 = 6, \qquad 2 \cdot 6 = 5 + 4 + 3. \tag{X.6.49}$$

At the two ends the equalities are $2 \cdot 1 = 2$ and $2 \cdot 2 = 4$. The remaining chain equalities follow from adjacent triples $(1, 2, 3)$, $(2, 3, 4)$, $(3, 4, 5)$ and $(4, 5, 6)$. This balance identifies the graph as the expected affine type; it does not construct the orientifold phase change. For the whole horizontal chain, writing the neighbor sum at each node also checks that the fork has been attached at the correct place,

$$(2,\ 1+3,\ 2+4,\ 3+5,\ 4+6,\ 5+4+3,\ 6+2,\ 4) = 2(1, 2, 3, 4, 5, 6, 4, 2). \tag{X.6.50}$$

Attaching the rank-three node to a neighboring rank-five or rank-four node would violate this equality and would define a different quiver. The position of the fork is therefore part of the source object, not a decorative way to draw a rank list.

The source also depicts a subtraction relation between the two physical branches. Its small graph has a nontrivial embedding in the large graph. The horizontal lists above cannot be aligned merely by adding leading zeros to $(1, 1)$ and subtracting componentwise. That operation would misidentify the transverse singularity. What we can verify directly is the three graph topologies, their effective ranks, and the balance of the specified slice. The brane creation and embedding are additional source premises. Chapter 7 will treat the transverse slice as a local geometric object rather than an arithmetic difference of rank lists.

It is useful to distinguish three geometries even though the same transition relates them. The outside-M9 Coulomb cone has complex dimension two and is smooth as a free quaternionic line. The large branch has complex dimension 60, with a free factor. The transverse minimal-E_8 cone has complex dimension 58 and a singular origin. The dimensions obey

$$\dim_{\mathbb{C}} \mathcal{C}_{\text{outside}} = 2, \quad \dim_{\mathbb{C}} \mathcal{C}_{\text{large}} = 60, \quad \dim_{\mathbb{C}} \mathcal{S}_{E_8} = 58. \tag{X.6.51}$$

The identity $60 - 2 = 58$ is compatible with a transverse slice, but does not construct its embedding. The graph of the slice and the source's transition supply more structure than the rank difference. Treating the large cone as 30 free quaternionic lines would match dimension while discarding its interacting E_8 singularity.

A restricted anomaly check makes the number 29 less accidental while showing its limit. For one hypothetical free six-dimensional hyper and one tensor, the purely gravitational contributions in the stated normalization are

$$I_H^{\text{grav}} = \frac{7p_1^2 - 4p_2}{5760}, \qquad I_T^{\text{grav}} = \frac{23p_1^2 - 116p_2}{5760}. \tag{X.6.52}$$

Condition on one lost tensor, a gain of 29 Higgs quaternionic directions and unchanged vector content. Then the irreducible p_2 coefficient cancels,

$$[p_2](29I_H^{\text{grav}} - I_T^{\text{grav}}) = \frac{-116 + 116}{5760} = 0, \tag{X.6.53}$$

but the reducible gravitational term survives,

$$29I_H^{\text{grav}} - I_T^{\text{grav}} = \frac{29 \cdot 7 - 23}{5760} p_1^2 = \frac{p_1^2}{32}. \tag{X.6.54}$$

The same arithmetic with 28 directions would leave a nonzero p_2 coefficient. This check concerns only the restricted gravitational coefficient. It does not include R-symmetry, flavor, or Green–Schwarz terms and does not prove full anomaly matching. The use of I_H here compares coefficients under a dimension-change assumption; it does not replace the interacting minimal-E_8 slice by 29 free hypers at its singular origin.

X.6.6 When quiver subtraction describes a transverse slice

A transverse slice is a local normal space to a stratum, so its location matters. A named $\mathfrak{sl}_5$ example supplies a controlled case in which aligned quiver subtraction produces such a slice. Both input gauge graphs are four-node chains. Their ranks and fundamental-flavor vectors are shown in Figure X.6.5; the smaller quiver's flavors are at the ends, whereas the larger quiver's flavors are in the middle. That difference is easy to miss if only gauge ranks are printed.

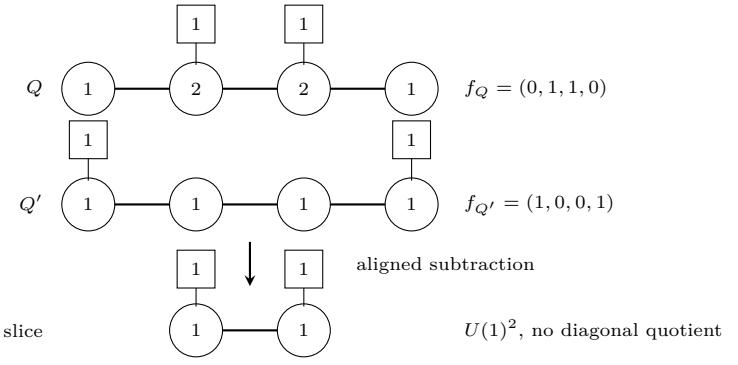


Figure X.6.5: Aligned four-node chains in the specified $\mathfrak{sl}_5$ example. The upper graph Q has ranks $(1, 2, 2, 1)$ and middle flavors $(0, 1, 1, 0)$. The lower graph Q' has ranks $(1, 1, 1, 1)$ and end flavors $(1, 0, 0, 1)$. Subtracting gauge ranks while retaining Q's flavor positions leaves two framed rank-one nodes with one connecting edge. The slice is taken at an interior point of orbit $(2, 1^3)$.

In the declared alignment, subtraction acts on gauge ranks and retains the larger graph's flavors. It gives

$$(1, 2, 2, 1) - (1, 1, 1, 1) = (0, 1, 1, 0), \tag{X.6.55}$$

$$f_Q = (0, 1, 1, 0) \quad \longrightarrow \quad \text{one fundamental at each surviving } U(1). \tag{X.6.56}$$

The two surviving gauge nodes have one bifundamental between them. Because each also has a fundamental, their simultaneous diagonal circle acts on matter and must be retained. The compact gauge group is $U(1) \times U(1)$, of rank two. Removing a common diagonal here would lower the predicted slice dimension and change the ring. The rule used for the unframed affine graphs is therefore not portable without checking the representation.

The matter incidence also makes the framed graph balanced. Each surviving rank-one node sees one neighboring rank-one gauge node and one fundamental flavor, for total matter rank two,

$$2r_1 = r_2 + f_1 = 1 + 1 = 2, \qquad 2r_2 = r_1 + f_2 = 1 + 1 = 2. \tag{X.6.57}$$

If the middle flavors had been replaced by the end flavors of Q' after subtraction, the surviving nodes would be unframed and the compact quotient would change. Flavor retention is therefore part of the local slice construction, not a harmless notation choice.

Let m, n be its two integral monopole charges. Its two fundamentals and one bifundamental yield

$$2\Delta(m,n) = |m| + |m-n| + |n|. \tag{X.6.58}$$

There are two independent degree-two vector scalars, and the same triangle expression encountered earlier now arises from a framed two-node graph rather than a three-node quotient. The finite series is

$$H_{\text{slice}}(t) = \frac{\sum_{m,n\in\mathbb{Z}} t^{|m|+|m-n|+|n|}}{(1-t^2)^2} = 1 + 8t^2 + 27t^4 + O(t^6). \tag{X.6.59}$$

Its quaternionic dimension is two. These coefficients match the minimal A_2 nilpotent cone in this named example; equality of the first two coefficients alone would not characterize an arbitrary cone.

The orbit geometry fixes the point at which the slice is meant. The larger quiver has Coulomb branch the closure of the orbit $(2^2, 1)$ in $\mathfrak{sl}_5$, and the smaller quiver has the closure of $(2, 1^3)$. For an $\mathfrak{sl}_5$ partition λ, the complex orbit dimension is $25 - \sum_i (\lambda_i^{\mathsf{T}})^2$. The two transposed partitions are $(3, 2)$ and $(4, 1)$, so

$$\dim_{\mathbb{C}} \mathcal{O}_{(2^2,1)} = 25 - (3^2 + 2^2) = 12, \qquad \dim_{\mathbb{C}} \mathcal{O}_{(2,1^3)} = 25 - (4^2 + 1^2) = 8. \tag{X.6.60}$$

Their complex dimension difference is four, consistent with a quaternionic two-dimensional transverse slice,

$$12 - 8 = 4 = 2 \dim_{\mathbb{H}} \mathcal{C}(Q_{\text{slice}}). \tag{X.6.61}$$

The specified slice is at a point inside orbit $(2, 1^3)$. Taking a boundary point of its closure would change the stabilizer and may give a larger local singularity. The named geometric example is known in the source treatment; its broader proposal that rank subtraction produces slices under orbit, inclusion, rank and flavor hypotheses is conjectural. The distinction is useful in Chapter 7, where a Hasse edge must name both the containing stratum and the point whose normal geometry it represents.

A matrix representative makes the word "interior" concrete. Let E_{12} have one unit entry in row one, column two and zeros elsewhere. Then

$$E_{12}^2 = 0, \qquad \operatorname{rank} E_{12} = 1, \qquad E_{12} \in \mathcal{O}_{(2,1^3)} \subset \mathfrak{sl}_5. \tag{X.6.62}$$

The larger closure consists of square-zero matrices of rank at most two; the smaller closure consists of those of rank at most one. Thus E_{12} lies on the rank-one orbit, while the zero matrix is a different, lower stratum. The relevant local normal slice is taken transverse to the rank-one orbit at E_{12}, not through the zero matrix. Dimension subtraction then refers to tangent directions normal to that orbit inside the larger closure. At the zero matrix the orbit tangent space is absent, so the same rank difference would not be a valid local-slice derivation.

The series also admits a representation check. The minimal $\mathfrak{sl}_3$ cone has degree-$2k$ piece of highest weight (k, k) and dimension $(k+1)^3$. Hence

$$H_{\min \mathrm{A}_2}(t) = \sum_{k \geq 0} (k+1)^3 t^{2k} = 1 + 8t^2 + 27t^4 + 64t^6 + \cdots . \tag{X.6.63}$$

The first two positive coefficients agree with the framed-quiver monopole calculation. Here the orbit construction supplies a named geometric target; the coefficient check tests the quiver representation of that target. In an unselected graph, matching a short series would not establish the required orbit inclusion or the point of slicing.

This example fixes the direction of the operation before Chapter 7 uses similar graph language. Here the inputs are an ambient orbit closure and a lower orbit closure; aligned gauge-rank subtraction, with the ambient physical fundamentals retained, produces the slice. The surviving framed nodes have no ineffective diagonal to remove. Chapter 7 instead starts with an ambient quiver and an embedded known slice. In its selected unframed examples, subtraction followed by rebalancing produces a quiver for the lower leaf, and the ineffective common diagonal is removed from that unframed graph. These are different roles for the inputs, not inverse algorithms for arbitrary quivers. A dimension difference checks a proposed slice or lower leaf only after the embedding and matter representation are fixed.

X.6.7 What the examples establish

The five-dimensional examples begin at massless infinite coupling. For E_4, a selected maximal five-subweb decomposition and the shared-seven-brane incidence lead to a weighted five-cycle. Its compact quotient and low-degree Coulomb series are exact once that graph is specified. For E_3, one web admits two maximal decompositions; the reduced-origin assumption gives a fiber-product union. The endpoint cancellation example proves that stable intersection by itself is insufficient even before a Hilbert sum is attempted.

The six-dimensional examples have different physical premises. The affine-D_4 graph belongs to a finite separated-M5 tensor phase. Its electric and magnetic dimension counts both give five, and its nonabelian monopole series begins $1 + 28t^2 + 300t^4$. The M5/M9 transition instead uses an orientifold phase change. Three sourced graphs

identify a free small branch, a large branch with a free factor, and a rank-29 interacting transverse slice. The restricted gravitational p_2 cancellation supports the rank jump under stated assumptions; its p_1^2 remainder forbids interpreting that check as full anomaly matching.

The $\mathfrak{sl}_5$ example clarifies what a slice calculation can actually do. Retaining the two flavor nodes turns the rank difference into a framed two-node quiver, with no diagonal quotient. Its local slice sits at an interior orbit point. These facts make it a useful model for the stratification in Chapter 7, while leaving the general subtraction prescription at its stated conjectural scope. The calculable three-dimensional rings sharpen each proposed branch correspondence. They cannot supply the web, M5, M9, or orientifold premises that selected those rings.

The five objects answer different questions, so it helps to keep their phase and mathematical test side by side in Table X.6.2. The table is also a warning against combining a finite-tensor affine D_4 count with the M5/M9 transition or using the E_3 union as if it were the single E_4 cycle.

object	physical phase that selects the graph	check after the graph is fixed
E_4 five-cycle	massless infinite-coupling $SU(2)$ with three flavors	ten endpoint pairs; $1 + 24t^2 + 200t^4$
E_3 union	massless infinite-coupling $SU(2)$ with two flavors	two compact ranks; fiber product $1 + 11t^2 + 32t^4$
affine D_4	two separated M5s on A_1 at finite tensor vev	rank five; nonabelian $1+28t^2+300t^4$
E_8 slice	single M5/M9 transition	three source graphs; effective ranks $1, 30, 29$
$\mathfrak{sl}_5$ slice	interior rank-one orbit point	framed rank two; $1+8t^2+27t^4$

Table X.6.2: The phase selects a particular three-dimensional object. The last column lists calculations for that object, not claims of complete cross-dimensional QFT equivalence.

X.6.8 Exercises

1. In the five-subweb $SU(2)$, $N_f = 3$ web, compute $E = SI + X - Y$ for all ten unordered color pairs in Table X.6.1. Give the five positive weighted edges and the quaternionic dimension after the primitive common diagonal is removed. Then explain why red–blue and red–green would be false links if one used stable intersection alone.

2. For the massless $SU(2)$, $N_f = 2$ web, calculate the three determinants in (X.6.20) and the compact ranks of the triangle and double-link quivers. Assuming their reduced cones meet at the reduced origin, derive the coefficients of t^0, t^2, t^4 for their union from the two component series. Explain the single constant that must be subtracted.

3. For two separated M5-branes on A_1, calculate the electric Higgs quaternionic dimension of the $SU(2)$ theory with four full fundamentals. Write the compact group of the four-leaf affine-D_4 magnetic quiver and its Coulomb rank. Use the equal and unequal central-flux dressings to obtain its t^0, t^2, t^4 coefficients.

4. The Appendix A endpoint fixture has $SI = 4$, $X = (0, 0, 2)$ and $Y = (1, 1, 4)$. Find the total opposite-side and same-side contributions and the resulting edge multiplicity. State why the zero-edge result alone does not furnish a good interacting monopole-series example.

5. Subtract the aligned gauge-rank vectors $(1, 2, 2, 1)$ and $(1, 1, 1, 1)$, retaining the first graph's middle fundamental flavors. Draw the surviving framed graph, state its compact gauge group and compute the sum of its nonzero gauge ranks. Use the two partition transposes to check the complex orbit-dimension difference.

6. Explain in words which steps in the E_4 web and separated-M5 examples depend on a physical brane construction, and which follow algebraically after the compact three-dimensional quiver is fixed. Distinguish finite tensor vev from a coincident-M5 phase and a branch correspondence from equality of complete quantum field theories.

X.6.9 Take-home message

Take-home message

A singular brane phase can supply a magnetic quiver for a proposed Higgs branch. Shared seven-brane endpoints turn the named E_4 five-subweb fixture into a unit five-cycle with $H = 1 + 24t^2 + 200t^4 + \cdots$; two different maximal decompositions keep the E_3 branch reducible. In six dimensions the finite separated-M5 A_1 system gives a four-leaf affine-D_4 quiver, while the M5/M9 transition has a rank-29 minimal-E_8 transverse slice. The $\mathfrak{sl}_5$ example shows how framed, aligned subtraction can describe a local slice at an interior orbit point. Compact quotients, weighted monopole counts and orbit dimensions are calculable for these fixed three-dimensional objects. The physical higher-dimensional branch identifications remain the sourced construction assumptions.

Status and sources

The five-dimensional subweb prescription and its status as Conjecture 1 come from Cabrera, Hanany, and Yagi (2019, PDF pp. 12–13, Fig. 7, Table 2, and pp. 18–19). The ten-pair endpoint incidence in Section X.6.2 is the named source fixture; the weighted-cycle and low-degree series calculations are [MATH] conditional on it. The source's web motion and five-dimensional branch identification are [GEO-E] and [CONJ+], respectively. The endpoint-cancellation fixture uses Cabrera, Hanany, and Yagi (2019, PDF pp. 46–48, Appendix A). The E_3 two-decomposition source is Cabrera, Hanany,

and Yagi (2019, PDF pp. 7–10, Figs. 2–4); its union series is [MATH] given a reduced-origin intersection. The monopole grading follows Cremonesi et al. (2014, PDF pp. 7–14, eqs. (2.4)–(3.20)).

The finite separated-M5/A_1 graph and electric comparison in Section X.6.4 follow Cabrera, Hanany, and Sperling (2019, PDF pp. 7–9, eqs. (2.4)–(2.10)) and its published erratum. The affine-D_4 rank and degree-four monopole sum are [MATH] for the stated compact group; the equality to the six-dimensional branch is the source's proposed [GEO-E] relation. Neutral NS5 adjoints are omitted only in the three-dimensional Coulomb count. Section X.6.5 uses the corrected complete article, PDF pp. 13–14 and 18, eqs. (2.14)–(2.20) and (2.31)–(2.32), with Cabrera, Hanany, and Sperling (2019, PDF pp. 10–12 and 14–15) as the arXiv version. Its three graph ranks and affine balance are [MATH]; the M5/M9 orientifold transition, graph embedding and minimal-E_8 physical slice are source premises. The restricted gravitational comparison uses Ohmori et al. (2014, PDF p. 26, Appendix A) and does not assert full anomaly matching. The corrected source uses inconsistent H_1/H_2 subscripts between its general subtraction passage and worked example; the outside, post-transition and slice names above refer to the actual graphs and phases. The $7 = 3 + 4$ and $8 = 2 \times 4$ counts use its displayed orientifold reconnection, not a separately established charge rule.

The framed $\mathfrak{sl}_5$ example in Section X.6.6 comes from Cabrera and Hanany (2018, PDF pp. 4–7, Secs. 2–3). Its named interior-orbit slice is a source-described geometric example; the broader subtraction rule is Conjecture 1 of that source. The rank, orbit-dimension and low-degree series calculations are [MATH] for the specified graphs. The web, branch and compact monopole conventions are those specified in the constructions above. No full QFT or metric equivalence, general M5/M9 circle lift, or all-degree D_4 Hilbert formula is inferred from these selected calculations.

References

Cabrera, S. and A. Hanany (2018). "Quiver Subtractions". In: *JHEP* 09, p. 008. DOI: 10.1007/JHEP09(2018)008. arXiv: 1803.11205 [hep-th].

Cabrera, S., A. Hanany, and M. Sperling (2019). "Magnetic quivers, Higgs branches, and 6d N=(1,0) theories". In: *JHEP* 06. [Erratum: JHEP 07, 137 (2019)], p. 071. DOI: 10.1007/JHEP06(2019)071. arXiv: 1904.12293 [hep-th].

Cabrera, S., A. Hanany, and F. Yagi (2019). "Tropical Geometry and Five Dimensional Higgs Branches at Infinite Coupling". In: *JHEP* 01, p. 068. DOI: 10.1007/JHEP01(2019)068. arXiv: 1810.01379 [hep-th].

Cremonesi, S., A. Hanany, and A. Zaffaroni (2014). "Monopole operators and Hilbert series of Coulomb branches of $3d$ $\mathcal{N} = 4$ gauge theories". In: *JHEP* 01, p. 005. DOI: 10.1007/JHEP01(2014)005. arXiv: 1309.2657 [hep-th].

Ohmori, K. et al. (2014). "Anomaly polynomial of general 6d SCFTs". In: *PTEP* 2014.10, 103B07. DOI: 10.1093/ptep/ptu140. arXiv: 1408.5572 [hep-th].

Chapter X.7

Hilbert series and the stratification of moduli spaces

X.7.1 One five-dimensional Higgs branch, two cones

At infinite coupling the massless five-dimensional $SU(2)$ theory with two fundamental hypermultiplets has a Higgs branch with two irreducible components. One is the closure of the minimal nilpotent orbit of $\mathfrak{sl}_3$; the other is the corresponding closure for $\mathfrak{sl}_2$. They meet only at the origin. A single cone would miss the possibility of moving away from the origin in two different ways. The web construction supplies this physical branch identification. Our task is to find what follows mathematically once it is accepted.

Write $X_2 = \overline{\mathcal{O}}_{\min}(\mathfrak{sl}_3)$ and $X_1 = \overline{\mathcal{O}}_{\min}(\mathfrak{sl}_2)$. At zero masses and zero Coulomb vev the sourced statement is

$$\mathcal{H}_\infty(SU(2), N_f = 2) = X_2 \cup_{\{0\}} X_1, \qquad \dim_{\mathbb{C}}(X_2, X_1, \{0\}) = (4, 2, 0). \tag{X.7.1}$$

Here the subscript is the five-dimensional coupling limit. The symbols X_2 and X_1 label components, not values of a flavor number. Each component has its own three-dimensional magnetic quiver. The affine A_2 triangle produces X_2 as a Coulomb branch, while the two-node doubled-edge affine A_1 quiver produces X_1. Chapter 6 explains the web decomposition from which these quivers are proposed; the later sections here compute inside the resulting three-dimensional theories.

The scheme structure matters for counting. Let $A = \mathbb{C}[X_2]$ and $B = \mathbb{C}[X_1]$. With a reduced common origin, evaluation at zero gives the coordinate ring of the union as a fiber product:

$$\mathbb{C}[X_2 \cup_{\{0\}} X_1] = A \times_{\mathbb{C}} B = \{(f, g) \in A \oplus B : f(0) = g(0)\}. \tag{X.7.2}$$

The defining exact sequence makes the overlap correction explicit:

$$0 \longrightarrow A \times_{\mathbb{C}} B \longrightarrow A \oplus B \xrightarrow{(f,g)\mapsto f(0)-g(0)} \mathbb{C} \longrightarrow 0. \tag{X.7.3}$$

Consequently, in the book grading $x = t^2$, the Hilbert series obeys

$$H_{\mathcal{H}_\infty}(t) = H_{X_2}(t) + H_{X_1}(t) - 1. \tag{X.7.4}$$

The subtraction removes one copy of the constant function. It does not remove a whole positive-dimensional branch.

One can see the component dimensions without reading a Hilbert-series denominator. A minimal nilpotent matrix for $\mathfrak{sl}_r$ can be written $M = uv^{\mathsf{T}}$ with $u, v \in \mathbb{C}^r$ and $v^{\mathsf{T}}u = 0$, modulo $(u, v) \sim (\lambda u, \lambda^{-1}v)$. Away from zero this gives

$$\dim_{\mathbb{C}} \overline{\mathcal{O}}_{\min}(\mathfrak{sl}_r) = 2r - 1 - 1 = 2r - 2. \tag{X.7.5}$$

For $r = 3$ and $r = 2$ this reproduces four and two. The matrix is traceless and satisfies $M^2 = u(v^{\mathsf{T}}u)v^{\mathsf{T}} = 0$. At $M = 0$ the orbit parametrization collapses; this is precisely the singular point shared by the two components. The dimension count therefore explains both why the open pieces differ in size and why their intersection must be treated separately when counting functions.

The minimal-orbit character series determine both components. For $\mathfrak{sl}_3$, the kth graded piece is the representation $[k, k]$ of dimension $(k+1)^3$. For $\mathfrak{sl}_2$, the corresponding dimension is $2k + 1$. Thus

$$H_{X_2}(t) = \sum_{k\geq 0}(k+1)^3 x^k = \frac{1 + 4x + x^2}{(1-x)^4}, \qquad H_{X_1}(t) = \sum_{k\geq 0}(2k+1)x^k = \frac{1+x}{(1-x)^2}. \tag{X.7.6}$$

Inserting these series into the fiber-product formula yields a concrete first check of the geometry:

$$H_{\mathcal{H}_\infty}(t) = 1 + 11t^2 + 32t^4 + 71t^6 + 134t^8 + O(t^{10}). \tag{X.7.7}$$

For instance the degree-two coefficient is $8 + 3 = 11$, while the constant coefficient is $1 + 1 - 1 = 1$. These numbers count operators on the reduced union; they do not tell us by themselves that there are two components. The first nonconstant terms also separate the two tangent spaces:

$$\dim A_2 = 8, \qquad \dim B_2 = 3, \qquad \dim(A \times_{\mathbb{C}} B)_2 = 8 + 3. \tag{X.7.8}$$

There is no positive-degree overlap to subtract, because the reduced intersection is a point. Were the intersection a nonreduced scheme, its Hilbert series could carry positive-degree terms; the simple minus-one rule would then be wrong. That is a geometric hypothesis, not a convention about the constant coefficient.

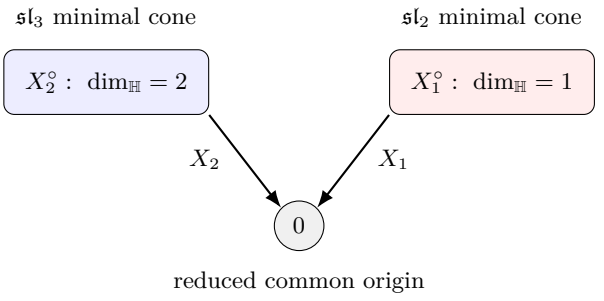


Figure X.7.1: The sourced infinite-coupling E_3 Higgs branch. The two upper nodes denote distinct open symplectic leaves of complex dimensions four and two; their closures meet at the lower origin. The component magnetic quivers are separate; the drawing does not combine them into one gauge theory.

The origin is a useful warning about what a Hilbert series cannot see. The series records dimensions of homogeneous vector spaces in a ring; it does not record their multiplication, their Poisson bracket, or the way their symplectic leaves meet. Conversely, the union statement alone does not determine the coefficients without the two graded component rings and the reduced-overlap assumption. This is why we will first learn to count operators and then return to the leaf geometry. The finite-coupling branch is a different physical limit and is not assigned the union in (X.7.1).

X.7.2 Magnetic flux and the monopole Hilbert sum

Which operators does a magnetic-quiver Hilbert series count? In a three-dimensional $\mathcal{N} = 4$ theory with compact gauge group G, a bare monopole insertion specifies magnetic flux on a small sphere around the insertion. Choose a maximal torus $T \subset G$. Conjugacy classes of homomorphisms $U(1) \to G$ are represented by the cocharacter lattice of T, modulo the Weyl group. The flux belongs to the cocharacter lattice $\Lambda_{\mathrm{cochar}}(G)$, modulo the Weyl group. The compact group, not merely its Lie algebra, fixes that lattice:

$$m \in \Lambda_{\mathrm{cochar}}(G)/W_G, \qquad \Lambda_{\mathrm{cochar}}(G) = \mathrm{Hom}(U(1), T). \tag{X.7.9}$$

All three-dimensional examples below are at zero real and complex masses and zero FI parameters, where available. A theory is good when $\Delta(m) > 1/2$ for every nonzero bare magnetic sector; it is ugly when $\Delta(m) \geq 1/2$ with saturation, which signals a free sector. Bad theories lie outside the use of the formula here. In a good or ugly theory, the ultraviolet monopole R charge supplies the protected grading used in the monopole formula. We use $t^{2\Delta}$ so that a residual complex scalar has degree two. This is the book grading throughout the chapter; any comparison with formulas written in t^{Δ} requires replacing their variable by t^2.

For weights ρ of full hypermultiplet representations and positive roots α of G, the charge entering the sum is written below. Each full hypermultiplet contributes the

weights of R once, not those of $R \oplus \overline{R}$ twice, as in Chapter 5:

$$2\Delta(m) = \sum_{\text{full hypers } R} \sum_{\rho \in R} |\rho(m)| - 2 \sum_{\alpha > 0} |\alpha(m)|. \tag{X.7.10}$$

The matter term counts charged zero modes; the negative root term accounts for the vector multiplet. Neither can be dropped in a nonabelian example. A bare flux can also be multiplied by invariant polynomials in the complex scalar of its residual centralizer $H_m \subset G$. If its independent Casimirs have ordinary polynomial degrees $d_i(H_m)$, their contribution is

$$P_G(t; m) = \prod_{i=1}^{\operatorname{rank} H_m} \frac{1}{1 - t^{2d_i(H_m)}}. \tag{X.7.11}$$

The Hilbert sum is therefore

$$H_G(t, \boldsymbol{w}) = \sum_{m \in \Lambda_{\text{cochar}}(G)/W_G} t^{2\Delta(m)} \boldsymbol{w}^{J(m)} P_G(t; m). \tag{X.7.12}$$

The optional fugacity $\boldsymbol{w}$ records an integral topological charge when the theory has one. It is not a universal $U(1)$ fugacity: compact $SU(2)$ has no continuous topological $U(1)$ of the type used for $U(1)$ gauge theory.

It is useful to inspect what one summand actually counts. At fixed m, a term $t^{2\Delta(m)}$ marks a bare monopole. Multiplication by the geometric factors in P_G counts all gauge-invariant polynomial dressings of that same flux. For compact $SU(2)$ with four doublets, the first three Weyl representatives already show the structure:

$$(k, 2\Delta(k), H_k) = (0, 0, SU(2)),\ (1, 4, U(1)),\ (2, 8, U(1)). \tag{X.7.13}$$

The $k = 1$ bare operator first appears at degree four, while its first dressing appears at degree six. The $k = 0$ scalar invariant first appears at degree four rather than degree two. These are statements about sectors of one theory, not about three different quivers.

The simplest nonabelian diagnostic is the residual group. For compact $SU(2)$, choose the integral coroot representative $m = \operatorname{diag}(k, -k)$ with $k \geq 0$. At $k = 0$, the full group survives and its quadratic Casimir has book degree four. At $k > 0$, the centralizer is $U(1)$ and its linear scalar has book degree two:

$$P_{SU(2)}(t; 0) = \frac{1}{1 - t^4}, \qquad P_{SU(2)}(t; k > 0) = \frac{1}{1 - t^2}. \tag{X.7.14}$$

This split is the reason a nonabelian flux sum cannot be obtained by putting a single common denominator in front of all sectors.

The two factors can be derived directly from scalar invariance. At zero flux, a complex Cartan scalar φ is still identified by the $SU(2)$ Weyl reflection $\varphi \mapsto -\varphi$. Hence only its even powers survive, and the invariant polynomial algebra is

$$\mathbb{C}[\varphi]^{\mathbb{Z}_2} = \mathbb{C}[\varphi^2], \qquad \deg \varphi^2 = 4. \tag{X.7.15}$$

For positive coroot flux the unbroken group is the Cartan $U(1)$. The chosen positive Weyl chamber no longer acts as a reflection inside this residual scalar algebra, so

$$\mathbb{C}[\varphi]^{U(1)} = \mathbb{C}[\varphi], \qquad \deg \varphi = 2. \tag{X.7.16}$$

These are precisely the denominators in (X.7.14). The example shows what dressing means in an operator count: one fixes a monopole sector first, then adjoins scalar polynomials invariant under its own residual gauge group.

The distinction also clarifies the relation between the formula and the physical branch of a higher-dimensional theory. The input to (X.7.12) is a compact three-dimensional group and its hypermultiplet representation. A web can motivate those data, but the web's Higgs branch is not defined by the sum. Only after the magnetic-quiver correspondence is supplied may the resulting graded ring be compared with that branch. This order prevents a successful coefficient match from being mistaken for an independent derivation of the web correspondence.

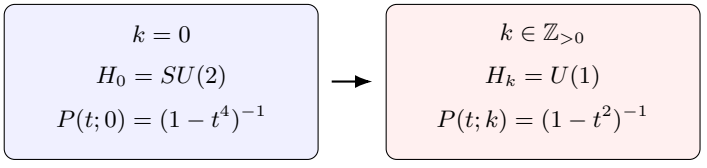


Figure X.7.2: The same compact $SU(2)$ theory in two flux sectors. The zero sector retains a quadratic invariant of book degree four. A nonzero integral coroot breaks the residual group to $U(1)$ and permits a degree-two scalar. The arrows mark sector change, not a physical flow.

The sum is a protected count for the specified three-dimensional gauge theory under the stated charge hypotheses. A proposed equality between that Coulomb branch and a five-dimensional Higgs branch uses an additional brane or magnetic-quiver argument. It does not follow by manipulating (X.7.12). In particular a compact quotient must be imposed before counting: an ineffective diagonal $U(1)$ leaves a common magnetic flux with zero charged matter and therefore infinitely many degree-zero terms. Sections X.7.5 and X.7.7 show this removal in actual quivers.

X.7.3 The A-series ring and Molien counting

Consider compact $U(1)$ with n charge-one full hypermultiplets. Its integer flux m has no root contribution, and every flux leaves the same residual $U(1)$ scalar Φ. Equation (X.7.10) becomes

$$m \in \mathbb{Z}, \qquad 2\Delta(m) = n|m|, \qquad P_{U(1)}(t;m) = \frac{1}{1-t^2}. \tag{X.7.17}$$

If w records topological flux, the zero sector and the two geometric tails can be summed separately:

$$H_n(t,w) = \frac{1}{1-t^2}\left(1 + \sum_{m\geq 1}(wt^n)^m + \sum_{m\geq 1}(w^{-1}t^n)^m\right). \tag{X.7.18}$$

Combining the tails gives the all-degree rational answer

$$H_n(t,w) = \frac{1-t^{2n}}{(1-t^2)(1-wt^n)(1-w^{-1}t^n)}. \tag{X.7.19}$$

The three denominator factors invite generators of degrees $2, n, n$; the numerator invites one degree-$2n$ relation. The sourced physical ring presentation identifies these as the scalar and unit monopoles:

$$\mathbb{C}[\mathcal{C}_{U(1),n}] = \mathbb{C}[\Phi, V_+, V_-]/(V_+V_- - \Phi^n), \qquad \deg(\Phi, V_+, V_-) = (2, n, n). \tag{X.7.20}$$

The generator degrees and the single relation can be read together:

Object	Book degree	Operator meaning
Φ	2	residual complex scalar
V_+	n	unit positive-flux monopole
V_-	n	unit negative-flux monopole
$V_+V_- - \Phi^n$	$2n$	one relation, not another generator

Table X.7.1: The three generators account for the denominator of (X.7.19); the relation accounts for its numerator. For $n = 2$ all generators have degree two and the relation degree four.

The rational function by itself is only a count. The operator product $V_+V_- = \Phi^n$ is part of the gauge-theory ring identification, not a logical consequence of equal coefficients.

An independent invariant-ring calculation reveals the surface behind this presentation. Let $\mathbb{Z}_n$ act on $\mathbb{C}[x, y]$ by $(x, y) \mapsto (\omega x, \omega^{-1}y)$, with $\omega^n = 1$ and $\deg x = \deg y = 1$. An invariant monomial $x^a y^b$ has $a - b \equiv 0 \pmod{n}$. Removing $\min(a, b)$ copies of xy leaves a pure power whose exponent is divisible by n. Thus every invariant has a normal form built from

$$X = x^n, \qquad Y = y^n, \qquad Z = xy, \qquad \deg(X, Y, Z) = (n, n, 2). \tag{X.7.21}$$

The only reduction needed between these generators is

$$XY = Z^n, \qquad \mathbb{C}[x, y]^{\mathbb{Z}_n} \simeq \mathbb{C}[X, Y, Z]/(XY - Z^n). \tag{X.7.22}$$

One may choose normal monomials $Z^c X^a$ or $Z^c Y^b$, counting the shared pure powers of Z once. This directly gives

$$H_{\mathbb{C}^2/\mathbb{Z}_n}(t,w) = \frac{1}{1-t^2}\left(1 + \frac{wt^n}{1-wt^n} + \frac{w^{-1}t^n}{1-w^{-1}t^n}\right). \tag{X.7.23}$$

Here w marks powers of X against powers of Y; its agreement with the monopole fugacity makes the dictionary transparent. Equivalently, the finite-group Molien projection enforces the same congruence:

$$H_{\mathbb{C}^2/\mathbb{Z}_n}(t) = \frac{1}{n}\sum_{j=0}^{n-1} \frac{1}{(1-\omega^j t)(1-\omega^{-j}t)}. \tag{X.7.24}$$

This is a second counting method, while the physical map from (X, Y, Z) to (V_+, V_-, Φ) still uses the sourced operator statement.

To derive the Molien projector rather than merely quote it, expand each factor before the group average. The sum over roots of unity then eliminates precisely the noninvariant monomials:

$$\frac{1}{n}\sum_{j=0}^{n-1}\omega^{j(a-b)} = \begin{cases} 1, & a-b \in n\mathbb{Z}, \\ 0, & a-b \notin n\mathbb{Z}. \end{cases} \tag{X.7.25}$$

Thus (X.7.24) and the normal-form argument impose the same condition by different routes. The normal form goes further: it provides an explicit set of generators and the reduction $XY \mapsto Z^n$. This is why it can support the invariant-ring isomorphism in (X.7.22), while the numerical Molien output alone cannot.

For $n = 3$, the first coefficients and the relation degree are

$$H_3(t, 1) = 1 + t^2 + 2t^3 + t^4 + 2t^5 + 3t^6 + 2t^7 + 3t^8 + O(t^9), \qquad \deg(V_+V_-) = 6. \tag{X.7.26}$$

The degree-three pair is precisely the two unit monopoles. At degree six, the naive monomials V_+V_- and Φ^3 collapse to one because of (X.7.20). This is a more informative check than matching the pole order alone: it locates the relation at the first degree where it can act. The resulting A_{n-1} Kleinian surface has complex dimension two. The affine A_2 quiver in Section X.7.5 carries the same Dynkin letter for a different reason and has a four-complex-dimensional Coulomb branch.

The refinement makes the first cancellation explicit. With $n = 3$, the degree-six invariant monomials before reduction include XY, Z^3, X^2 and Y^2. The relation identifies the first two, while the last pair retain opposite topological charge:

$$[t^6]H_3(t, w) = 1 + w^2 + w^{-2}. \tag{X.7.27}$$

At degree three the coefficient is $w + w^{-1}$, and at degree five it is again $w + w^{-1}$ after multiplying each unit monopole by Φ. The unrefined sequence therefore hides a useful selection rule: a polynomial in Φ stays at zero topological charge, whereas V_+ and V_- occupy opposite charge sectors. The cyclic normal form accounts for these charges without assuming an operator product in the gauge theory.

There is also a simple geometric consistency check. The quotient map $(x, y) \mapsto (x^n, y^n, xy)$ is generically finite onto the hypersurface $XY = Z^n$. One polynomial relation among three complex coordinates leaves complex dimension two:

$$\dim_{\mathbb{C}} \mathbb{C}[X, Y, Z]/(XY - Z^n) = 3 - 1 = 2. \tag{X.7.28}$$

This agrees with the rank-one Coulomb branch and the order-two pole of (X.7.19) at $t = 1$ after setting $w = 1$. Dimension agreement is a check, whereas the normal-form argument establishes the invariant-ring presentation. The same check illustrates the limits of counting: two nonisomorphic graded rings can share a Hilbert series and a dimension. Here the explicit cyclic monomial reduction proves the algebraic quotient presentation, while the identification of its generators with physical monopole operators is supplied separately. A reader can therefore use the coefficient calculation as a diagnostic without silently promoting it into a claim about operator multiplication.

X.7.4 A nonabelian sum and the D-series surface

The difference between zero and nonzero flux becomes decisive for compact $SU(2)$ with $n > 2$ fundamental full hypermultiplets. The compact group fixes an integral coroot lattice: after Weyl reflection we take $m = \mathrm{diag}(k, -k)$, $k = 0, 1, 2, \ldots$. A fundamental has weights $+k$ and $-k$; the positive root evaluates to $2k$. Therefore the two terms of (X.7.10) are

$$\sum_{\text{hypers, weights}} |\rho(m)| = 2nk, \qquad 2\sum_{\alpha>0} |\alpha(m)| = 4k. \tag{X.7.29}$$

Their difference is

$$2\Delta(k) = 2(n-2)k. \tag{X.7.30}$$

For $n > 2$ every positive flux has positive degree. This is the range used here; changing the matter content can make the ultraviolet charge assignment unsuitable for the same sum.

Keeping the residual centralizers distinct, the full unrefined series is

$$H_{SU(2),n}(t) = \frac{1}{1-t^4} + \sum_{k=1}^{\infty} \frac{t^{2(n-2)k}}{1-t^2}. \tag{X.7.31}$$

The positive-flux sectors form a geometric series, so

$$H_{SU(2),n}(t) = \frac{1}{1-t^4} + \frac{t^{2n-4}}{(1-t^2)(1-t^{2n-4})}. \tag{X.7.32}$$

Putting this over a common denominator gives the complete-intersection form

$$H_{SU(2),n}(t) = \frac{1-t^{4n-4}}{(1-t^4)(1-t^{2n-4})(1-t^{2n-2})}. \tag{X.7.33}$$

Its three generator degrees and one relation degree match the sourced D_n surface presentation. The pole at $t = 1$ has order two, hence complex dimension two. This is a compact-$SU(2)$ Coulomb surface; its D_n name describes the Kleinian singularity, not the number of magnetic gauge nodes.

The familiar weighted-hypersurface model makes the relation visible. With coordinates z, x, y of book degrees $4, 2n-4, 2n-2$, one may write the D_n surface in the form

$$y^2 + zx^2 + z^{\,n-1} = 0. \tag{X.7.34}$$

Every term has degree $4n-4$. Removing one relation from the freely generated polynomial ring therefore gives exactly (X.7.33). This comparison checks degree compatibility; the sourced monopole-operator presentation supplies the gauge-theoretic identification with this hypersurface. There is no need to guess an equation merely from the factorized numerator.

For $n = 4$, the bare first monopole has degree four, the zero-flux Casimir has degree four, and the third generator has degree six. Their relation has degree twelve:

$$(\deg A, \deg B, \deg C; \deg R) = (4, 4, 6; 12). \tag{X.7.35}$$

Expansion of (X.7.31) now reads

$$H_{SU(2),4}(t) = 1 + 2t^4 + t^6 + 3t^8 + 2t^{10} + 4t^{12} + O(t^{14}). \tag{X.7.36}$$

At degree four, one operator is the zero-flux quadratic Casimir and one is the first bare monopole. The degree-six coefficient comes from dressing that monopole with one residual $U(1)$ scalar. At degree twelve, the relation removes one monomial from the complete intersection's naive polynomial count. Thus the first few coefficients can be read sector by sector, not merely copied from a rational function. For example, at degree eight the contributions are the second power of the zero-sector Casimir, the twice-dressed $k = 1$ monopole and the bare $k = 2$ monopole:

$$[t^8]H_{SU(2),4} = 1_{k=0} + 1_{k=1} + 1_{k=2} = 3. \tag{X.7.37}$$

At degree ten the zero sector contributes nothing; the $k = 1$ and $k = 2$ sectors contribute one dressing each. This sector reading explains why the coefficient sequence is not the polynomial-ring sequence of three independent generators.

Replacing the zero-sector factor by $(1 - t^2)^{-1}$ would produce a degree-two operator that the compact $SU(2)$ invariant ring does not have. More precisely, the altered series differs by

$$\frac{1}{1 - t^2} - \frac{1}{1 - t^4} = \frac{t^2}{1 - t^4}. \tag{X.7.38}$$

The error is already visible at degree two, well before the D_4 relation. It is caused by treating the unbroken nonabelian scalar as though it were a gauge-invariant linear scalar.

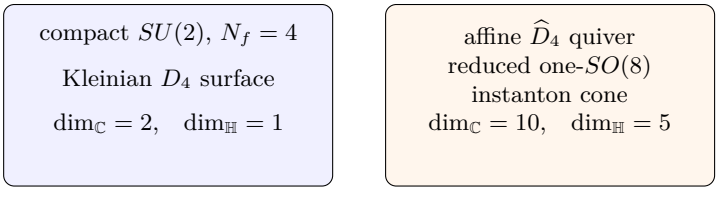


Figure X.7.3: Two objects carrying the D_4 name. The compact $SU(2)$ theory with four fundamentals has a Kleinian D_4 Coulomb surface of quaternionic dimension one. The affine D_4 quiver Coulomb branch is the reduced one-$SO(8)$-instanton space of quaternionic dimension five. The diagram compares objects, not a deformation between them.

The affine D_n quiver gives the contrast. Its Coulomb branch is the reduced one-$SO(2n)$-instanton space, or minimal nilpotent orbit closure in this example, with quaternionic dimension $2n - 3$. For $n = 4$ this is five, whereas the compact $SU(2)$ surface has quaternionic dimension one:

$$\dim_{\mathbb{H}} \mathcal{C}_{SU(2),N_f=4} = 1, \qquad \dim_{\mathbb{H}} \mathcal{C}_{\widehat{D}_4} = 5. \tag{X.7.39}$$

The source also compares relevant Higgs branches under mirror symmetry; one must keep track of which branch is being named. Substituting an $SO(3)$ flux lattice into the compact $SU(2)$ sum would change the theory, and doublets would not define ordinary $SO(3)$ matter. Neither the Dynkin label nor a Hilbert-series resemblance licenses that change.

X.7.5 The affine A2 quiver and its missing center

An affine triangle has three unitary gauge circles joined pairwise by one bifundamental hypermultiplet. The common diagonal $U(1)$ acts trivially on all three edges. The effective compact group and a primitive integral flux slice are

$$G_{\widehat{A}_2} = U(1)^3/U(1)_{\mathrm{diag}}, \qquad (m_0, m_1, m_2) \sim (m_0 + c, m_1 + c, m_2 + c), \qquad m_0 = 0. \tag{X.7.40}$$

The same quotient removes one neutral complex scalar. Thus each flux sector has exactly two independent degree-two residual scalars, giving the dressing factor $(1-t^2)^{-2}$. The triangle's three charged edges give

$$2\Delta(m_1, m_2) = |m_1| + |m_1 - m_2| + |m_2|, \qquad P_{\widehat{A}_2}(t; m_1, m_2) = \frac{1}{(1-t^2)^2}. \tag{X.7.41}$$

The center removal is simultaneously a statement about magnetic flux and residual scalar dressings. Removing only one of them is not a definition of the same effective gauge theory.

The primitive quotient can be described without choosing a favorite node. A triple of integral fluxes represents a class in $\mathbb{Z}^3/\mathbb{Z}(1,1,1)$. Subtracting its first entry produces the unique representative $(0, m_1 - m_0, m_2 - m_0)$:

$$[(m_0, m_1, m_2)] \longmapsto (m_1 - m_0, m_2 - m_0) \in \mathbb{Z}^2. \tag{X.7.42}$$

This map is an isomorphism of integer lattices, not only of real vector spaces. Dually, the three complex vector-multiplet scalars lose their common diagonal combination, leaving two independent degree-two invariants. If one first removes the common flux but retains all three scalars, the mismatch in (X.7.51) follows. If one keeps all fluxes, the infinite orbit of common shifts cannot be repaired by a scalar normalization.

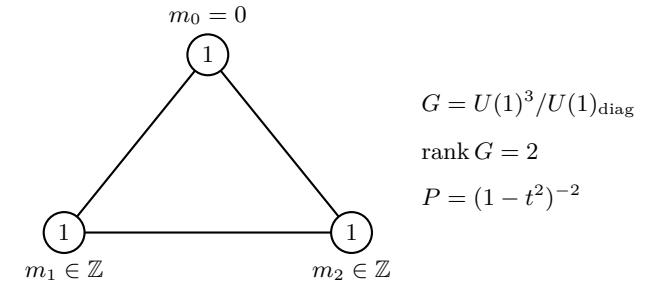


Figure X.7.4: The affine A_2 triangle and a primitive flux slice. All three circles are gauge nodes and every line is one bifundamental hyper. The common flux shift and its neutral scalar are both removed by the diagonal quotient; fixing $m_0 = 0$ leaves $(m_1, m_2) \in \mathbb{Z}^2$.

The degree function has hexagonal level sets. For $j \geq 1$, the number of integer pairs with $2\Delta = 2j$ is $6j$. One way to see it is to walk around the six sides of the hexagon with vertices $(j,0), (j,j), (0,j), (-j,0), (-j,-j), (0,-j)$; each side has j new lattice points after corners are counted once. Hence the undressed sum is

$$\sum_{m_1,m_2\in\mathbb{Z}} t^{2\Delta(m_1,m_2)} = 1 + \sum_{j\geq 1} 6j t^{2j} = 1 + \frac{6t^2}{(1-t^2)^2}. \tag{X.7.43}$$

For $j = 1$, these are exactly the six nearest primitive fluxes:

$$(m_1, m_2) = (1,0), (1,1), (0,1), (-1,0), (-1,-1), (0,-1). \tag{X.7.44}$$

Dressing the zero flux by two scalar directions contributes two degree-two operators, so the total degree-two coefficient is $6 + 2 = 8$. At the next shell, there are twelve bare fluxes. The degree-four coefficient receives their twelve operators, twelve first dressings of the six earlier fluxes, and three quadratic monomials in the two zero-flux scalars:

$$[t^4] H_{\widehat{A}_2} = 12 + 6 \cdot 2 + 3 = 27. \tag{X.7.45}$$

This sector decomposition is a direct check of the first two nontrivial character dimensions before invoking the all-degree identity. Multiplying by the two-scalar dressing gives

$$H_{\widehat{A}_2}(t) = \frac{1 + 4t^2 + t^4}{(1-t^2)^4}. \tag{X.7.46}$$

This is an all-degree equality, not just a coefficient fit. In terms of $x = t^2$, the identity

$$\frac{1 + 4x + x^2}{(1-x)^4} = \sum_{k\geq 0} (k+1)^3 x^k = \sum_{k\geq 0} \dim_{SU(3)}[k,k] x^k \tag{X.7.47}$$

recognizes the graded coordinate ring of the reduced one-$SU(3)$- instanton space, equivalently the minimal $\mathfrak{sl}_3$ orbit closure. The series begins

$$H_{\widehat{A}_2}(t) = 1 + 8t^2 + 27t^4 + 64t^6 + 125t^8 + O(t^{10}). \tag{X.7.48}$$

There are no odd powers. The pole order four in (X.7.46) agrees with complex dimension four.

The representation comparison uses the $SU(3)$ dimension formula

$$\dim[p,q] = \frac{(p+1)(q+1)(p+q+2)}{2}. \tag{X.7.49}$$

For $p = q = k$ this gives $(k+1)^3$. Chapter 5 used the corresponding generating identity; in the present grading the identity is

$$\sum_{k\geq 0}(k+1)^3 x^k = \frac{1+4x+x^2}{(1-x)^4}. \tag{X.7.50}$$

The shell enumeration and representation calculation therefore agree for every grade. The further statement that this particular three-dimensional Coulomb branch is the one-instanton space is the sourced interpretation of the fixed quiver, not a new conclusion about arbitrary affine graphs.

If the common scalar alone were erroneously retained while the flux slice $m_0 = 0$ were still imposed, the result would be

$$H_{\text{extra scalar}}(t) = \frac{H_{\widehat{A}_2}(t)}{1-t^2} = 1 + 9t^2 + 36t^4 + \cdots . \tag{X.7.51}$$

The degree-two error is immediate. Retaining the entire unremoved common flux is worse: every integer shift c has zero bare degree, so the constant term diverges. These are distinct errors. By contrast, removing a second $U(1)$ would erase a genuine flux and scalar direction. The effective rank of the triangle is two, exactly the quaternionic dimension of its Coulomb branch.

The A_2 in this section is an affine quiver label. It produces the four-dimensional complex minimal-orbit cone just used as one component of the E_3 union. The $n = 3$ theory of Section X.7.3 produces the complex surface $\mathbb{C}^2/\mathbb{Z}_3$. A shared Lie-theoretic letter does not identify their Coulomb rings. This distinction will also matter for D-type labels in a Hasse edge.

X.7.6 Symplectic leaves and the Hasse diagram

A Hilbert series assigns one number to each graded piece of a coordinate ring. A singular symplectic variety carries additional local information. At a smooth point its Poisson bracket is nondegenerate along a symplectic leaf; at singular points the rank can drop. A symplectic leaf is a maximal connected immersed submanifold tangent to the Hamiltonian vector fields, the image of the Poisson tensor. Its induced Poisson structure is nondegenerate, and its dimension equals the Poisson rank. The closure order of leaves is

$$L' \preceq L \quad \Longleftrightarrow \quad L' \subseteq \overline{L}. \tag{X.7.52}$$

A cover $L \succ L'$ means that no other leaf lies strictly between them. Near a generic point of L', a transverse slice $S_{L,L'}$ describes the singular directions normal to that leaf.

Its expected quaternionic dimension is the drop

$$\dim_{\mathbb{H}} S_{L,L'} = \dim_{\mathbb{H}} L - \dim_{\mathbb{H}} L'. \tag{X.7.53}$$

The dimension check is necessary, but it does not identify the slice: many singularities share a dimension. A Hasse diagram records the cover relations and attaches the local slice type to each edge.

Before drawing a branching diagram, let us find the leaves of one surface already encountered in Section X.7.3. Use the traceless matrix convention

$$M = \begin{pmatrix} z & x \\ y & -z \end{pmatrix}, \qquad X = \{(x,y,z) \in \mathbb{C}^3 : f = xy + z^2 = 0\}. \tag{X.7.54}$$

This is the $n = 2$ surface, with the sign of one generator changed from $XY = Z^2$. Restrict the Lie-Poisson bracket of matrix entries, displayed below in (X.7.62). Its three independent brackets are

$$\{z, x\} = x, \qquad \{z, y\} = -y, \qquad \{x, y\} = 2z. \tag{X.7.55}$$

They give a bracket on the surface because the defining relation is preserved. For example, the Leibniz rule gives

$$\{f, x\} = x\{y, x\} + 2z\{z, x\} = -2xz + 2zx = 0, \qquad \{f, y\} = \{f, z\} = 0. \tag{X.7.56}$$

Thus Hamiltonian motion stays on $f = 0$. In the coordinate order (x, y, z) the matrix of brackets is

$$P = \begin{pmatrix} 0 & 2z & -x \\ -2z & 0 & y \\ x & -y & 0 \end{pmatrix}. \tag{X.7.57}$$

At $p = (1, 0, 0)$, a point on the surface, P has rank two. More generally, its three principal two-by-two minors are $4z^2, x^2, y^2$. At any nonzero point at least one is nonzero, while a three-by-three antisymmetric matrix has determinant zero. Hence

$$\operatorname{rank} P_p = 2 \quad (p \neq 0), \qquad \operatorname{rank} P_0 = 0. \tag{X.7.58}$$

The surface is smooth away from zero: $df = (y, x, 2z)$ vanishes only there. Its smooth locus is connected, and the Hamiltonian directions span its two-dimensional complex tangent space. It is consequently one symplectic leaf; the origin is the other. The Hasse diagram has precisely one cover,

$$X \setminus \{0\} \;\succ\; \{0\}, \qquad \dim_{\mathbb{H}} L = 1 \;\longrightarrow\; 0. \tag{X.7.59}$$

At the zero-dimensional leaf there are no tangent directions to remove, so the transverse cone is X itself. At a nonzero point the local surface is smooth and the transverse slice to its open leaf is a point. These are different local questions on the same variety. Figure X.7.5 records the calculation before we use it on a reducible union.

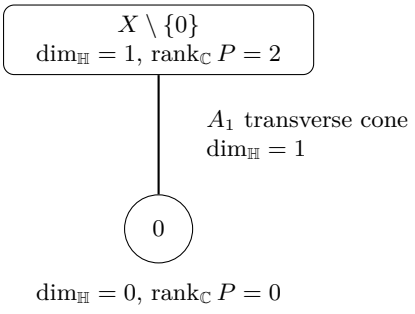


Figure X.7.5: The A_1 surface supplies the smallest Hasse example. The Poisson tensor has complex rank two everywhere on the connected open leaf and rank zero at the origin. Node labels give quaternionic leaf dimensions. The edge is labelled by the transverse A_1 cone at the lower leaf; it does not represent a trajectory of a vacuum in time.

The two-cone E_3 example makes the distinction tangible. Each minimal orbit closure has an open symplectic leaf and the zero leaf. The two open leaves lie in different components and neither contains the other in its closure. The union consequently has precisely the three leaves

$$\mathcal{L}(\mathcal{H}_\infty) = \{X_2 \setminus \{0\},\, X_1 \setminus \{0\},\, \{0\}\}, \qquad \dim_{\mathbb{H}} = (2, 1, 0). \tag{X.7.60}$$

Its Hasse graph is a fork with two covers, each open leaf descending to the origin. The two full component cones are the corresponding origin slices:

$$S_{X_2\setminus\{0\},\,0} = X_2, \qquad S_{X_1\setminus\{0\},\,0} = X_1. \tag{X.7.61}$$

These are unequal slices, of quaternionic dimensions two and one. There is no edge directly between the two open leaves.

The Poisson structure can be assembled as carefully as the graded ring. On each minimal nilpotent orbit closure, matrix-coordinate functions inherit the Lie-Poisson bracket from the ambient $\mathfrak{sl}_r^*$:

$$\{M_{ij}, M_{kl}\} = \delta_{jk} M_{il} - \delta_{il} M_{kj}, \qquad r = 3 \text{ or } 2. \tag{X.7.62}$$

The maximal ideal of the origin is Poisson, because all right-hand sides vanish there. Therefore the fiber product in (X.7.2) inherits the componentwise bracket

$$\{(f_2, f_1), (g_2, g_1)\} = (\{f_2, g_2\}_{X_2}, \{f_1, g_1\}_{X_1}). \tag{X.7.63}$$

The resulting ring is reduced and Poisson, but reducible. Calling it a single irreducible normal orbit closure would discard its defining geometry. Its Hilbert series (X.7.7) cannot recover this fork without the product and bracket data.

One multiplication rule already detects the two branches. Let $f \in A$ and $g \in B$ vanish at their respective origins. Then $(f, 0)$ and $(0, g)$ are valid functions on the fiber product, but

$$(f, 0)(0, g) = (0, 0). \tag{X.7.64}$$

Positive-degree functions supported on different components annihilate one another. The Hilbert series adds their vector-space dimensions and sees no such cross product. The zero divisors in (X.7.64) encode reducibility directly, while the componentwise Poisson bracket in (X.7.63) ensures that each open branch carries its own symplectic geometry. This is a concrete reason to draw the fork after calculating the series.

There is a second reason to draw rather than guess a Hasse graph. The same five-dimensional electric gauge theory can have a different Higgs-branch stratification at finite and infinite coupling. For massless $SU(3)$ with six fundamentals and Chern–Simons level zero, the finite-coupling source diagram has a three-leaf chain of quaternionic dimensions $10, 5, 0$. Its two edges carry different minimal-orbit slices:

$$10 \xrightarrow{d_4,\ \dim_{\mathbb{H}} 5} 5 \xrightarrow{a_5,\ \dim_{\mathbb{H}} 5} 0. \tag{X.7.65}$$

Here d_4 denotes the minimal nilpotent $SO(8)$ orbit closure, with quaternionic dimension five. It is not the compact-$SU(2)$ D_4 Kleinian surface of Section X.7.4, which has quaternionic dimension one. Likewise a_5 is the minimal nilpotent $SU(6)$ orbit closure, not a generic A_5 Kleinian surface.

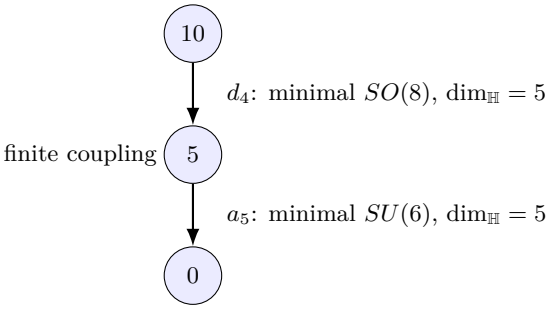


Figure X.7.6: Finite-coupling 5d $SU(3)$, $N_f = 6$, level-zero chain. Node numbers are quaternionic leaf dimensions; each edge names a transverse minimal-orbit slice and its quaternionic dimension. This is the three-leaf finite-coupling source diagram, separate from the infinite-coupling five-leaf graph in Figure X.7.7.

At infinite coupling the sourced diagram has five leaves: a top leaf of quaternionic dimension twelve, a central leaf of dimension five, two distinct side leaves of dimension one, and the origin. It has six covers. The central route and each side route satisfy the dimension drops

$$12 = 7 + 5, \quad 5 = 5 + 0, \qquad 12 = 11 + 1, \quad 1 = 1 + 0. \tag{X.7.66}$$

The top-to-central slice is d_5, the minimal $SO(10)$ orbit closure; central-to-origin is a_5. Each top-to-side slice is an e_6 minimal orbit closure, and each side-to-origin slice is a_1. The two side leaves have equal dimensions and equal labels on their edges, but they are distinct leaves in the source geometry. Merging them would turn six covers into four and lose an actual branch of the poset.

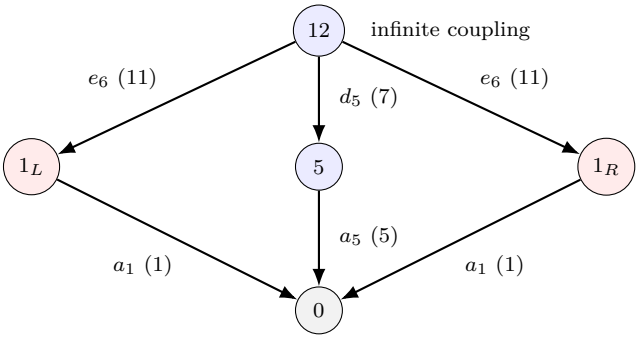


Figure X.7.7: Infinite-coupling $5d$ $SU(3)$, $N_f = 6$, level-zero Hasse graph redrawn from the sourced five-leaf, six-cover object. Numbers denote quaternionic leaf dimensions. The central d_5 route and two separate e_6 routes have different slice dimensions, although all begin at the same top leaf.

A Hasse edge is a local statement about a generic point on the lower leaf. In a magnetic-quiver construction, assigning a higher-dimensional Higgs branch to a three-dimensional Coulomb branch remains a physical premise. The Hilbert count can check graded dimensions of a proposed component or slice, and rank arithmetic can check a dimension drop; neither alone establishes the physical coupling transition or the local analytic isomorphism. The two diagrams above are kept separate because the extra infinite-coupling leaves are part of the physics, not a relabelling of the finite chain. The coupling distinction is the same one encountered in Chapter 6 when a web admits different maximal subweb decompositions; a stratification attaches local geometry to each resulting branch.

X.7.7 What quiver subtraction can and cannot decide

Chapter 6 and the examples here use subtraction with different inputs. Keeping the geometric roles visible avoids reversing the answer. In the framed $\mathfrak{sl}_5$ example of Section 6.6, the two input quivers describe an ambient orbit closure and a lower orbit closure. Their aligned rank difference, with the stated retained framing, describes the proposed transverse slice. Here we instead start with an ambient magnetic quiver and an embedded elementary slice quiver. After subtracting that slice, the specified rebalancing produces a quiver for the lower leaf closure. The two directions can be summarized as

$$\begin{aligned} &\text{Chapter 6:} && (Q_{\text{ambient}}, Q_{\text{lower}}) \longmapsto Q_{\text{slice}}, \\ &\text{this section:} && (Q_{\text{ambient}}, D_{\text{slice}}) \longmapsto Q_{\text{lower}} \quad \text{after rebalancing.} \end{aligned} \tag{X.7.67}$$

These arrows specify the roles in the selected examples, not an invertible identity between arbitrary quivers. In particular, the framed example retains physical fundamental matter, so its surviving diagonal circle acts on that matter. The unframed graphs below instead remove an ineffective common diagonal; the added rebalancing node changes the rank

sum before that quotient. The same dimension identity

$$\dim_{\mathbb{H}} \mathcal{C}(Q_{\text{ambient}}) = \dim_{\mathbb{H}} \mathcal{S} + \dim_{\mathbb{H}} \overline{L}_{\text{lower}} \tag{X.7.68}$$

checks both constructions, but does not determine which input describes the slice. That role must be fixed before manipulating node ranks.

Can a graph operation propose the slice on a Hasse edge? For the particular unitary quivers below, an aligned subquiver has a nonnegative rank vector D inside a larger graph with rank vector Q. Subtracting node ranks gives a remainder $S = Q - D$; one then restores balance to obtain a candidate quiver for the lower leaf. This operation uses an assumed inclusion of leaves and a specified embedding of the subquiver. It is not a theorem that arbitrary rank subtraction produces a transverse slice. In the selected source example the subtraction and its physical interpretation can both be examined, with their roles kept distinct.

First take finite-coupling five-dimensional $SU(3)$ with $N_f = 6$ and level zero. Order the magnetic gauge nodes along a length-five horizontal chain as (L_2, L_1, C, R_1, R_2), with two upper tips (U_L, U_R) attached to C. All seven nodes are gauge circles, no magnetic flavor squares are present, and the effective group removes one common diagonal $U(1)$. In this order the source graph and the embedded affine-D_4 slice have ranks

$$Q_{\text{fin}} = (1, 2, 3, 2, 1, 1, 1), \qquad D_{\widehat{D}_4} = (0, 1, 2, 1, 0, 1, 1). \tag{X.7.69}$$

The original effective gauge rank is

$$\dim_{\mathbb{H}} \mathcal{C}(Q_{\text{fin}}) = (1 + 2 + 3 + 2 + 1 + 1 + 1) - 1 = 10. \tag{X.7.70}$$

The embedded slice has effective rank

$$\dim_{\mathbb{H}} \mathcal{C}(D_{\widehat{D}_4}) = (1 + 2 + 1 + 1 + 1) - 1 = 5. \tag{X.7.71}$$

The slice's affine-D_4 name here denotes the minimal $SO(8)$ orbit closure. Its five quaternionic dimensions exactly match the upper edge of the finite Hasse chain.

Nodewise subtraction leaves five unit ranks on the horizontal chain, with zero upper tips:

$$S_{\text{fin}} = Q_{\text{fin}} - D_{\widehat{D}_4} = (1, 1, 1, 1, 1, 0, 0). \tag{X.7.72}$$

The fixed finite graph has horizontal edges $L_2L_1, L_1C, CR_1, R_1R_2$ and upper edges CU_L, CU_R. Applying the balance formula to the full graph gives, in the same node order as (X.7.69),

$$b(Q_{\text{fin}}) = (0, 0, 0, 0, 0, 1, 1), \qquad b(S_{\text{fin}}) = (-1, 0, 0, 0, -1, 1, 1). \tag{X.7.73}$$

The two upper tips have zero rank in the remainder and are then discarded. Its five positive-rank nodes consequently form a chain, with precisely the two deficient ends shown in the balance vector. The two end nodes of this chain are underbalanced by one. Introduce one unit gauge node and join it to both ends; the resulting six-node cycle is balanced affine A_5. Its effective gauge rank is

$$Q'_{\text{fin}} = (1, 1, 1, 1, 1, 1)_{\widehat{A}_5}, \qquad \dim_{\mathbb{H}} \mathcal{C}(Q'_{\text{fin}}) = 6 - 1 = 5. \tag{X.7.74}$$

The last five dimensions form the lower leaf closure, while the subtracted $D_{\widehat{D}_4}$ proposes the transverse d_4 slice. Its own lower-to-origin a_5 edge is a separate statement. The finite chain is thus arithmetically consistent:

$$\dim_{\mathbb{H}} \mathcal{C}(Q_{\mathrm{fin}}) = \dim_{\mathbb{H}}(d_4) + \dim_{\mathbb{H}} \mathcal{C}(Q'_{\mathrm{fin}}) = 5 + 5 = 10. \tag{X.7.75}$$

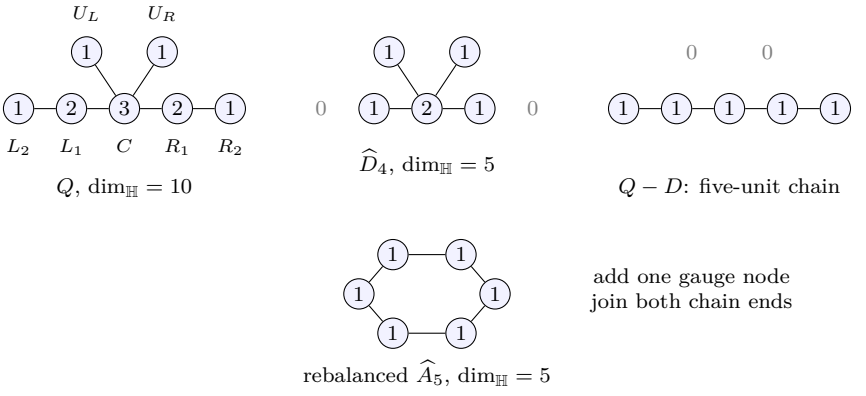


Figure X.7.8: Finite-coupling rank subtraction in the fixed seven-node magnetic graph. The upper row keeps node order $(L_2, L_1, C, R_1, R_2; U_L, U_R)$ across Q, the embedded d_4 slice and the remainder. The lower cycle is the rebalanced affine-A_5 quiver. Circles are gauge nodes; gray zeros mark omitted positions. Every flavor vector is zero; the six fundamentals belong to the electric theory.

Balance makes the added node intelligible rather than cosmetic. For a simply laced unitary gauge node i with no flavor square, write

$$b_i = \sum_{j \sim i} r_j - 2r_i. \tag{X.7.76}$$

Along the five-unit remainder chain, the two ends have $b = -1$ and the three interior nodes have $b = 0$. Joining a new unit node to both ends raises each deficient balance to zero; the new node sees two unit neighbors and also has zero balance. A single extra edge or a single-sided attachment would fail this check. The rank sum and the balance calculation are deterministic properties of these graphs; the identification of the corresponding slice with the five-dimensional transverse geometry is the sourced physical step.

The infinite-coupling graph is a different eight-node object. Retain the same five horizontal labels, but now an upper rank-two node U joins the central rank-three node and branches to two unit tips (U_L, U_R). Its ranks are

$$Q_\infty = (1, 2, 3, 2, 1, 2, 1, 1), \qquad \dim_{\mathbb{H}} \mathcal{C}(Q_\infty) = 13 - 1 = 12. \tag{X.7.77}$$

The graph has zero flavor squares and one effective diagonal quotient. It must not be silently replaced by the seven-node finite graph. Its horizontal edges are unchanged, but

the upper edges are CU, UU_L, UU_R rather than CU_L, CU_R. This extra rank-two upper node changes both the effective dimension and the central slice type. In the eight-node order,

$$b(Q_\infty) = (0,0,0,0,0,1,0,0). \tag{X.7.78}$$

The arithmetic says that the graph is not merely the finite graph with an extra free unit node: the new node sits inside the connected charge network and changes the balance data. The source's central d_5 slice is embedded with

$$D_{\widehat{D}_5} = (0,1,2,1,0,2,1,1), \qquad \dim_{\mathbb{H}} \mathcal{C}(D_{\widehat{D}_5}) = 8-1 = 7. \tag{X.7.79}$$

Subtracting this vector gives

$$Q_\infty - D_{\widehat{D}_5} = (1,1,1,1,1,0,0,0). \tag{X.7.80}$$

The same end-to-end unit-node rebalancing produces affine A_5, with lower-leaf dimension five. Thus the central cover passes the independent dimension test $12-5=7$, now for a d_5 rather than a d_4 slice.

Two other embeddings inside the same infinite graph account for the side leaves. Each is a balanced affine-E_6 graph of effective rank eleven, obtained by omitting a different unit upper tip:

$$D^{(L)}_{\widehat{E}_6} = (1,2,3,2,1,2,0,1), \qquad D^{(R)}_{\widehat{E}_6} = (1,2,3,2,1,2,1,0). \tag{X.7.81}$$

Their two remainders are different unit tips,

$$Q_\infty - D^{(L)}_{\widehat{E}_6} = (0,0,0,0,0,0,1,0), \qquad Q_\infty - D^{(R)}_{\widehat{E}_6} = (0,0,0,0,0,0,0,1). \tag{X.7.82}$$

Adding one unit node with two edges to the remaining tip produces an affine-A_1 doubled-edge quiver. After its diagonal quotient, its Coulomb branch has quaternionic dimension one. Each e_6 upper slice therefore has dimension eleven, and each distinct lower arm has a final a_1 slice of dimension one:

$$12 = 7+5 = 11+1, \qquad 5 = 5+0, \qquad 1 = 1+0. \tag{X.7.83}$$

The affine-A_1 lower arm also admits a short operator check. Fixing one of its two unit fluxes to zero, the double edge gives $2\Delta(m) = 2|m|$ and one residual scalar. Its series is

$$H_{\widehat{A}_1}(t) = \frac{1}{1-t^2}\sum_{m\in\mathbb{Z}} t^{2|m|} = \frac{1+t^2}{(1-t^2)^2} = 1+3t^2+5t^4+\cdots. \tag{X.7.84}$$

It has a pole of order two, as required for a quaternionic one-dimensional arm. In this special a_1 case, the minimal $SU(2)$ orbit closure is also the A_1 Kleinian surface. That coincidence must not be extended to the d_4 and d_5 upper minimal-orbit slices, whose dimensions already rule out the corresponding Kleinian surfaces. These equations account for all six covers of the infinite graph: one d_5, one a_5, two e_6, and two a_1. They do not collapse the two side arms simply because their dimensions agree.

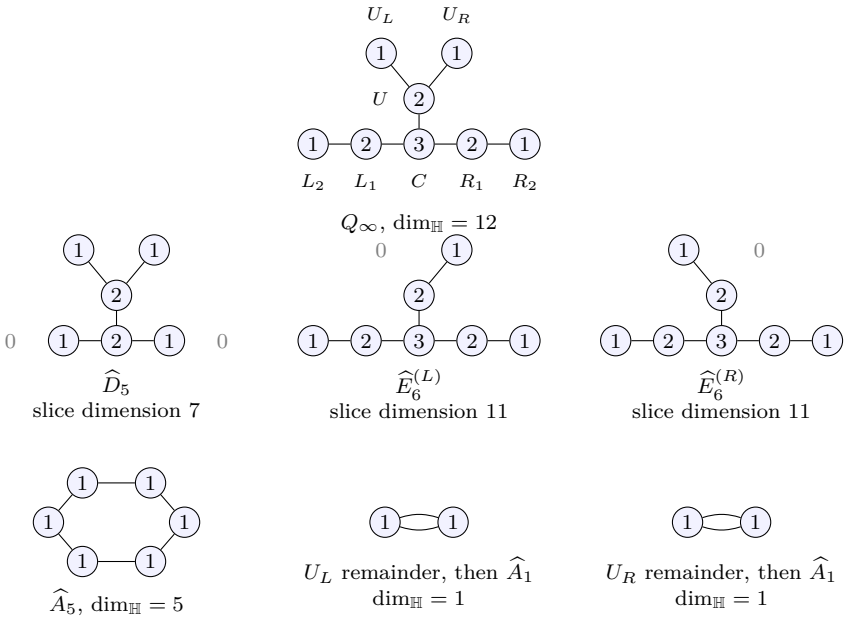


Figure X.7.9: The separate infinite-coupling eight-node graph and its three source-aligned embedded slices. The top panel fixes node names; gray zeros mark omitted positions in each aligned embedding. The central d_5 embedding leaves a five-unit chain and the two e_6 embeddings leave opposite unit tips. The lower graphs are respectively affine A_5 and two distinct affine A_1 arms.

Quiver subtraction is useful precisely because it forces such specific tests: an embedding must be nodewise nonnegative, the remainder must have the advertised balance restoration, and the effective rank must equal the proposed dimension drop. For a five-dimensional theory the existence of the magnetic-quiver description, the inclusion of the selected Higgs leaves, and the identification of the local transverse slice remain physical or geometric inputs. The general subtraction prescription remains conjectural under orbit and embedding hypotheses. The finite and infinite diagrams used here are the particular source examples just transcribed. A Hilbert series can support a particular protected fingerprint, but it does not turn those inputs into a theorem. Six-dimensional applications need their own tensor-branch and brane assumptions, as in Chapter 4.

X.7.8 Exercises

1. For compact three-dimensional $U(1)$ with three charge-one full hypermultiplets, sum the positive and negative flux tails. Give the unrefined series through book degree eight, or an exact rational series, and the degree of the relation $V_+V_- = \Phi^3$. Explain which part of the ring identification cannot be deduced from coefficients

alone.

2. For compact $SU(2)$ with four fundamental full hypermultiplets, keep the zero-flux and positive-flux dressings separate. Find their Casimir degrees, the Hilbert series through book degree twelve (or exactly), and the degree of the sourced D_4 relation. Show the first coefficient that would change if zero flux were dressed as $U(1)$.

3. For the affine A_2 triangle, specify its compact effective group, fix a primitive flux coordinate, and count the hexagonal shells. Give the series through book degree eight (or exactly), and the number of independent degree-two residual scalars. State the effect of keeping a neutral diagonal scalar.

4. Accept the sourced infinite-coupling, massless five-dimensional $SU(2)$, $N_f = 2$ two-cone union at the reduced origin. Calculate its Hilbert series through book degree eight (or exactly), state the number of irreducible components and the complex dimension of the intersection, and explain why the same statement has not been made at finite coupling.

5. Draw the three-leaf Hasse fork for that E_3 union and label both component slices. Explain why the compact-$SU(2)$ D_n Coulomb surface and the affine-D_n quiver Coulomb branch are different objects. Identify the physical premise needed to assign a proposed five- or six-dimensional Higgs branch to a magnetic quiver. This exercise calls for a diagram and written reasoning.

X.7.9 Take-home message

Take-home message

The monopole sum counts a graded three-dimensional Coulomb ring once its compact flux lattice, matter weights and residual Casimirs are fixed. Cyclic normal forms, nonabelian dressing and the primitive affine-A_2 quotient show how much information a Hilbert series can check. A reducible five-dimensional Higgs branch needs component rings and their intersection; its Hasse graph needs Poisson leaves and local slices. In the sourced $SU(3)$ example, finite coupling gives a $10 \to 5 \to 0$ chain, while infinite coupling gives a distinct five-leaf graph with d_5 and two e_6 upper routes. Rank subtraction checks these named graphs under their physical embedding assumptions.

Status and sources

Section 7.1. The massless, infinite-coupling E_3 Higgs-branch identification is a brane-web construction [GEO-E], using Cabrera, Hanany, and Yagi 2019, Section 2.1 and Figures 1–3. The reduced-origin fiber product, its exact sequence and the resulting Hilbert-series identity are conditional algebra [MATH]; they do not establish the physical identification or its finite-coupling analogue.
Section 7.2. The protected monopole count and its good/ugly ultraviolet grading use Cremonesi et al. 2014, Section 2, Eqs. (2.4)–(2.5) [CONJ+]. The specified compact group,

integral cocharacters and residual Casimirs are inputs to that formula; no bad-theory generalization is asserted.

Section 7.3. Geometric resummation, the cyclic invariant-monomial normal form and the roots-of-unity projection are exact algebra [MATH]. The separate Coulomb-ring/OPE identification uses Cremonesi et al. 2014, Section 3.1 [CONJ+]; a Hilbert-series match alone does not supply it. Sections 6.1–6.3 of that source give the separate abelian mirror and Molien comparisons.

Section 7.4. The compact $SU(2)$ sum is evaluated exactly, conditional on the monopole formula [MATH]. Its D_n Coulomb-ring presentation is sourced from Cremonesi et al. 2014, Section 3.3, Eqs. (3.9)–(3.12) [CONJ+]. The distinct affine-D_n quiver's reduced one-$SO(2n)$-instanton interpretation uses its Section 3.4 [CONJ+]; it is not the D_n surface.

Section 7.5. The primitive quotient, hexagonal shell count and all-degree rational/representation identities are conditional calculations [MATH]. Identifying the affine-A_2 Coulomb branch with the reduced one-$SU(3)$-instanton space uses Cremonesi et al. 2014, Section 3.2, Eqs. (3.5)–(3.8) [CONJ+].

Section 7.6. The Poisson fiber algebra and its three-leaf fork follow from the stated component rings and reduced intersection [MATH], after the physical premise of Section 7.1. The finite $SU(3)$, $N_f = 6$ stratification and its subtraction use Bourget et al. 2020, Figure 4, Appendix A.2, Eq. (A.3), and Figure 22. Its separate infinite-coupling stratification uses Figures 13–14. These source-specific physical/slice identifications remain conditional [CONJ+].

Section 7.7. Rank subtraction, balance and the stated dimension checks are exact arithmetic on the displayed source graphs [MATH]. Their transverse-slice interpretation is source-specific [CONJ+], with the general proposal in Cabrera and Hanany 2018, Section 3, Conjecture 1, and the worked graphs in Bourget et al. 2020 at the locations just given. The particular orbit example in Section 2 of the former source has narrower scope. These calculations do not establish a universal higher-dimensional Higgs/Coulomb dictionary, full quantum-field-theory equivalence or a metric identification.

References

Bourget, A. et al. (2020). "The Higgs mechanism — Hasse diagrams for symplectic singularities". In: *JHEP* 01, p. 157. DOI: 10.1007/JHEP01(2020)157. arXiv: 1908.04245 [hep-th].

Cabrera, S. and A. Hanany (2018). "Quiver Subtractions". In: *JHEP* 09, p. 008. DOI: 10.1007/JHEP09(2018)008. arXiv: 1803.11205 [hep-th].

Cabrera, S., A. Hanany, and F. Yagi (2019). "Tropical Geometry and Five Dimensional Higgs Branches at Infinite Coupling". In: *JHEP* 01, p. 068. DOI: 10.1007/JHEP01(2019)068. arXiv: 1810.01379 [hep-th].

Cremonesi, S., A. Hanany, and A. Zaffaroni (2014). "Monopole operators and Hilbert series of Coulomb branches of $3d$ $\mathcal{N} = 4$ gauge theories". In: *JHEP* 01, p. 005. DOI: 10.1007/JHEP01(2014)005. arXiv: 1309.2657 [hep-th].

Chapter X.8

An atlas of webs and magnetic quivers

X.8.1 A source object becomes an atlas row

A five-brane face can measure a magnetic string tension, while a three-dimensional monopole sum counts functions on a Coulomb branch. Both calculations start with a physical object. They do not use the same object, and a matching number does not supply the map between them. This atlas follows selected constructions through the step at which a source interpretation becomes a calculable invariant. The reader can then ask a sharper question of each row: which part is a brane or field-theory premise, which part is algebra, and in which phase does the relation hold?

The pure $SU(2)$ web provides a first model. Its ordered external (p, q) charges and its moving face belong to a particular five-brane configuration. The source identifies the face width with an instanton mass and its height with a W-boson mass. Once those identifications are supplied, multiplying width by height computes an area, and differentiating a prepotential computes a local metric. Neither operation recovers the discrete theta angle. Chapters 1 and 3 develop the web and gauge descriptions; the present chapter keeps their common object in view while comparing it with other engines.

Three further distinctions organize the atlas. A five-dimensional Higgs branch proposed from a web may have several components. A magnetic quiver then computes a three-dimensional Coulomb ring for each proposed component. In six dimensions, a tensor vev specifies a phase of an electric theory before a magnetic quiver is introduced. Finally, a compact $SU(2)$ Coulomb surface and an affine-D_4 unitary quiver space have the same Dynkin label but different dimensions and different rings. Their distinction will be tested explicitly below.

Table X.8.1 fixes the complete inventory. The dimension column gives quaternionic dimensions for Higgs and magnetic Coulomb spaces, but a real dimension for the five-dimensional Coulomb or six-dimensional tensor coordinate. Each phase qualifier belongs to the object in its own row.

Object and phase	Actual compact group or source lattice	Calculated size or invariant
Pure $SU(2)$ web, finite face	5d web, no magnetic group	real Coulomb rank 1; area $\phi(m_0+\phi)$
$E_1, \widetilde{E}_1, E_0$ flows	source webs with distinct theta or endpoint	one real Coulomb modulus; no $SU(2)$ chart at E_0
Ordered $BCBC$ junctions	seven-brane prongs, no 3d gauge group	two simple roots; pairing rank 1
Finite $SU(4) \times SU(4)$ chain	6d electric gauge cover	two relative real tensors
Three-flavor SQED	3d compact $U(1)$	Coulomb $\dim_{\mathbb{H}} = 1$
Affine A_2 triangle	$U(1)^3/U(1)_{\mathrm{diag}}$	Coulomb $\dim_{\mathbb{H}} = 2$
Infinite-coupling E_3 origin	triangle and doubled edge, separately quotiented	two components $\dim_{\mathbb{H}} = 2, 1$
Separated $M5/A_1$, no $M9$	$[U(2) \times U(1)^4]/U(1)_{\mathrm{diag}}$	electric Higgs and magnetic Coulomb $\dim_{\mathbb{H}} = 5$
Infinite-coupling E_4 cycle	$U(1)^5/U(1)_{\mathrm{diag}}$	proposed Higgs, magnetic Coulomb $\dim_{\mathbb{H}} = 4$
Compact $SU(2)$, four flavors	3d traceless integral cocharacters	D_4 surface $\dim_{\mathbb{H}} = 1$
Aligned $\mathfrak{sl}_5$ subtraction	framed $U(1)^2$, no diagonal quotient	transverse slice $\dim_{\mathbb{H}} = 2$

Table X.8.1: The eleven source-qualified objects. The E_3 entry is one physical origin with two separate component quivers. The five-dimensional and six-dimensional entries carry physical branch proposals; compact three-dimensional groups specify the protected ring computations.

The table is a map for reading, not a universal correspondence. In particular, the finite tensor phase in its eighth row is distinct from the coincident-M5 and $M9$ configurations, while the E_3 and E_4 rows sit at infinite five-dimensional coupling. Chapters 5–7 give the magnetic-quiver and Hilbert-series techniques used below. The planned Part I foundations will supply a broader account of decoupling, three-dimensional mirror dynamics, anomaly theory and IIA/M-theory units; the present calculations use their stated local inputs rather than assuming those later foundations have been written.

X.8.2 The pure SU(2) face, scalar map and theta fork

What can a moving five-brane face actually calculate? In the selected pure $SU(2)$ web, set $L = m_0 + \phi$, with $m_0, \phi \geq 0$. The web lies in the x^6–x^5 plane, with D5 direction horizontal and NS5 direction vertical. Its four ordered corners and the outward rays are

$$(x^6, x^5) = \left(\pm\frac{L}{2}, \pm\frac{\phi}{2}\right) \quad \text{with all four sign choices,} \tag{X.8.1}$$

and the four outward rays, read clockwise from the upper right, carry

$$(p,q) = (1,1),\ (1,-1),\ (-1,-1),\ (-1,1). \tag{X.8.2}$$

The source names ϕ as the W mass and L as the instanton mass. The suspended D3 magnetic string measures the rectangle's area in this normalization. Its area and its first derivative are

$$A_{\text{face}} = \phi L = m_0\phi + \phi^2, \qquad \frac{\partial A_{\text{face}}}{\partial \phi} = m_0 + 2\phi. \tag{X.8.3}$$

The geometric multiplication is elementary; the physical statement that this area is the string tension uses the selected web frame.

The same derivative appears in the source-native prepotential,

$$\mathcal{F}_{\text{AHK}}(\phi) = \frac{m_0}{2}\phi^2 + \frac{1}{3}\phi^3, \qquad \mathcal{F}'_{\text{AHK}} = m_0\phi + \phi^2, \qquad \mathcal{F}''_{\text{AHK}} = m_0 + 2\phi. \tag{X.8.4}$$

Thus $\mathcal{F}' = A_{\text{face}}$ in this magnetic-string unit, and $\mathcal{F}''$ is the local gauge kinetic function in the source coordinate. For example, at $\phi = m_0 > 0$, the face has width $2m_0$, height m_0, area $2m_0^2$ and metric $3m_0$. At $\phi = 0$ with $m_0 > 0$, the height vanishes but the width remains m_0. The face becomes a segment, and the local metric stays positive. It collapses to a point only when both m_0 and ϕ vanish.

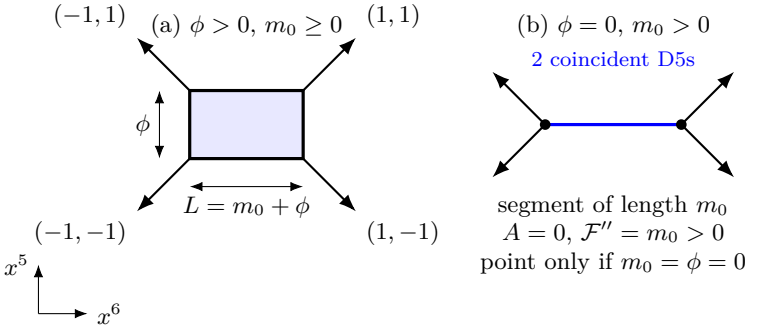


Figure X.8.1: The actual four-corner pure $SU(2)$ face, drawn with the house outward $(D5, NS5)$ charges. Panel (b) changes only ϕ and preserves $m_0 > 0$; the collapsed segment carries two coincident D5s, with the same four outgoing charge rays. Its nonzero segment and positive metric distinguish an edge degeneration from the joint $m_0 = \phi = 0$ collapse.

There is a second scalar coordinate, and equating symbols without a charge map would obscure the comparison. In the compact $SU(2)$ gauge frame let $\Phi = a\,\mathrm{diag}(1,-1)$, $a \geq 0$. The roots have charges $\pm 2a$, whereas a full fundamental has weights $\pm a$. Matching the W mass gives $\phi = 2a$. The IMS prepotential in this frame is

$$\mathcal{F}_{\text{IMS}}(a) = m_0 a^2 + \frac{4}{3}a^3, \qquad \mathcal{F}''_{\text{IMS}}(a) = 2m_0 + 8a. \tag{X.8.5}$$

With the source magnetic unit and m_0 identified only after this map, direct substitution gives

$$\phi = 2a, \qquad \mathcal{F}_{\mathrm{AHK}}(2a) = 2\mathcal{F}_{\mathrm{IMS}}(a), \qquad \mathcal{F}''_{\mathrm{IMS}}(a) = 2\mathcal{F}''_{\mathrm{AHK}}(2a). \tag{X.8.6}$$

For instance, at $a = m_0/2$ the two metrics are $6m_0$ and $3m_0$, respectively, as the last factor of two requires. The factor is a coordinate and normalization statement. It is not an extra physical flavor or an identification of all line operators. Chapter 1 derives the brane charges behind this relative normalization, and Chapter 3 uses the IMS coordinate for mass chambers.

The pure cubic does not select the discrete theta angle. The source webs distinguish E_1 and $\widetilde{E}_1$ even though this local polynomial is shared. A further E_0 endpoint is another source flow, without an asserted pure-$SU(2)$ gauge description. The one-flavor negative-mass route makes the limit especially concrete. Write the source-native mass as $m = -\mu$, with $\mu > 0$, and let

$$s = m_{0,\mathrm{MS}} - 4\mu. \tag{X.8.7}$$

The old gauge expression applies for $s > 0$. The equality $s = 0$ is the limiting $\widetilde{E}_1$ wall. For $s < 0$ the source uses its separate continuation, with the origin held fixed; continuing the old gauge cubic into that region would change the object. Likewise, positive $\mathcal{F}''$ is a necessary local gauge-phase condition, not a UV-existence theorem and not a theta detector. This fork is why the atlas stores a phase and a global label separately from the face area.

X.8.3 Charge and tensor data that do not become a magnetic ring

Several atlas rows calculate something precise without introducing a three-dimensional flux lattice. In the ordered seven-brane chart $BCBC$, the brane charges are

$$z_1 = z_3 = (1, -1), \qquad z_2 = z_4 = (1, 1). \tag{X.8.8}$$

Write $Z = (z_1\ z_2\ z_3\ z_4)$ for the map from the four prong charges to the asymptotic charge. Prong vectors $r_1 = (1, 0, -1, 0)$ and $r_2 = (0, 1, 0, -1)$ have vanishing asymptotic charge. Using the ordered junction intersection form gives

$$-\big(r_i \cdot r_j\big)_{i,j=1,2} = \begin{pmatrix} 2 & -2 \\ -2 & 2 \end{pmatrix}, \qquad Z(1, 1, -1, -1)^{\mathsf{T}} = 0. \tag{X.8.9}$$

This is affine-root arithmetic in a flavor junction lattice. The null-asymptotic vector is not the radical of the full unconstrained intersection lattice. The total ordered monodromy in this chart is $\left(\begin{smallmatrix} 1 & 8 \\ 0 & 1 \end{smallmatrix}\right)$, not the identity. Chapter 2 develops the cut and braid conventions. Neither the matrix nor its monodromy asserts that each lattice root is a BPS particle, and neither turns a flavor root into a magnetic cocharacter.

The six-dimensional interval row asks a different question. Take two internal D6 intervals of rank four between three NS5 branes, with exterior flavor ranks $(4, 4)$ and no internal D8 branes. The source charge-balance equation gives

$$2V_i - V_{i-1} - V_{i+1} = W_i, \qquad (V_0, V_1, V_2, V_3) = (4, 4, 4, 4), \qquad (W_1, W_2) = (0, 0). \tag{X.8.10}$$

Thus the selected semisimple electric gauge cover is $SU(4) \times SU(4)$. The relative string pairing is the A_2 matrix. Here X is the two-component Green–Schwarz four-form vector in the source I_i basis used in Chapter 4, so its pairing is A, not A^{-1}. In this example $X = (s_1/2 + 4c, s_2/2 + 4c)^{\mathsf{T}}$, where $s_i = \mathrm{tr}_{\mathrm{f}}\, F_{O,i}^2$, $c = c_2(R)$ and $F_O = -iF_{\mathrm{phys}}/(2\pi)$ as in that chapter:

$$A_{ij} = \begin{pmatrix} 2 & -1 \\ -1 & 2 \end{pmatrix}, \qquad I_{\mathrm{GS}} = \frac{1}{2} X^{\mathsf{T}} A X. \tag{X.8.11}$$

The irreducible gauge-anomaly residual vanishes in both intervals. In the stated flavor-curvature-zero, simply connected gauge-cover frame, the restricted background polynomial is

$$I_8\big|_{F_{\mathrm{flavor}}=0} = \frac{89}{6} c_2(R)^2 - \frac{7}{12} c_2(R) p_1(T) + \frac{43}{1440} p_1(T)^2 - \frac{19}{360} p_2(T). \tag{X.8.12}$$

These are charge and anomaly checks in a six-dimensional tensor branch. Its two relative tensor coordinates are real. Finite positive values describe the separated interval phase; the putative SCFT lies at vanishing relative vevs. The free center tensor has been omitted from the local interacting count, while trace $U(1)$ factors are massive in the source frame. Neither operation is a quotient of a three-dimensional magnetic diagonal. Chapter 4 develops the interval and anomaly derivations, which this row records without importing a new magnetic ring.

X.8.4 The E3 origin is a union of unequal cones

At the massless $SU(2)$ theory with two flavors, take inverse five-dimensional coupling, flavor masses and Coulomb vev all to zero. The sourced web has two maximal subweb decompositions. Their proposed magnetic quivers are a triangle of three rank-one nodes with unit edges and a two-node doubled-edge graph. Each loses one primitive diagonal $U(1)$. The proposed five-dimensional Higgs branch is the union of the two corresponding three-dimensional Coulomb spaces at this infinite-coupling origin. The physical identification and their reduced common origin are source inputs. We can calculate what these inputs entail.

For the triangle choose the integral quotient slice $m_0 = 0$, so its magnetic fluxes are $(0, m_1, m_2)$. In the book fugacity $t^{2\Delta}$, the bare monopole degree and residual scalar dressing are

$$d_{A_2}(m_1, m_2) = |m_1| + |m_1 - m_2| + |m_2|, \qquad P_{A_2}(t) = \frac{1}{(1 - t^2)^2}. \tag{X.8.13}$$

The first nonzero shell has six fluxes at degree two. More generally the hexagonal shell

of radius $r > 0$ has $6r$ fluxes at degree $2r$. Writing $x = t^2$ yields

$$H_{A_2}(t) = \frac{1 + \sum_{r\geq 1} 6r x^r}{(1-x)^2} = \frac{1 + 4x + x^2}{(1-x)^4} = 1 + 8x + 27x^2 + O(x^3). \tag{X.8.14}$$

The quaternionic Coulomb rank follows independently from $3 - 1 = 2$. The source identifies this ring with the reduced minimal $\mathfrak{sl}_3$ orbit closure. The series checks its graded dimensions but cannot establish that identification by itself.

For the doubled edge use a primitive slice $(0, m)$. Two edges each contribute $|m|$ to the bare degree, and one residual scalar remains. The complete sum is

$$H_{A_1}(t) = \frac{1 + 2\sum_{r\geq 1} x^r}{1-x} = \frac{1+x}{(1-x)^2} = 1 + 3x + 5x^2 + O(x^3). \tag{X.8.15}$$

Its effective rank is $2 - 1 = 1$. This is the reduced minimal $\mathfrak{sl}_2$ orbit closure in the sourced description. The triangle and doubled edge have distinct graphs, ranks and component dimensions.

Let A and B denote the two reduced graded coordinate rings. If their intersection is exactly the common origin, the ring of the union consists of pairs of functions with the same value there:

$$\mathbb{C}[X_{A_2} \cup_{\{0\}} X_{A_1}] = A \times_{\mathbb{C}} B = \{(f, g) \in A \oplus B \mid f(0) = g(0)\}. \tag{X.8.16}$$

The exact sequence $0 \to A \times_{\mathbb{C}} B \to A \oplus B \to \mathbb{C} \to 0$ removes one constant function. Hence

$$H_{E_3,\infty}(t) = H_{A_2}(t) + H_{A_1}(t) - 1 = 1 + 11t^2 + 32t^4 + O(t^6). \tag{X.8.17}$$

Degree two contains eight triangle functions and three doubled-edge functions. Degree four contains $27 + 5 = 32$. The intersection has coefficients $(1, 0, 0, 0, 0)$ through t^4.

This union has complex Krull dimension four, the maximum of its components' complex dimensions four and two. It has no single equidimensional quaternionic dimension. The Hasse fork in Figure X.8.2 records two open pieces above one origin, but a Hilbert series alone could not recover that adjacency. Chapter 6 supplies the web decompositions and Chapter 7 explains the Poisson leaves. The construction changes at finite coupling or nonzero mass, where the source does not assert this same union. One cannot sum the two series without the origin correction.

The elementary three-flavor SQED ring provides another check on what a magnetic computation knows. For compact $U(1)$ with three full charge-one hypers, the sourced monopole relation and book degrees are

$$V_+V_- = \varphi^3, \qquad \deg(\varphi, V_+, V_-) = (2, 3, 3), \qquad H(t) = \frac{1 - t^6}{(1-t^2)(1-t^3)^2}. \tag{X.8.18}$$

It begins $1 + t^2 + 2t^3 + t^4 + 2t^5 + 3t^6 + 2t^7 + 3t^8$. The odd degrees are genuine monopole sectors. The relation is a sourced operator statement; summing fluxes or matching a cyclic Molien count tests the grading. This compact surface is neither E_3 component merely because all are small quivers.

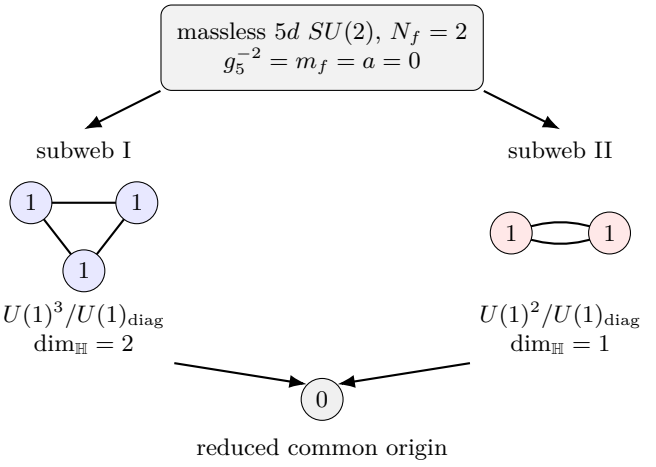


Figure X.8.2: The same massless E_3 origin supplies two sourced subweb phases. Their compact magnetic graphs have quaternionic dimensions two and one. The arrows to the reduced common origin encode the source's intersection premise, after which the fiber-product calculation gives the union series.

X.8.5 Separated M5s, electric four flavors and the D4 star

The six-dimensional path begins with a local physical construction. Two $M5$ branes sit on an A_1 singularity, are separated along x^6, and have a positive finite relative tensor vev. The initial equal-rank IIA/M lift here contains no $M9$ plane. The source's electric interval theory has one $SU(2)$ gauge factor and four full hypermultiplets. Its regular Higgs quaternionic dimension follows from the hyperkähler quotient count,

$$\dim_{\mathbb{H}} \mathcal{H}_{\text{electric}} = 4 \dim_{\mathbb{C}} \mathbf{2} - \dim_{\mathbb{R}} SU(2) = 8 - 3 = 5. \tag{X.8.19}$$

The relative separation is one real tensor coordinate, separate from this Higgs dimension. The source literature proposes a magnetic quiver in this finite separated phase. Its D8 rearrangement and magnetic prescription are additional physical steps after the local no-$M9$ lift.

The resulting compact three-dimensional group is

$$G_{D_4} = \frac{U(2) \times U(1)^4}{U(1)_{\text{diag}}}, \qquad \operatorname{rank} G_{D_4} = 2 + 4 - 1 = 5. \tag{X.8.20}$$

The affine-D_4 graph has one central rank-two node, four distinct rank-one leaves and four unit edges. Removing the primitive common diagonal removes one flux and its scalar. It does not remove a six-dimensional Higgs factor. Figure X.8.3 keeps the physical and magnetic objects side by side.

To see what the magnetic graph computes, fix one leaf flux to zero as an integral slice of the primitive quotient. Write the central $U(2)$ fluxes as $a \leq b$ and the four leaf

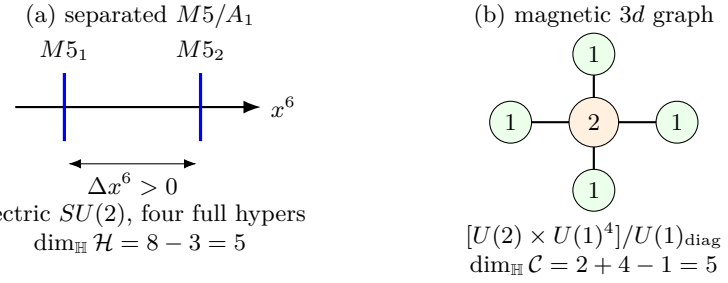


Figure X.8.3: A finite positive x^6 separation defines the no-$M9$ electric phase in panel (a). Panel (b) shows the sourced magnetic star, with four separate unit leaves and a central rank-two node. The map between panels is a physical magnetic-quiver proposal; the dimension counts and monopole coefficients are separate calculations.

fluxes as l_i, with $l_0 = 0$. The matter weights and central positive root give

$$d(a,b;\boldsymbol{l}) = \sum_{i=0}^{3} \big(|a - l_i| + |b - l_i|\big) - 2|a - b|. \tag{X.8.21}$$

For $a \le b$, the identity

$$|a - l| + |b - l| = (b - a) + 2\,\mathrm{dist}(l, [a,b]) \tag{X.8.22}$$

turns it into the nonnegative form

$$d(a,b;\boldsymbol{l}) = 2(b - a) + 2\sum_{i=0}^{3} \mathrm{dist}(l_i, [a,b]). \tag{X.8.23}$$

The central root subtraction is essential. For $d \le 4$ the bound is

$$(b - a) + \sum_{i} \mathrm{dist}(l_i, [a,b]) \le 2, \qquad l_0 = 0. \tag{X.8.24}$$

It implies $|a|, |b|, |l_i| \le 2$. Sum all integral sectors satisfying this inequality; the interval $[a,b]$ need not contain zero. For example, $a = b = 1$ and $(l_0, l_1, l_2, l_3) = (0,1,1,1)$ has $d = 2$. At $a = b$, the residual central factor contributes a degree-four Casimir together with four degree-two factors. At $a < b$, the five residual Casimirs all have degree two. This dressing distinction matters as much as the bare degree.

With these fluxes and dressings, the finite sum gives

$$H_{G_{D_4}}(t) = 1 + 28t^2 + 300t^4 + O(t^6). \tag{X.8.25}$$

The 28 degree-two functions fit the adjoint dimension of $\mathfrak{so}_8$; the source identifies the space with the reduced minimal $SO(8)$ orbit of quaternionic dimension five. The agreement of $8 - 3$ with $2 + 4 - 1$, and the low Hilbert coefficients, check the proposed

dictionary once its physical map is supplied. They do not derive that map or establish a complete six-dimensional and three-dimensional QFT equivalence. Chapter 5 develops the flux lattice, while Chapter 7 explains residual dressing.

There is a dangerous same-name comparison. Compact three-dimensional $SU(2)$ with four doublets has a D_4 Kleinian Coulomb *surface* of quaternionic dimension one. Its source ring has generator degrees $(4, 4, 6)$ and one relation of degree twelve, giving

$$H_{SU(2),N_f=4}(t) = \frac{1-t^{12}}{(1-t^4)^2(1-t^6)} = 1+2t^4+t^6+3t^8+2t^{10}+4t^{12}+O(t^{14}). \quad \text{(X.8.26)}$$

There is no degree-two term here. The rank-one compact $SU(2)$ cocharacter lattice and residual Casimirs differ from the rank-five affine-D_4 unitary quotient. The same Dynkin letter labels different singularities. The finite separated no-$M9$ construction does not establish a coincident-$M5$ or later $M9$ extension.

X.8.6 Cycles and aligned subtraction

The last two rows show how much source structure a graph calculation needs. For the massless five-dimensional $SU(2)$ theory with three flavors at infinite coupling, the sourced E_4 web decomposition has five colored subwebs. Their magnetic edge prescription combines a stable intersection with opposite-side and same-side shared-endpoint corrections,

$$E_{ij} = SI(W_i, W_j) + X_{ij} - Y_{ij}. \quad \text{(X.8.27)}$$

Red–blue and red–green each have $(SI, X, Y) = (1, 0, 1)$, so those apparent stable intersections give no edge. Orange–red and purple–red each have $(0, 1, 0)$ and do give an edge. Blue–green has $(1, 0, 0)$. Applying the fixed source incidences to all ten pairs yields precisely the unit cycle

$$\text{orange} \leftrightarrow \text{red} \leftrightarrow \text{purple} \leftrightarrow \text{green} \leftrightarrow \text{blue} \leftrightarrow \text{orange}. \quad \text{(X.8.28)}$$

The effective group is $U(1)^5/U(1)_{\text{diag}}$, so its magnetic Coulomb dimension is four. Fixing one primitive flux, its bare shells have counts $1, 20, 110$ in degrees $0, 2, 4$. Four scalar dressings produce

$$H_{E_4}(t) = \frac{1+20t^2+110t^4+O(t^6)}{(1-t^2)^4} = 1+24t^2+200t^4+O(t^6). \quad \text{(X.8.29)}$$

This is a calculation for the specified source graph, not a proof of a general endpoint rule. Replacing one unit edge by a doubled edge would change the early series, including an odd-degree term. The physical assignment of the five-cycle to the five-dimensional Higgs branch remains the source prescription.

Quiver subtraction uses a different operation. Inside the ambient $\mathfrak{sl}_5$ orbit closure $\overline{\mathcal{O}}_{(2^2,1)}$, choose a point in the smaller orbit $\mathcal{O}_{(2,1^3)}$ itself, for example E_{12}. The two sourced gauge chains are aligned on the same four nodes with unit edges. Their rank vectors are

$$Q = (1, 2, 2, 1), \qquad Q' = (1, 1, 1, 1), \qquad Q - Q' = (0, 1, 1, 0). \quad \text{(X.8.30)}$$

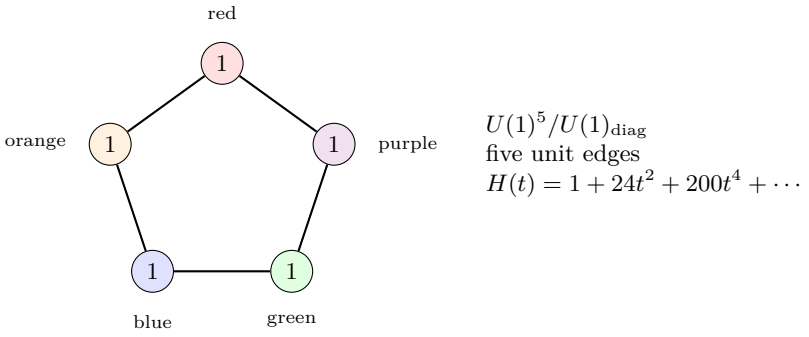


Figure X.8.4: The E_4 source incidence prescription gives five unit edges in this order. Each node has magnetic rank one; the primitive diagonal is removed. The low-degree series belongs to this cycle in the massless infinite-coupling phase.

Their flavor vectors are respectively $(0, 1, 1, 0)$ and $(1, 0, 0, 1)$. Subtraction retains the framing of Q. Deleting the two zero-rank nodes leaves a framed $U(1)$–$U(1)$ chain with one unit edge and one fundamental on each node. The framing is retained, so no common diagonal is quotiented. Its quaternionic Coulomb rank is two, and its checked low-degree series is $1 + 8t^2 + 27t^4 + O(t^6)$. The named slice at this interior orbit point is the minimal $\mathfrak{sl}_3$ orbit closure, a known geometric example in the source. The broader section-three subtraction prescription is conjectural, and arbitrary nonaligned graph subtraction has no such interpretation. This contrasts with the E_3 union, where component rings are glued at an origin rather than one quiver being subtracted from another.

X.8.7 Exercises

1. In the stated pure-$SU(2)$ source conventions take $\mathcal{F}_{\mathrm{AHK}} = m\phi^2/2 + \phi^3/3$ and $\mathcal{F}_{\mathrm{IMS}} = ma^2 + 4a^3/3$. Find c in $\phi = ca$, the ratios $\mathcal{F}_{\mathrm{AHK}}(ca)/\mathcal{F}_{\mathrm{IMS}}(a)$ and $\mathcal{F}''_{\mathrm{IMS}}(a)/\mathcal{F}''_{\mathrm{AHK}}(ca)$, and the area of a face of width $m + \phi$ and height ϕ.

2. For compact three-dimensional $U(1)$ with three charge-one full hypermultiplets, use $t^{2\Delta}$. Find the degrees of φ, V_+ and V_-, the exponent in $V_+V_- = \varphi^n$, and every Hilbert coefficient from t^0 through t^8, including the odd degrees.

3. At the massless, zero-Coulomb-vev, infinite-coupling E_3 origin, use the sourced unit-edge triangle and doubled-edge graph, each with its primitive diagonal removed. Give both quaternionic Coulomb dimensions, both series through t^4, the common-origin intersection series and the union series through t^4.

4. For two separated $M5$s on A_1 at finite positive relative tensor vev and with no $M9$, draw the effective five-node magnetic graph with all ranks and unit edges. State whether a primitive diagonal $U(1)$ is removed. Calculate the electric four-flavor $SU(2)$ Higgs quaternionic dimension, the magnetic Coulomb quaternionic

dimension and its coefficients through t^4. Keep the finite separated phase as an input to the calculation.

5. Explain in writing why the compact $SU(2)$, four-flavor D_4 Coulomb surface cannot be identified with the affine-D_4 reduced $SO(8)$ orbit of quaternionic dimension five. Explain also why the local no-$M9$ lift of separated $M5/A_1$ does not establish an $M9$ extension. Give an exact source locator for each boundary.

X.8.8 Take-home message

Take-home message

The pure $SU(2)$ web computes a face area and local prepotential derivatives after its source mass map is fixed; it does not determine theta. At the infinite-coupling E_3 origin, two sourced subwebs lead to two distinct compact magnetic rings, and their reduced common origin gives the fiber-product series $1+11t^2+32t^4+\cdots$. Separated $M5$s on A_1 at finite tensor vev supply a different electric six-dimensional object and a sourced affine-D_4 magnetic star with series $1 + 28t^2 + 300t^4 + \cdots$. The compact $SU(2)$ D_4 surface is a separate rank-one object. Charges, anomalies, endpoint incidences and graph subtraction calculate their own invariants within stated phases; a cross-dimensional physical map requires its own source premise.

Status and sources

The pure face, area, tension and source prepotential follow Aharony, Hanany, and Kol 1998, Section II.A–B, Figure 1(b) and equations (24)–(25), together with the compact gauge prepotential of Intriligator et al. 1997, Section 2.3, equation (2.22). The relative scalar map and its derivative factors use the stated charge normalization of Chapter 1. The distinct E_1, $\widetilde{E}_1$ and E_0 flow labels use Morrison and Seiberg 1997, Section 2, equations (2.8)–(2.10), and Aharony and Hanany 1997; DeWolfe, Hanany, et al. 1999. The signed negative-mass chamber, wall and separate continuation follow the source's equations (2.9)–(2.10); the shared cubic alone does not fix theta or UV existence.

The ordered $BCBC$ junction and its charge conventions use DeWolfe, Hanany, et al. 1999, Section 4 and Appendix, with the flavor-root boundary in DeWolfe and Zwiebach 1999, Section 3.1. The local six-dimensional interval ranks use Hanany and Zaffaroni 1998, Section 2.1, while the restricted anomaly and tensor pairing use Ohmori et al. 2014, Appendix A. The displayed rank, junction, pairing and polynomial values are calculations within those selected frames. They assert no BPS-spectrum existence from root arithmetic and no global six-dimensional completion from local charge balance.

The compact monopole formula, SQED operator ring, affine-A_2 triangle and two distinct D_4 constructions use Cremonesi et al. 2014, Sections 2 and 3.1–3.4. The E_3 two-subweb physical union and reduced-origin intersection use Cabrera, Hanany, and Yagi 2019, Section 2.1, equations (2.1)–(2.4) and Figures 2–4. Its E_4 five-cycle and endpoint incidences use Section 2.2, Figure 7, Table 2 and Summary 1; the general rule in Section 3 is conjectural. The separate three-dimensional series and fiber-product

identity are algebraic consequences of the sourced graphs and reduced-intersection premise, not proofs of the five-dimensional branch identifications.

The finite separated $M5/A_1$ electric and magnetic objects use Cabrera, Hanany, and Sperling 2019, Section 2.3, equations (2.4)–(2.10), with its corrected published erratum, and Hanany and Zafrir 2018, equations (2.17)–(2.19). The local no-$M9$ lift, D8 rearrangement, magnetic star and Higgs/Coulomb identification are distinct physical source steps. The compact star rank, finite degree-four flux sum and electric $8-3$ quotient are calculations under those steps. The aligned $\mathfrak{sl}_5$ example uses Cabrera and Hanany 2018, Section 2, equations (2.1)–(2.14); its general Section 3 prescription is conjectural. These protected coefficients do not establish a universal higher-dimensional Higgs/Coulomb dictionary, a metric identification or a complete QFT duality. Later Part I foundations remain interfaces for gravity decoupling, three-dimensional mirror dynamics, six-dimensional anomalies and IIA/M units.

References

Aharony, O. and A. Hanany (1997). "Branes, superpotentials and superconformal fixed points". In: *Nucl. Phys. B* 504, pp. 239–271. DOI: 10.1016/S0550-3213(97)00472-0. arXiv: hep-th/9704170.

Aharony, O., A. Hanany, and B. Kol (1998). "Webs of (p,q) five-branes, five-dimensional field theories and grid diagrams". In: *JHEP* 01, p. 002. DOI: 10.1088/1126-6708/1998/01/002. arXiv: hep-th/9710116.

Cabrera, S. and A. Hanany (2018). "Quiver Subtractions". In: *JHEP* 09, p. 008. DOI: 10.1007/JHEP09(2018)008. arXiv: 1803.11205 [hep-th].

Cabrera, S., A. Hanany, and M. Sperling (2019). "Magnetic quivers, Higgs branches, and 6d N=(1,0) theories". In: *JHEP* 06. [Erratum: JHEP 07, 137 (2019)], p. 071. DOI: 10.1007/JHEP06(2019)071. arXiv: 1904.12293 [hep-th].

Cabrera, S., A. Hanany, and F. Yagi (2019). "Tropical Geometry and Five Dimensional Higgs Branches at Infinite Coupling". In: *JHEP* 01, p. 068. DOI: 10.1007/JHEP01(2019)068. arXiv: 1810.01379 [hep-th].

Cremonesi, S., A. Hanany, and A. Zaffaroni (2014). "Monopole operators and Hilbert series of Coulomb branches of $3d$ $\mathcal{N} = 4$ gauge theories". In: *JHEP* 01, p. 005. DOI: 10.1007/JHEP01(2014)005. arXiv: 1309.2657 [hep-th].

DeWolfe, O., A. Hanany, et al. (1999). "Five-branes, seven-branes and five-dimensional E(n) field theories". In: *JHEP* 03, p. 006. DOI: 10.1088/1126-6708/1999/03/006. arXiv: hep-th/9902179.

DeWolfe, O. and B. Zwiebach (1999). "String junctions for arbitrary Lie algebra representations". In: *Nucl. Phys. B* 541, pp. 509–565. DOI: 10.1016/S0550-3213(98)00743-3. arXiv: hep-th/9804210.

Hanany, A. and A. Zaffaroni (1998). "Branes and six-dimensional supersymmetric theories". In: *Nucl. Phys. B* 529, pp. 180–206. DOI: 10.1016/S0550-3213(98)00355-1. arXiv: hep-th/9712145.

Hanany, A. and G. Zafrir (2018). "Discrete Gauging in Six Dimensions". In: *JHEP* 07, p. 168. DOI: 10.1007/JHEP07(2018)168. arXiv: 1804.08857 [hep-th].

Intriligator, K. A., D. R. Morrison, and N. Seiberg (1997). "Five-dimensional supersymmetric gauge theories and degenerations of Calabi-Yau spaces". In: *Nucl. Phys. B* 497, pp. 56–100. DOI: 10.1016/S0550-3213(97)00279-4. arXiv: hep-th/9702198.

Morrison, D. R. and N. Seiberg (1997). "Extremal transitions and five-dimensional supersymmetric field theories". In: *Nucl. Phys. B* 483, pp. 229–247. DOI: 10.1016/S0550-3213(96)00592-5. arXiv: hep-th/9609070.

Ohmori, K. et al. (2014). "Anomaly polynomial of general 6d SCFTs". In: *PTEP* 2014.10, 103B07. DOI: 10.1093/ptep/ptu140. arXiv: 1408.5572 [hep-th].